

6 BIOLOGICAL ENVIRONMENT

6.1 General Setting

The nodule provinces found in the CCZ typically provide hard substrates in the form of the nodules and soft substrates in the red clays that surround them. Thus, there are organisms that live in the sediment, on the sediment, attached to the nodules and those that are free swimming (Snelgrove & Smith, 2002). The overarching framework for the biological baseline studies has been structured to characterize the biotic communities in each of these habitat types.

6.2 Baseline Studies

NORI has completed a total of nine campaigns to the CCZ during the period Q4/2019 to Q4/2021 and committed to a further 4 campaigns prior to the submission of the commercial ESIA.

Table 6-1 lists the contractors, institutions, principal investigators, and area of study that have been contracted by NORI to conduct the biological baseline studies for the commercial ESIA.

Table 6-1. Contractors, institutions, principal investigators, and areas of study

| INSTITUTION (Abbreviation - Country) | PRINCIPAL INVESTIGATORS | AREA OF STUDY |
|---|---|--|
| Natural History Museum (NHM; UK) | Dr Adrian Glover | <ul style="list-style-type: none"> Benthic macrofauna (nodules and sediments) |
| University of Gothenburg (UG; SE) | Dr Thomas Dahlgren | <ul style="list-style-type: none"> Benthic macrofauna (nodules and sediments) |
| National Oceanography Centre (NOC; UK) | Dr Daniel Jones | <ul style="list-style-type: none"> Benthic megafauna |
| University of Leeds (UL; UK) | Dr Claire Woulds | <ul style="list-style-type: none"> Sediment geochemistry |
| Heriot Watt University (HWU; UK) | Dr Andrew Sweetman / Dr. Theodore Henry | <ul style="list-style-type: none"> Benthic scavengers. Sediment respiration Benthic ecotoxicology |
| Florida State University (FSU; US) | Dr Jeroen Ingels | <ul style="list-style-type: none"> Meiofauna |
| Cawthorn Institute (CI; NZ) | Dr. Olivier Laroche / Dr. Xavier Pochon | <ul style="list-style-type: none"> Microbes (sediment) |
| University of Southern Florida (USF; US) | Dr. Patrick Schwing / Bryan O'Malley | <ul style="list-style-type: none"> Foraminifera |
| University of Hawaii at Manoa (UH; US) | Dr Jeff Drazen | <ul style="list-style-type: none"> Micronekton assemblage Bioacoustic mid-water ROV transects, Upper trophic levels of food web study |
| | Dr Angel White | <ul style="list-style-type: none"> Microbial assemblages Phytoplankton community and productivity Particles |
| | Dr Brian Popp | <ul style="list-style-type: none"> Stable isotopes Food web linkages |
| | Dr Sara Ferron | <ul style="list-style-type: none"> Phytoplankton productivity |

| INSTITUTION (Abbreviation - Country) | PRINCIPAL INVESTIGATORS | AREA OF STUDY |
|--|--|--|
| | Dr Mariko Hatta / Dr Chris Measures | <ul style="list-style-type: none"> • Chemical oceanography • Trace metals |
| | Dr Erika Goetze | <ul style="list-style-type: none"> • Zooplankton, metabarcoding • Mid-water eDNA • DNA barcoding • ROV transects |
| University of Maryland (UMD; US) | Dr Dana Sackett | <ul style="list-style-type: none"> • Microneckton ecotoxicology |
| Japan Agency for Marine-Earth Science and Technology (JAMSTEC; JP) | Dr Dhugal Lindsay | <ul style="list-style-type: none"> • Gelatinous zooplankton • Mid-water ROV transects |
| Texas A&M University (TA&M; US) | Dr Jessica Fitzsimmons | <ul style="list-style-type: none"> • Chemical oceanography • Trace metals |
| CSA Ocean Sciences Inc. (CSA; US) | Dr Chris Kelly | <ul style="list-style-type: none"> • Metocean moorings |
| Fathom Pacific (FP; AU) | Dr Adrian Flynn | <ul style="list-style-type: none"> • Surface Biology |

The baseline campaign schedule is now complete and analysis of samples, specimens and data collected at sea is a time-consuming process, with research institutions requiring up to 12 months post-campaign to conduct a full post-campaign analysis. Information that will not be available prior to the Collector Test has been highlighted in Table 6-2.

The sub-set of baseline findings presented in this chapter are considered appropriate for the small scale Collector Test and is consistent with Annex III of ISA Recommendations (ISBA/25/LTC/6/Rev.1) which states that the assessment of impacts from activities on the seafloor ***should be appropriate to the nature and extent of the activity being considered*** and should also ensure that no significant harm is caused by the activities conducted during exploration.

Table 6-2. Baseline campaign and reporting schedule for NORI-D*

| # | CAMPAIGN ID | START DATE | END DATE | # DAYS | FOCUS | INSTITUTION | DATA STATUS | REPORTING STATUS |
|---|----------------|------------|----------|--------|--|----------------------|---------------------------------|--------------------------|
| 1 | Campaign 4A | 2/10/19 | 23/10/19 | 21 | Deployment of three oceanographic moorings within NORI-D to collect continuous metocean data. Water sampling and oceanographic profiling also conducted. | CSA | All data collected and analysed | Report received 04/01/20 |
| 2 | Ocean Infinity | 23/05/20 | 30/05/20 | 7 | Over 25K seabed images collected from PRZ and CTA used for megafauna identification and quantification. | Ocean Infinity / NOC | Preliminary data presented | Report due 01/04/22 |
| 3 | Campaign 4D | 16/6/20 | 15/7/20 | 29 | Serviced the oceanographic moorings deployed at NORI-D during Campaign 4A. Conducted additional oceanographic profiling. | CSA | All data collected and analysed | Report received 18/12/20 |

| # | CAMPAIGN ID | START DATE | END DATE | # DAYS | FOCUS | INSTITUTION | DATA STATUS | REPORTING STATUS |
|----|------------------------|------------|----------|--------|--|--|---|---------------------------------|
| 4 | Campaign 5A | 16/10/20 | 30/11/20 | 45 | Collected data on the benthic biology, sediment geochemistry and surface biology of NORI-D using box-core, multicore and floating hydrophones. | NHM / UG / UL / FSU / USF / FP | Preliminary data presented | Annual Reports received 12/2021 |
| 5 | Campaign 5B | 5/3/21 | 14/4/21 | 40 | Pelagic biology studies of NORI-D supported by ROV, CTDs, MOCNESS nets and rosette water quality samplers for trace metals. | UH / TA&M / JAMSTEC /UMD | Preliminary data presented | Annual Reports received 12/2021 |
| 6 | Campaign 5D | 27/4/21 | 12/6/21 | 45 | Collected seasonal data on the benthic biology, sediment geochemistry and surface biology of NORI-D using box-core, multicore and floating hydrophones. Lander deployments for scavengers, respiration and ecosystem function | NHM / UG / UL / FSU / USF / BU / HWU / FP / CI | Data currently with contractor for analysis | Final reports due 12/22 |
| 7 | Campaign 4E | 6/7/21 | 29/7/21 | 21 | Serviced the oceanographic moorings deployed at NORI-D during Campaign 4A. Conducted additional oceanographic profiling. | CSA | Preliminary data presented | Report received 01/2022 |
| 8 | Campaign 5C | 21/9/21 | 2/11/21 | 42 | Seasonal pelagic biology studies of NORI-D supported by CTDs, MOCNESS nets and rosette water quality samplers for trace metals. | UH / TA&M / UMD | Data currently with contractor for analysis | Final reports due 12/2022 |
| 9 | Campaign 5E | 12/11/21 | 22/12/21 | 40 | ROV pelagic and benthic transects and sample collection. Collection of seasonal seabed images collected from PRZ and CTA used for megafauna identification and quantification. Lander deployments for scavengers, respiration and ecosystem function | JAMSTEC / HWU / NOC / NHM / UG | Data currently with contractor for analysis | Final reports due 12/22 |
| 10 | Pre/Mid-Collector Test | Q2/2022 | TBA | TBA | Studies before and during the Collector Test will be conducted during this campaign. | TBA | NA | Q1/2023 |
| 11 | Campaign 4F | Q2/2022 | TBA | TBA | Serviced the oceanographic moorings deployed at NORI-D during Campaign 4A. | TBA | NA | Q3/2022 |

| # | CAMPAIGN ID | START DATE | END DATE | # DAYS | FOCUS | INSTITUTION | DATA STATUS | REPORTING STATUS |
|----|-----------------------|------------|----------|--------|--|-------------|-------------|------------------|
| | | | | | Conducted additional oceanographic profiling. | | | |
| 12 | Post - Collector Test | Q3/2022 | TBA | TBA | Disturbance studies during and after the Collector Test will be conducted. | TBA | NA | Q1/2023 |
| 13 | Campaign 4G | Q2/2023 | TBA | TBA | Serviced the oceanographic moorings deployed at NORI-D during Campaign 4A. Conducted additional oceanographic profiling. | TBA | NA | Q3/2023 |

Note: data from highlighted campaigns will not be available prior to the Collector Test

The following sections provide a brief overview of relevant studies from the wider CCZ region with descriptions of preliminary data from NORI-D based on the Annual Reports submitted in December 2021. These source reports are available to the LTC on request.

6.3 Benthic Baseline

6.3.1 Benthic Megafauna

Benthic megafauna (i.e., metazoans >1 cm) of the CCZ comprise a variety of fauna from scavengers/bait-attending communities (including fish, amphipods and shrimp); deposit feeders (dominated by the echinoderms) and suspension-feeding organisms (including sponges, anemones, corals and other cnidarians). Together, these communities play an important role in functioning of deep-sea ecosystems, in terms of phytodetrital consumption, bioturbation (Smith *et al.* 2008) and benthic carbon flow through the abyssal food web (Stratmann and Voorsmit *et al.* 2018).

Although biomass is reported to be low, the CCZ is thought to have one of the highest levels megafaunal species richness in the deep sea (Kamenskaya, Melnik, and Gooday 2013; Tilot *et al.* 2018). Previous studies of areas targeted for mining, indicate morphospecies richness estimations from imagery data can rise above 150 taxa (for example, UK-1; (Amon *et al.* 2016); NORI-A; (Tilot *et al.* 2018)) with variations in megafaunal density observed between different geofoms (e.g., hills, plains, troughs) and nodule coverage (Simon-Lledó *et al.* 2020)

Sessile epifauna (particularly suspension feeders) are shown to have increased numerical densities in locations with higher nodule coverage (Vanreusel *et al.* 2016) with up to 50% of the overall megafauna identified thought to depend on them (Amon *et al.* 2016). In nodule-free areas, echinoderms (asteroids, echinoids, and holothuroids) are shown to represent a high-proportion of the deposit-feeding megafauna (De Smet *et al.* 2021; Stoyanova 2012).

Regional differences in the community composition of benthic megafauna and scavengers in the CCZ has been observed, with a decrease in density with increasing water depth (Simon-Lledó *et al.* 2020; Leitner *et al.* 2017). Fish densities detected from AUV imagery are reported to be much higher in the CCZ (Simon-Lledó *et al.* 2020; 2019; Simon-Lledó *et al.* 2019c; Drazen *et al.* 2019a) than those from other abyssal plain areas of the global ocean (e.g., Porcupine abyssal plain; Milligan *et al.* 2016a).

On regional scales, the overall density of megafauna decreases with increasing water depths from the east to the west of the CCZ and has shown not to be correlated to regional productivity gradients (Simon-Lledó *et al.* 2020; Leitner *et al.* 2017) suggesting that the presence and density of nodules (Simon-Lledó *et al.* 2019a; Vanreusel *et al.* 2016; De Smet *et al.* 2021; Leitner *et al.* 2017) as well as typology (e.g.,

shape and volume; Simon-Lledó *et al.* 2020; 2019) may play an important role in driving the abundance and community composition of both mobile and sessile megafauna.

6.3.1.1 Purpose & scope

The following section describes the work conducted between 2020-2021 by the National Oceanographic Centre (NOC) to characterise natural baseline conditions in megafaunal communities in the NORI-D contract area. The scope, the survey planning and the sampling methodologies carried out to ecologically characterise seabed megafaunal communities align with International Seabed Authority ISBA/25/LTC/6 Rev 1. Annex 1 section 41(a) Biological communities: Megafauna, to provide baseline data requirements under Recommendations III.A.13; III.B.14; III.B.15.(d).(i)–(ii); IV.B.22. Results obtained from assessments of seabed image data conducted during Year 1 of the project are provided here.

6.3.1.2 Baseline investigations

The methods and proposed survey array for both the Collector Test and long-term environmental studies on NORI-D will provide data to meet the following objectives:

1. Establish the standing stocks (in both abundance and biomass terms), diversity and community structure of key megafauna in the sampled areas. Including comparisons between baseline conditions in areas planned for nodule collection and reference sites (e.g., preservation reference zones. APEIs and other abyssal areas).
2. Compare the megafauna of the NORI-D to the regional distribution patterns of megafaunal morphotypes across the CCZ.
3. Examine how megafaunal communities respond to spatial variation in the environment.
4. Examine whether visible physical conditions (e.g., turbidity. nodule position. sediment cover) changes over time and determine if this affects the biology.

To characterise the abundance, biomass, morphotype structure and diversity of megafauna from scaled photographic transects, the methodologies for data acquisition, image processing and analysis proposed also follow those already published in the peer reviewed literature (e.g., Simon-Lledó *et al.* 2019) to allow for local (within NORI-D) and regional (wider CCZ) comparisons as part of the operational ESIA.

6.3.1.3 Campaign activities

(a) Site selection, survey design and image collection

(i) Site selection

Quantitative megafaunal assessments were planned at NORI-D in four study areas:

- Disturbance sites – Areas within the CTA that will be subjected to disturbance, including the test mining zone (MIN centred: 10° 22.4' N. 117° 9.6' W) and an assumed plume dispersal zone (PLU, centred: 10° 25.5' N. 117° 11.9' W)
- Control sites - Control site to MIN and PLU (CNT centred: 10° 27' N. 116° 46' W)
- Preservation reference zone - (PRZ centred: 10° 54.273' N. 116° 15.026' W)

These sites are at approximately similar depth and some level of representation of each different nodule facies type (see Table 5-4).

The selection of each site was based on the following criteria:

Disturbance Sites

This area of seafloor (depth range: 4250 - 4340 m) will be subject to different levels of disturbance from Collector Test. The low topographical complexity (“Flatter areas” or “Plains” slopes < 3°) facilitates nodule collection and the high abundances of small nodules in this area facilitate nodule collection operations. Preliminary mapping (Section 5.17) suggests a predominance of Type I nodule facies and the existence of some Type II-III patches towards the NE sector of this area. Two different study areas were originally planned to be surveyed within the CTA:

- MIN: this area that will be subject to direct disturbance from the PCV (i.e., nodule removal, sediment removal, sediment compaction, and sediment redeposition).
- PLU: this area is immediately adjacent to MIN, this area was originally anticipated to receive sediment redeposition (decreasing with distance from near field: 100 m; to far field: 10 km) generated during test nodule mining operations. e.g., selected in accordance with the modelled predominant bottom current direction (SE to NW; CSA 2020).

However, based on expanded knowledge of plume distribution patterns (GSR-Patania II testing, Haeckel *et al.* 2021) and new hydrodynamic models conducted at NORI-D’s test mining area (DHI 2021) the PLU study area will be reallocated up from Year 2 (C5E, Nov 2021) surveys (more detail below in section iii below under *Campaign 5E*).

Control site (CNT) (depth range: 4160 – 4300 m)

The control site was allocated in an area thought sufficiently distant from the CTA (~ 40 km) to not be affected by sediment redeposition but sufficiently close to be representative. Models suggest this area has with both Type I and Type II-III nodule facies. This area was selected for its high geomorphological similarity with MIN and PLU areas. As with the MIN and PLU area, it is a generally flat area surrounded by hills (around 100 m higher). CNT and PRZ were planned to serve as no impact reference sites to assess the effect of disturbance from the Collector Test. This adding statistical rigor to the comparisons and mitigating any issues of biological representativity between the MIN and PLU areas and these reference sites.

Preservation reference zone (PRZ)

The PRZ (depth range: 4000* - 4400 m; excluding seamounts which are at a depth of 3600m) is allocated in an area distant from the CTA, not expected to receive any level of mining disturbance. Like the CTA, models suggest it has patches with both Type I and Type II-III nodule facies, but a higher predominance of the latter. Although the topography in this area is different from the CTA, the delineated PRZ sector (25 x 25 km) does have some “flatter areas” (predominant geoform in MIN and PLU areas). which were set as target of survey operations. Subsequent baseline ecological characterisation is planned to assess the rate of similarity between the biological communities found in “flatter areas” (and potentially other geoforms) within PRZ and those in MIN and PLU.

(ii) Survey design

A stratified random sampling design (Andrew & Mapstone, 1987) with even sample replication across study areas was planned to be applied to collect photographic transects (1 transect = 1 sample). In each study area, a zig-zag survey design with random start point will be conducted within each given area of interest to maximise sampling efficiency while minimising design-based bias in the spatial distribution of the replicate samples (Buckland *et al.* 2001; Strindberg & Buckland, 2004). A total of 5 transects, the straight-line zig and zag sections, will be surveyed in each study area per sampling event. Transect length was set to 2 km to encompass a minimum of 500 individuals per sample unit, following recommendations for optimal image-based megafauna sampling at the CCZ (Ardron *et al.* 2019; Simon-Lledó *et al.* 2019a). and based on faunal abundance data reported in nearby CCZ locations (Jones *et al.* 2021). Standardised

image collection protocols (e.g., determining survey features such as image resolution, camera altitude and angle, speed, shooting interval, angle, interval, etc) were designed for optimal acquisition of image data.

(iii) *Image collection*

Ocean Infinity Campaign (23/05/20 - 30/05/20)

High resolution vertical-facing seabed images (and oblique HD video) were collected by Ocean Infinity in June 2020 using the ROV *Kystdesign Supporter 31* from the *Pacific Constructor* during the “WROV Photo Sampling Environmental Survey”, a campaign commissioned by NORI. A total of four image surveys were conducted across NORI-D, following the original project plan designed by NOC. As such, 5 zig-zag shaped transects (each 2 km long) were collected in each of the study areas originally delineated (PRZ, CNT, PLU, and MIN (Figure 6-1)).

A total of 26,916 images were collected during the survey e.g., 6,383 – 6,995 images in each target study area (Table 6-3). Images were obtained with some (~10 %) overlap, which was removed based on survey navigation and image scaling data. Image edges were removed, by cropping the central part of each image (80%), to minimise light distortion detected in these and thus homogenise fauna detectability within and across images. This process yielded non-overlapping images that covered a total of 24,836 m² of seabed. e.g., 6147 – 6266 m² per study area (Table 6-3). Transect-scale survey features are provided in Table 6-4.

Table 6-3 ROV survey features and imagery obtained during Ocean Infinity campaign at NORI-D in June 2020. Mean values across each survey provided for depth, longitude and latitude (data in WGS 1984 coordinate system)

| AREA | DEPTH (m) | LATITUDE (deg) | LONGITUDE (deg) | IMAGES (total) | AREA (m ²) (no overlap) |
|------|-----------|----------------|-----------------|----------------|-------------------------------------|
| MIN | 4285 | 10.36572652 | -117.1635736 | 6995 | 6240 |
| PLU | 4285 | 10.42289974 | -117.1952685 | 6924 | 6183 |
| CNT | 4223 | 10.44988102 | -116.7571656 | 6614 | 6147 |
| PRZ | 4202 | 10.99027955 | -116.152183 | 6383 | 6266 |

Table 6-4 ROV survey features and imagery obtained in each transect collected during Ocean Infinity campaign at NORI-D in June 2020. Mean values across each transect provided for depth, longitude and latitude (data in WGS 1984 coordinate system)

| TRANSECT | LATITUDE (deg) | LONGITUDE (deg) | DEPTH (m) | AREA (m ²) (no overlap) |
|----------|----------------|-----------------|-----------|-------------------------------------|
| MIN_01 | 10.33800372 | -117.174874 | 4278 | 1341 |
| MIN_02 | 10.35209939 | -117.1691889 | 4271 | 1145 |
| MIN_03 | 10.36562928 | -117.1634905 | 4287 | 1277 |
| MIN_04 | 10.37947116 | -117.1578042 | 4295 | 1155 |
| MIN_05 | 10.39390514 | -117.1522945 | 4299 | 1322 |
| PLU_01 | 10.40314515 | -117.1725421 | 4298 | 1283 |
| PLU_02 | 10.41318049 | -117.184468 | 4299 | 1226 |
| PLU_03 | 10.42308661 | -117.195539 | 4283 | 1202 |
| PLU_04 | 10.4328443 | -117.2066113 | 4279 | 1207 |
| PLU_05 | 10.44300814 | -117.2180659 | 4270 | 1264 |
| CNT_01 | 10.47596444 | -116.7724322 | 4233 | 1364 |
| CNT_02 | 10.46265948 | -116.7644283 | 4220 | 1137 |
| CNT_03 | 10.44981727 | -116.7570578 | 4219 | 1135 |
| CNT_04 | 10.43684684 | -116.7497336 | 4223 | 1201 |
| CNT_05 | 10.42383986 | -116.7419986 | 4223 | 1308 |
| PRZ_01 | 10.96208117 | -116.1625372 | 4225 | 1309 |
| PRZ_02 | 10.97654848 | -116.157359 | 4198 | 1204 |

| TRANSECT | LATITUDE (deg) | LONGITUDE (deg) | DEPTH (m) | AREA (m ²) (no overlap) |
|----------|----------------|-----------------|-----------|--|
| PRZ_03 | 10.99023479 | -116.152093 | 4182 | 1269 |
| PRZ_04 | 11.004317 | -116.146811 | 4187 | 1135 |
| PRZ_05 | 11.01888669 | -116.1418175 | 4216 | 1349 |

Campaign 5E (12/11/21 - 22/12/21)

High resolution vertical-facing seabed images (and oblique HD video) were collected using the ROV *Odysseus* from the MSS Launcher during Campaign 5E. A total of four image surveys were conducted across NORI-D.

To study temporal variations in NORI-D megafauna communities seabed imagery was obtained repeating the survey design implemented during the OI campaign (May '20) in two study areas. These were within the Collector Test Area (MIN) and the Preservation Reference Zone (PRZ), the two most geographically distant locations previously surveyed (separated by 125 km).

In total, 5 image transects (each 2 km in length) were planned to be collected in each study area, matching the start/end positions where transects were collected 1.5 years before. An additional image survey, also encompassing 5 (2 km) transects, was planned in the Test Field (TF), to enable future monitoring of nodule mining impacts.

The TF was delimited (1.8 x 4.2 km rectangle) within the southern western sector of the CTA by NORI after the first ROV megafauna survey was conducted in 2020.

The nodule Collector Test operations are planned to be most intensive within an even smaller rectangle (630 x 1330 m) enclosed within the TF (see Section 3.3.2). The Collector Test sediment plume modelling suggests that potentially biologically relevant levels of sedimentation (i.e., >0.1mm) might extend 6-8 kms from the point of plume generation (see Section 7.2.2.5(j)).

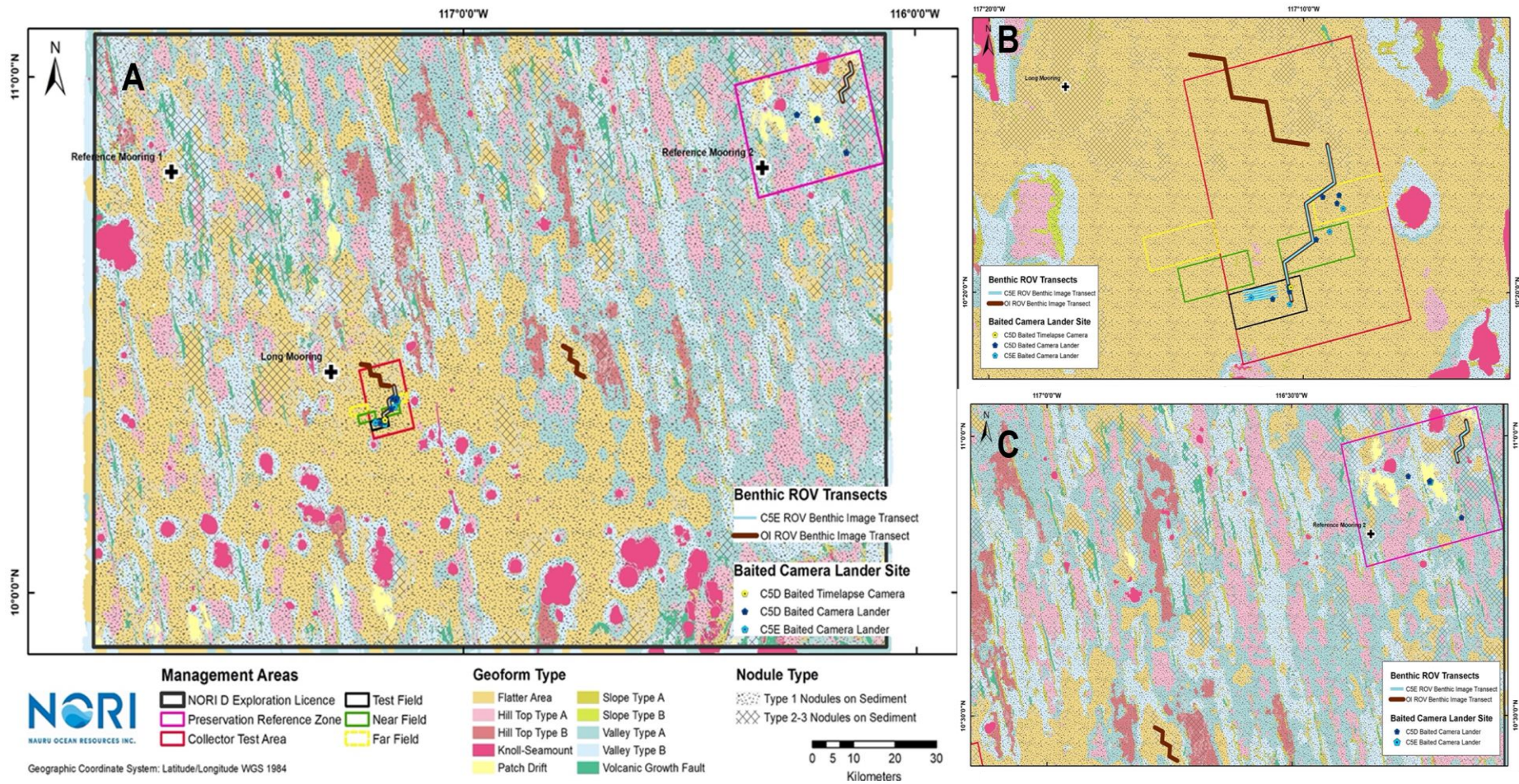
Consequently, the use of the PLU site as baseline to quantify the effect of the redeposition of sediments potentially generated during Collector Tests was deemed not suitable, as the distance between these transects and the TF is too large (e.g. 7.5-12 km), particularly considering the results of the Patania II nodule collection test in 2021 by GSR (plumes travelling < 5 km before re-depositing; Haeckel *et al.* 2021).

Survey planning up from Year 2 of the project had to consequently be modified to fulfil the scientific objectives of the quantitative benthic megafauna studies and align these with the analyses of other working groups (e.g., Campaigns 5B, 5C and 5D).

ROV surveys completed in November 2021 (Campaign 5E; refer to Figure 6-1) included:

- Repeating PRZ, CNT, and MIN surveys as per the 2020 ROV survey
- No revisiting of PLU
- Creating a new tighter survey at the test field. This was positioned using random positions within a tight space to overlay the area we think is most likely to get the most disturbance.

Figure 6-1. A) Overview of ROV and baited camera and time-lapse camera operations within NORI-D; B) Collector Test Area (CTA); C) Preservation Reference Zone (PRZ)



Benefits of the adapted plan:

1. Temporal changes between 2020 and 2021 can be assessed by making direct comparisons at 3 sites (PRZ, CNT and MIN)
2. More spatial scales covered with the 2021 survey.
3. Sets us up for having the best chance of being able to repeat a survey after the test that has maximal disturbance
4. The MIN line will allow some indication of plume spread after mining.

It appears that there may be little variability between PLU and MIN. If this is the case, then the variability between MIN and the test field will test homogeneity at another scale. If these are similar, then a very robust baseline in space and time for the mining area (with extensive representative data from MIN, PLU and test) will be established. In the contrary case, the new survey plan provides more handle on the extent and scales of variability over a relatively small area, which is important. Either way, a site that is very close in space to the area disturbed will be sampled to make a direct comparison to change after the Collector Test.

A total of six ROV dives were conducted to collect the 15 image transects (5 transects at CTA, 5 at MIN; and 5 at PRZ) during Campaign 5E. Further comparison between data collected at a control site (CNT) in 2020 was planned but owing to operational constraints, was not completed during the campaign.

Oblique 4K video was recorded during all dives along with the vertically facing stills. A total of 33,738 quantitative images were collected. Table 6-5 summarises benthic transecting operations, images collected and associated navigation. Note that overlap between consecutive images was observed during some transects thus, the number of images in the quantitative dataset collected for ecological analysis is expected to be somewhat smaller after overlap removal.

Table 6-5 ROV survey features and imagery obtained during C5E at NORI-D in November 2021. Mean values across each survey provided for depth, longitude and latitude (data in WGS 1984 coordinate system)

| AREA | DEPTH (m) | LATITUDE (deg) | LONGITUDE (deg) | IMAGES (total) |
|------|-----------|----------------|-----------------|----------------|
| CTA | 4277 | 10.33266 | -117.19152 | 10839 |
| MIN | 4288 | 10.36574 | -117.16546 | 12527 |
| PRZ | 4205 | 10.99097 | -116.15188 | 10372 |

To confirm identifications of morphospecies from photographs and to undertake DNA taxonomy on any new species, megafauna specimens were used that had been collected during macrofauna box-core studies; preserved as part of earlier baseline resource campaigns (Campaign 6A and Campaign 6B) or; targeted through ROV sampling on Campaign 5E (see Appendix 2).

(b) Long-term benthic camera lander

The time lapse camera lander was deployed at the edge of the CTA to quantify natural variability and document the arrival and impacts of any natural sediment plume events. Time lapse cameras have also been deployed on Reference Mooring #1 and #2 (Table 6-6). Time-lapse images will be assessed to qualitatively examine the physical dynamics of surface sediment and the frequency of resuspension events. Any visible changes in the physical environment (e.g., visible turbidity, nodule coverage, sedimentation) will be documented. Time-lapse images will also be used to document the activity levels of surface megafauna. Deposit feeding rates for abundant taxa will be quantified by measuring the creation rates of their associated traces.

Table 6-6. Camera deployments on Reference Moorings

| CAMPAIGN | DEPLOYMENT | INTERVALS | DURATION |
|-----------------|----------------------|-----------|---------------------|
| C4D (recovered) | Reference mooring #1 | 1 hour | 15/10/19 - 19/10/19 |
| | | 4 hours | 21/10/19 - 16/11/19 |
| | | 4 hours | 17/11/19 - 23/01/20 |
| | | 4 hours | 24/01/20 - 23/04/20 |
| | Reference mooring #2 | 2 hours | 14/10/19 - 18/10/19 |
| | | 8 hours | 19/10/19 - 12/02/20 |
| C5E (recovered) | Reference mooring #1 | 1 hour | 30/06/20 - 06/07/20 |
| | | 8 hours | 06/07/20 - 29/12/20 |
| | Reference mooring #2 | 2 hours | 02/07/20 - 07/07/20 |
| | | 8 hours | 07/07/20 - 02/11/20 |
| C5E (deployed) | Reference mooring #1 | 1 hour | 22/07/21 - 31/07/21 |
| | | 8 hours | 23/07/21 - 31/07/22 |
| | Reference mooring #2 | 0.5 hours | 17/07/21 |
| | | 8 hours | 18/07/21 - 01/08/22 |

6.3.1.4 Preliminary results & discussion

From the May 2020 Ocean Infinity survey, a total of 295 non-overlapping images (encompassing a total seabed area of 597 m²) selected at random across the four NORI-D study areas were quantitatively assessed for megafauna to conduct a preliminary exploration of baseline ecological conditions at NORI-D. In these, 605 metazoan megafauna specimens and 2657 xenophyophore tests (all > 1 cm) were identified (Table 6-7). A total of 72 metazoan megafauna morphotypes (e.g., Figure 6-2) were encountered in the ~600 m² of seabed analysed.

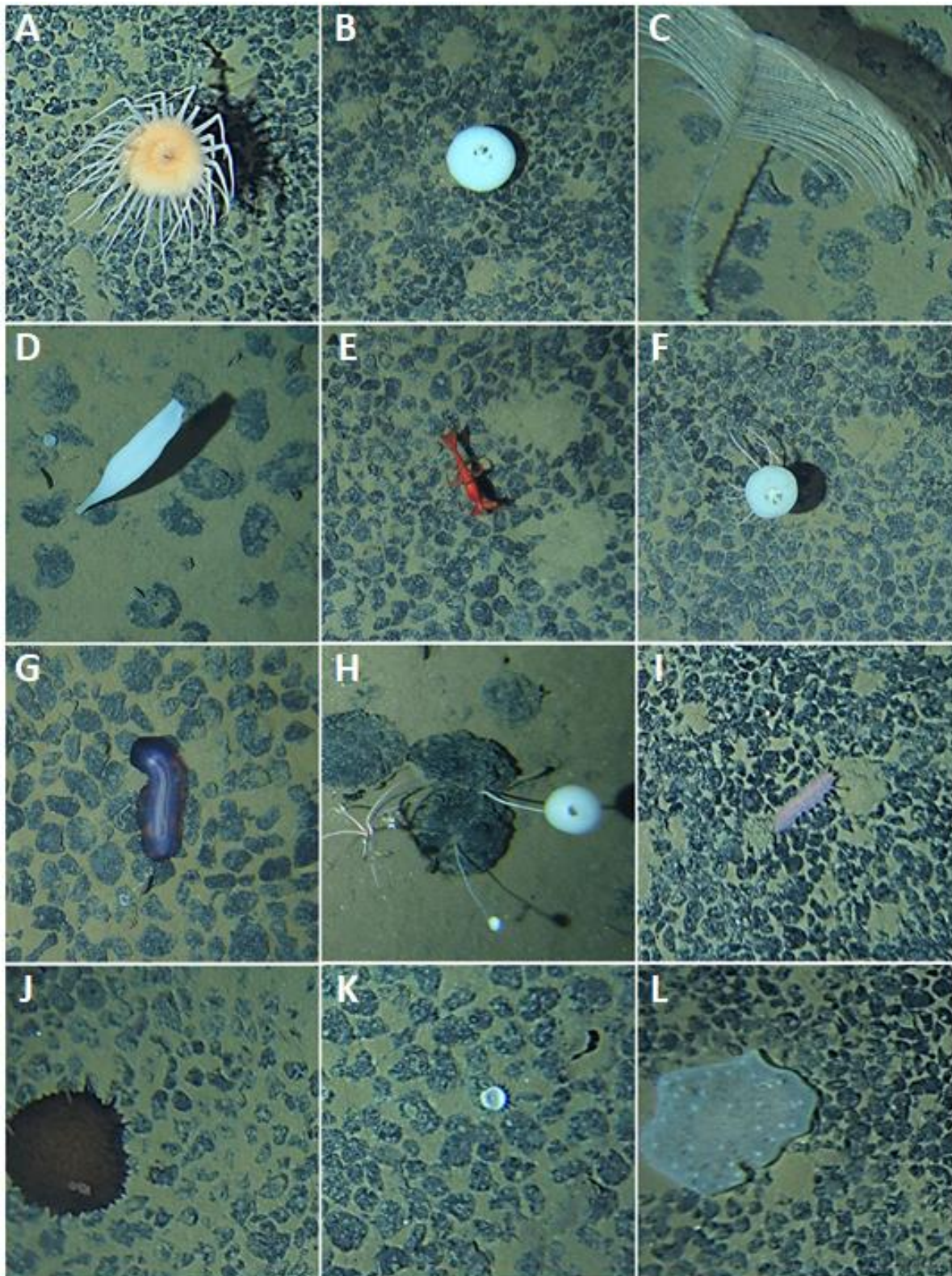
The three most abundant morphotypes so far encountered at NORI-D were: the primnoid soft coral *Abyssoprimnoa gemina* sp inc. (ALC_008; 80 occurrences), the small nodule-encrusting sponge Porifera indet. (POR_002; 31 occurrences), and the primnoid soft coral *Callozostron bayeri* sp inc. (ALC_009; 25 occurrences). About 72% of the metazoan megafauna encountered was found attached to nodules (Table 6-7), amid a high dominance of sessile taxa in this area.

Table 6-7 Preliminary biological exploration of seabed images collected across NORI-D. Images were selected at random within each study area.

| TRANSECT | IMAGES | AREA (m ²) | XENOPHYOPHORES (n) | METAZOANS ON NODULES (n) |
|----------|--------|------------------------|--------------------|--------------------------|
| PLU_01 | 18 | 35.3 | 121 | 41 (76%) |
| PLU_02 | 15 | 29.2 | 130 | 25 (84%) |
| PLU_03 | 11 | 21.3 | 63 | 32 (77%) |
| PLU_04 | 12 | 23.7 | 67 | 25 (74%) |
| PLU_05 | 24 | 47.6 | 155 | 40 (86%) |
| MIN_01 | 16 | 31.5 | 96 | 30 (80%) |
| MIN_02 | 12 | 22.9 | 64 | 27 (81%) |
| MIN_03 | 13 | 25.5 | 101 | 29 (77%) |
| MIN_04 | 9 | 18 | 84 | 15 (69%) |
| MIN_05 | 20 | 39 | 160 | 47 (81%) |

| TRANSECT | IMAGES | AREA (m ²) | XENOPHYOPHORES (n) | METAZOANS ON NODULES (n) |
|--------------|------------|------------------------|--------------------|--------------------------|
| CNT_01 | 15 | 32.4 | 155 | 14 (60%) |
| CNT_02 | 9 | 17.6 | 94 | 20 (62%) |
| CNT_03 | 19 | 38.6 | 191 | 34 (79%) |
| CNT_04 | 12 | 24.5 | 117 | 25 (68%) |
| CNT_05 | 22 | 45.9 | 229 | 53 (77%) |
| PRZ_01 | 11 | 23.2 | 108 | 27 (26%) |
| PRZ_02 | 14 | 29.7 | 162 | 38 (47%) |
| PRZ_03 | 19 | 41.8 | 259 | 34 (72%) |
| PRZ_04 | 8 | 17.3 | 101 | 18 (90%) |
| PRZ_05 | 16 | 32.6 | 200 | 31 (74%) |
| Total | 295 | 597.4 | 2657 | 605 (72%) |

Figure 6-2 Examples of metazoan megafauna morphotypes from the Ocean Infinity encountered during preliminary assessment of seabed images at NORI-D.



A) Anemone. Actiniaria mtp 75; B) Sponge *Hyalonema (Corynonema) depressum* sp. inc.; C) Black coral *Alternatipathes* sp. indet.; D) From left to right: sponge Porifera mtp 33; sponge *Holascus taraxacum* sp. inc.; E) Shrimp *Cerataspis monstrosus* sp. inc.; F) Top to bottom; sponge *Hyalonema (Onconema) clarioni* sp. inc.; (on stalk) brisingid *Freyastera* sp. indet.; G) Holothurian *Paelopatides* sp. indet.. mtp 1; H) Left to right: brittle star. Ophiuroidea indet.; barnacle *Catherinum* sp. indet.; sponge *Cladorhiza* sp. indet.; sponge *Hyalonema (Corynonema) tylostylum* sp. inc.; I) Holothurian *Synallactes* sp. indet. mtp 2.; J) Nudibranch *Bathydoris* sp. indet.; K) Anemone. Actiniaria mtp 4; L) Sponge *Docosaccus maculatus* sp. inc.

Figure 6-3 Variations in (A) megafaunal and (B) xenophyophore test density across different study areas surveyed at NORI-D.

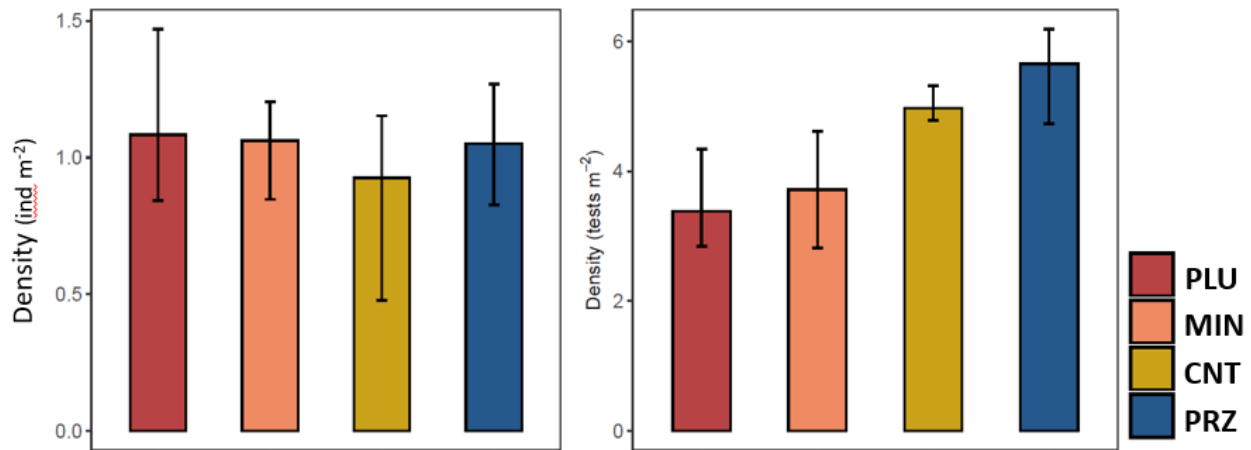
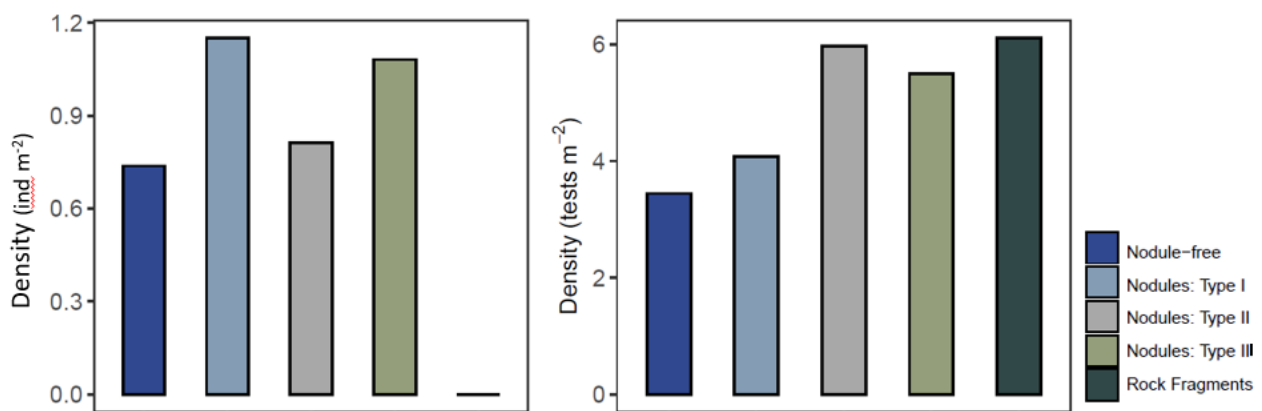


Figure 6-4 Variations in (A) megafaunal and (B) xenophyophore test density across different seabed types surveyed at NORI-D. Note that sample sizes surveyed in each of these seabed types were not equivalent. (see Section 5.17 for a description of sea bed types).



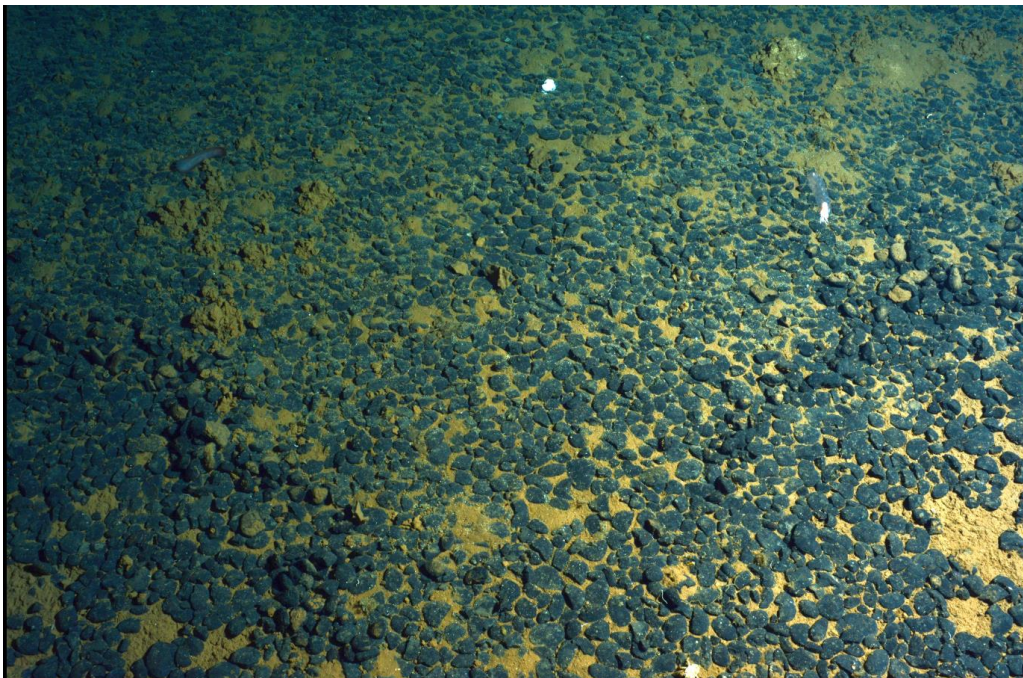
Only direct comparisons of faunal density were drawn between different study areas, as the sample size assessed per site was so far insufficient for quantitative assessment of diversity and community composition traits (see e.g., minimum sample size requirements for CCZ megafauna; Simon-Lledó *et al* 2019a; Ardron *et al* 2019). No notable variations in metazoan density were observed between the four study areas (Figure 6-3). Metazoan megafauna density was relatively homogenous across NORI-D, ranging between 0.93 – 1.08 specimens per meter square of seabed (Figure 6-3). In contrast, substantially different xenophyophore test densities were found between study areas (Figure 6-3), as significantly higher densities of these thecae were found at the PRZ site (mean: 5.6 tests m⁻²) compared to MIN (mean: 3.7 tests m⁻²) and PLU (mean: 3.4 tests m⁻²) sites. As expected from other CCZ studies, nodule-free areas at NORI-D appeared to harbour a lower megafaunal density, both in metazoan megafauna and xenophyophore test occurrence (Figure 6-4).

Quantitative analyses of the megafauna in the ROV images from Campaign 5E are currently ongoing, but preliminary assessments reveal the quality of the images are more than sufficient for megafaunal (> 2 cm) identifications (see Figure 6-5 for examples).

Figure 6-5 Examples of metazoan megafauna morphotypes from the Campaign 5E encountered during preliminary assessment of seabed images at NORI-D⁶.



Figure 6-6 Image of the seabed during the long-term lander deployment (date: 11/06/21)



⁶ Codes in CCZ standardised megafauna catalogue: a) HOL_008. b) ACT_010. c) HEX_019. d) ACT_075. e) HOL_041. f) ALC_004. g) COR_XX. h) DEC_001. i) AST_002.

The lander was deployed on 31 May 2021 during Campaign 5A and retrieved on 17 November 2021 during Campaign 5E. A total of 1019 images were collected by the camera; however, the seabed was only visible in a total of 543 images (before the strobe battery ran out), between the 31/05/2021 and the 20/08/2021. An example (auto colour adjusted) image is provided in Figure 6-6. Time-lapse images from the reference moorings are awaiting re-analysis in-line with ongoing studies.

6.3.2 Scavenging Megafauna

In abyssal regions, the vast majority of the top predators, including large mobile fishes, shrimps and amphipods, are also scavengers (Drazen *et al.* 2008). Predators and scavengers can have important influences on deep-sea ecosystems, controlling prey biomass, redistributing organic material, exerting selective pressures, and altering the behaviour and habitat choices of potential prey (Sweetman *et al.* 2014). Few data exist for scavenger biodiversity and community structure in the CCZ; data have been collected in just 4 studies using baited-camera landers, fish traps and ROV footage in the western APEIs (1, 4 and 7); Singapore (OMS – Ocean Minerals Singapore); United Kingdom (UK1) and; German (BGR – The Federal Institute for Geosciences and Natural Resources) licence areas (Amon *et al.* 2016; Harbour *et al.* 2020; Leitner *et al.* 2017).

A relatively high diversity of bait-attending scavengers has been observed in the BGR (Harbour *et al.* 2020) and UK1 and OMS contract areas (Leitner *et al.* 2017) however, community structure between these contract areas has been shown to be significantly different (Harbour *et al.* 2020).

Meta-analysis by Drazen *et al.* (2021) reveals that CCZ communities are different to other communities elsewhere in the abyssal Pacific. Given that most fishes and scavengers tend to have very large ranges, these differences were attributed to varying abundances of species, rather than species presence/absence. Seamounts have also been shown to have significantly different scavenger communities than neighboring abyssal plains. thereby contributing to regional diversity (Drazen *et al.* (2021) and Leitner *et al.* (2020).

6.3.2.1 Purpose & scope

The following section describes the work conducted between 2020-2021 by Heriot-Watt University to characterise natural baseline conditions in scavenger communities in the NORI-D contract area. The scope, the survey planning and the sampling methodologies carried out to ecologically characterise scavenging communities align with International Seabed Authority ISBA/25/LTC/6 Rev 1. Annex 1 section 41(g) Biological communities: Demersal fishes and scavengers to provide baseline data requirements under Recommendations III.A.13; III.B.14; III.B.15.(d) Results obtained from preliminary assessments of seabed image data conducted during Year 1 of the project are provided here.

6.3.2.2 Baseline investigations

The methods and proposed survey array for both the Collector Test and long-term environmental studies on NORI-D will provide data to meet the following objectives:

1. Establish the baseline predator and scavenger assemblage (diversity and relative abundance) in NORI-D and determine baseline scavenging rates.
2. Examine how scavenging fauna changes with environmental parameters within NORI-D and determine relationships to seafloor geology (e.g., presence of seamounts. nodule abundance, etc.)
3. Examine how scavenging biodiversity and activity changes inter-annually within the NORI-D.
4. Compare the baseline scavenger diversity, sediment physical and benthic biogeochemical/ ecological function parameters following the Collector Test.

6.3.2.3 Campaign activities

During Campaign 5D and 5E, lander deployments were conducted opportunistically amid other operations throughout benthic and ROV campaigns. Deployments were spread geographically to measure depth and spatial variability (Figure 6-1).

(a) Campaign 5D

During Campaign 5D, the lander was deployed 7 times in the CTA and 3 times at the PRZ of the NORI-D contract area (Table 6-8). Each lander deployment lasted approx. 24 hrs at the seafloor.

Pacific mackerel (*Scomber japonicus*) was used as bait to attract scavengers. Approximately 2 kg of bait was attached using cable ties to a bait plate suspended between the legs of the lander. The bait was weighed before and after deployment so that a consumption rate could be calculated.

Table 6-8 Baited camera deployments at NORI-D during Campaign 5D (data in WGS 1984 coordinate system)

| DEPLOYMENT | AREA | LATITUDE (deg) | LONGITUDE (deg) | DEPTH (m) |
|------------|------|----------------|-----------------|-----------|
| AKS266 | CTA | 10.3303 | -117.1829 | 4283 |
| AKS270 | CTA | 10.3359 | -117.1744 | 4285 |
| AKS272 | CTA | 10.3786 | -117.1477 | 4304 |
| AKS274 | CTA | 10.3748 | -117.1489 | 4308 |
| AKS275 | CTA | 10.3778 | -177.1472 | 4310 |
| AKS277 | CTA | 10.3337 | -117.1741 | 4287 |
| AKS278 | CTA | 10.3303 | -117.1829 | 4283 |
| AKS280 | PRZ | 10.9188 | -116.2178 | 4301 |
| AKS283 | PRZ | 10.8537 | -116.1528 | 4122 |
| AKS285 | PRZ | 10.9280 | -116.2618 | 4257 |

After recovery of the lander following each deployment, the images were downloaded from the camera to hard drives, and current meter data was downloaded from the Aquadopp ADCP. Any remaining bait was also removed and weighed so a scavenger rate could be calculated.

For each photograph, the maximum number of animals of a specific species were counted (MaxN), along with their time of first arrival (Tarr). Animals were identified based on their morphology to the lowest taxonomic level possible. To estimate the absolute abundance of *Coryphaenoides* sp. in the NORI-D region, the “Time of first arrival” model by Priede and Merrett (1996) was used. This model uses the time of first arrival (Tarr), the average current velocity (V_w) recorded by Anonyx’s in situ ADCP, and the average swimming speed of *Coryphaenoides* sp. (V_f). (0.072 m s^{-1}) (Leitner *et al.* 2017), to infer absolute abundances of *Coryphaenoides* sp. assuming an even distribution of fish.

(b) Campaign 5E

Campaign 5E was completed on 21/12/2021, preliminary data are not yet available. See Figure 6-1 for deployment locations.

6.3.2.4 Preliminary results & discussion

Fifteen bait-attending fauna were identified over 10 deployments (Table 6-9; Figure 6-8) similar to those numbers reported by Harbour *et al.* 2020; Leitner *et al.* 2017). The most abundant were the rattail *Coryphaenoides* sp. with a mean MaxN of 5 ± 0.6 (SE $n = 10$) (Table 6-9). The next most abundant species were the cusk eel *Barathrites iris* and the eelpout *Pachycara nazca* with mean MaxN’s of 6 ± 0.7 SE and 6 ± 0.6 (SE $n = 10$), respectively (Table 6-9). The large Aristeidae shrimp, *Cerataspis monstrosus* had a mean MaxN of 2 ± 0.2 (SE $n = 10$), and the Solenoceridae shrimp *Hymenopenaeus nereus* 2 ± 0.3

(SE $n = 10$) (Table 6-9). The mean Simpson's Diversity Index ($1-\lambda$) for the NORI-D licence area was 0.80 ± 0.1 (SE $n = 10$)

Table 6-9 MaxN of the species observed during each deployment NORI-D from Campaign 5D

| DEPLOYMENT | AREA | <i>Coryphaenoides</i> sp. | <i>Barathrites iris</i> | <i>Pachycara nazca</i> | <i>Bassozetus</i> sp. | <i>Bathyonus caudalis</i> | <i>Cerataspis monstrosus</i> | <i>Hymenopenaeus naealis</i> | Small shrimp 2 | <i>Eurythenes</i> sp. 1 | <i>Eurythenes</i> sp. 2 | <i>Mundulopsis</i> sp. | <i>Bassozetus</i> juvenile | <i>Ilyophis anyx</i> | Holothuroid 1 | Holothuroid 2 | GRAND TOTAL | |
|-------------------|------|---------------------------|-------------------------|------------------------|-----------------------|---------------------------|------------------------------|------------------------------|----------------|-------------------------|-------------------------|------------------------|----------------------------|----------------------|---------------|---------------|-------------|----|
| AKS266 | CTA | 5 | 3 | 3 | 2 | 0 | 2 | 1 | 0 | 0 | 0 | 0 | 0 | 0 | 0 | 0 | 0 | 16 |
| AKS270 | CTA | 3 | 2 | 2 | 1 | 0 | 2 | 1 | 0 | 0 | 0 | 0 | 1 | 0 | 0 | 0 | 0 | 12 |
| AKS272 | CTA | 4 | 2 | 0 | 0 | 0 | 2 | 1 | 1 | 1 | 0 | 0 | 0 | 0 | 1 | 0 | 0 | 12 |
| AKS274 | CTA | 4 | 3 | 5 | 1 | 0 | 2 | 2 | 1 | 0 | 0 | 0 | 0 | 0 | 0 | 0 | 0 | 18 |
| AKS275 | CTA | 5 | 1 | 1 | 1 | 0 | 3 | 1 | 0 | 0 | 0 | 0 | 0 | 0 | 0 | 0 | 0 | 12 |
| AKS277 | CTA | 6 | 4 | 3 | 0 | 0 | 2 | 0 | 0 | 0 | 0 | 0 | 0 | 1 | 0 | 0 | 0 | 16 |
| AKS278 | CTA | 3 | 1 | 4 | 1 | 1 | 3 | 2 | 0 | 1 | 1 | 0 | 0 | 0 | 1 | 0 | 0 | 18 |
| AKS280 | PRZ | 7 | 3 | 2 | 2 | 0 | 2 | 4 | 0 | 0 | 1 | 0 | 0 | 0 | 0 | 0 | 0 | 21 |
| AKS283 | PRZ | 8 | 8 | 7 | 1 | 0 | 2 | 1 | 0 | 1 | 0 | 1 | 0 | 0 | 0 | 0 | 1 | 30 |
| AKS285 | PRZ | 2 | 1 | 4 | 1 | 0 | 1 | 2 | 0 | 2 | 0 | 0 | 0 | 0 | 0 | 0 | 0 | 13 |
| Total MaxN | | 47 | 28 | 31 | 10 | 1 | 21 | 15 | 2 | 5 | 2 | 1 | 1 | 1 | 2 | 1 | 168 | |

Figure 6-7 Mean species accumulation curve for the NORI-D licence area ($n = 10$) generated from 9.999 permutations.

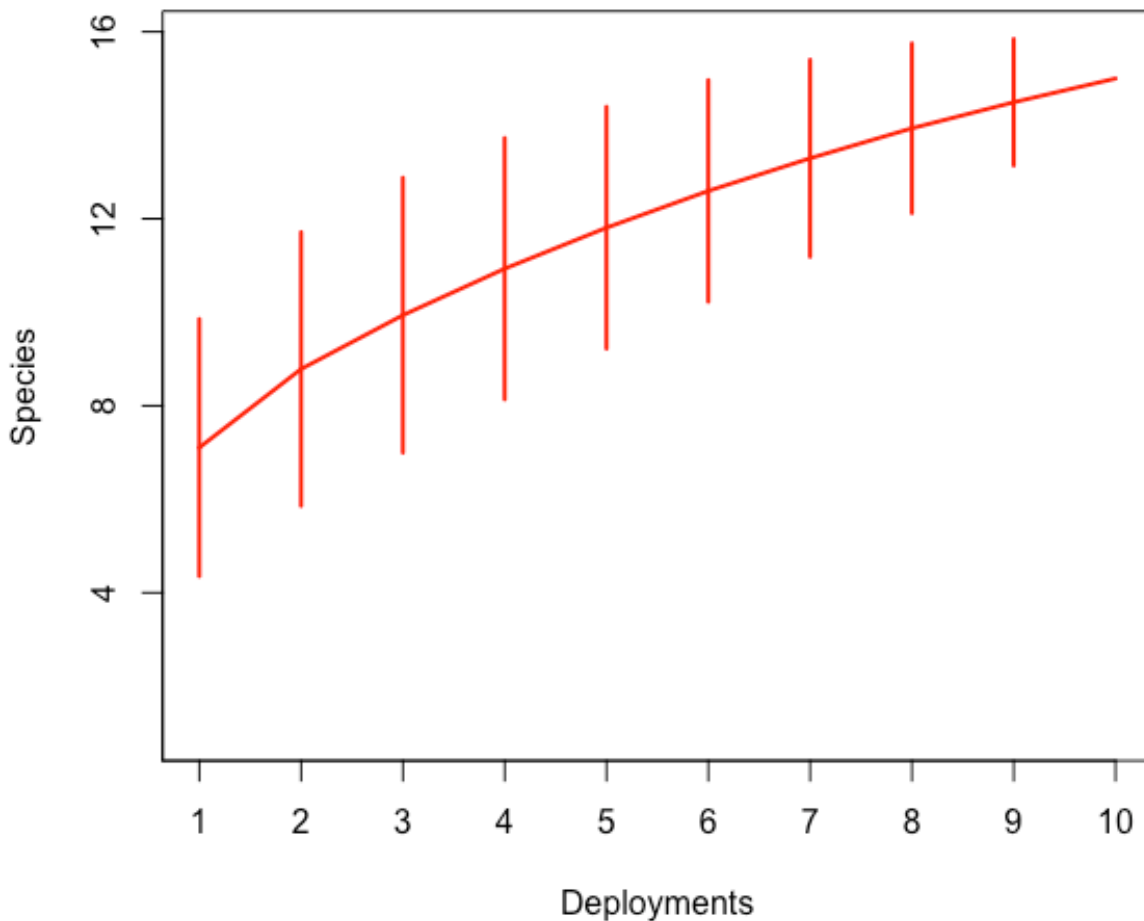
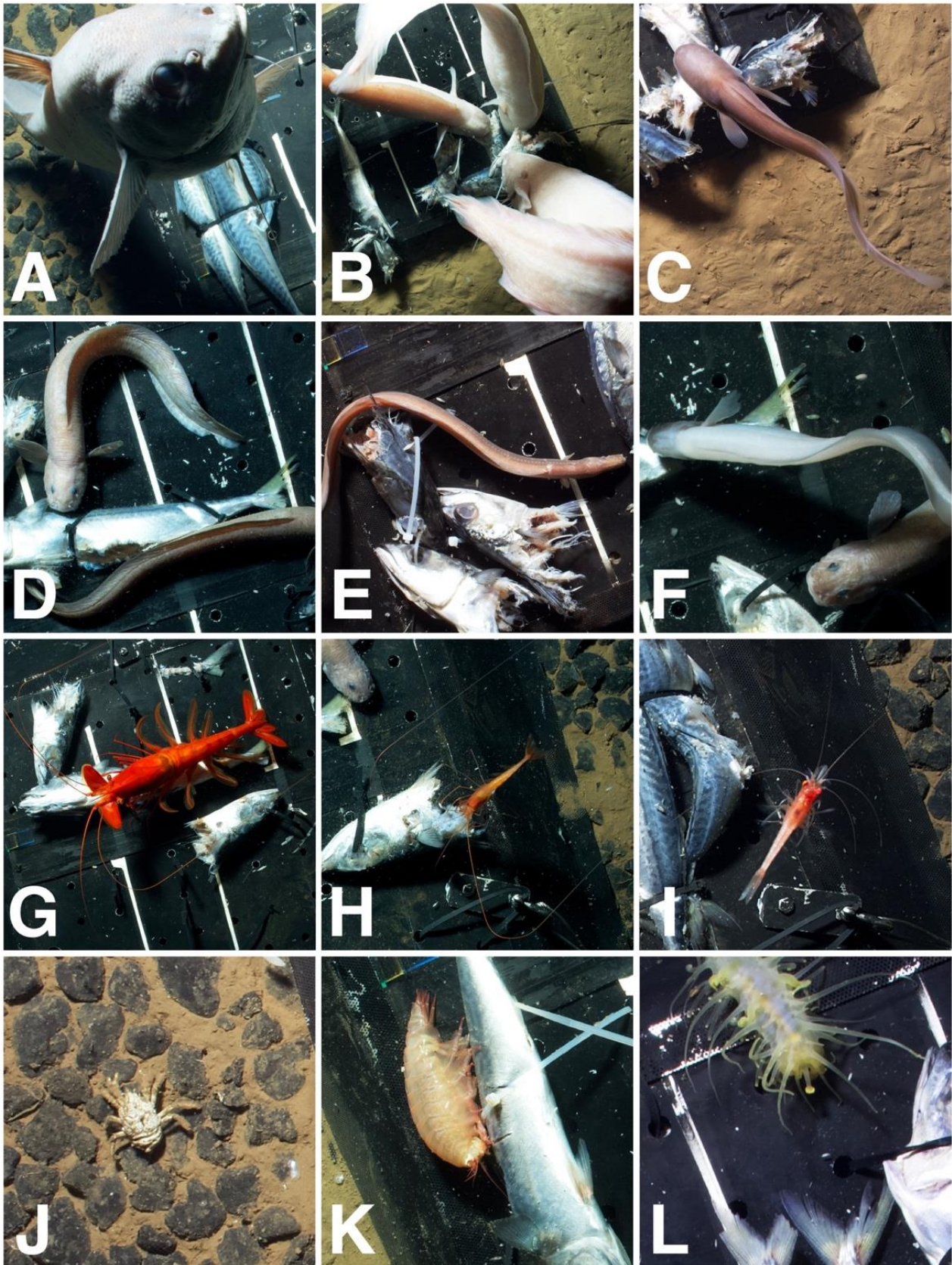


Figure 6-8. Commonly observed scavengers in the NORI-D licence are of the CCZ.



(A) *Coryphaenoides* sp. (B) *Barathrites iris* (n = 3) (C) *Bassozetus* sp. (D) *Pachycara nazca* (n = 2) (E) *Ilyophis aryx* (F) *Bassozetus* sp. juvenile (top) and *Pachycara nazca* (bottom) (G) *Cerataspis monstrosus* (H) *Hymenopenaeus nereus* (J) *Munidopsis* sp. (K) *Eurythenes* sp. (L) *Holothuridea*

After 10 baited camera deployments the species accumulation curve for NORI-D had not reached an asymptote (Figure 6-7). Further sampling has been completed November 2021 during Campaign 5E and based on a power analysis carried out by Harbour *et al.* (2020), this should be sufficient to gain a more complete picture of scavenger species richness in this region.

Using the Priede and Merrett (1996) model, estimates of *Coryphaenoides* sp. in the NORI-D licence area ranged from 9–782 fish km⁻¹, with a mean abundance of 221 ± 82.20 (SE n = 10) (Table 6-10).

Patterns of succession in terms of scavenger arrival times were seen in three out of the top five scavengers. *Coryphaenoides* sp. were usually first to arrive, with a mean Tarr of 45 ± 9 mins (SE n = 10) (Figure 6-9). The large shrimp *Cerataspis monstrosus* had a mean Tarr of 112 ± 27 mins (SE n = 10) but the smaller *Hymenopenaeus nereus* were generally much later to arrive (mean Tarr 464 ± 135 mins SE n = 10) (Figure 6-9), which seemed to be related to lower abundances of larger predators by this stage in the deployment. Similarly, *Pachycara nazca* were also late to arrive with a mean Tarr 572 ± 79 mins (SE n = 10), but the same individuals tended to stay on the bait plate for the remainder of the deployment (Figure 6-9).

Table 6-10 The absolute abundance of *Coryphaenoides* sp. (fish km⁻¹) in NORI-D. calculated using the Priede and Merrett (1996) time of first arrival model.

| DEPLOYMENT | AREA | TIME OF ARRIVAL (mins) | MEAN SPEED (ms ⁻¹) | ABUNDANCE (km ⁻²) |
|------------|------|------------------------|--------------------------------|-------------------------------|
| AKS266 | CTA | 98 | 0.012 | 112 |
| AKS270 | CTA | 16 | 0.044 | 562 |
| AKS272 | CTA | 22 | 0.048 | 264 |
| AKS274 | CTA | 20 | 0.179 | 101 |
| AKS275 | CTA | 46 | 0.057 | 50 |
| AKS277 | CTA | 82 | 0.097 | 9 |
| AKS278 | CTA | 22 | 0.048 | 266 |
| AKS280 | PRZ | 24 | 0.020 | 782 |
| AKS283 | PRZ | 74 | 0.049 | 23 |
| AKS285 | PRZ | 44 | 0.103 | 31 |

A considerable amount of bait was consumed during 10 deployments. In most deployments just the heads of the bait fish were left, and in other cases, the bait was hollowed out by amphipod feeding activity. The mean scavenging rate in NORI-D (1687.68 ± 138.27 SE. n = 10) was significantly higher than in the BGR licence area (878.4 g d⁻¹ ± 113.61 SE n = 9) (independent samples t-test, p < 0.0001). The mean current speed calculated from measurements taken by the ADCP during the deployments was 0.051 m s⁻¹ ± 0.0009 (SE n = 10) (Figure 6-10).

Figure 6-9 The 5 most observed species in the NORI-D licence area plotted by their appearance; data generated using mean MaxN values across 10 deployments. Shaded areas represent $\pm 95\%$ confidence intervals.

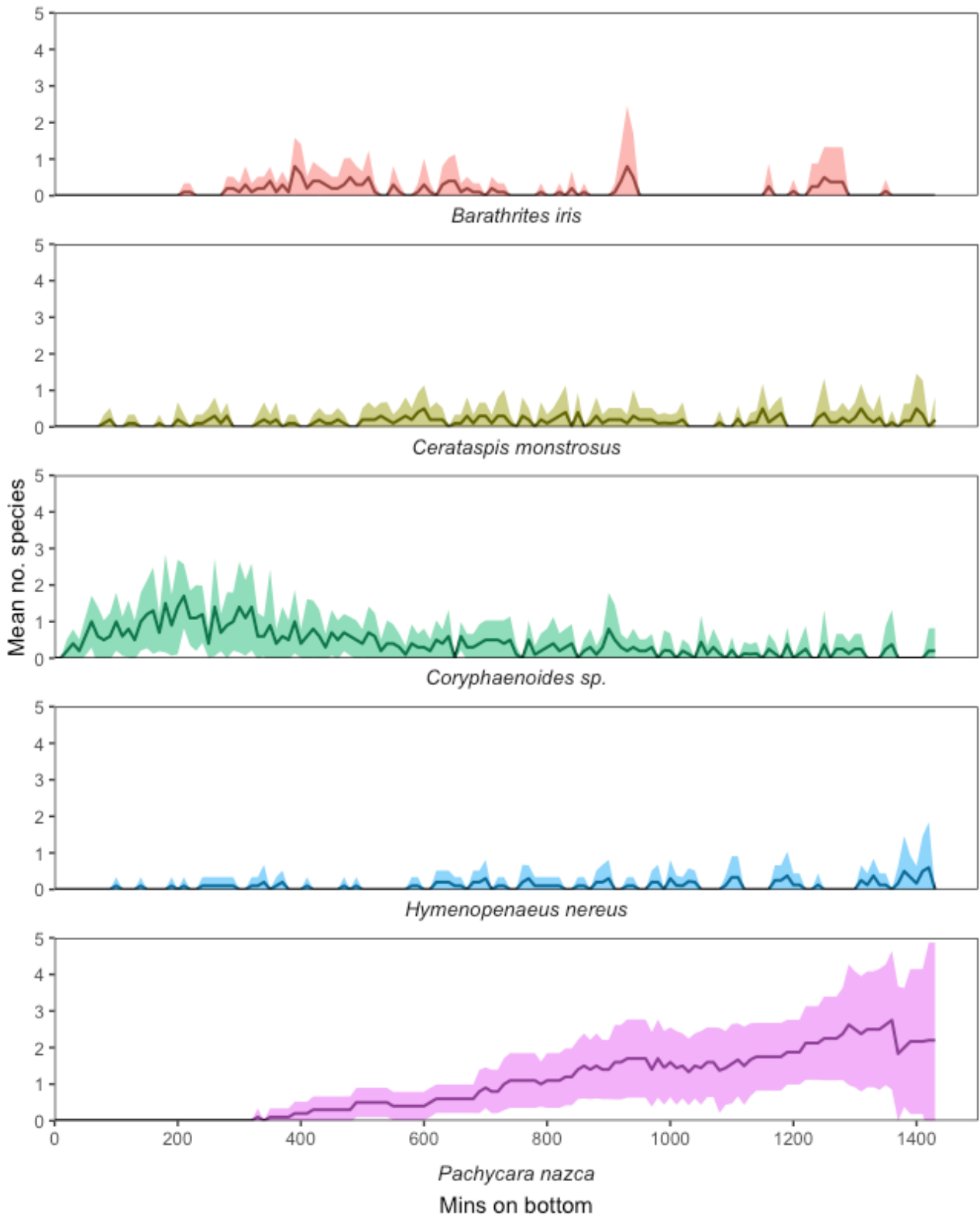
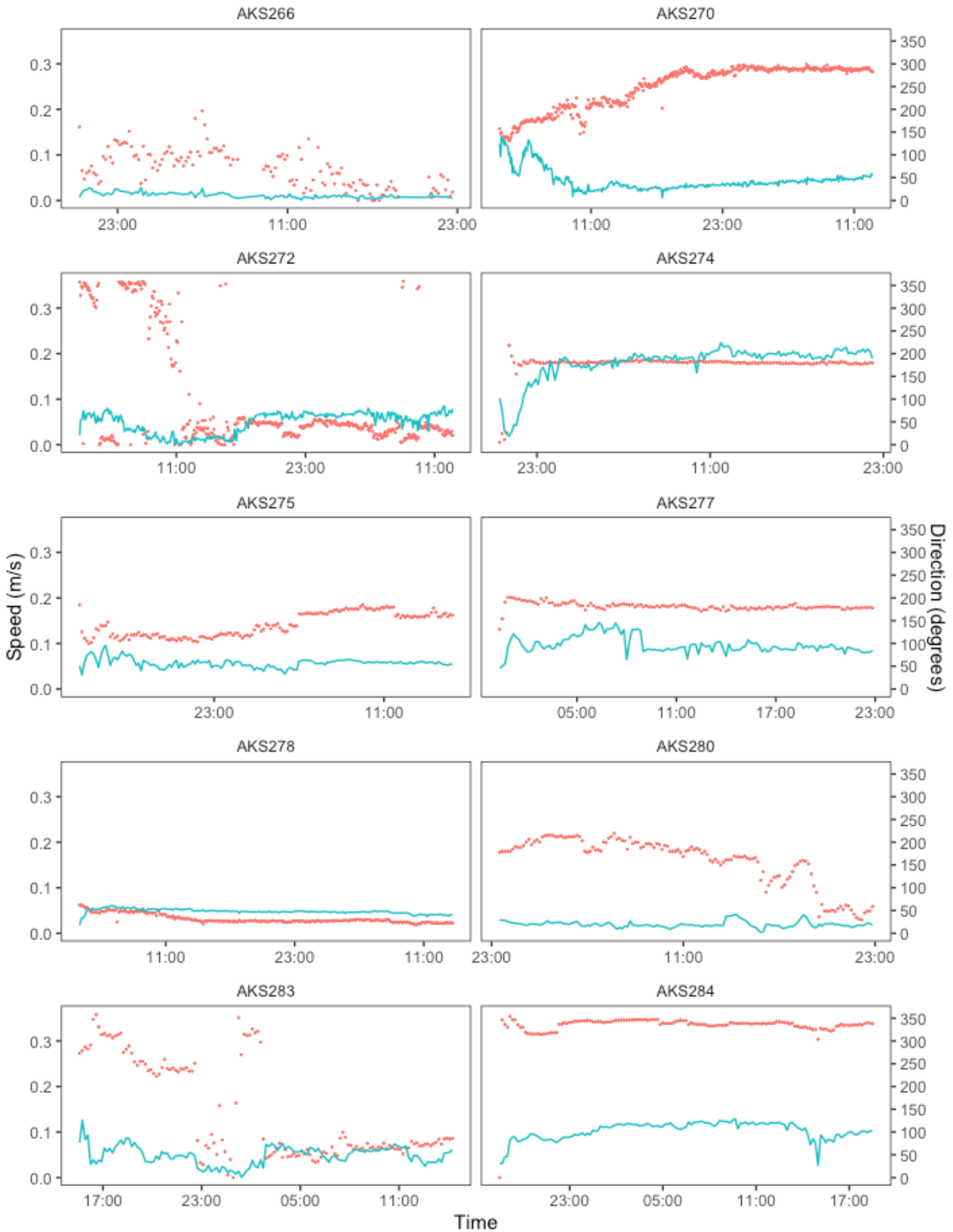


Figure 6-10 Current speed (m/s. blue line) and current direction (degrees. red points) measured by an Aquadopp 6000 ADCP attached to the Anonyx baited-camera lander during 10 deployments in May / June 2021.



6.3.3 Macrofauna

Owing to the commencement of the NOAA and later, Scripps Institution of Oceanography, organised surveys in the 1970s and 1980s (Hecker & Paul, 1977; Spiess *et al.* 1987), there is a relatively long history of careful quantitative sampling of metazoan infauna using boxcores in the CCZ. Macrofaunal abundance measured using the methods developed by Robert Hessler, who pioneered the use of the USNEL Spade Box Core for abyssal studies (Hessler & Jumars, 1974; reviewed by Glover *et al.* 2016) can therefore provide a useful benchmark for monitoring and is probably the least controversial or complex of CCZ baseline biological measurements.

Macrofauna (considered to be animals retained on 250 µm - 300 µm sieves) are primarily sediment-dwelling, with communities from the CCZ numerically dominated by polychaete worms and crustaceans (including Tanaidacea, and Isopoda) (Borowski & Thiel 1998; De Smet *et al.* 2017; Wilson 2017; Francesca *et al.* 2021; Washburn *et al.* 2021).

Most macrofaunal abundance is found at the sediment–water interface with abundance, diversity and community structure varying across the CCZ in response to variations in particulate organic carbon (POC) flux, variations in sediment characteristics and nodule abundance (De Smet *et al.* 2017; Washburn *et al.* 2021; Chuar *et al.* 2020; Wilson 2017). At local scales, however, (e.g., within contract areas; GSR), there is no significant difference in the community composition of the soft sediment macrofauna in relation to the presence/absence of nodules (Francesca *et al.* 2021) and some known common macrofaunal species have shown to have spatial ranges from hundreds to thousands of kilometres across the CCZ (Washburn *et al.* 2021; Wilson 2017; Brix *et al.* (2020); Taboada *et al.* (2018)).

6.3.3.1 Purpose & scope

The following section describes the work conducted between 2020-2021 by the Natural History Museum (NHM) and the University of Gothenburg (UoG) and the National Oceanographic Centre (NOC) to characterise natural baseline conditions in macrofaunal communities in the NORI-D contract area. The scope, the survey planning and the sampling methodologies carried out to ecologically characterise seabed macrofaunal communities align with International Seabed Authority ISBA/25/LTC/6 Rev 1. Annex 1 section 41(b) Biological communities: Macrofauna. to provide baseline data requirements under Recommendations III.A.13; III.B.14; III.B.15.(d).(i)–(ii); IV.B.22. Results obtained from preliminary assessments of box core analysis conducted during Year 1 of the project are provided here.

6.3.3.2 Baseline investigations

The methods and proposed survey array for both the Collector Test and long-term environmental studies on NORI-D will provide data to meet the following objectives:

- Establish the biodiversity in terms of species richness estimators in the NORI-D sampled regions.
- Compare the baseline diversity in impacted areas (e.g., the IRZ) to reference sites (e.g., the PRZ, other control sites, APEIs and other abyssal locations).
- Compare the regional distribution patterns (species ranges and biogeographic patterns confirmed with DNA analysis) of fauna in impacted sites to other areas in the CCZ and globally.
- For taxa that are present in more than one site, and in sufficient numbers to enable analysis, determine the degrees of population connectivity as measured using population genetic methods (e.g., analyses of haplotype diversity, frequencies and distribution), and discern any demographic patterns such as the stability of populations.
- Determine the abundance, community composition and diversity of metazoan sessile nodule fauna (macrofauna and megafauna) and examine variation across the sampled sites.

- Determine the abundance, community composition and diversity of metazoan macrofauna within quantitative samples taken with replicate box cores from within three sample strata (including PRZ and CTA) in the NORI-D contract area, and examine temporal and spatial variation.

In addition to addressing these questions, the Natural History Museum (NHM) and the University of Gothenburg (UoG) team will also undertake integrative DNA taxonomy on new species recovered from the sampling, directly benefiting the iterative development of knowledge of not only NORI-D but the wider CCZ.

6.3.3.3 Campaign activities

(a) Survey design & site selection

For Campaign 5A, box core locations were selected to represent the diversity of geoform and substrate types across NORI-D including sufficient replication within the CTA and PRZ (Figure 6-11A). For post-Collector Test and long-term monitoring studies, replication within the Level 2/3 “Flatter area” geoform with Type I nodule facies is critical to the BACI design to ensure statistical robustness. As such, a randomized stratified survey design (*sensu* Etter, 2002) was employed during Campaign 5D to ensure sufficient replication on both spatial and temporal scales within the CTA (Figure 6-11B). Replicates for temporal variation were also conducted within the PRZ (Figure 6-11C).

(b) Campaign 5A & Campaign 5D

Launch and recovery of the box core was the responsibility of the Maersk crew. The macrofauna team followed established DNA-taxonomy protocols (Glover *et al.* 2016) for the collection of box core samples and data at-sea. Once the box core was secured on deck, the temperature of top water was measured, a downward-facing image of the box core was taken with top water intact, the top water was siphoned off, and a further image was taken with top water removed (Figure 6-12). The box core sample quality was assessed based on whether the top water was retained and the sediment surface undisturbed, both which had to be met in order for the sample to be accepted for quantitative work.

During Campaigns 5A and 5D, all planned deliverables were met, and additional tasks carried out including opportunistic sampling of macrofauna from cores recovered by the multicore. All box core samples recovered by the team (C5A n=53; C5D n=35) were examined by the onboard macrofauna team and samples taken for future environmental baseline analyses.

Following recovery and quality assessment, quantitative box cores (C5A n=48; C5D n=30) were sampled quantitatively for megafauna, nodule fauna, and macrofauna, with a live-sort of a 15x15cm² subsample (sampled at 0-2cm and 2-5cm depth layers). All remaining sediment was sieved on 300micron sieves sliced in 0-2cm, 2-5cm and 5-10cm layers and the residue retained on 300micron sieves bulk fixed in non-denatured ethanol. In the live-sorting process, all specimens were imaged, and preliminary identifications were given, with most specimens individually preserved in 80% ethanol in barcoded sample jars or tubes linked to a database. Sediment residues from the 15x15cm² live-sort were returned to respective bulk-fixed depth layers following the removal and processing of animals.

Box core sampling was considered highly successful. For Campaign 5A, of the 53 box cores examined (out of n=57 due to four failed deployments); 48 were processed for full quantitative sampling and five for live-sort sampling only. For Campaign 5D of the 35 box cores examined, 30 were processed for full quantitative sampling and five for live-sort sampling only. Additional macrofaunal samples were collected from all other gears onboard.

Figure 6-11. A) Overview of box-core operations within NORI-D; B) Collector Test Area (CTA); C) Preservation Reference Zone (PRZ)

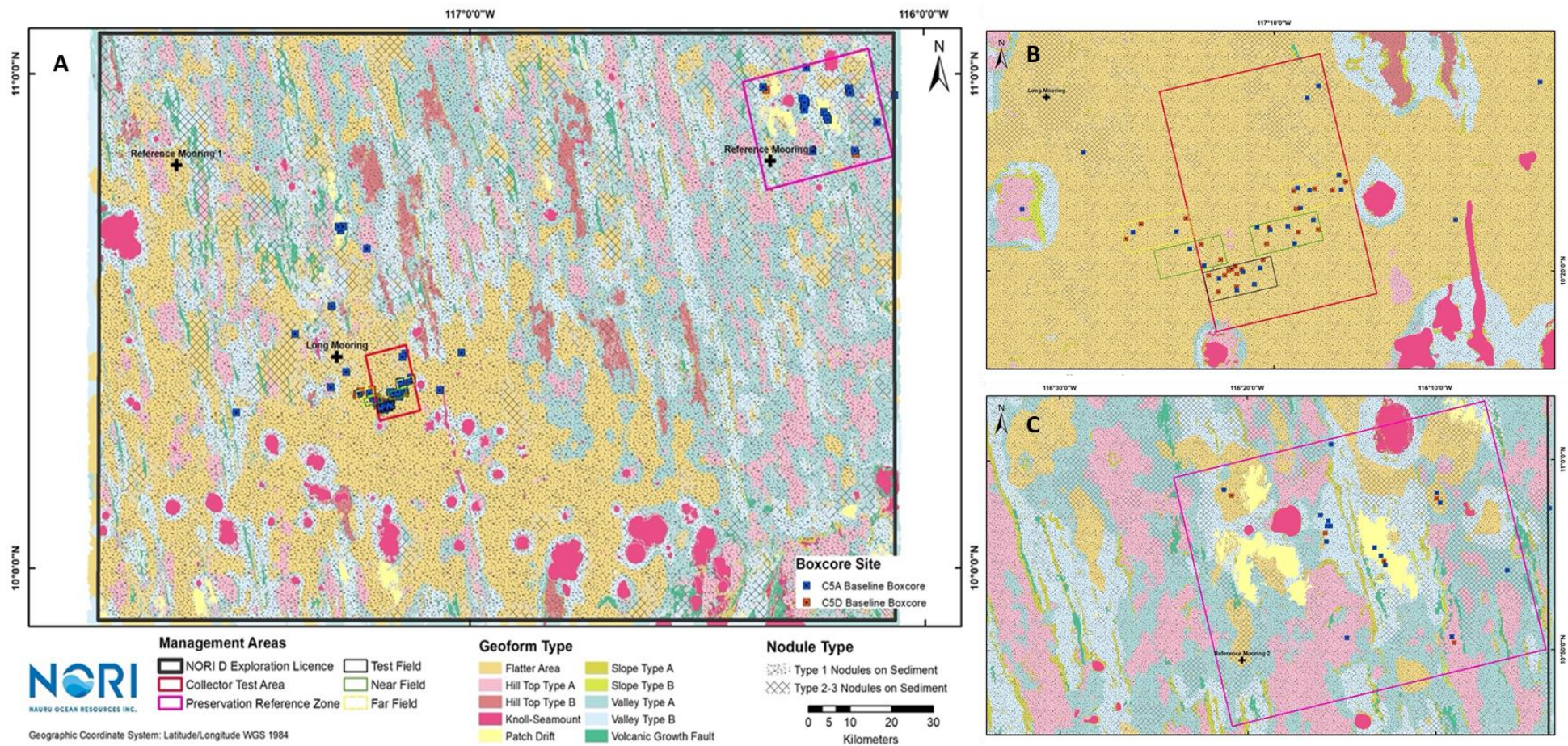


Figure 6-12 Images of box cores after the topwater was siphoned out.

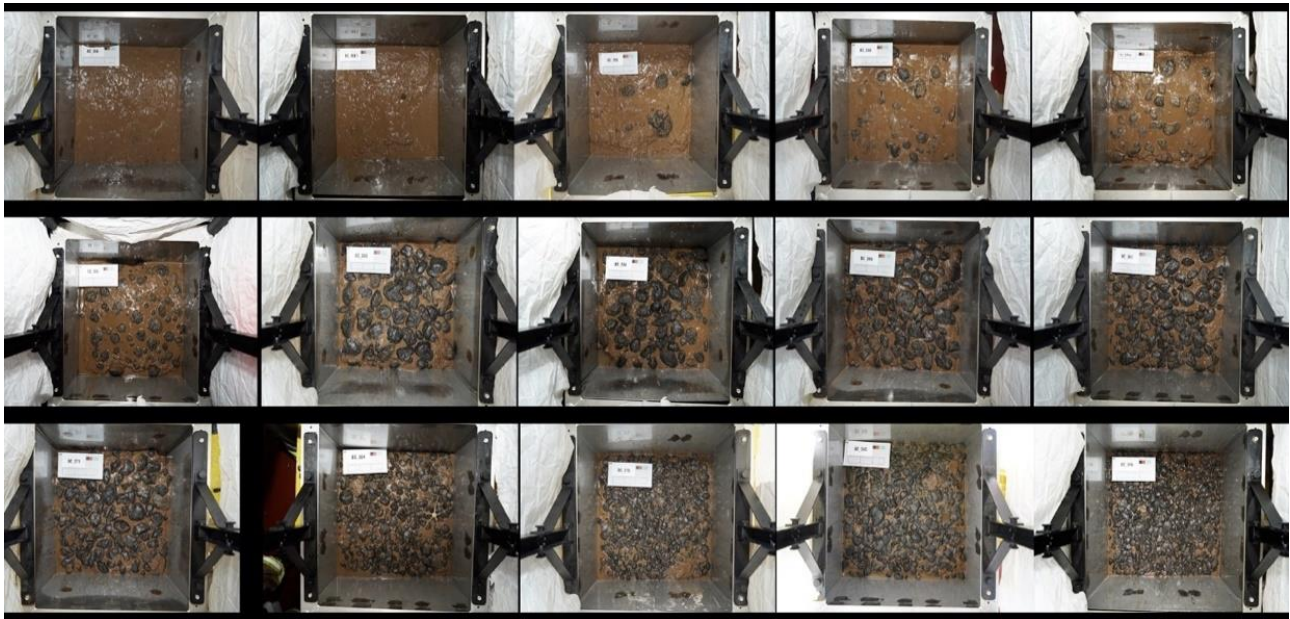


Image credit: C Dalglish and T Adamson

6.3.3.4 Preliminary results & discussion

Preliminary identifications carried out at sea during the live-sorting of box core subsamples (Glover *et al.* 2016) facilitate initial at-sea analyses of both data and community structure.

(a) Campaign 5A

In total 4825 specimens were collected with the box core, and 71 with the multicore.

In total, 2100 preserved samples were collected, of which 145 were bulk fixed samples for quantitative analyses and 1955 live-sorted samples. Most live-sorted samples consisted of individually processed specimens with a preliminary taxonomic identification and imagery of key features. A total of 5533 images were taken of these specimens (e.g., Figure 6-13 & Figure 6-14).

Five Porifera specimens were subsampled in RNA later for further work by Dominique Anderson at Heriot-Watt University, Edinburgh, UK. Eleven specimens of Bryozoa, Cnidaria and Porifera were subsampled and frozen at -20°C for further work by Leeds University, UK.

(b) Campaign 5D

In total 3257 specimens were collected with the box core, 47 with the multicore, 18 with the Trap Lander, 11 with the Camera Lander, and one subsample from the Respirometer Lander.

In total, 2057 preserved samples were collected, of which 111 were bulk fixed samples for quantitative analyses and 1946 live-sorted samples. Most live-sorted samples consisted of individually processed specimens with a preliminary taxonomic identifications and imagery of key features. A total of 3995 images were taken of these specimens (e.g., Figure 6-13 & Figure 6-14).

Seven specimens of Bryozoa and Cnidaria were subsampled, and the subsamples were frozen at -20°C for further work by Leeds University, UK.

Figure 6-13 Images of the nodule fauna collected by the Macrofauna team taken with the Canon 100mm macrophotography workstation.

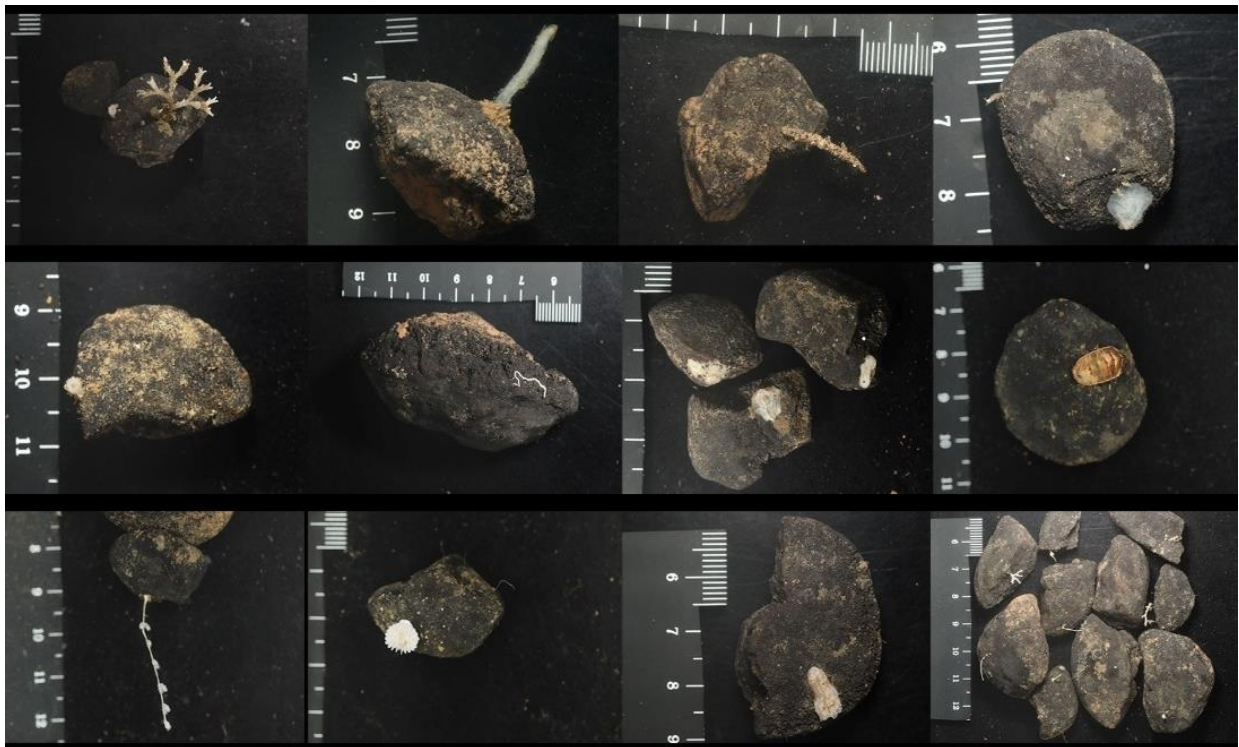


Image credit: H Wiklund, R Drennan, C Boolukos, G Bribiesca Contreras.

Figure 6-14 Images of the live-sorted macrofauna collected by the Macrofauna team taken with the Leica photomicroscopy workstation.



Image credit: H Wiklund, R Drennan, C Boolukos, G Bribiesca Contreras.

Table 6-11 Number of specimens collected during the Campaigns 5A and 5D by phylum, with details of number of individuals photographed, number of DNA extractions performed, and number of sequences generated to date.

| PHYLUM | # INDIVIDUALS | # PHOTOGRAPHED | # DNA EXTRACTIONS | # SEQUENCES |
|-----------------|---------------|----------------|-------------------|-------------|
| Annelida | 1978 | 1734 | 241 | 117 |
| Appendicularia | 1 | 1 | - | - |
| Arthropoda | 2450 | 2207 | 3 | 3 |
| Brachiopoda | 75 | 74 | 20 | 17 |
| Bryozoa | 1560 | 1557 | 17 | 10 |
| Chaetognatha | 24 | 22 | - | - |
| Chordata | 30 | 30 | - | - |
| Cnidaria | 764 | 764 | 41 | 81 |
| Ctenophora | 1 | 1 | - | - |
| Echinodermata | 110 | 105 | 80 | 51 |
| Metazoa indet. | 79 | 78 | 4 | 1 |
| Mollusca | 559 | 510 | 97 | 39 |
| Nematoda | 101 | 35 | - | - |
| Nemertea | 13 | 11 | - | - |
| Platyhelminthes | 2 | 2 | - | - |
| Porifera | 1033 | 1031 | 39 | 19 |
| Entoprocta | - | - | 3 | - |
| TOTAL | 8780 | 8162 | 545 | 338 |

Table 6-12 Number of individuals identified to species level, with details on the number of species per phylum and number of specimens identified from morphological and molecular data.

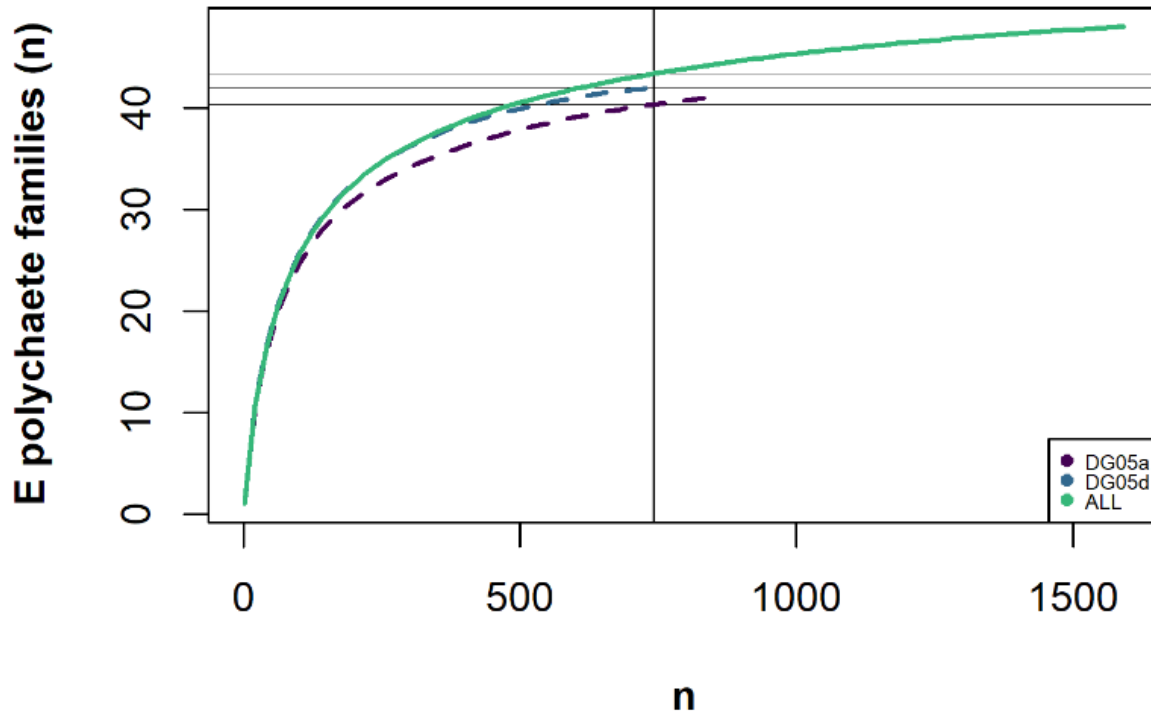
| PHYLUM | # INDIVIDUALS IDENTIFIED (molecular) | # INDIVIDUALS IDENTIFIED (morphology) | # INDIVIDUALS IDENTIFIED (total) | # SPECIES |
|---------------|--------------------------------------|---------------------------------------|----------------------------------|------------|
| Annelida | 93 | 0 | 93 | 57 |
| Arthropoda | 3 | 0 | 3 | 2 |
| Brachiopoda | 14 | 58 | 72 | 6 |
| Cnidaria | 28 | 4 | 32 | 9 |
| Echinodermata | 47 | 32 | 79 | 19 |
| Mollusca | 14 | 0 | 14 | 13 |
| TOTAL | 199 | 94 | 293 | 106 |

(c) DNA Taxonomy and Biodiversity

To date, DNA has been extracted from 545 specimens, from which 338 sequences have been generated (Table 6-11). So far, 293 specimens have been assigned to species based on genetic data (199) or morphological data (94; Table 6-12). These represent 106 species from 6 different Phyla (Cnidaria, Echinodermata, Annelida, Brachiopoda, Arthropoda, and Mollusca), with annelids representing the most diverse so far (57 species). Only 18 of those species represent described species, with the rest possibly representing new species.

Sampling effort was assessed via a rarefaction curve based only on polychaete samples that have been assigned to family level. As observed in Figure 6-15, the curves are plateauing, suggesting that most families of polychaetes found in the area have been collected, and hence we can expect most other taxa to be well represented in the samples.

Figure 6-15 Rarefaction curves of polychaete samples that have been assigned to families. x axis represents the number of individuals (n), and the y axis the number of polychaete families. Rarefaction curves for samples from both Campaigns 5A and 5D are indicated in dashed lines, with samples from both campaigns indicated in a straight line.



(d) Biogeographic patterns and species ranges

From the 106 species identified, only 18 represent described species. The remaining species represent undescribed species that, at this stage, are only comparable using genetic data. For the 103 delimited species for which we have generated genetic data, 47 have only been found at NORI-D, and 56 have been found in other areas (Table 6-13). Species with wide distributions such as *Bathyglycinde cf. profunda*, the cosmopolitan *Porcellanaster cereulus* and *Pelagodiscus atlanticus*, as well as the widespread *Styracaster paucispinus* and *Silax daleus* were also found within the NORI-D samples.

Table 6-13 Total number of specimens identified from genetic data in NORI-D, indicating whether they have been somewhere else or if they are unique to the site.

| PHYLUM | # TOTAL spp. | # UNIQUE NORI-D spp. | # KNOWN ELSEWHERE spp. |
|---------------|--------------|----------------------|------------------------|
| Annelida | 56 | 17 | 39 |
| Arthropoda | 2 | 1 | 1 |
| Brachiopoda | 4 | 0 | 4 |
| Cnidaria | 9 | 7 | 2 |
| Echinodermata | 18 | 12 | 6 |
| Mollusca | 14 | 10 | 4 |
| TOTAL | 103 | 47 | 56 |

(e) Genetic connectivity

Some taxa that have been found in other CCZ areas in high enough numbers to be useful for genetic connectivity analyses include several species of annelids, one sponge and one bivalve (Stewart *et al.* in prep). The molecular work on material from NORI-D is in progress, and so far, only one of the CCZ connectivity target taxa has been confirmed with sequences, the annelid species *Bathyglycinde cf. profunda*. Other taxa that have been documented in NORI-D based on morphology only are the bivalve *Nucula profundorum*, the annelid *Lumbrinerides cf. laubieri* and the sponge *Plenaster craigi*, but these samples have not been sequenced yet.

(f) Quantative nodule fauna assessment

Nodule fauna is an important component of the biodiversity of the CCZ and hence it is important to analyse this separately. At sea, all nodule fauna was photographed while still attached to the nodules, and images of detailed structures were also taken under the microscope. Both morphological and molecular work is still ongoing for these samples, but they are confidently identified to Phylum, and we present some preliminary results here.

A total of 2864 samples were included, representing all nodule-associated metazoans found in the 69 box cores taken at the six areas of interest (TF, Near Field East, Far Field East, Near Field West, Far Field West, and PRZ) during NORI-D Campaigns 5A and 5D. In average, the number of nodule-associated specimens found per box core ranged from 39.4 ± 15.6 to 44.7 ± 13 for the different areas (Table 6-14). Abundance is reported in Figure 6-16.

Table 6-14 Number of metazoans associated to nodules found in each box core during the NORI-D Campaigns 5A and 5D. The number of box cores taken at each area is also indicated, with mean number of individuals per box core and per m².

| AREA | # BOX CORES | # INDIVIDUALS | MEAN # INDIVIDUALS PER BOX CORE | MEAN # INDIVIDUALS PER m ² |
|-----------------|-------------|---------------|-----------------------------------|---------------------------------------|
| TF | 20 | 788 | 39.4 ± 15.6 | 157.6 ± 62.5 |
| Near field east | 11 | 491 | 44.6 ± 11.2 | 178.5 ± 44.9 |
| Far field east | 10 | 447 | 44.7 ± 13 | 178.8 ± 52 |
| Near field west | 5 | 213 | 42.6 ± 13.1 | 170.4 ± 52.3 |
| Far field west | 5 | 215 | 43 ± 14.2 | 172 ± 56.7 |
| PRZ | 18 | 710 | 39.4 ± 19.3 | 157.8 ± 77.3 |
| TOTAL | 69 | 2864 | 41.5 ± 15.2 | 166 ± 60.7 |

In addition to abundance being similar between regions, the relative abundance of different phyla seems consistent between sites (Figure 6-17). However, sponges (Porifera) represented nearly half of the samples collected in the PRZ, where annelid worms were less abundant than in the other areas. This is strongly suggestive that the PRZ is different in community composition to the other sites, not unexpected given the distances involved and observational reports from the Campaign field teams. Identification to species level is still ongoing, and these conclusions are preliminary.

Figure 6-16 Bar plot indicating mean number of nodule-associated individuals found per m² in each of the six areas sampled during the NORI-D Campaigns 5A and 5D. Standard deviation is indicated by error bars.

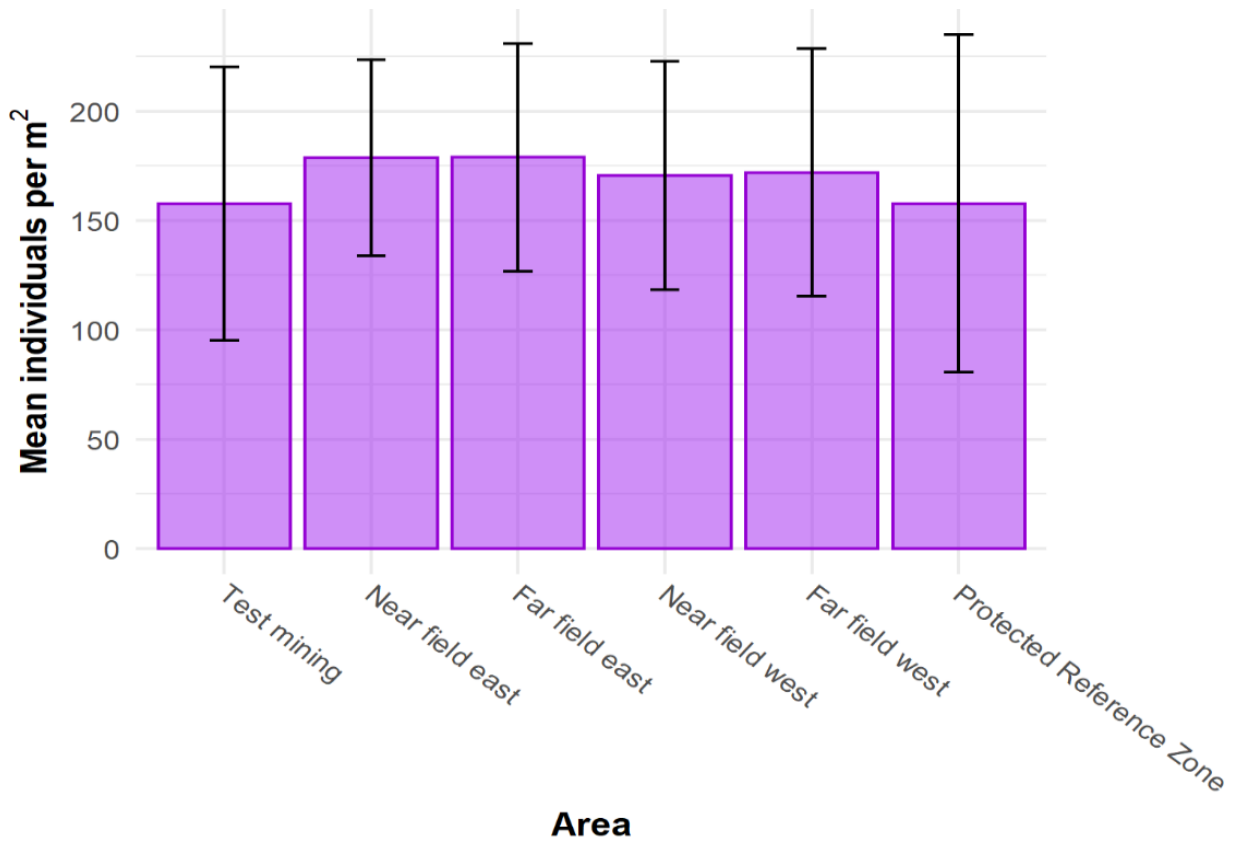
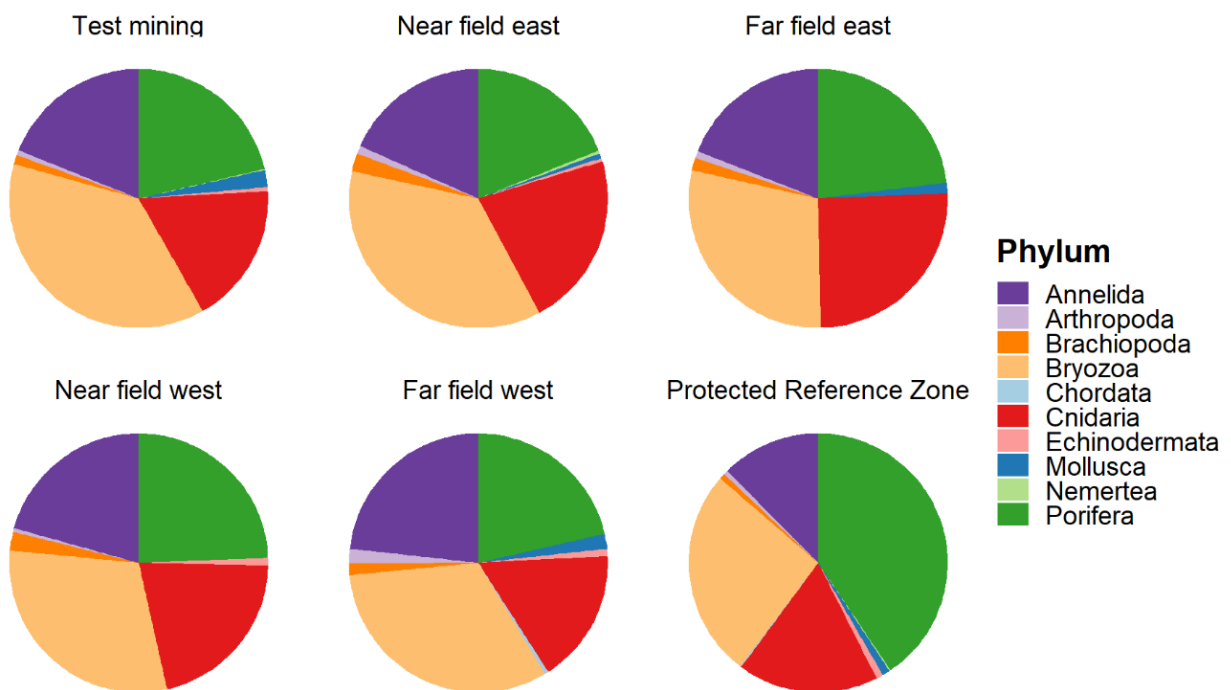


Figure 6-17 Community composition of the macrofauna across NORI-D



(g) Quantitative sediment macrofauna assessment

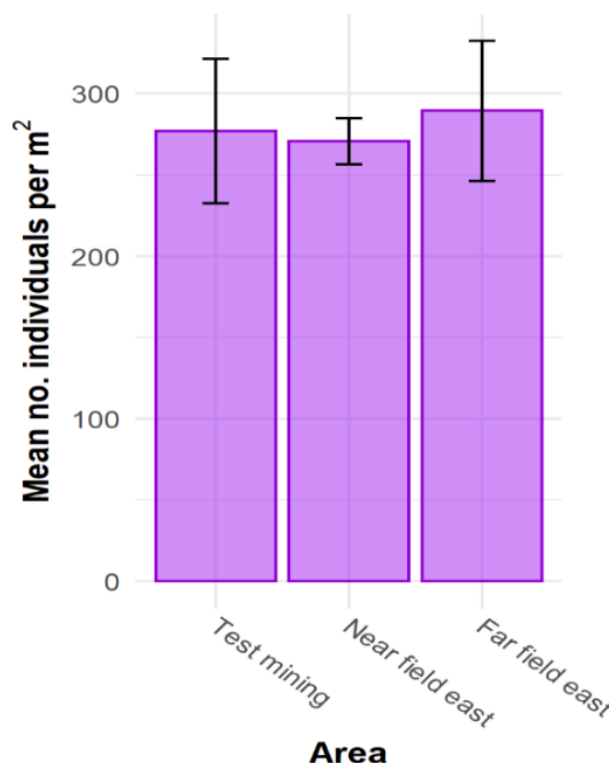
Quantitative work is being carried out for a total of at least 30 box cores. Due to shipping issues, bulk-fixed samples from the box cores collected during the NORI-D Campaign 5A arrived much later than those of 5D, and hence the preliminary data shown herein is from 5D samples, only. Bulk-fixed samples belonging to all sediment layers (0-2 cm, 2-5 cm, and 5-10 cm depth) have been sorted in the laboratory for a total of 10 box cores, 4 from the TF, 3 from the Near field east, and 3 from the Far field east. Nodule fauna (sponges, bryozoans, ascidians, and brachiopods) were removed from the preliminary analyses presented, as well as ostracods, nematods, and copepods which are usually considered meiofauna. Chaetognaths, appendicularians and ctenophores were removed, as most of these are probably contamination from surface water.

A total of 697 individuals, from 10 box cores, were considered for the quantitative analyses (Table 6-15). On average, 67.7-72.3 specimens were recovered per box core across the three different areas, with up to 289.3 individuals found per m², with abundance being similar between the three areas (Figure 6-18). The close grouping of these numbers is also suggestive of a high-quality of sampling at sea by the team.

Table 6-15 Detail of number of box cores and mud-dwelling specimens collected in the three areas (TF, Near field east, and Far field east) during the NORI-D Campaign 5D, with average number of individuals found per box core and per m².

| AREA | # BOX CORES | # INDIVIDUALS | MEAN # INDIVIDUALS PER BOX CORE | MEAN # INDIVIDUALS PER m ² |
|-----------------|-------------|---------------|---------------------------------|---------------------------------------|
| Test mining | 4 | 277 | 69.3 ± 11.1 | 277 ± 44.3 |
| Near field east | 3 | 203 | 67.7 ± 3.5 | 270.7 ± 14 |
| Far field east | 3 | 217 | 72.3 ± 10.8 | 289.3 ± 43.1 |
| Total | 10 | 697 | 69.7 ± 8.6 | 278.8 ± 34.3 |

Figure 6-18 Bar plot indicating the mean number of mud-dwelling specimens found per m² in each of the three areas sampled in the NORI-D Campaign 5D.



The relative abundance of the different Phyla present also seems to be similar between the three regions (Figure 6-19), although annelid worms were less abundant in the Far field east and arthropods (mainly amphipods and isopods) were more abundant.

Figure 6-19. Relative abundance of the different phyla of mud-dwelling fauna collected in three different areas during the NORI-D Campaign 5D

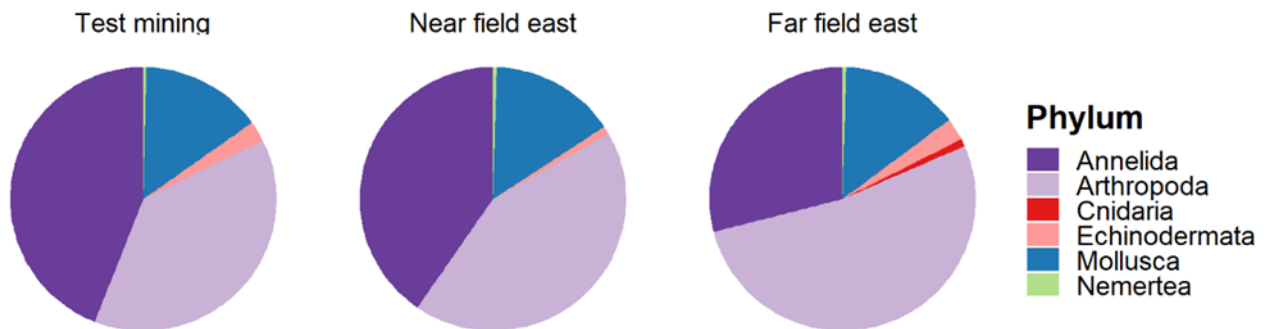


Figure 6-20 Relative abundance of polychaete families collected in three different areas during the NORI-D Campaign 5D.

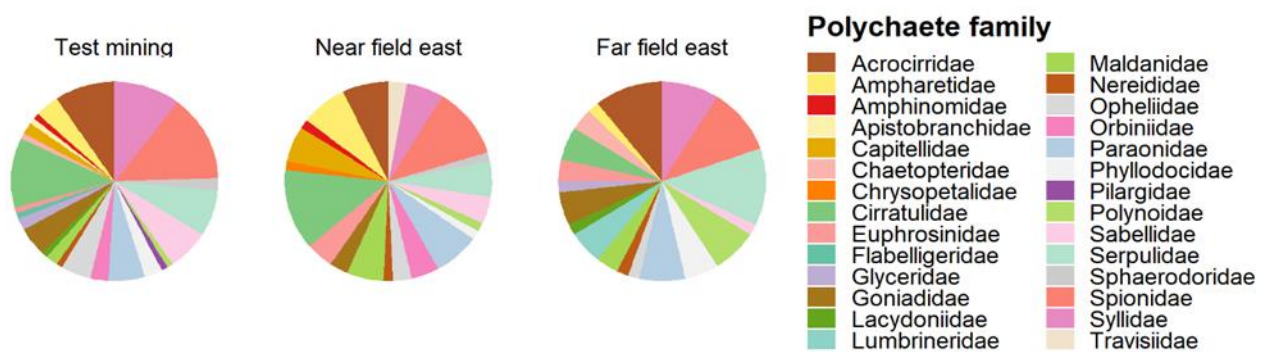
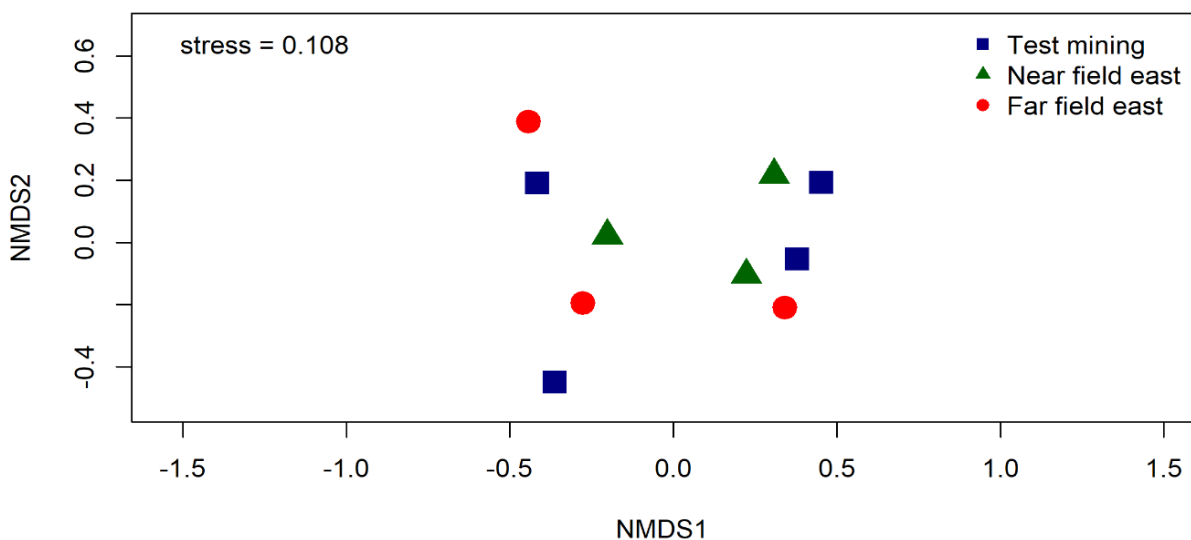


Figure 6-21 Non-metric multidimensional indicating similarities in abundance of polychaete families from different box cores. Different shapes and colours indicate the three different areas that were sampled during the NORI-D Campaign 5D.



While the species identification is still ongoing, most polychaete worms have been identified to family. Looking at compositional assemblages of polychaete families, these are roughly similar; with none of the families dominating in any of the three areas (

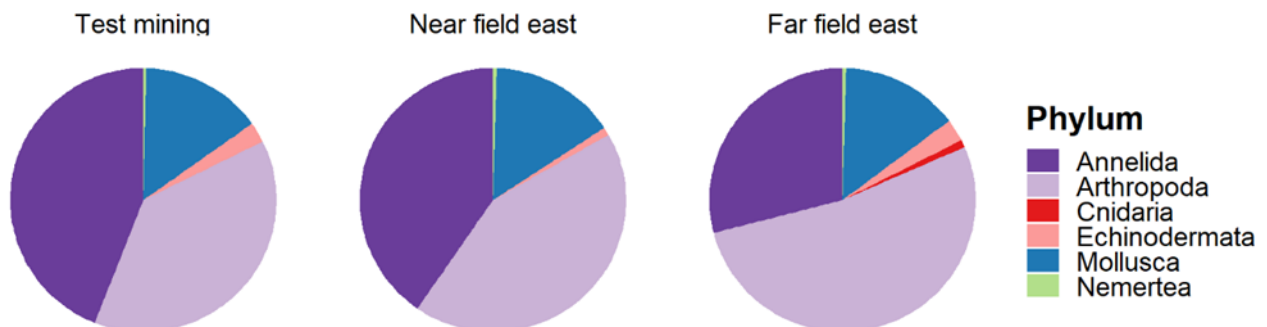


Figure 6-20). This can also be observed in the NMDS analysis (Figure 6-21), with all no obvious sample structure being driven by site. At the family level, there are minor differences. For instance, Lumbrineridae was only found in the Far field east, where also Serpulidae was relatively more abundant and Cirratulidae was less abundant than in other areas.

Preliminary results support the survey design. All sites within the CTA, including the TF, appear very similar in terms of abundance and community composition which is a promising result for properly monitoring future changes with an experimental Collector Test activity. The PRZ is likely to be somewhat different in terms of its composition but is similar in abundance to the CTA. This is to be expected given its distance. Future species-level studies will confirm the levels of species and genetic overlap between the PRZ and the CTA, it is expected there will be some new taxa at the PRZ but some overlaps.

6.3.4 Meiofauna

Benthic meiofauna is defined (ISBA/25/LTC/6/Rev.1) as the interstitial fauna found in seafloor sediments and are operationally defined as those organisms that remain on a 32 µm mesh sieve. Meiofauna are distinct from larger organisms such as macro- and megafauna in terms of their ecology and evolutionary history and occupy the space in between the sediment grains, rather than pushing the sediment away to create living space such as macrofauna.

Meiofauna are the most abundant components of the metazoan meiobenthos in the deep sea (Rex & Etter, 2010), dominating the metazoan biomass below 3000 m water depth (Wei *et al.* 2010) and are often the dominant metazoan size-class in food-limited abyssal waters, with the CCZ being no exception (Hauquier *et al.* 2019; Miljutina *et al.* 2010; Pape *et al.* 2017; Uhlenkott *et al.* 2021). In the north-eastern Pacific abyss, including the CCZ, a relatively high number of meiofauna taxa have been found (including but not limited to nematodes, harpacticoid copepods, ostracods, kinorhynchs, tardigrades, gastrotrichs, halacarid mites, loriciferans, meiofauna-sized polychaetes). Nematodes especially dominate the metazoan meiofauna in these abyssal plains, followed by copepods as the second most-abundant taxon. Both groups are very diverse in terms of genus/species richness, with up to 246 and 62 genera of nematodes and harpacticoids, respectively (Miljutina *et al.* 2010; Radziejewska, 2014) although these numbers may be conservative, given the number of studies that are being conducted currently which expand the overall study area, and the fact that many undescribed taxa (mostly species and genera) are being recovered.

Meiofauna abundance is expected to exhibit generally limited spatial and temporal variability in the wider region (Bik *et al.* 2010; Bik *et al.* 2012; Zeppilli *et al.* 2011) although distinct differences between habitat, geofom and nodule classifications can be expected on small-to-medium sized spatial scales (Hauquier

et al. 2019; Pape *et al.* 2021; Pape *et al.* 2017; Thiel, 1993; Thiel *et al.* 1993; Uhlenkott *et al.* 2020; Uhlenkott *et al.* 2021).

Recent evidence has shown that similar meiofaunal assemblages (although still in differing orders of dominance and rarity) may also occur in both nodule bearing, and nodule free sediment samples within the CCZ (Pape *et al.* 2017), potentially supporting the concept of low-level endemism for meiofauna taxa and nematode genera in the deep sea (Bik *et al.* 2010; Bik *et al.* 2012; Zeppilli *et al.* 2011). However, more morphological, and molecular studies support high meiofauna/nematode rarity levels and phylogenetic clustering across various licensing areas and APEIs, suggesting potential vulnerability to localized polymetallic nodule extraction (Hauquier *et al.* 2019; Macheriotou *et al.* 2020).

6.3.4.1 Purpose & scope

The following section describes the work conducted between 2020-2021 by Florida State University (FSU) to characterise natural baseline conditions in metazoan meiofauna communities in the NORI-D contract area. The scope, the survey planning and the sampling methodologies carried out to ecologically characterise seabed metazoan meiofauna communities align with International Seabed Authority ISBA/25/LTC/6 Rev 1 Annex 1 section 41(b) Biological communities: Metazoan meiofauna. to provide baseline data requirements under Recommendations III.A.13; III.B.14; III.B.15.(d).(i)–(ii); IV.B.22. Results obtained from preliminary assessments of multicore analysis conducted during Year 1 of the project are provided here.

6.3.4.2 Baseline investigations

The methods and proposed survey array for both the Collector Test and long-term environmental studies on NORI-D will provide data to meet the following objectives:

1. Establish meiofauna (32 µm – 300 µm) benthic biology/ecology time-series (two sampling campaigns and Collector Test) from selected sites in the Collector Test area, adjacent plume impact areas, control sites, and preservation reference zone to enable a baseline study, including spatio-temporal aspects, and study of conditions pre- and post-impact.
2. Characterize meiofauna biological communities (i.e., metazoan meiofauna higher taxa, and Nematode genera as dominant taxon (> 85% abundance)) living within or on seafloor sediments and hard substrates in the investigated areas.
3. Characterize the environmental drivers of meiofauna communities in the investigated areas.
4. Investigate the relationship between habitat heterogeneity (e.g., nodule abundance and type), sediment type and meiofauna communities.
5. Develop a meiofauna dataset of baseline seafloor sediment ecological status (based on community structure, biodiversity, and functional traits) that can be used to guide management actions during future operations.

6.3.4.3 Campaign activities

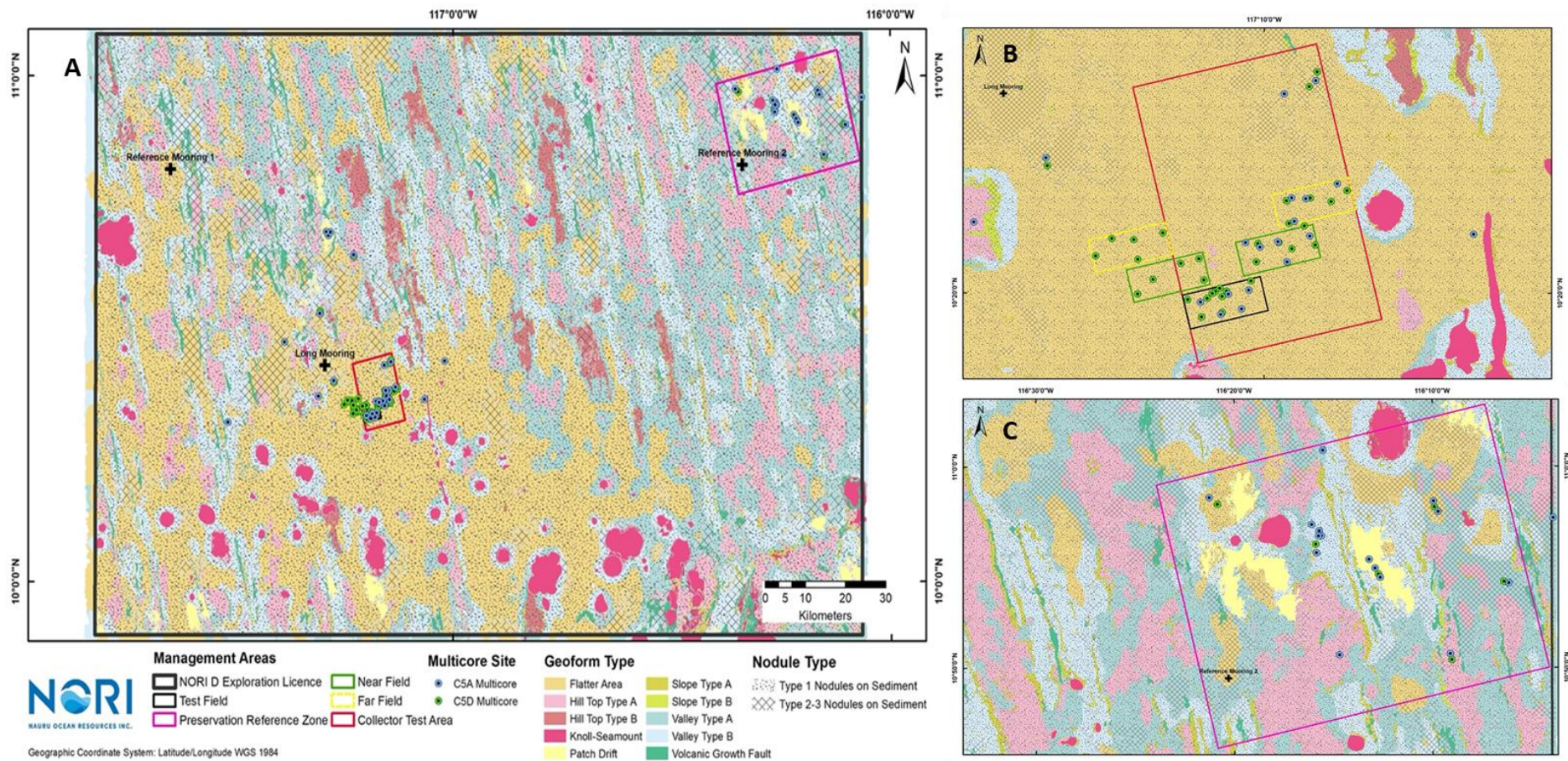
(a) Survey design & site selection

For Campaign 5A, OKTOPUS MC20 multicore deployment locations were selected to represent the diversity of geoform and substrate types across NORI-D including sufficient replication within the CTA, wider NORI-D and PRZ . For post-Collector Test and long-term monitoring studies, replication within the Level 2/3 Flatter area geoform with Type I nodule facies is critical to the BACI design to ensure statistical robustness. As such, a randomized stratified survey design (sensu Etter. 2002) was employed during

Campaign 5D to ensure sufficient replication on both spatial and temporal scales within the CTA (Figure 6-22B). Replicates for temporal variation were also conducted within the PRZ. (Figure 6-22C).

The sampling strategy in the baseline surveys maximized data collection to fill in knowledge gaps in spatial variability of infaunal communities in terms of community structure, richness, diversity/evenness, taxonomic distinctness, and functional diversity metrics, as well an assessment of these metrics that indicate ecological quality status in the context of a future Collector Test. The latter two are reliable indicators of disturbance which have been demonstrated in numerous publications and different types of habitats, as well as for different types of disturbances including physical disturbance and sedimentation. These metrics include trophic diversity index (TDI), Maturity Index (MI), and Ecological Quality Status (EcoQS). Calculating these metrics will be important to demonstrate the level of impact of the Collector Test in the direct impact area, the plume settlement zone and the control or reference areas.

Figure 6-22. A) Overview of multicores operations within NORI-D; B) Collector Test Area (CTA); C) Preservation Reference Zone (PRZ)



(b) Campaign 5A & Campaign 5D

During Campaign 5A, 183 cores from 55 deployments at 44 different sites were collected for meiofauna analyses, yielding a total of 732 samples (including 0-1, 1-3, 3-5, and 5-10 cm sediment slices for each core, 480 samples covering the 0-5 cm sediment horizon).

During Campaign 5D, 141 cores from 37 stations were collected for meiofauna analyses, yielding a total of 564 samples (423 samples covering the 0-5 cm sediment horizon). These samples were taken across the entire NORI-D area, focusing on the Mining Test Zone/Collector Test Area (MTZ/CTA), the areas surrounding the CTA, and the PRZ in the northeast of NORI-D.

While ISA (ISBA/25/LTC/6 Rev 1.) recommends collecting the 0-5 cm slice of the sediment core, we opted to sample the 0-1 cm, 1-3 cm, 3-5 cm, and the 5-10 cm slices from each sediment core for meiofauna analysis (Figure 6-23). This will allow a better understanding of vertical meiofauna distributions and enable comparisons with macrofaunal and biogeochemical sediment profiles. Studies have shown that >90% of the meiofauna resides in the top 3 cm of the sediment, with distinct community differences along the vertical sediment core profile (Radziejewska, 2014). Data can be pooled to provide 0-5 cm data for standard comparisons with other studies. The 5-10 cm samples will not be processed unless data shows high abundance in 3-5 cm sediment layers, but they are available for future research. Pseudo replication of at least three cores per deployment was included to assess small-scale spatial variability and reproducibility, an important factor in collecting accurate quantitative data.

In addition, at each of seven sampling sites, surface nodules were collected from an individual core to investigate meiofauna presence in/on nodule material. Thiel *et al.* (1993) and Bussau *et al.* (1995) have demonstrated that nodule crevices, which are filled with sediment, harbour distinct meiobenthos from the surrounding sediments. Further research is needed to determine the extent and relative importance of these differences, and whether they are maintained for different nodule types and across the region.

Figure 6-23 Sediment slicing for meiofauna analysis.



A) Using the aluminium plates, mud was sliced in between the core tube and the slicing ring. B) The plate was slid off the tube with light downward pressure (without pushing the core tube down further onto the extruder), removing the slicing ring and mud with it. C&D) Presence of nodules at the sediment surface and in the deeper sediment layers.

6.3.4.4 Preliminary results & discussion

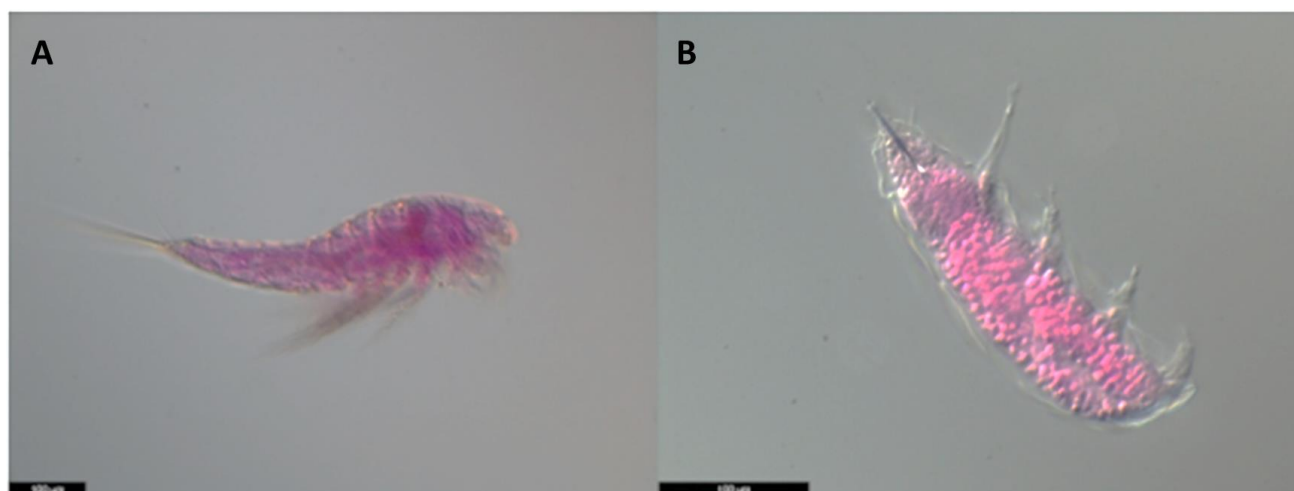
As of December 2021, all Campaign 5A and 5D samples have been processed (washed, sieved, density centrifugation to extract fauna). Samples were split 50/50 to avoid incidental loss during sorting, post-processing, or the identification process. Of these, 199 samples have been identified for meiofauna higher taxa, and 150 samples for nematode genera. By May 2022 all 480 Campaign 5A samples will have been identified, and samples from Campaign 5D are expected to be finished by end 2023.

Data presented here are based on the identification of nearly 30,000 meiofauna individuals from 199 samples (Figure 6-24), and >9,000 nematodes from a total of 152 samples (mostly 0-1 cm sediment slices) However, given the large number of samples that still await analysis, interpretations of these limited data should be made with caution and results/data presented below will differ from the final results.

(a) Meiofauna higher taxa

A total of 21 higher taxa have been observed (Table 6-15). Note that higher taxa mostly correspond to higher taxonomic levels but does include categories such as nauplii (larval forms copepods, crustaceans) and larval polychaetes, which do not have a recognized taxonomic status, but can be considered to have different behaviour and ecologies.

Figure 6-24 Light microscope images of meiofauna taxa recovered from NORI-D samples



A) harpacticoid copepod; B) tardigrade

Table 6-16 Overview of counts, abundances, and densities of meiofauna higher taxa. Abundance and density values are average values for all samples analysed thus far

| TAXA | TOTAL COUNTS* | AVERAGE ABUNDANCE PER SAMPLE** | AVERAGE DENSITY (ind. 10cm ⁻²)** |
|--------------|---------------|--------------------------------|--|
| Acari | 47 | 0.47 | 0.0666 |
| Ciliophora | 201 | 2.02 | 0.2850 |
| Cnidaria | 4 | 0.04 | 0.0057 |
| Copepoda | 2,987 | 30.02 | 4.2352 |
| Cumacea | 1 | 0.01 | 0.0014 |
| Gastrotricha | 22 | 0.22 | 0.0312 |
| Isopoda | 9 | 0.09 | 0.0128 |
| Kinorhyncha | 33 | 0.33 | 0.0468 |
| Loricifera | 10 | 0.10 | 0.0142 |

| TAXA | TOTAL COUNTS* | AVERAGE ABUNDANCE PER SAMPLE** | AVERAGE DENSITY (ind. 10cm ⁻²)** |
|---------------------|---------------|--------------------------------|--|
| Nauplii | 2,872 | 28.86 | 4.0722 |
| Nematoda | 20,025 | 201.26 | 28.3931 |
| Nemertea | 1 | 0.01 | 0.0014 |
| Oligochaeta | 39 | 0.39 | 0.0553 |
| Ostracoda | 460 | 4.62 | 0.6522 |
| Polychaeta (larval) | 250 | 2.51 | 0.3545 |
| Polychaeta | 151 | 1.52 | 0.2141 |
| Priapulida | 14 | 0.14 | 0.0199 |
| Sipuncula | 3 | 0.03 | 0.0043 |
| Tanaidacea | 11 | 0.11 | 0.0156 |
| Tardigrada | 409 | 4.11 | 0.5799 |
| Turbellaria | 2,155 | 21.66 | 3.0555 |
| Total | 29,704 | 298.53 | 42.1167 |

*Based on 50% of each sample

**Average across all samples currently analysed, including 0-1, 1-3, and 3-5 cm sediment horizons

Total meiofauna density per cores (0-5 cm) across the NORI-D area ranged 26.0 – 204.3 ind. 10cm⁻², averaging 70.0 ± 42.0 ind. 10cm⁻² (Table 6-16). Total meiofauna density per cores (0-5 cm) across the NORI-D area ranged 26.0 – 204.3 ind. 10cm⁻², averaging 70.0 ± 42.0 ind. 10cm⁻² (Table 6-16). These average values are relatively low compared to similar other studies, possibly linked to the variability in presence and density of nodules and sediment conditions such as the very high amounts of silicious remains of radiolarians and diatoms, and biogeochemical conditions. Upon completing the dataset, meaningful comparative analyses will be conducted.

The sampling procedure allowed to assess the differences in density and taxa composition between sediment layers. Preliminary data shows that on average 68.8% of meiofauna abundance resides in the top 0-1 cm sediment layer (51.0 ± 33.9 ind.10cm⁻²), 23.3% in the 1-3 cm layer (17.3 ± 12.4 ind.10cm⁻²), and 7.9% in the 3-5 cm layer (5.9 ± 4.1 ind.10cm⁻²), confirming findings from previous CCZ studies that the top 3 cm hosts most of the organisms (92.1%) of the 0-5 cm core sediment (Figure 6-25).

In terms of higher taxon richness this pattern is even more pronounced, with all 21 higher taxa occurring in the top 0-1 cm, 12 in 1-3 cm, and 10 in the 3-5 cm (Figure 6-26). The same is true for the nematode genera (Figure 6-32). It can therefore be argued that analyses on the surface layers at this stage of sample completion is most informative. Based on 0-1 cm samples, the three main NORI-D zones (CTA (46.5 ± 33.1 ind.10cm⁻²), PRZ (44.8 ± 28.9 ind.10cm⁻²), Western area surrounding the CTA (67.6 ± 37.3 ind.10cm⁻²) do not differ statistically in terms of meiofauna density (Figure 6-25). Within the CTA, however, 0-1 cm density differences are observed between the proposed test mining area (TF, 61.6 ± 44.0 ind.10cm⁻²) and the near-field area (NF, 27.8 ± 12.2 ind.10cm⁻², p=0.01), and between the NF and far-field area (FF, 52.7 ± 30.2 ind.10cm⁻², p=0.003), but not between the TF and FF (p=0.489) (Figure 6-25).

Figure 6-25 Average meiofauna densities and standard deviation along the vertical sediment profile (left), and 0-1 cm meiofauna densities per NORI-D Zone (middle) and within the CTA (TF: Test Field, NF: near field, FF: far field).

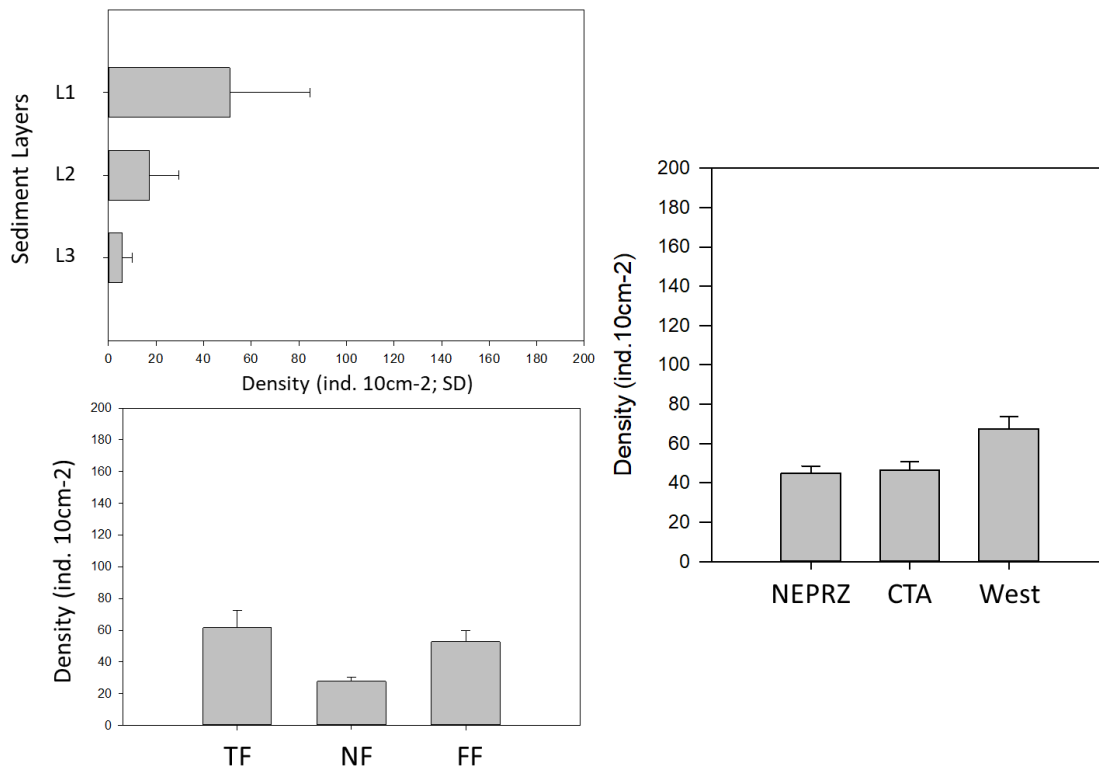
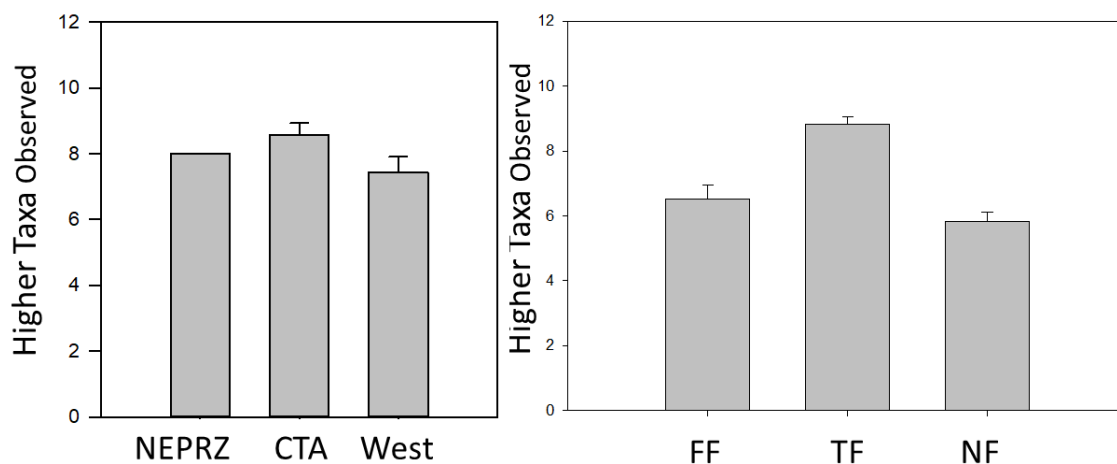


Figure 6-26 Average meiofauna higher taxa observations in 0-1 samples for NORI-D Zones (left), and areas within the CTA (TF: Test Field, NF: near field, FF: far field).

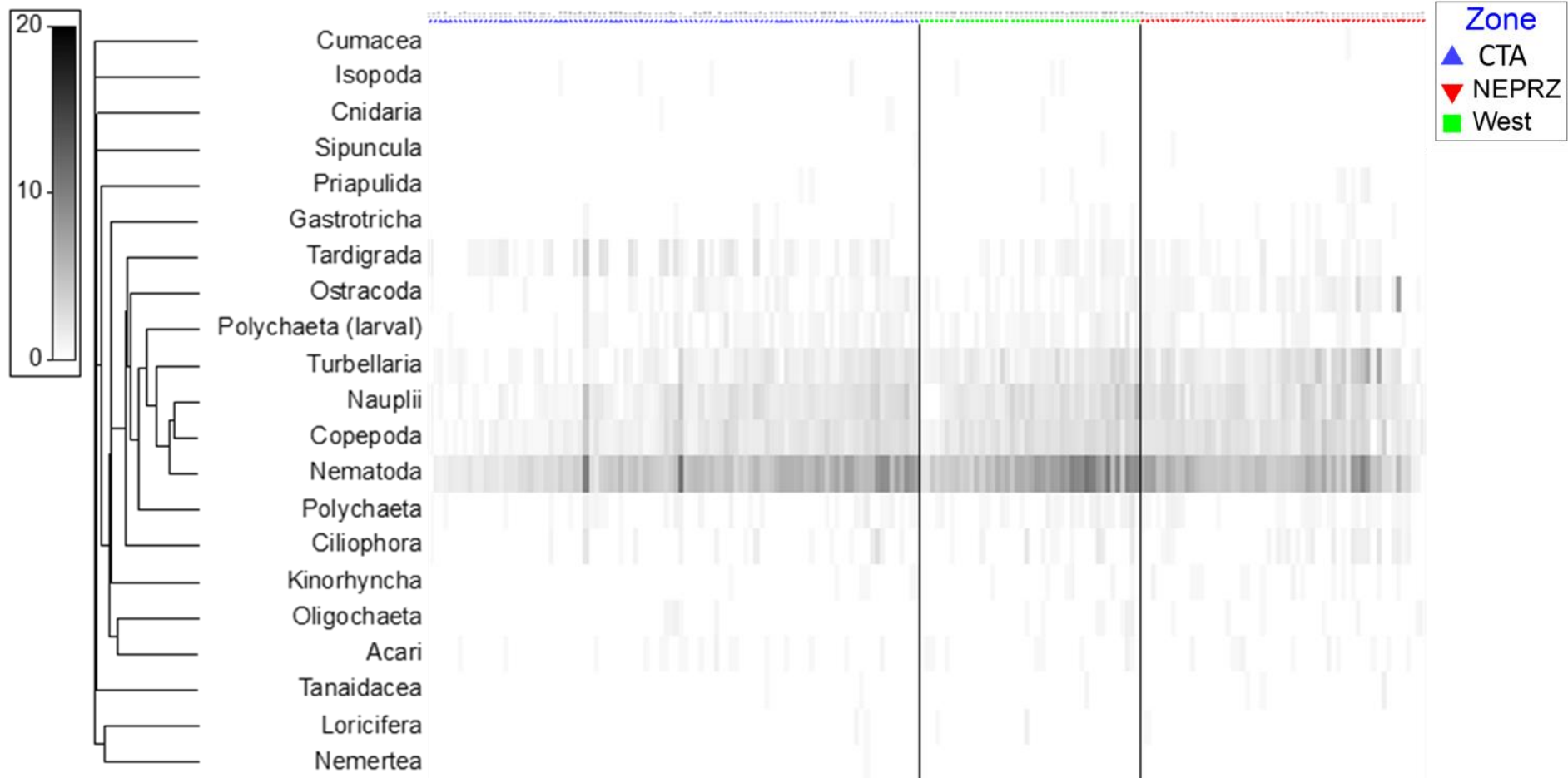


The number of meiofauna higher taxa observed varies little between zones, likely linked to the small sample size of the 0-1 cm sediment slice relative to the spatial area under consideration; significant differences were not observed (Figure 6-26).

Based on meiofauna higher taxa community composition from the 0-1 cm samples there are distinct differences between the CTA/TM, surrounding Western area, and the NEPRZ (nMDS based on centroids of samples per station (

Figure 6-28), PERMANOVA $p=0.001$, PERMDISP: n/s). Within the CTA,

Figure 6-27 Matrix shade plot of meiofauna higher taxa with associated taxon cluster profile based on similarities in presence and abundance of higher taxa across all samples. A darker shade implies greater density in the sample. Samples (left to right) are ranked according to zone in the NORI-D area. CTA: Collector Test Area; West: Western area CTA; NEPRZ: NE Preservation Zone.



communities differed also, with significant differences between the TF and NF/FF ($p=0.001$), whereas no significant differences were observed between NF and FF ($p=0.163$). However, our data show that most taxa are shared across the entire NORI-D Area (17 occur in all three NORI-D Zones, Figure 6-29).

This is in part supported by a RELATE analysis (comparison between meiofauna dissimilarity matrix and dissimilarity matrix based on sample locations/coordinates, $Rho: 0.017$, $P:0.237$; Figure 6-27), showing that the differences in meiofauna assemblages do not correspond with distance between the physical locations of the samples across NORI-D. Spatial patterns purely based on physical distance within NORI-D are likely the result of other factors such as habitat or geform and associated sedimentary conditions.

Figure 6-28 nMDS based on meiofauna higher taxa in the 0-1cm samples, using distance among centroids per station. TM: Trial Mining Zone or Collector Test Area; West: area surrounding CTA; NEPRZ: NE Special Preservation Zone.

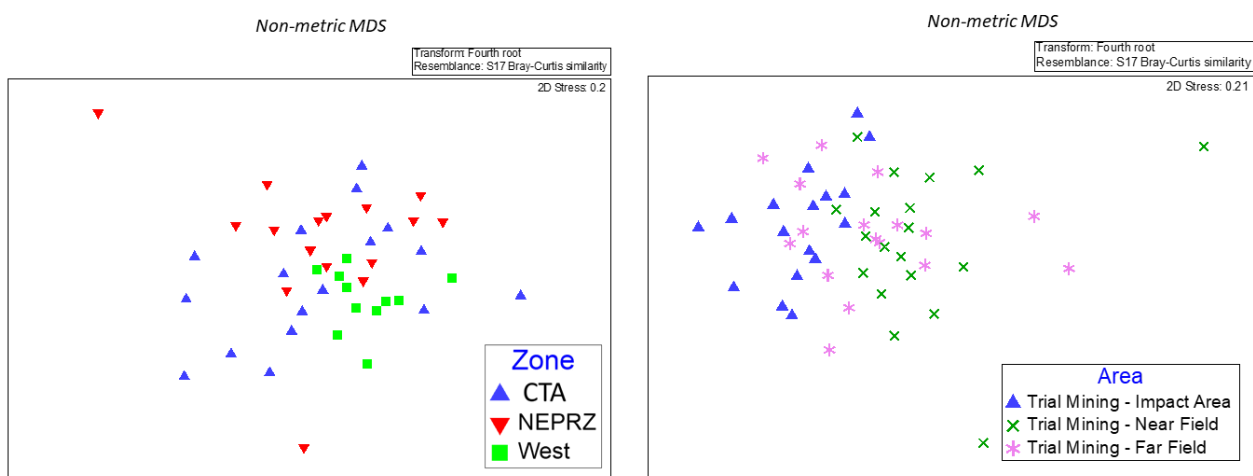
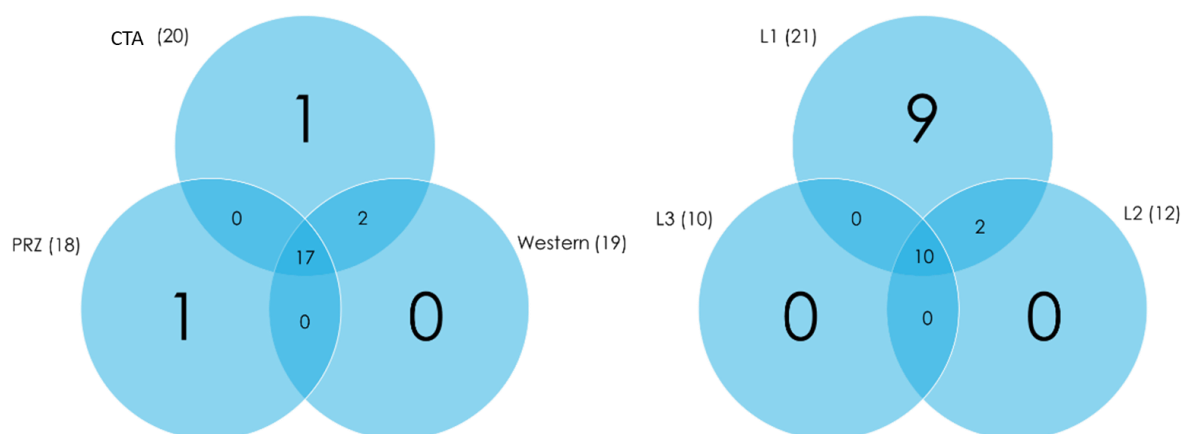


Figure 6-29 Venn diagrams of meiofauna higher taxa numbers and their presence in the different NORI-D Zones (CTA; Western area surrounding the CTA, and the PRZ) (left), and in the different sediment layers (L1:0-1 cm, L2: 1-3 cm, L3: 3-5 cm) (right).



(b) Nematodes

So far, a total of 116 nematode genera (Figure 6-30) have been documented from NORI-D, which is very similar to other studies in different license areas (Hauquier *et al.*, 2019; Pape *et al.*, 2017), and lies within the expectations considering the 156 genera observed in Hauquier *et al.* (2019) who compared data from four different license areas and the APEI-3 area. Despite the observed diversity, the communities are characterized by a high abundance of only a limited number of taxa, with many low-abundance genera

making up most of the community, and rare genera with only a few occurrences across all the samples (Figure 6-35).

Figure 6-30. Light microscope images of head regions of nematode specimens recovered from the NORI-D area.



Overall diversity was assessed using genera accumulation curves and rarefaction plots using the Chao1 estimator for all samples and the three different NORI-D zones (CTA, Western area surrounding the CTA, and the NEPRZ) (Figure 6-31). These curves give us an idea of how complete the current sampling effort is in capturing the total number of genera in the area, and how many genera can be expected (Chao1). Figure 6-31 shows that the rate of nematode genera being added to the total genus pool is decreasing with each new sample added, and Chao1 indicates that total genus diversity is estimated to be around 136, exhibiting flattening and progression to an asymptote after 100 samples; this also seems to be the case for the CTA and NEPRZ based on the current limited number of samples finalized.

The number of nematode genera observed per sample varies little between zones, likely linked to the small sample size of the 0-1 cm sediment slice relative to the spatial area under consideration; significant differences were not observed (Figure 6-32). Comparing nematode genera numbers between areas within the CTA, however, the near-field area samples hosted significantly less genera than the far-field (FF) and TF areas. As was the case for the meiofauna higher taxa, nematode genera predominantly reside in the surface sediment layer (0-1cm), with only 2 and 4 genera restricted to 1-3 cm and 3-5 cm, respectively (Figure 6-32). supporting the use of the 0-1cm later in assessing nematode genera richness and diversity.

Figure 6-31 Left: Nematode genera accumulation curves for total number of samples processed so far in NORI-D, and for the three different zones (CTA, Western area surrounding the CTA, and the NEPRZ). Right: Chao1 genera richness estimator rarefaction curves for total number of samples processed so far in the NORI-D region, and for the three different zones (TMZ, Western area surrounding the TMZ, and the NEPRZ).

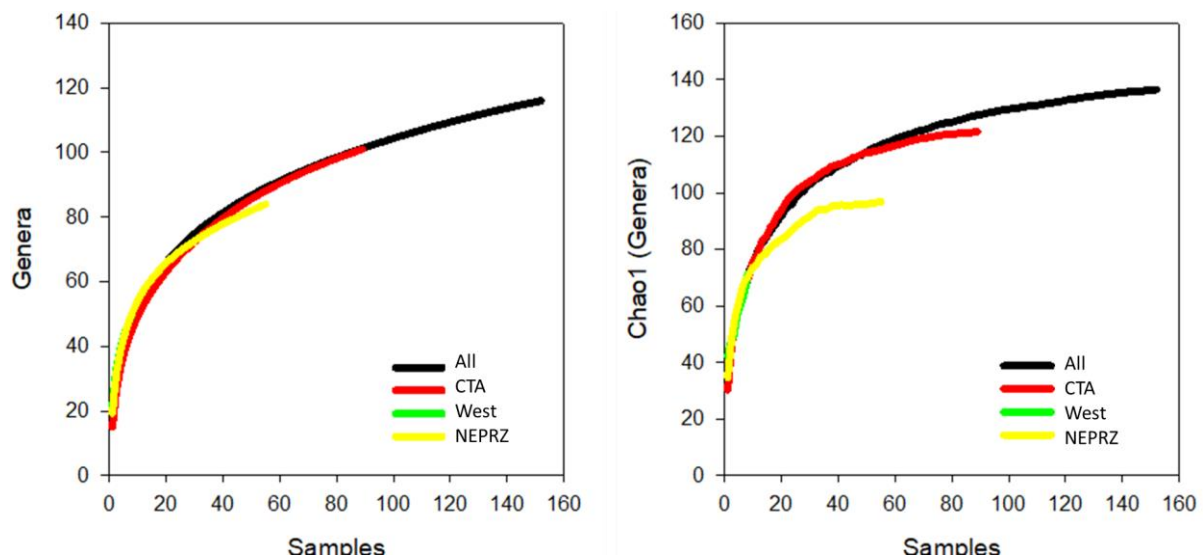
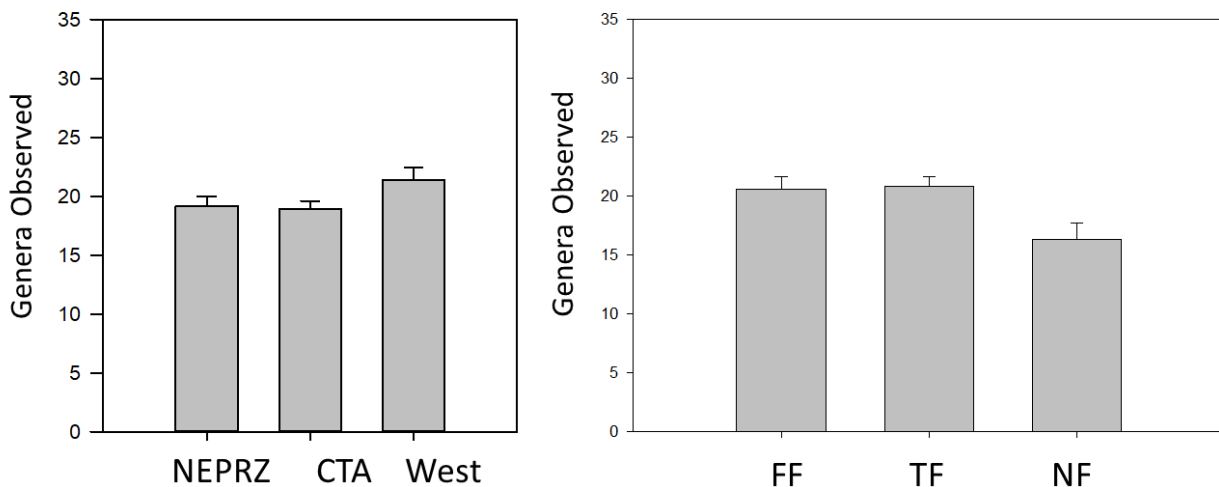


Figure 6-32 Average number of nematode genera observed in 0-1 samples for NORI-D Zones (left), and areas within the CTA (TF: Test Field, NF: near field, FF: far field).



Based on nematode genera community composition from the 0-1 cm samples there are distinct differences between the CTA/TM, surrounding Western area, and the NEPRZ (nMDS based on centroids of samples per station (Figure 6-33), PERMANOVA $p=0.001$, PERMDISP: n/s). Within the CTA, communities differed also ($p=0.005$), with significant differences between the TMA and NF/FF ($p=0.007$, $p=0.03$, respectively), whereas no significant differences were observed between NF and FF ($p=0.113$). However, our data show that most nematode genera are shared across the entire NORI-D Area (Figure 6-34). Correlation analysis (comparison between meiofauna dissimilarity matrix and dissimilarity matrix based on sample locations/coordinates; RELATE analysis; Figure 6-35) showed that the differences in nematode genera assemblages correspond with distance between the physical locations of the samples across NORI-D, suggesting a substantial role of physical distance within NORI-D in determining nematode genera community structure, although other factors such as habitat or geofom and associated sedimentary conditions will be compared to nematode community structure as they are likely important community assembly driving forces.

Figure 6-33 nMDS based on nematode genera in the 0-1cm samples, using distance among centroids per station. TM: Trial Mining Zone or Collector Test Area; West: area surrounding TMZ/CTA; NEPRZ: NE Special Preservation Zone.

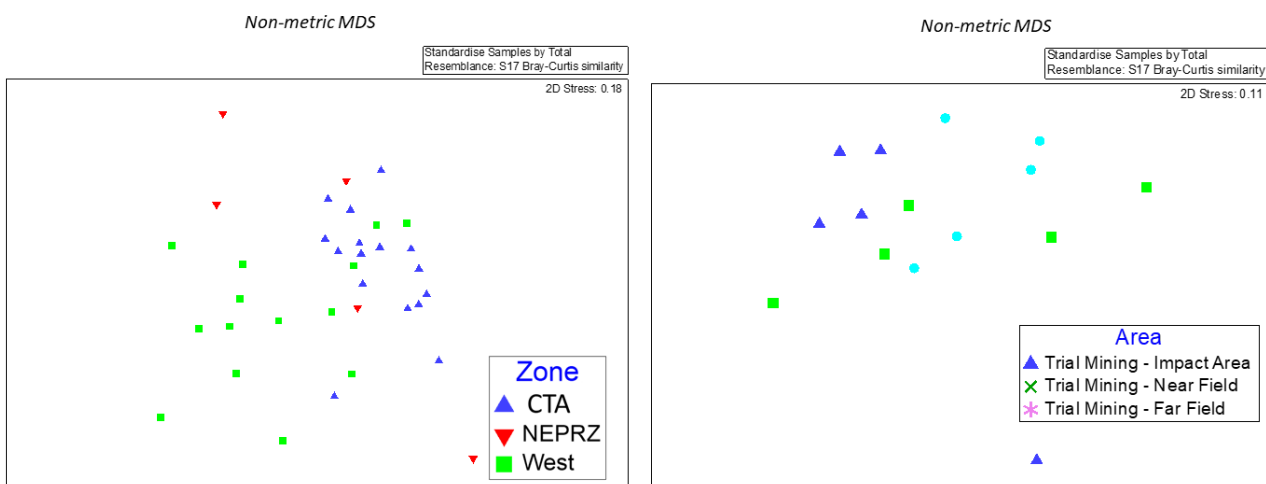


Figure 6-34 Venn diagrams of genera numbers and their presence in the different NORI-D Zones (TMZ/CTA; Western area surrounding the CTA, and the PRZ) (left), and in the different sediment layers (L1:0-1 cm, L2: 1-3 cm, L3: 3-5 cm) (right).

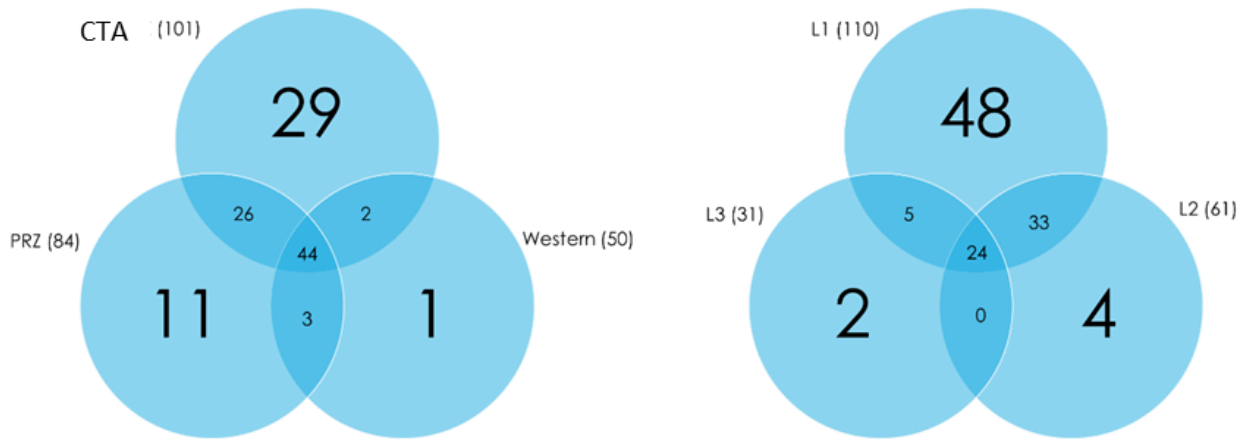
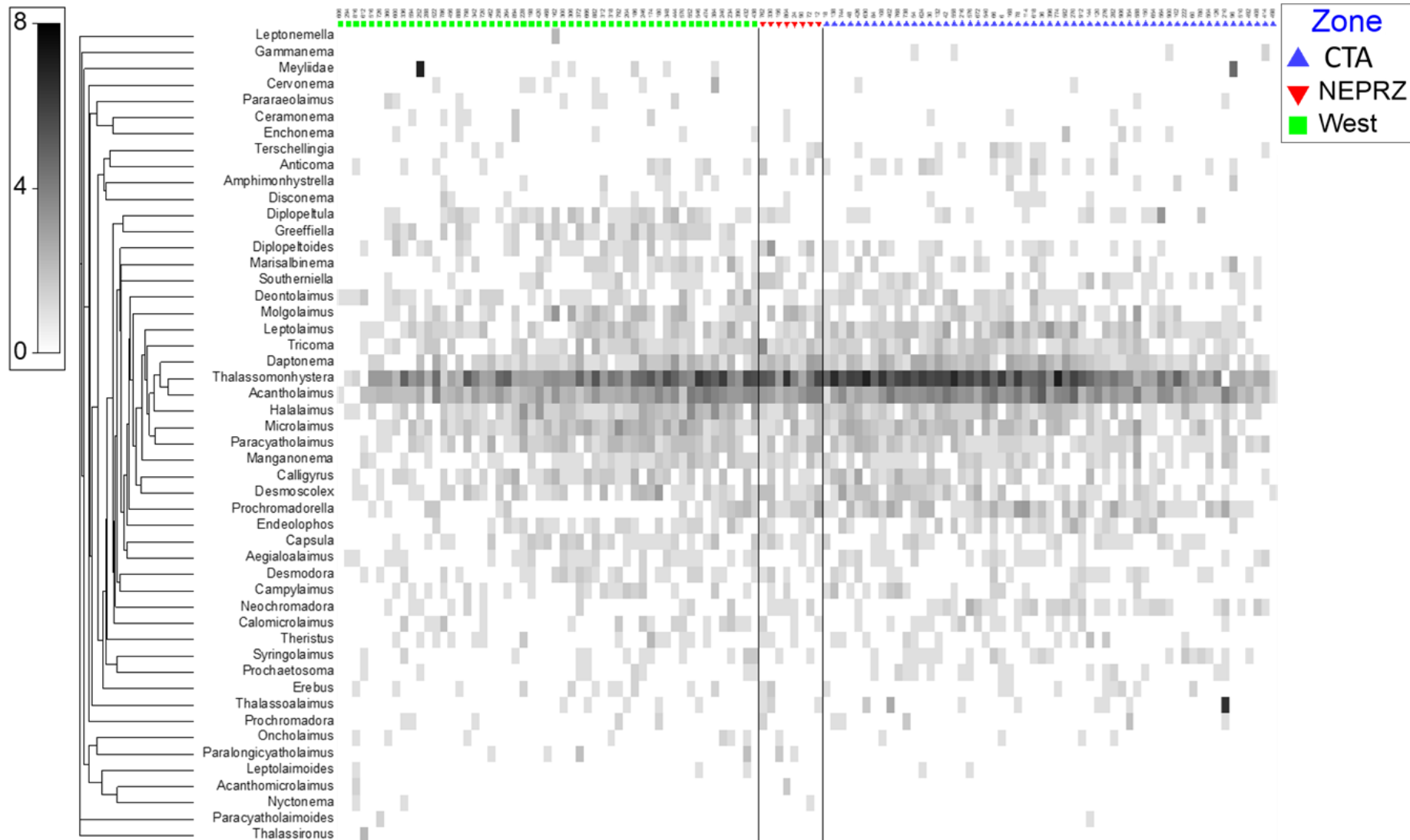


Figure 6-35 Matrix shade plot of nematode genera with associated taxon cluster profile based on similarities in presence and abundance of nematode genera across all samples. A darker shade implies greater density in the sample. Samples (left to right) are ranked according to zone in the NORI-D area. TM: Trial Mining Zone or Collector Test Area; West: area surrounding TMZ/CTA; NEPRZ: NE Special Preservation Zone.



6.3.5 Foraminifera Meiofauna

6.3.5.1 Benthic foraminifera

Benthic foraminifera are single-celled protists that are ideal bioindicators for ecological monitoring because of their high biodiversity, short turnover rate, low trophic status, varying degrees of environmental sensitivities, and high abundance in all marine environments (Schwing *et al.* 2018; Lei *et al.* 2015; Morvan *et al.* 2004; Mojtahid *et al.* 2006).

Over the past two decades, a renewed interest in deep-sea mining spurred a rise in benthic ecological studies, including the first quantitative foraminiferal surveys of the region (Nozawa *et al.* 2006; Goineau & Gooday, 2017, 2019). Nozawa *et al.* (2006) published a study of stained or 'live' foraminifera from 3 stations in the Kaplan East, which found 252 morphospecies with over two thirds being monothalamous.

The most abundant (>5% relative abundance) species found in these samples were komokiaceans, tube species, *Nodellum* sp. and *Lagenammina* sp. (Nozawa *et al.*, 2006). The Fisher's alpha values for these three sites were generally high and ranged from 27.4 to 41.8 with an average value of 36.8 (Nozawa *et al.* 2006). In 2015, as part of the ABYSSLINE study (UK-1), Gooday *et al.* examined epilithic foraminifera and discovered 86 species that rely on polymetallic nodules as a hard surface for habitat (Gooday *et al.*, 2015). The ABYSSLINE study also included a quantitative report on sedimentary foraminifera from five sites, in which Goineau and Gooday (2017) found 416 morphospecies. Seventy-six percent of these species were monothalamids and a vast majority of the species discovered were considered 'undescribed' (Goineau & Gooday, 2017). The Fisher alpha values for these five sites ranged from 46.4 to 74.8, which represent higher diversity than both abyssal Atlantic assemblages and deep Gulf of Mexico assemblages (Gooday *et al.* 1996, 1998, 1999, Goineau & Gooday, 2017, Schwing *et al.* 2018). Goineau and Gooday's 2019 study from UK-1 and Ocean Minerals Singapore (OMS) expanded from five sites to eleven sites and another 164 species were added to the initial 416 morphospecies discovered making a total of 580 morphospecies found in the eastern CCZ. This study reinforces the high diversities of the region as well as the dominance of monothalamids among the benthic fauna (Goineau & Gooday, 2019). Foraminiferal assemblages have been found to be highly diverse, yet very similar across nodule-rich sites within contract areas in the eastern CCZ (Goineau & Gooday, 2019; 2017) with approximately 400 individual morphospecies (Goineau & Gooday, 2017).

Some species of benthic foraminifera have been shown to colonize areas that have been exposed to episodic organic enrichment, physically disturbed sediment, and anoxia (Schwing *et al.* 2015; Romero *et al.* 2016), with biodiversity and biomass shown to rapidly decline after episodic plume settling events with faster documented recoveries than comparable macrofauna (Schwing, *et al.* 2018; Romero *et al.* 2016).

As such, foraminifera represent a good candidate as indicator species, and internationally recognized and standardized marine biotic indices based on foraminifera assemblages such as the AZTI Marine Biotic Index (ForamAMBI) have also proven essential in monitoring benthic ecological quality status (EcoQS) and determining benthic habitat suitability (Borja *et al.* 2000; Alve *et al.* 2015; Jorissen *et al.* 2018; O'Malley *et al.* 2021).

(a) Chlorophyll-a & phaeopigments

Abyssal plain benthic faunal abundance, vertical profiles and food webs are influenced by the quality and quantity of phytodetritus deposition, which is a function of pelagic primary productivity, sinking rates, and degradation (Stephens *et al.*, 1997; Nomaki *et al.*, 2021). Phytopygments have been commonly used in abyssal settings as tracers of the phytodetrital contribution (as much as 25-100%) to the organic carbon budget (Stephens *et al.*, 1997; Danovaro, 2010) and despite high degradation rates, remain on the seafloor for up to several months (Smith *et al.*, 1996; Stephens *et al.*, 1997; Witbaard *et al.*, 1999). Phytodetrital accumulation is seasonally driven in equatorial regions by latitudinal migration of convergence zones (Smith *et al.*, 1996). Abyssal meiofaunal abundance varies with phytopigment

concentrations (Moens *et al.*, 2013; Lins *et al.*, 2014) and should be included as a driving environmental variable for abyssal benthic communities. However, the predominance of phytodetritus as a driver of meiofaunal abundance may be confounded by other factors in the CCZ such as nodule density, water depth and sediment texture (Hauquier *et al.*, 2019) considering the oligotrophic nature of the CCZ (Volz *et al.*, 2018).

(b) Organic matter determination

Organic matter availability is a key limiting factor in the function of abyssal benthic ecosystems (Nugteren *et al.*, 2009). The ISA requires that grain-size and total organic matter be measured as a baseline to track a discharge plume as well as contextualize the benthic meiofaunal and macrofaunal communities. Although these parameters were measured by the University of Leeds for the 14 priority 1 sites, sediment composition analysis was also quantified by Eckerd College for the priority 2 and 3 sites as this was crucial in understanding the meiofaunal and macrofaunal distribution and how a redistribution of this organic matter would affect the benthos.

These parameters were also crucial in identifying opportunistic indicator species as the Foram-AMBI assigns species as tolerant or sensitive based on their response to organic enrichment (O'Malley *et al.*, 2021). Including measurements of grain size and total organic matter at the priority 2 and 3 sites also provided a statistically robust calibration of the Foram-AMBI to produce EcoQS for the study area.

6.3.5.2 Purpose & scope

The following section describes the work conducted between 2020-2021 by Eckerd College, to characterise natural baseline conditions in Foraminiferal meiofauna in the NORI-D contract area. The scope, the survey planning and the sampling methodologies carried out to ecologically characterise seabed Foraminiferal meiofauna communities align with International Seabed Authority ISBA/25/LTC/6 Rev 1. Annex 1 section 41(d) Biological communities: Foraminiferal meiofauna. to provide baseline data requirements under Recommendations III.A.13; III.B.14; III.B.15.(d).(i)–(ii); IV.B.22. The ISA also requires that grain-size and total organic matter be measured as a baseline to track a discharge plume as well as contextualize the benthic meiofaunal and macrofaunal communities under Recommendations III.A.13; III.B.15.(b).(ii); III.B.15.(d).(iv). Results obtained from preliminary assessments of multicore analysis conducted during Year 1 of the project are provided here.

6.3.5.3 Baseline investigations

The methods and proposed survey array for both the Collector Test and long-term environmental studies on NORI-D will provide data to meet the following objectives:

1. Establish foraminiferal biodiversity baselines using traditional taxonomic methods
2. Establish foraminiferal biomass baselines
3. Determine the chlorophyll-a, phaeopigments and total organic matter to contextualize the benthic meiofaunal and macrofaunal communities within NORI-D
4. Identify opportunistic indicator species
5. Calibrate the Foram-AMBI and calculate baseline pre-mining Ecological Quality Statuses.

6.3.5.4 Campaign activities

(a) Survey design and site selection

See 6.3.4.3(a) Meiofauna survey design and site selection

(b) Campaign 5A

Multicore samples (2 x core) were collected from 44 successful multicore deployments during Campaign 5A. Foraminifera samples were sliced in the following sections 0-1 cm, 1-2 cm, 2-3 cm, 3-4 cm, 4-5 cm, 5-10 cm yielding 288 samples. Samples recovered for phaeopigments and organic matter determination were sampled at 0-1 cm, 1-2 cm, 2-3 cm, 3-4 cm, 4-5 cm sections.

(c) Campaign 5D

Multicore samples (2 x core) were collected from 42 successful multicore deployments during Campaign 5D. Foraminifera samples were sliced in the following sections nodules, 0-1 cm, 1-2 cm, 2-3 cm, 3-4 cm, 4-5 cm, 5-10 cm yielding 292 samples. Samples recovered for phaeopigments and organic matter determination were sampled at 0-1 cm, 1-2 cm, 2-3 cm, 3-4 cm, 4-5 cm sections.

6.3.5.5 Preliminary results & discussion

(a) Benthic Foraminifera

To date, a total of 23 cores from Campaign 5A have been analysed for benthic foraminiferal community assemblage data. 115 samples were analysed as 1-cm increments from 0-5 cm from each core (65 samples from CTA sites, 20 samples from wider NORI-D (WND) sites and 30 from PRZ sites). A total of 25,965 foraminifera were identified, with 9,736 considered stained (living) and a total species count of 487. There were 224 species found in WND, 353 species found in CTA, and 248 species found in PRZ.

The average foraminiferal density of all sites was 392 stained and complete individuals per 5 cm² (all increments integrated) with a range of 255 to 743 individuals per 50 cm². The average density of individuals in the CTA region was 393 individuals per 50 cm² with a range of 255 to 654 individuals per 50 cm². The average density of individuals in the WND region was 430 individuals per 50 cm² with a range of 288 to 743 individuals per 50 cm². The average density of individuals in the PRZ region was 411 individuals per 50 cm² with a range of 338 to 484 complete individuals per 50 cm².

Figure 6-36 Micrograph plate of example species identified in NORI-D



1) *Spirillina denticulata* 2) *Cribrostomoides subglobosum* 3) *Reophax* sp 17 4) *Ammodiscus tenuis* 5) *Cyclammina subtrullissata* 6) Komokiacean sp. 5 7) *Cystammina pauciloculata* 8) *Fissurina orbignyana* 9) *Fissurina staphyllearia* 10) *Francuscia extensa* 11) *Psammosphaera* sp. 3 12) Agglutinated Sphere sp. 6 13) *Resigella moniliformis* 14) *Lagenammina difflugiformis* 15) *Saccorhiza ramosa* 16) *Verneuilinulla propinqua* 17) *Vanhoeffenella* sp 2 18) *Reophax dentaliniformis* 19) *Fissurina stschedrinae*

Figure 6-37 Sample-based rarefaction curve (red line) based on complete stained (“live”) specimens from 23 sites from Campaign 5A in NORI-D. The outer blue lines represent the 95% confidence interval.

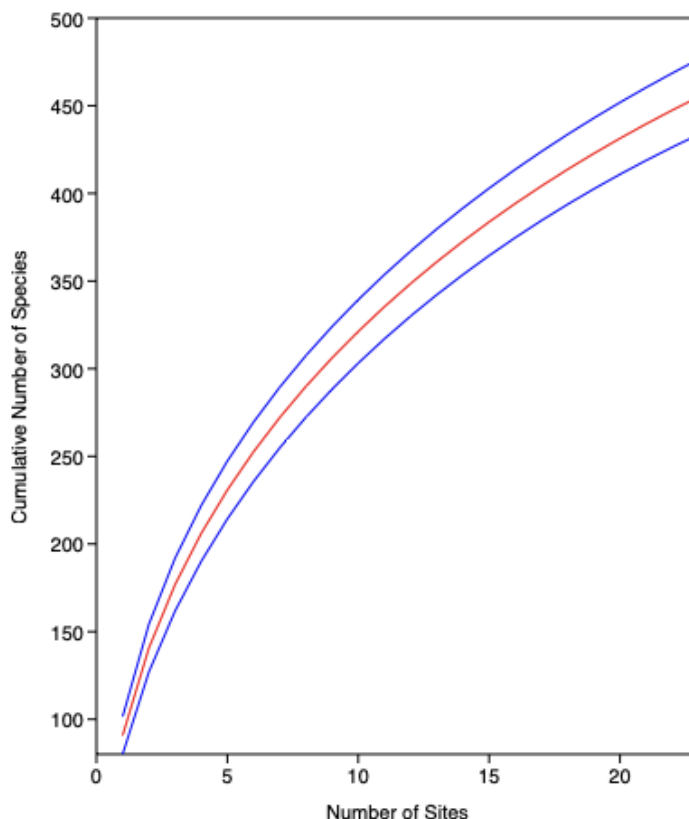


Table 6-17 The number of stained benthic foraminifera taxa (# of taxa), Shannon, Fisher’s alpha, and density for each site (all increments/horizons integrated).

| SITE | AREA | # OF TAXA | SHANNON | EVENESS | FISHERS ALPHA | DENSITY (50cm ²) |
|--------|------|-----------|---------|---------|---------------|------------------------------|
| STM001 | CTA | 75 | 3.712 | 0.5457 | 23.23 | 563 |
| STM002 | CTA | 82 | 4.024 | 0.6818 | 38.17 | 289 |
| STM003 | CTA | 88 | 4.151 | 0.7217 | 35.34 | 391 |
| STM004 | CTA | 89 | 3.901 | 0.5559 | 27.82 | 654 |
| STM005 | CTA | 96 | 4.253 | 0.7325 | 44.90 | 336 |
| STM007 | CTA | 101 | 4.065 | 0.5771 | 35.27 | 583 |
| STM008 | CTA | 93 | 3.932 | 0.5483 | 34.33 | 481 |
| STM010 | CTA | 79 | 3.815 | 0.5745 | 34.44 | 307 |
| STM012 | CTA | 100 | 4.414 | 0.8257 | 60.60 | 255 |
| STM013 | CTA | 114 | 4.349 | 0.6789 | 54.29 | 389 |
| STM014 | CTA | 84 | 4.049 | 0.6824 | 36.29 | 331 |
| STM015 | CTA | 85 | 4.152 | 0.7474 | 44.09 | 259 |
| STM016 | CTA | 85 | 4.096 | 0.7071 | 43.30 | 265 |
| SWM018 | WND | 85 | 4.092 | 0.7045 | 35.29 | 357 |
| SWM019 | WND | 121 | 3.851 | 0.3887 | 41.01 | 743 |
| SWM025 | WND | 85 | 4.125 | 0.7278 | 40.68 | 288 |
| SWM026 | WND | 96 | 4.253 | 0.7323 | 45.48 | 330 |
| SPR033 | PRZ | 99 | 4.106 | 0.6132 | 40.86 | 420 |
| SPR034 | PRZ | 82 | 4.042 | 0.6941 | 32.58 | 371 |
| SPR036 | PRZ | 84 | 3.792 | 0.5280 | 32.29 | 403 |
| SPR037 | PRZ | 88 | 3.998 | 0.6193 | 31.47 | 484 |
| SPR039 | PRZ | 67 | 3.819 | 0.6801 | 25.06 | 338 |
| SPR041 | PRZ | 112 | 4.233 | 0.6155 | 48.00 | 447 |

The number of species per site (all increments integrated) ranged from 67-121 species (mean: 91 ± 13 , $n=23$), Shannon ranged from 3.7-4.4 (mean: 4.1 ± 0.2), evenness ranged from 0.4-0.8 (mean: 0.6 ± 0.1) and Fisher's alpha ranged from 23.2-60.6 (mean: 38.5 ± 8.8) (Table 6-17).

The number of stained taxa at CTA sites (mean: 90 ± 3 , $n=13$) were similar to the number at WND (mean: 97 ± 8 , $n=4$) and PRZ sites (mean: 89 ± 2 , $n=6$). Shannon at CTA sites (mean: 4.1 ± 0.1 , $n=13$) was also very similar to the WND (mean: 4.1 ± 0.1 , $n=4$) and PRZ (mean: 4.0 ± 0.1 , $n=6$) sites. Evenness was also very similar between the site groups ($0.6-0.7 \pm 0.1$, $n=23$). Fisher's Alpha at CTA sites (mean: 39.4 ± 2.8 , $n=13$) and WND sites (mean: 40.6 ± 2.1 , $n=4$) were higher than PRZ sites (mean: 35.0 ± 3.3 , $n=6$)

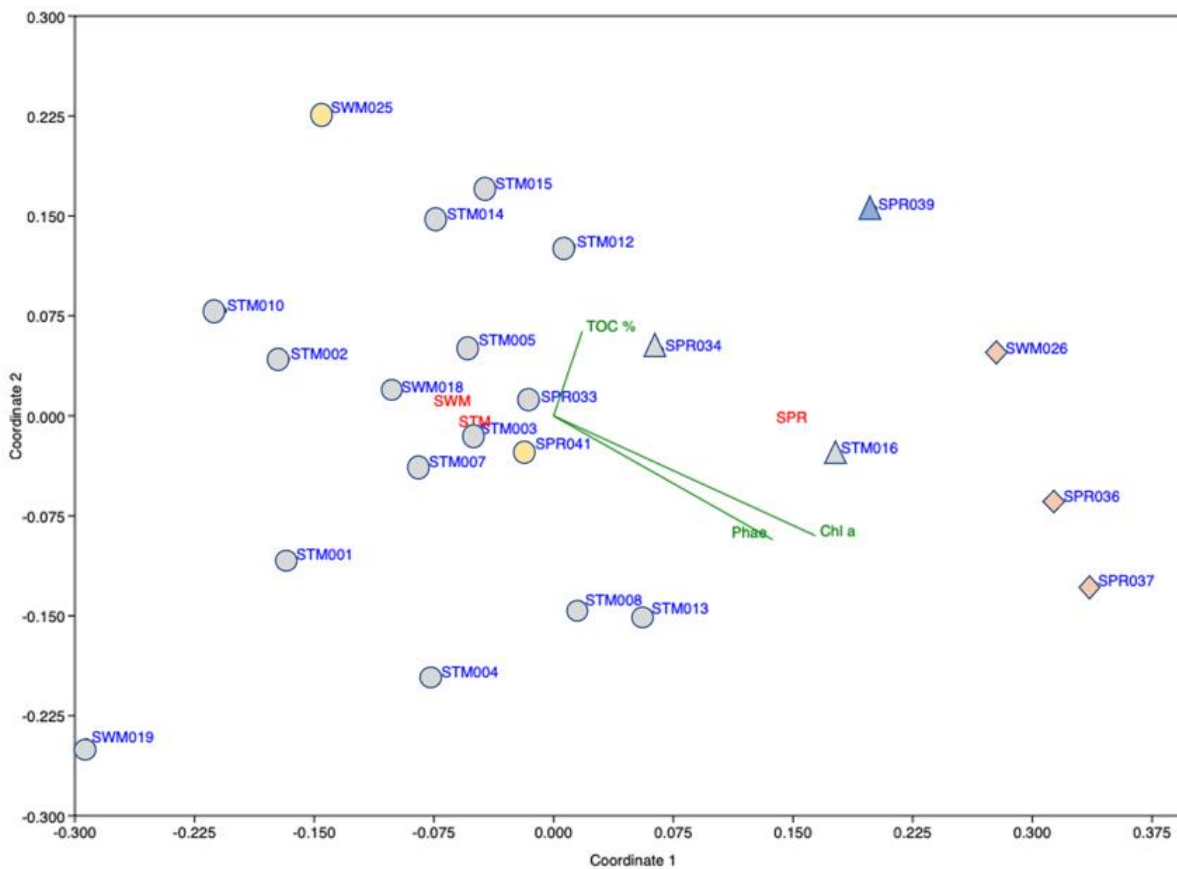
The number of benthic foraminifera taxa (coincident with Fisher's alpha) remained relatively high from the surface down to 4 cm at certain CTA sites (Figure 6-40), whereas these parameters both decreased gradually with depth at WND and PRZ sites.

This study represents one the most comprehensive quantitative foraminifera baseline studies from a mining contract area in the CCZ with 487 species identified and >25,000 individuals counted from 23 sites across PRZ, CTA, and WND. The total species number is comparable to the two previous major CCZ studies from Nozawa *et al.* (2006) and Gooday & Goineau (2019) who found 252 species and 580 species respectively. A sample-based rarefaction curve was generated based on the total amount of stained ("live") individuals found in all increments (0-1 cm, 1-2 cm, 2-3 cm, 3-4 cm, 4-5 cm) from all sites (Figure 6-37).

Over half (>250 species) of all species found in the NORI-D samples were considered monothalamous forms. This is consistent with previous studies from the UK-1, OMS, Kaplan East, and APEI-6 regions where monothalamids were largely dominant (Nozawa *et al.*, 2006; Kamenskaya *et al.*, 2012; Goineau and Gooday, 2017, 2019). Monothalamids are important for establishing diversity considering their dominance across abyssal plain systems. Since monothalamids are extremely fragile, we developed a gentle freeze-drying method capable of drying them without cellular distortion.

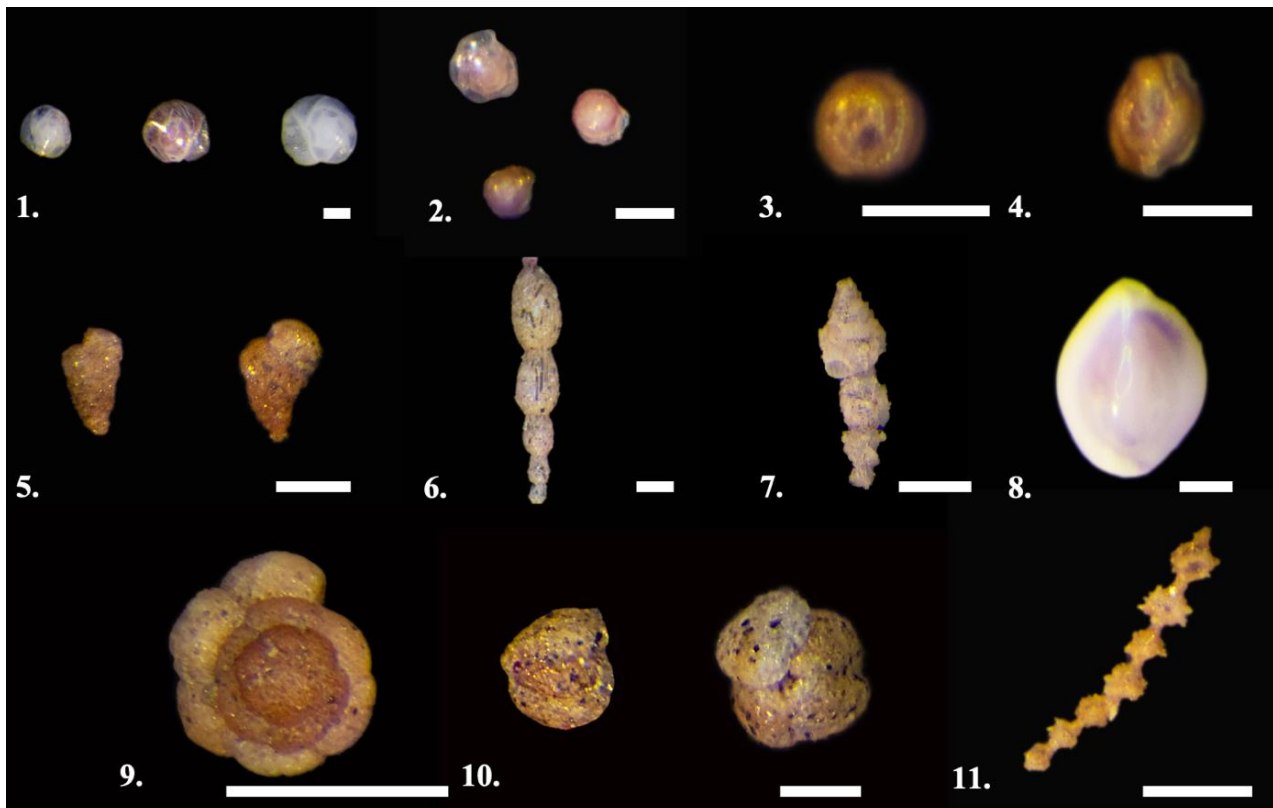
The baseline foraminiferal diversities (Table 6-17), calculated from 23 sites in the NORI-D contract area, ranged from 23.2-60.6 (Fisher's alpha) and 3.7-4.4 (Shannon Index), which is comparable to a similar study in the Ocean Mineral Singapore (OMS) and UK-1 contract areas by Goineau and Gooday (2019) that ranged from 27.4-85.0 (Fisher's alpha) and 3.2-4.6 (Shannon Index). These baseline diversities will be monitored for natural seasonal variability from Campaign 5D samples, then compared to future post-Collector Test samples to quantify disturbance.

Figure 6-38 Non-metric MDS plot of 23 multi-core sites in NORI-D including all complete stained (“live”) foraminifera. Green vectors represent environmental controls [%TOC (Total Organic Carbon), Phae (Phaeophytin), Chl-a (Chlorophyll-a)].



In order to determine the utility of the PRZ region as an appropriate control site, a non-metric MDS plot was generated using stained foraminifera to visualize qualitative groupings amongst sites and regions (Figure 6-38). Three of the six PRZ sites (SPR033, SPR034, SPR041) shared similarities with the CTA region, while the other three (SPR036, SPR037, SPR039) were dissimilar and grouped on their own. The SPR sites (SPR036, SPR037, SPR039) that grouped away from the STM sites were non-nodule sites so this may account for the difference in foraminiferal communities. Phytopigments (chl-a, phaeophytin), as depicted with the green vectors in Figure 6-38, also drive this difference in assemblage. The sites without nodules had an overall higher concentration of chlorophyll-a and phaeophytin. As a control region, the nodule sites in the PRZ, had comparable foraminiferal assemblages to the CTA region making these specific sites a good control. However, due to the heterogeneity of nodule type and geofom in the PRZ, not all sites are representative of this CTA region. The nodule-less sites in the PRZ may be a good predictor of future foraminiferal communities in CTA after Collector Test trials.

Figure 6-39 Micrograph plate of bioindicator species identified in the NORI-D contract area. Scale bar =100µm.



1) *Epistominella exigua* 2) *Alabaminella weddellensis* 3) *Glomospira charoides* 4) *Glomospira gordialis* 5) *Textularia agglutinans* 6) *Reophax dentaliniformis* 7) *Reophax scorpiurus* 8) *Quinqueloculina seminulum* 9) *Trochammina* sp. 1. 10) *Adercotryma glomeratum*. 11) *Hormosinelloides guttifer*.

Preliminary analysis also identified the presence of small indicator species *Epistominella exigua*, *Alabaminella weddellensis*, *Glomospira charoides*, and *Glomospira gordialis* (Figure 6-39) which have been deemed “opportunists” based on literature from sediment plume settling events (e.g. Deepwater Horizon blowout, Mt. Pinatubo ashfall, turbidites). It will be important to monitor the relative abundances of these species post-Collector Test as they will likely be the first to recolonize affected areas on a short-term timescale (months). At least one of these “opportunist” species have been identified at every site except for SPR036. The CTA region had a baseline average relative abundance of “opportunists” of 5.70% with a range of 0.38% to 9.97%. The WND region had a baseline average relative abundance of “opportunists” of 4.30% with a range of 1.21% to 6.72%. The PRZ region had a baseline average relative abundance of “opportunists” of 2.86% with a range of 0% to 5.39%. The total baseline average relative abundance of “opportunists” at all sites was 4.72% with a range of 0% to 9.97%.

This study also identified the presence of noted first-wave Pinatubo recolonizers (Kaminski *et al.*, 1988, 1995; Hess *et al.*, 2001): *Textularia* sp., *Reophax dentaliniformis*, *Reophax scorpiurus*, and *Quinqueloculina seminulum* (Figure 6-39). These infaunal first-wave recolonizing species dominated for up to three years after the ashfall event (Hess *et al.*, 2001). The CTA region had a baseline average relative abundance of “first-order recolonizers” of 2.35% with a range of 0.91% to 4.52%. The WND region had a baseline average relative abundance of “first-order recolonizers” of 3.55% with a range of 1.39% to 5.25%. The PRZ region had a baseline average relative abundance of “first-order recolonizers” of 2.79% with a range of 2.24% to 4.55%. The total baseline average relative abundance of “first-order recolonizers” at all sites was 2.67% with a range of 0.91% to 5.25%.

Second-wave recolonizers, such as *Trochammina* sp., *Adercotryma glomeratum* and *Hormosinelloides guttifer* (Figure 6-39), which were found to dominate three years after the Pinatubo ashfall, were also

identified at all 23 sites in NORI-D. The CTA region had a baseline average relative abundance of “second-order recolonizers” of 6.94% with a range of 1.80% to 11.55%. The WND region had a baseline average relative abundance of “second-order recolonizers” of 3.95% with a range of 2.12% to 7.00%. The SPRZ region had a baseline average relative abundance of “second-order recolonizers” of 3.95% with a range of 2.12% to 7.00%.

In the wake of nodule collection, a succession of these bioindicator types is expected. Foraminiferal recolonization rates are more rapid than cohabitating macrofauna (Kaminski *et al.*, 1988). First, the relative abundance of opportunists is expected to increase in the months-to-year timeframe. The “first-order recolonizers” should be coincidentally monitored as they are expected to increase in abundance as the opportunists decrease after the consumption of the organic matter from the initial sedimentation pulse. After the Pinatubo event, “second-order recolonizers” increased in abundance after three years, increasing diversity and competition, proving these species to be more useful in determining long-term recovery (Hess *et al.*, 2001). Monitoring these species will be crucial in understanding the impacts of deep-sea mining, the resilience of the benthic community, and the timetable for foraminiferal recovery.

(b) Sedimentology

At all sites and depths, silt and clay size particles (mud fraction) were predominant (Table 6-18). Overall (all sites and depths), gravel percentages ranged from 0.0-56.0% (mean: $3.4 \pm 0.7\%$, $n = 193$), sand percentages ranges from 0.0-51.0% (mean: $6.2 \pm 0.8\%$, $n = 193$), silt percentages ranged from 4.0-91.0% (mean: $67.2 \pm 1.2\%$, $n = 193$), and clay percentages from 4.0-52.0% (mean: $23.1 \pm 0.5\%$, $n = 193$). Gravel percentages were highest at CTA sites (mean: $5.1 \pm 1.4\%$, $n = 80$) when compared to WND sites (mean: $1.2 \pm 0.6\%$, $n = 50$) and PRZ sites (mean: $3.1 \pm 1.1\%$, $n = 63$). Sand percentages were higher at CTA (mean: $6.5 \pm 1.2\%$, $n = 80$) and PRZ (mean: $6.6 \pm 1.4\%$, $n = 63$) sites compared to WND sites (mean: $5.2 \pm 1.3\%$, $n = 50$). Silt was generally uniform throughout all CTA (mean: $66.2 \pm 2.2\%$, $n = 80$), PRZ (mean: $67.4 \pm 2.1\%$, $n = 63$) and WND (mean: $68.5 \pm 1.8\%$, $n = 50$) sites. Clay percentages were generally higher at WND sites (mean: $25.0 \pm 1.0\%$, $n = 50$) than both CTA (mean: $22.2 \pm 0.8\%$, $n = 80$) and PRZ (mean: $22.8 \pm 0.7\%$, $n = 63$).

There were higher gravel and sand percentages in the surface intervals (0-1 and 1-2 cm) primarily at CTA and PRZ (Figure 6-40). There were relatively low silt percentage in the surface interval (0-1 cm) and uniformly higher percentages with depth (1-4 cm) at CTA sites. Texture remains relatively uniform with depth at WND sites. Clay percentages were highest in the surface intervals (0-1) and uniformly lower at depth (1-4 cm) at PRZ sites. Silt was proportionately lower in surface intervals (0-1, 1-2 cm) and proportionately higher at depth (2-4 cm) at PRZ sites.

(c) Organic matter determination

At all sites and depths, total organic carbon (TOC) ranged from 0.5-1.1% (mean: $0.7 \pm 0.0\%$, $n = 40$). TOC was generally uniform amongst sampling areas as the mean TOC was $0.7 \pm 0.0\%$ for CTA ($n = 16$), WND ($n = 10$), and SPR ($n = 14$) individually as well. However, the upper TOC range was highest at WND(1.1%) as compared to CTA (0.8%) and WND (0.8%). The low TOC concentrations found in NORI-D are typical of abyssal plain sediments under oligotrophic conditions. These values are also consistent with TOC values from the BGR region (Volz *et al.*, 2018).

Table 6-18 Summary statistics (n: number of measurements, min: minimum, max: maximum, mean, and Std. error) for all sedimentary measurements [Chlorophyll-A concentrations (ug/g), phaeophytin concentrations (ug/g), gravel percentage, sand percentage, silt percentage, clay percentage, mud (silt+clay) percentage, and total organic carbon (TOC) percentage], presented for all sites and depth increments (depth, cm), STM sites, SWM sites, and SPR sites.

| SUMMARY STATISTICS | chl-a (ug/g) | phaeo (ug/g) | % GRAVEL | % SAND | % SILT | % CLAY | % MUD | % TOC |
|--------------------------|--------------|--------------|----------|--------|--------|--------|-------|-------|
| All Sites, Depths | | | | | | | | |
| N | 185 | 185 | 193 | 193 | 193 | 193 | 193 | 40 |
| Min | 1 | 2 | 0 | 0 | 4 | 4 | 9 | 0 |
| Max | 325 | 619 | 56 | 51 | 91 | 52 | 100 | 1 |
| Mean | 31.0 | 54.8 | 3.4 | 6.2 | 67.2 | 23.1 | 90.3 | 0.7 |
| Std. error | 2.8 | 5.2 | 0.7 | 0.8 | 1.2 | 0.5 | 1.4 | 0.0 |
| CTA | | | | | | | | |
| N | 80 | 80 | 80 | 80 | 80 | 80 | 80 | 16 |
| Min | 2.6 | 5.7 | 0 | 0.7 | 4.1 | 3.6 | 9.2 | 0.5 |
| Max | 137 | 246.4 | 56 | 49 | 91.1 | 46.3 | 99.3 | 0.8 |
| Mean | 26.6 | 47.2 | 5.1 | 6.5 | 66.2 | 22.2 | 88.4 | 0.7 |
| Std. error | 2.7 | 4.8 | 1.4 | 1.2 | 2.2 | 0.8 | 2.4 | 0.0 |
| WND | | | | | | | | |
| N | 45 | 45 | 50 | 50 | 50 | 50 | 50 | 10 |
| Min | 6.5 | 8.9 | 0 | 0.8 | 16.2 | 5.3 | 21.5 | 0.6 |
| Max | 111 | 200.1 | 28.2 | 50.3 | 84.7 | 52 | 99.2 | 1.1 |
| Mean | 31.1 | 54.1 | 1.2 | 5.2 | 68.5 | 25.0 | 93.5 | 0.7 |
| Std. error | 3.8 | 7.1 | 0.6 | 1.3 | 1.8 | 1.0 | 1.9 | 0.0 |
| PRZ | | | | | | | | |
| N | 60 | 60 | 63 | 63 | 63 | 63 | 63 | 14 |
| Min | 1.3 | 1.8 | 0 | 0.4 | 12.4 | 11.6 | 23.9 | 0.6 |
| Max | 325 | 619.1 | 43.3 | 51.1 | 86.8 | 37.4 | 99.6 | 0.8 |
| Mean | 36.9 | 65.5 | 3.1 | 6.6 | 67.4 | 22.8 | 90.2 | 0.7 |
| Std. error | 7.3 | 13.7 | 1.1 | 1.4 | 2.1 | 0.7 | 2.3 | 0.0 |

(d) Chlorophyll-a and phaeopigments

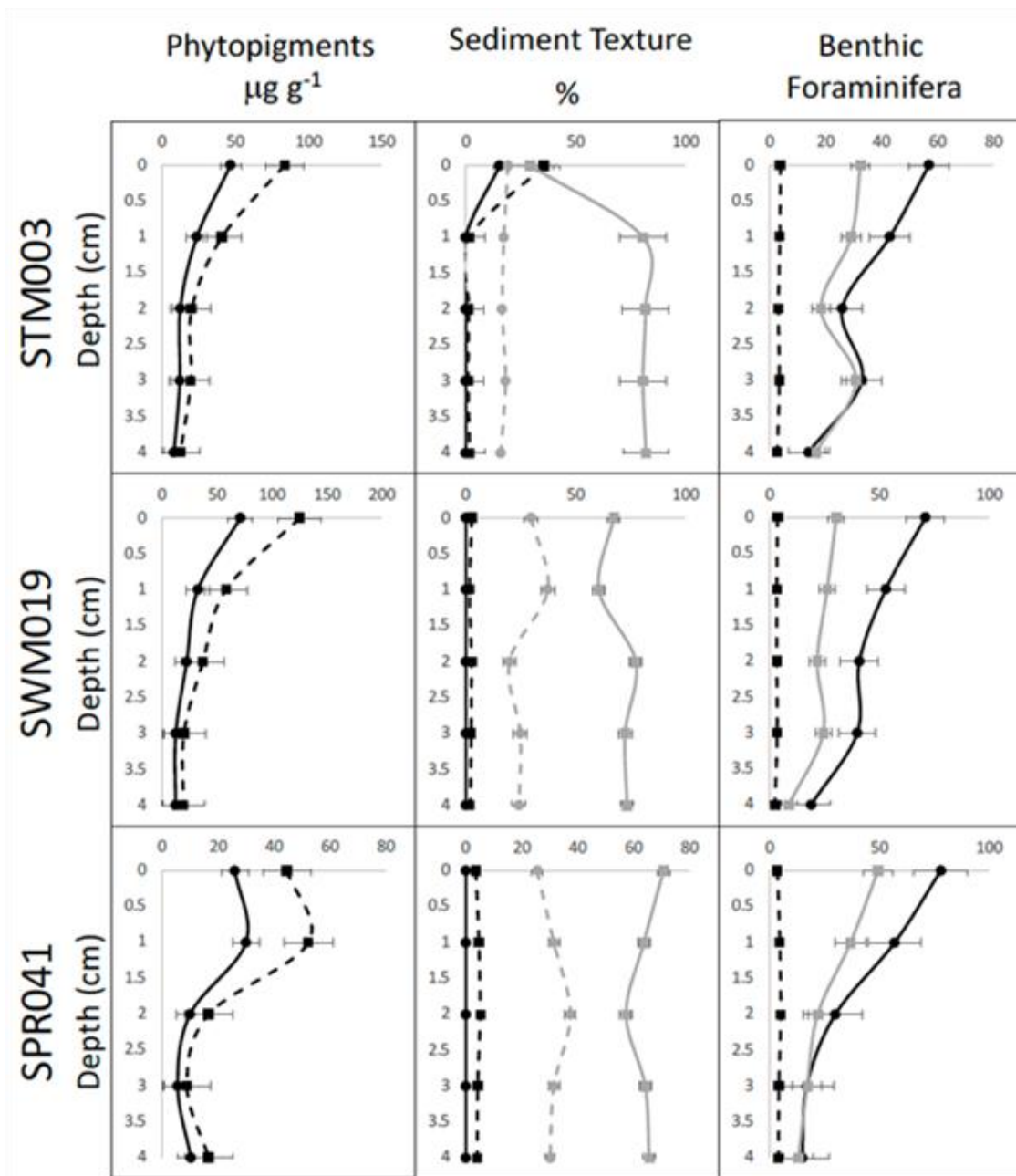
At all sites and depths, chlorophyll-a concentrations ranged from 1.0-325.0 $\mu\text{g g}^{-1}$ (mean: $31.0 \pm 2.8 \mu\text{g g}^{-1}$, n = 185) and phaeophytin concentrations ranged from 2.0-619.0 $\mu\text{g g}^{-1}$ (mean: $54.8 \pm 5.2 \mu\text{g g}^{-1}$, n = 185) (Table 2). Chlorophyll-a concentrations were highest at PRZ sites (mean: $36.9 \pm 7.3 \mu\text{g g}^{-1}$, n = 60) with lower concentrations at WND (mean: $31.1 \pm 3.8 \mu\text{g g}^{-1}$, n = 45) and lowest at CTA (mean: $26.6 \pm 2.7 \mu\text{g g}^{-1}$, n = 80) sites. Phaeophytin concentrations were highest at PRZ sites as well (mean: $65.5 \pm 13.7 \mu\text{g g}^{-1}$, n = 60) with lower concentrations at WND (mean: $54.1 \pm 7.1 \mu\text{g g}^{-1}$, n = 45) and lowest at CTA (mean: $47.2 \pm 4.8 \mu\text{g g}^{-1}$, n = 80) sites. While all other phaeophytin concentrations were near or below 200 $\mu\text{g g}^{-1}$, the surface increment (0-1 cm) phaeophytin concentration at site SPR035 was $619.1 \pm 24.9 \mu\text{g g}^{-1}$ and at site SPR037 was $551.6 \pm 16.1 \mu\text{g g}^{-1}$. These samples were measured six times during two separate subsampling events to ensure accuracy and quality control.

There were relatively high concentrations of both chlorophyll-a and phaeophytin in the surface intervals (0-1 cm) at CTA and WND sites and both gradually decreased with depth (Figure 6-40) with a step-wise decrease in the underlying layers (below 3 cm).

There were higher concentrations of TOC, phytopigments, gravel (within the CTA) and benthic foraminifera taxa (coincident with Fisher's Alpha) in the surface intervals (0-1 cm) at most sites that decreased gradually with depth. At certain PRZ sites, these parameters remained high from 0-2 cm depth. Considering the low accumulation rates of particulate matter in abyssal settings, this trend was consistent with deposition of the most labile TOC and phytopigments at the surface serving as the primary food source for this system (Hauquier *et al.*, 2019 and references therein). Below the surface layer, this labile particulate organic matter has likely been consumed or degraded. The presence of higher TOC and

phytopigment concentrations in the 1-2 cm layer in some cases may have been caused by bioturbation or potentially less consumption (lower consumer abundance) in these areas (Mayor *et al.*, 2012). Additional comparisons with meiofaunal and macrofaunal results will help ascertain the cause and better characterize food source consumption and carbon cycling.

Figure 6-40 Depth profiles from three example cores from each sampling area (STM003, SWM019, SPR041). Phytopigments are plotted in $\mu\text{g g}^{-1}$ with depth (cm), the solid black line is chlorophyll-a concentration and the dashed black line is phaeophytin concentration. Sediment texture is plotted in percentage (%) with depth (cm), gravel is the solid black line, sand is the dashed black line, silt is the solid gray line, and clay is the dashed gray line. Error bars represent standard error. Benthic foraminifera parameters include the number of taxa (solid black line), Shannon (dashed black line) and Fisher's Alpha (solid gray line).



6.3.6 eDNA-based Bioassessment of Eukaryotes

The monitoring of marine biodiversity is traditionally performed using morph-taxonomy-based methods (described above), focusing on selected morphologically identifiable biological quality elements (mega-, macro-, and meio- fauna).

As significant taxon gaps in DNA databases have been shown to limit the use of marine metabarcoding of macrofauna (Hestetun *et al.* 2020) environmental DNA (eDNA) can be used to complement these traditional methods (Valencia *et al.* 2016) and can be used to characterize microeukaryote communities (Shulse *et al.*, 2017).

To facilitate taxonomic studies and potential use of metabarcoding for future environmental impact assessments within the CCZ, new species are being described with type material stored in museums and DNA sequences uploaded to NCBI GenBank (e.g., Wiklund *et al.* 2019).

6.3.6.1 Purpose & scope

The following section describes the work conducted between 2020-2021 by the University of Hawaii and the Cawthron Institute to characterise natural baseline conditions of eDNA for eukaryote communities in the NORI-D contract area. The scope, the survey planning and the sampling methodologies carried out to ecologically characterise eukaryote communities align with International Seabed Authority ISBA/25/LTC/6 Rev 1. While not a requirement, NORI intend to carryout eukaryote DNA analysis simultaneously with traditional morpho taxonomic methods.

6.3.6.2 Baseline investigations

The methods and proposed survey array for both the collector test and long-term environmental studies on NORI-D will provide data to meet the following objectives:

1. Determine deep-sea eukaryotes diversity and biotic indices using sedimentary eDNA.
2. Determine the taxonomic composition of eukaryotes communities and identify abundant species.
3. Compare these data with data from other CCFZ regions.
4. Compare these data with morphotaxonomy-based methods.

6.3.6.3 Campaign activities

(a) Survey design and site selection

See 6.3.4.3(a) Meiofauna survey design and site selection

(b) Campaign 3

A collection of 112 sediments sub-samples were obtained from Campaign 3 resource box cores and samples were kept frozen at -80°C until analysis. Twenty-five samples were selected for analysis (Figure 6-41). For each sample, 2 sub-samples were selected for a total of 50 subsamples analysed.

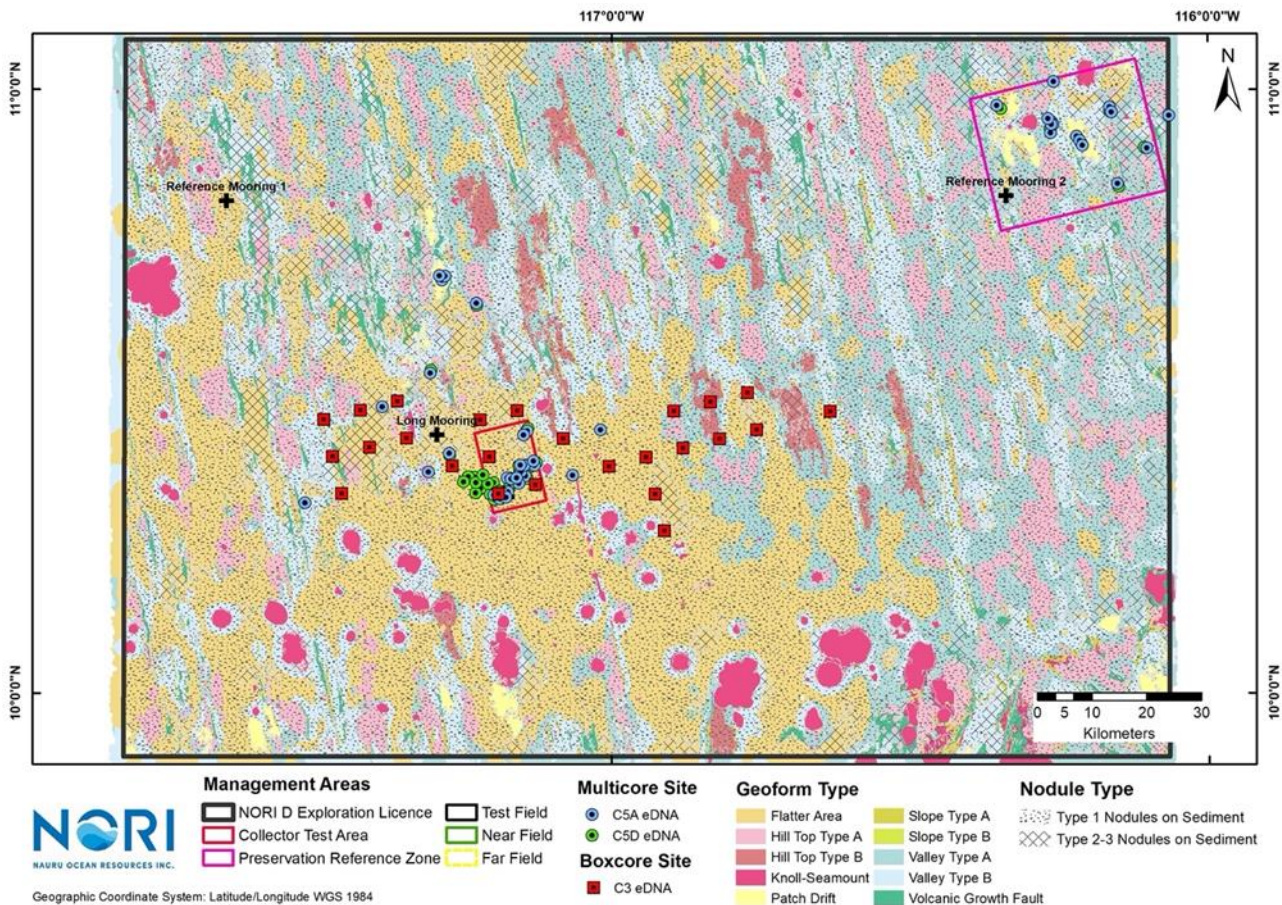
(c) Campaign 5A & 5D

Multicore samples (1 x core) were collected from 44 (C5A) and 42 (C5dD successful multicore deployments during the benthic campaigns. eDNA samples were sliced in the following sections (including nodules) 0-2 cm, 3-5 cm yielding 561 (C5A) and 558 (C5D), respectively.

6.3.6.4 Preliminary results & discussion

As a preliminary study, fifty sediment samples within NORI-D from Campaign 3 were collected from box-cores and shipped to ID-Gene ecodiagnosics in Switzerland for analysis.

Figure 6-41. Overview of eDNA samples collected within NORI-D



Over 60 million high-quality sequences were obtained for two nuclear ribosomal markers (18S V1V2 and 18S V9) targeting wide range of eukaryotic taxa (ID Gene ecodiagnosics, 2019).

Using eDNA analysis, eukaryotic OTUs were classified into 6 different categories (Alveolata, Excavata, Metazoa, Rhizaria, Stramenopiles and Others) (Figure 6-42). This was done for both markers (V1V2 and V9). Metazoa were classified into 5 categories (Annelida, Arthropoda, Nematoda, Nemertea and Other). The most abundant Metazoa OTUs assigned to the genus/species were reported in Figure 6-43. The taxonomic composition as depicted by the two markers presented a significance dominance of Nematoda and Annelida.

Fifty-seven sediment samples from the UK exploration area were analysed using the same protocol as with V9 marker. Alpha-diversity, beta-diversity and biotic indices were calculated and compared with the results obtained for NORI-D samples. While alpha-diversity and biotic indices did not significantly differ between the two sites (Figure 6-44), eukaryotic communities profiles showed a clear separation between NORI and UK samples. NORI samples communities also appeared less spread than the UK samples communities, indicating less variations in the composition of communities (Figure 6-44).

Figure 6-42 Taxonomic composition of eukaryotic communities using V1V2 and V9 markers and considering the richness (number of OTUs) or the abundance (number of reads).

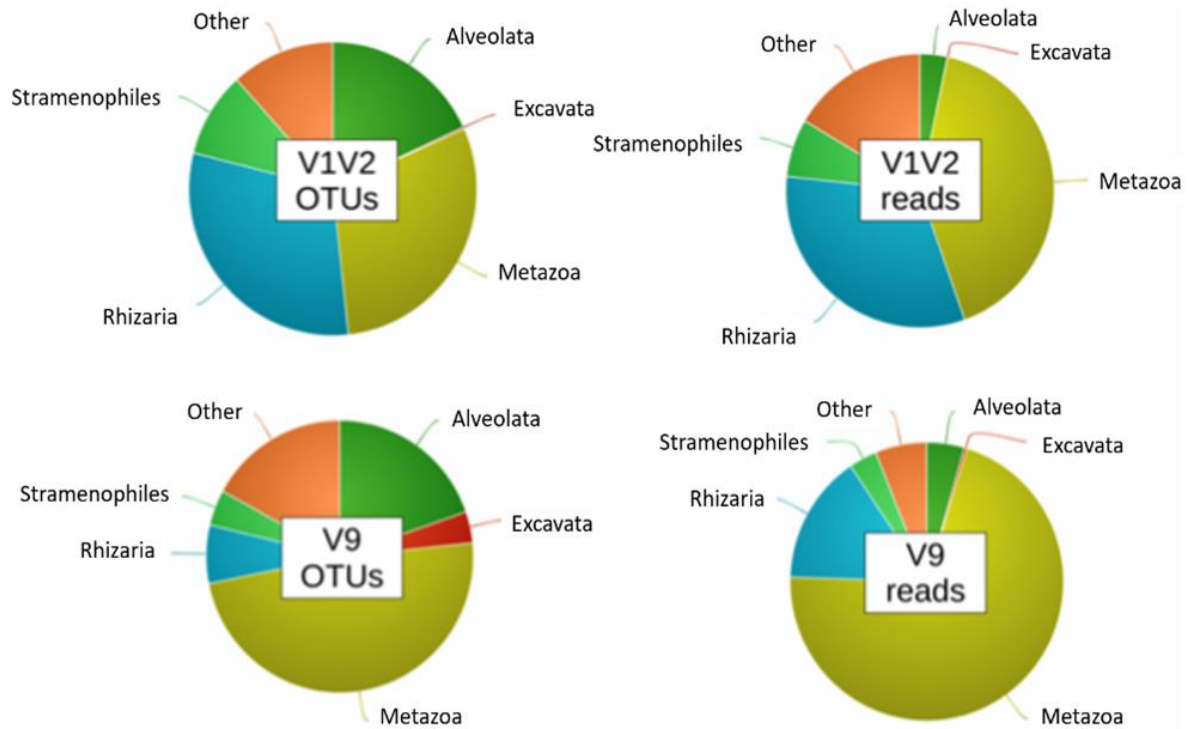


Figure 6-43 Taxonomic composition of Metazoa communities using V1V2 and V9 markers and considering the presence (OTUs) or the abundance (reads) of each OTU.

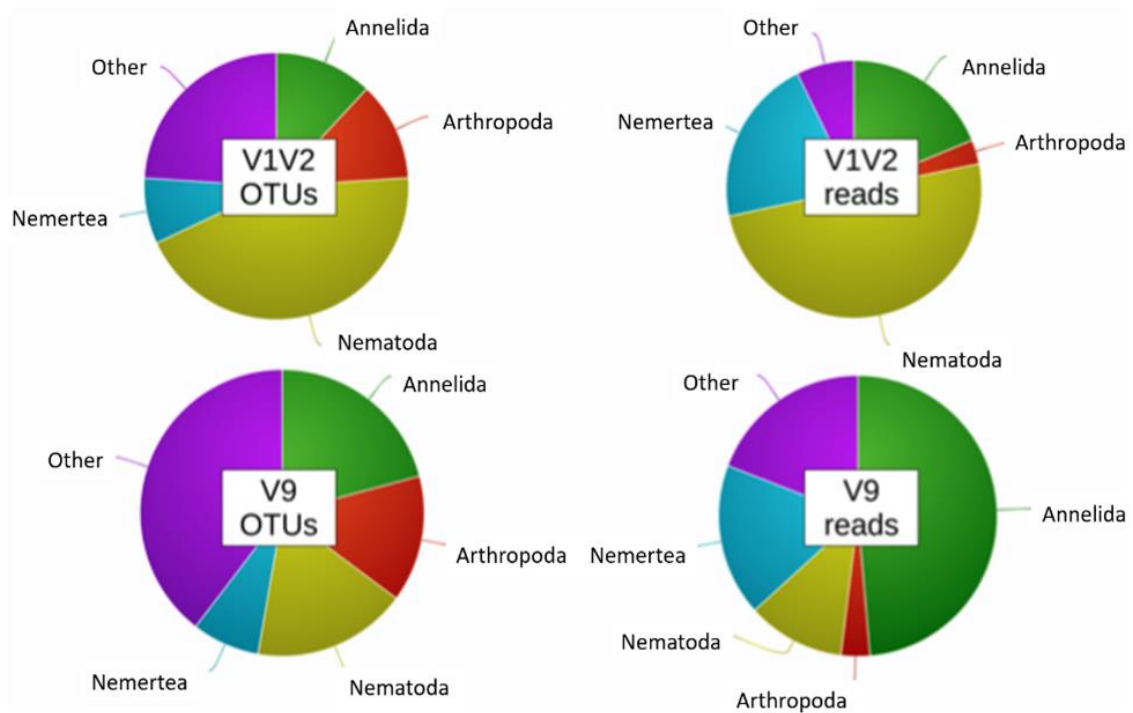
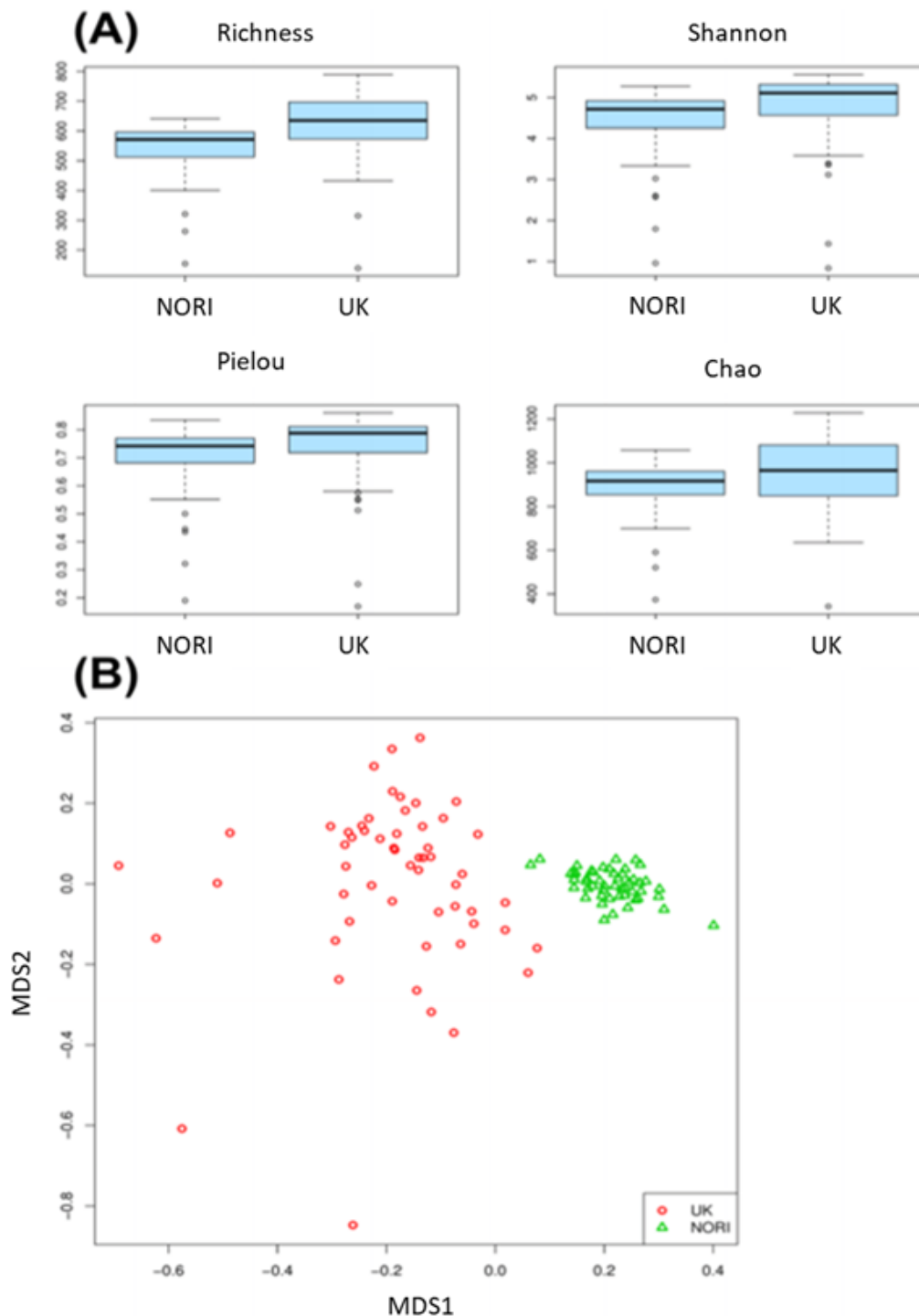


Figure 6-44 (A) alpha-diversity indices (B)NMDS calculated using V9 marker for UK area samples (red) and for NORI_D samples (green).



At the technical level, our analyses indicate that the 18S V1V2 and V9 markers provide a complementary view of deep-sea diversity. Although the taxonomic resolution of V1V2 barcode is not optimal for some taxonomic groups, numerous V1V2 sequences can be assigned to higher taxonomic level and more assigned OTUs are obtained providing better overview of total eukaryotic diversity changes.

Owing to Covid-19, samples from C5A and C5D have not yet been shipped to our contractor in New Zealand. These samples are still awaiting analysis.

6.3.7 Microbial Prokaryotes

To comprehensively characterize microbial communities, metabarcoding represents a convenient and efficient tool for deep-sea surveys due to its high sensitivity, high throughput, and low volumes of material needed. A few recent studies have taken advantage of eDNA metabarcoding to unveil the prokaryote assemblages associated with sediments and nodules within the CCZ (e.g., Wang *et al.* 2010; Dong *et al.* 2016; Lindh *et al.* 2017; 2018; Shulse *et al.* 2017).

Studies to date suggest regional similarity in taxonomic diversity and community composition across sampled areas of the CCZ, but clear differences per habitat type (i.e., sediment and nodule versus seawater samples) and cruises (likely due to differences in high-throughput sequencing library preparation) (ISBA 2020). While the available literature reveals some insights on microbial communities populating sediments and nodules within the CCZ, it is acknowledged that the current information provides poor temporal and spatial resolution, with most data deriving from sampling conducted in 2015 in the north-eastern section (including UK1, Ocean Mineral Singapore (OMS), and APEI 6 sites).

6.3.7.1 Purpose & scope

The following section describes the work conducted between 2020-2021 by the Cawthron Institute to characterise natural baseline conditions in microbiota in the NORI-D contract area. The scope, the survey planning and the sampling methodologies carried out to ecologically characterise the microbiota align with International Seabed Authority ISBA/25/LTC/6 Rev 1. Annex 1 section 41(e) Biological communities: Microbiota. to provide baseline data requirements under Recommendations III.A.13; III.B.14; III.B.15.(d).(i)–(ii); IV.B.22.

6.3.7.2 Baseline investigations

The methods and proposed survey array for both the Collector Test and long-term environmental studies on NORI-D will provide data to meet the following objectives:

- Characterize the relative abundance, composition, diversity, and the spatio-temporal variability of the taxonomic and functional prokaryotic community (focusing primarily on bacteria) within sediment core samples.

6.3.7.3 Campaign activities

(a) Survey design & site selection

See 6.3.4.3(a) Meiofauna survey design and site selection

(b) Campaign 5A & 5D

Multicore samples (1 x core) were collected from 44 (C5A) and 42 (C5dD successful multicore deployments during the benthic campaigns. eDNA samples were sliced in the following sections (including nodules) 0-2 cm, 3-5 cm yielding 561 (C5A) and 558 (C5D), respectively.

6.3.7.4 Preliminary results & discussion

Owing to COVID-19, samples from C5A and C5D have not yet been shipped to our contractor in New Zealand. These samples are still awaiting analysis.

6.3.8 Metazoan & Microbial Metabolic Activity

Upper-ocean dynamics (e.g., stratification) fluctuate through the year in open-ocean environments, which alters surface ocean primary production, and the export of particulate organic carbon (POC) to the

seafloor. At the seafloor, POC is either remineralised (Nomaki, 2005; Miller *et al.*, 2021; Arrigo, 2005; Hammond *et al.*, 1996) or shunted into deep-sea sediments by bioturbation where some of it becomes buried for millennia (Dunlop *et al.*, 2016; Dunne *et al.*, 2007; Hammond *et al.*, 1996). In areas where chemosynthesis does not occur, POC is thought to be one of the most important sources of organic matter for sustaining deep-sea ecosystems (Smith *et al.*, 2008; Danovaro *et al.*, 2008, Smith *et al.*, 2009).

Previous studies have observed an increase in the rate of surface primary production, and hence POC flux, to abyssal depths from the north to south and from the west to east in the CCZ (Lutz *et al.*, 2007; Smith *et al.*, 1997; Berelson *et al.*, 1997; Cecchetto, in prep) because of enhanced upwelling along the western side of the America's and along the equator. In the eastern CCZ, the annual flux of POC is approximately $1 \text{ g C m}^2 \text{ y}^{-1}$ (Amon *et al.*, 2016). This is twice the rate of the flux that occurs in the western CCZ (Smith *et al.* 1997; Smith and Demopoulos 2003) but is still relatively low in comparison to other abyssal regions (e.g., PAP in the northeast Atlantic, Station M in the northeast Pacific; Amon *et al.*, 2016). Seasonal changes in surface productivity and POC flux are well documented, but interannual changes have seldom been documented in the eastern CCZ.

Sediment Community Oxygen Consumption (SCOC) and seafloor nutrient flux estimates are commonly used state-of-the-art methods to measure the overall benthic activity and biogeochemical processes and thus, seafloor ecosystem function. In situ measurements carried out directly at the seafloor are the optimal technique to quantify fluxes across sediment-water interface, since in situ hydrodynamics are not readily reproduced in laboratories. Samples can be altered chemically, physically and biologically, while being sampled at the seafloor, brought to the surface and processed on board; core recovery will change oxygen penetration and availability (through core heating, pressure release and lysis of labile organic matter). In situ exchange rates across the water-sediment interface are commonly measured by two approaches: 1) enclosed benthic chamber systems and; 2) O_2 concentration profiles in the benthic boundary layer determined by microsensors. Fluxes measured by benthic chamber incubations following the change in dissolved oxygen or nutrient concentration over time represent the total consumption (or total flux) including diffusion, as well as advective transport across the sediment-water interface due to benthic organisms (micro-, meio-, macrofaunal) activity flushing their burrows with overlying water (bio-irrigation). In contrast to total fluxes measured by chamber incubations, diffusive O_2 fluxes can also be measured by micro-profiling.

While the aforementioned benthic ecosystem functioning methods (e.g., SCOC, nutrient flux rates) provide information on seafloor respiration and nutrient cycling rates, they do not allow for the quantification of microbial metabolic activities or the metabolic activities of metazoans. Both functions are, however, key to regulating the amount of organic C that is ultimately sequestered in seafloor sediments – a key ecosystem function and service (Thurber *et al.* 2014). Previous investigations have measured microbial metabolic activities *ex situ* (i.e., onboard the ship) using recovered seawater samples or sediment cores (e.g., Bianchi and Garcin 1994, Tamburini *et al.* 2002, Molari *et al.* 2013).

However, shipboard experiments are subject to experimental artefacts from decompression and warming and can either stimulate or reduce microbial activity relative to in situ levels (Bianchi and Garcin 1994, Tamburrini *et al.*, 2002). Moreover, most metazoan organisms die when being retrieved from abyssal depths such that *ex situ* metazoan metabolic studies are not possible. In situ studies to measure benthic organism metabolic activities are therefore necessary. Pulse-chase experiments using isotopically enriched substrates are a powerful technique to quantify the metabolic activities of sediment-dwelling organisms, and the total amount of organic and inorganic carbon that is processed (Middelburg *et al.* 2000, van Oevelen *et al.* 2006, Sweetman *et al.* 2009, 2010, 2014b, 2016, 2019). In short, an isotope labeled substrate (e.g., ^{13}C -labeled algae or bicarbonate) is injected over the seafloor in situ inside a benthic chamber, and the uptake of ^{13}C is tracked into sediment-dwelling organisms. This makes it possible to quantify the rate of C-processing (i.e., metabolic activity), and identify the main groups of organisms responsible. Pulse-chase experiments have been carried out throughout the CCZ in the UK1

and OMS license areas (Sweetman *et al.* 2019) as well as in the western CCZ in APEI 1, 4 and 7 (Cecchetto *et al.* submitted).

6.3.8.1 Purpose & scope

The following section describes the work conducted between 2020-2021 by Heriot-Watt University to characterise natural baseline conditions in metazoan and microbial metabolic activity in NORI-D. The scope, the survey planning and the sampling methodologies are designed to ecologically characterise metabolic activity align with International Seabed Authority ISBA/25/LTC/6 Rev 1. Annex 1 section 41(e) Biological communities: Microbiota. to provide baseline data requirements. Results obtained from preliminary assessments of box core analysis conducted during Year 1 of the project are provided below.

6.3.8.2 Baseline investigations

The methods and proposed survey array for both the Collector Test and long-term environmental studies on NORI-D will provide data to meet the following objectives:

1. Establish the baseline benthic ecosystem function properties (inc. sediment respiration, metabolic activities of the benthos, nutrient fluxes).
2. Determine how these change with the abundance and type of nodules, as well as spatially and temporally across NORI-D.

6.3.8.3 Campaign activities

(a) Survey design and site selection

During Campaign 5D and 5E, lander deployments were conducted, with deployments spread geographically to capture depth and spatial variability (Figure 6-45).

(b) Campaign 5D

A benthic respirometer lander (Figure 6-46) was deployed eight times across eight abyssal sites – two within the PRZ and six in the CTA. Lander deployments ranged from 4127 to 4306 m in depth (Table 6-19). In total, four deployments were used to conduct pulse chase experiments, two for chemoautotrophy experiments and two for cold, filtered seawater injection (one including and one excluding sediment). All chambers where the injector failed to deploy were kept and processed as normal for background data.

Figure 6-45. A) Overview of lander operations within NORI-D; B) Collector Test Area (CTA); C) Preservation Reference Zone (PRZ)

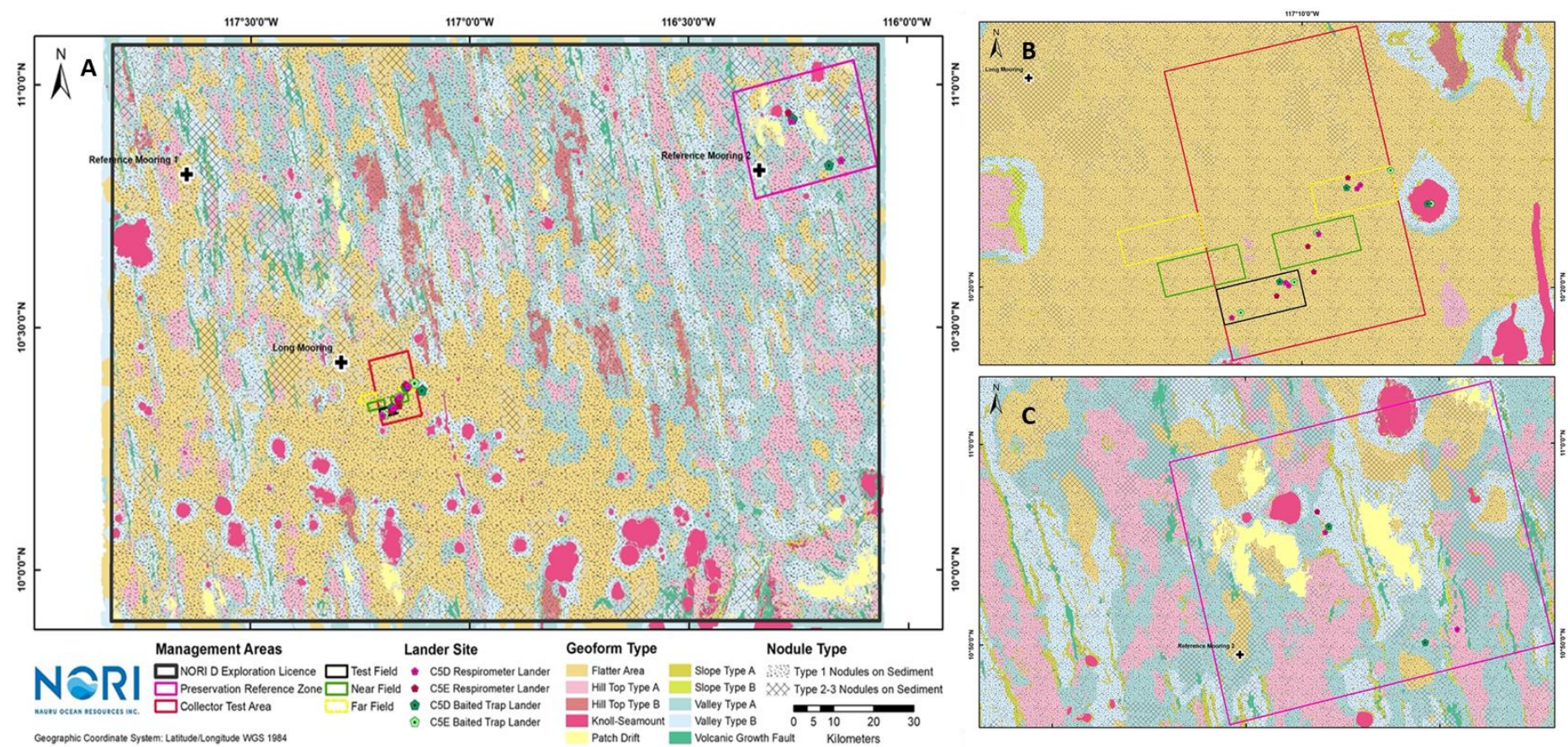


Figure 6-46 Front and side views (right to left) of the benthic respirometer lander used aboard Campaign 5D to conduct in situ incubation experiments



(c) Campaign 5E

Campaign 5E was completed on 21/12/2021, and as a result, preliminary data are not yet available. See (Figure 6-45) for deployment locations.

Table 6-19 Benthic respirometer lander deployments and experiments conducted during Campaign 5D. (During AKS287, sediment was excluded from the experiment as the chambers closed without penetrating the seafloor)

| DEPLOYMENT | AREA | LATITUDE (deg) | LONGITUDE (deg) | DEPTH (m) | INJECTED MATERIAL | # OF EXPERIMENTS |
|------------|------|----------------|-----------------|-----------|---|------------------|
| AKS268 | CTA | 10.3341 | -117.1727 | 4285 | Labelled <i>P. tricornutum</i> | 1 |
| AKS271 | CTA | 10.3353 | -117.1741 | 4284 | Labelled <i>P. tricornutum</i> | 0 |
| AKS273 | CTA | 10.3784 | -117.1412 | 4306 | Labelled <i>P. tricornutum</i> | 2 |
| AKS276 | CTA | 10.3801 | -117.1397 | 4306 | 1.75 g NaCl, 170 mg ¹³ HCO ₃ , 40 μM ¹⁵ NH ₄ Cl and 20 μM HPG | 2 |
| AKS279 | CTA | 10.3576 | -117.1589 | 4280 | Cold, 0.5-μm filtered seawater | 2 |
| AKS282 | PRZ | 10.9264 | -116.2649 | 4245 | Labelled <i>P. tricornutum</i> and 30 μM HPG | 1 |
| AKS286 | PRZ | 10.8453 | -116.1515 | 4127 | 1.75 g NaCl, 170 mg ¹³ HCO ₃ , 40 μM ¹⁵ NH ₄ Cl and 20 μM HPG | 1 |
| AKS287 | CTA | 10.3199 | -117.1990 | 4277 | Cold, 0.5-μm filtered seawater | 2 |
| AKS268 | CTA | 10.3341 | -117.1727 | 4285 | Labelled <i>P. tricornutum</i> | 1 |

| DEPLOYMENT | AREA | LATITUDE (deg) | LONGITUDE (deg) | DEPTH (m) | INJECTED MATERIAL | # OF EXPERIMENTS |
|------------|------|----------------|-----------------|-----------|-------------------------------|------------------|
| AKS271 | CTA | 10.3353 | -117.1741 | 4284 | Labelled <i>P. tricoratum</i> | 0 |

6.3.8.4 Preliminary results & discussion

(a) Sediment community oxygen dynamics

In all chamber incubations, O₂ optode sensors mounted in the lid of the chambers detected an initial increase in O₂ concentration from 184.6 ± 3.1 μmol L⁻¹ (n = 7) for approximately the first 4.5 hrs (Figure 6-47). Oxygen concentrations then continued to increase in 4 out of 6 in situ incubation experiments and peaked at 357.0 – 527.5 μmol L⁻¹ (Figure 6-47), which corresponded to a 187 – 285 % increase in seafloor O₂ concentration. Mean abyssal (3000-6000m water depth) sediment community oxygen consumption (SCOC) rates throughout the world's Ocean have been estimated to be 1.3 ± 0.2 mmol O₂ m⁻² d⁻¹ (± 1 standard error of the mean [SEM], n=308, Stratmann *et al.* 2019). While optode data showed an initial increase in O₂ concentration for the first hours in all the chambers, two experiments amended with DIC+NH₄ (AKS286-C3) and algae (AKS282-C3) showed net O₂ consumption rates of 0.9 - 1.1 mmol O₂ m⁻² d⁻¹ between 4.5 – 48 hrs that correspond well to the mean abyssal SCOC rate reported by Stratmann *et al.* (2019), as well as SCOC rates measured near to our study region (Khripunoff *et al.* 2006, Sweetman *et al.* 2019).

Independent Winkler analysis on seawater samples collected periodically over the course of the experiments also revealed increasing O₂ concentrations consistent with the optode data, thus providing evidence that the O₂ dynamics observed in the optode data was not caused by malfunctioning optode sensors. The O₂ concentrations derived from the Winkler analysis were, however, always lower than the optode measurements - a mismatch most likely explained by off-gassing of O₂ as indicated by the presence of bubbles in the syringes when the lander resurfaced. In the 4 algal incubations, Winkler-derived O₂ concentrations increased significantly from a mean of 194.2 ± 13.4 μM (SEM, n = 4) at 0.1 hr to 303.5 ± 48.2 μM (SEM, n=4) after 47 hr (weighted least-squares regression model, r² = 0.31, P = 0.005, n = 24), which corresponded to a seafloor O₂ production rate of 4.4 mmol O₂ m⁻² d⁻¹. No significant change in Winkler-derived O₂ concentrations was detected in the 3 DIC + NH₄ treatments although increasing O₂ concentrations were observed in the optode and Winkler data from one incubation experiment (AKS276-Ch3). To assess whether the O₂ increase observed in the algal incubations was due to the injection of the labelled algae culture, 2 extra in situ benthic experiments were undertaken to measure the seafloor response to the injection of cold, 0.45-μm filtered seawater. Again, both optode and Winkler datasets showed increasing O₂ concentrations in the chambers over the course of the experiment (optode-derived O₂ production: 16.1 mmol O₂ m⁻² d⁻¹, Winkler-derived O₂ production: 4.3 mmol O₂ m⁻² d⁻¹).

(b) Bacterial carbon uptake at seafloor

Bacterial carbon uptake rates decreased from 0.047 ± 0.012 mg C m⁻² d⁻¹ (n = 4, ±SE) to 0.009 ± 0.004 mg C m⁻² d⁻¹ (n = 3, ±SE), respectively between 0-2 and 2-5cm sediment depth (Figure 6-48). Bacterial carbon uptake rates ranged from 0.055 mg C m⁻² d⁻¹ (n = 1) at ASK268 (CTA), to 0.063 ± 0.064 mg C m⁻² d⁻¹ (n = 2, ±SE) at AKS273 (CTA) and 0.035 mg C m⁻² d⁻¹ (n = 1) at AKS282 (PRZ). Statistically significant differences between all locations cannot yet be determined as there are insufficient sample sizes. However, bacterial C uptake appears to not significantly differ between sample sites (Figure 6-49).

Figure 6-47 Change in oxygen concentration through time in different benthic chamber experiments. The green lines refer to incubations with isotopically labelled algae; the blue lines refer to incubations with labelled $D^{13}C$ and $^{15}NH_4$, and the red line is from an experiment where cold filtered (0.45-micron) seawater was injected. The black line is O_2 data recorded from outside the chamber.

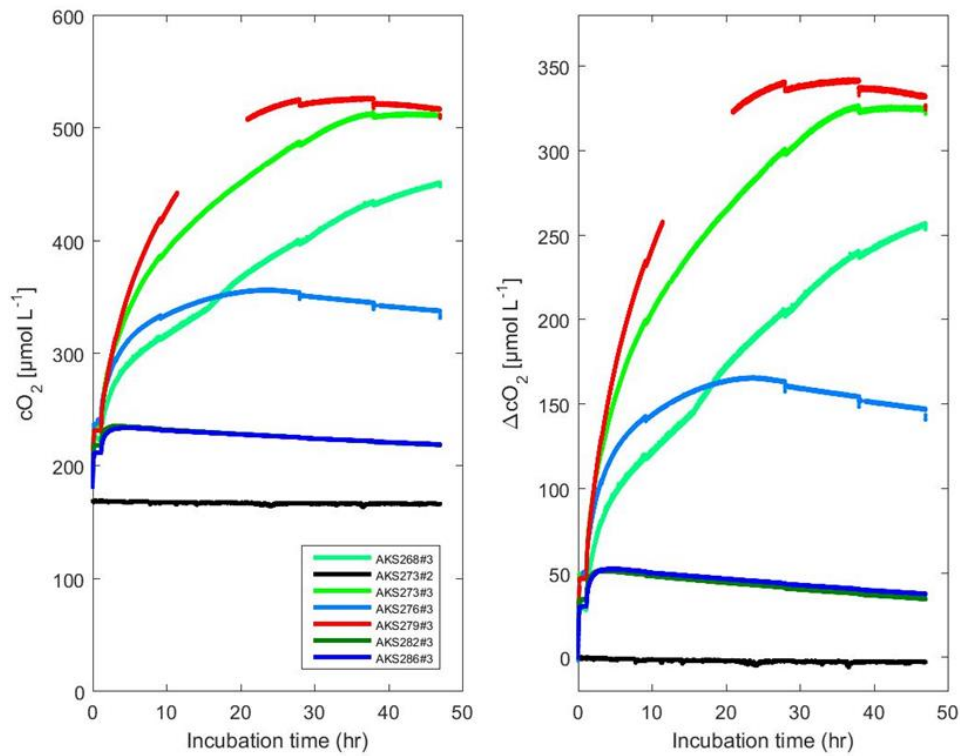


Figure 6-48 Average bacterial C uptake ($\text{mg C m}^{-2} \text{d}^{-1}$) between 0 to 2 ($n = 4, \pm \text{SE}$) and 2 to 5 cm ($n = 3, \pm \text{SE}$) sediment depths from the algal addition experiments.

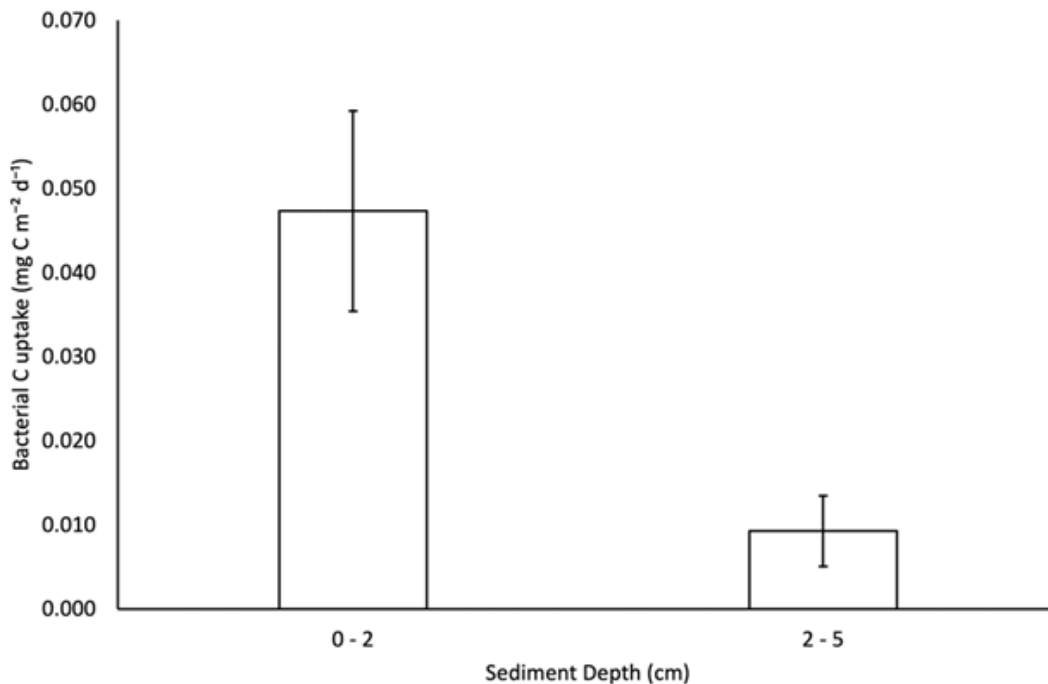


Figure 6-49 Average bacterial carbon uptake rates ($\text{mg C m}^{-2} \text{d}^{-1}$) between deployment locations AKS268 ($n = 1$), AKS273 ($n = 2, \pm \text{SE}$) and AKS282 ($n = 1$).

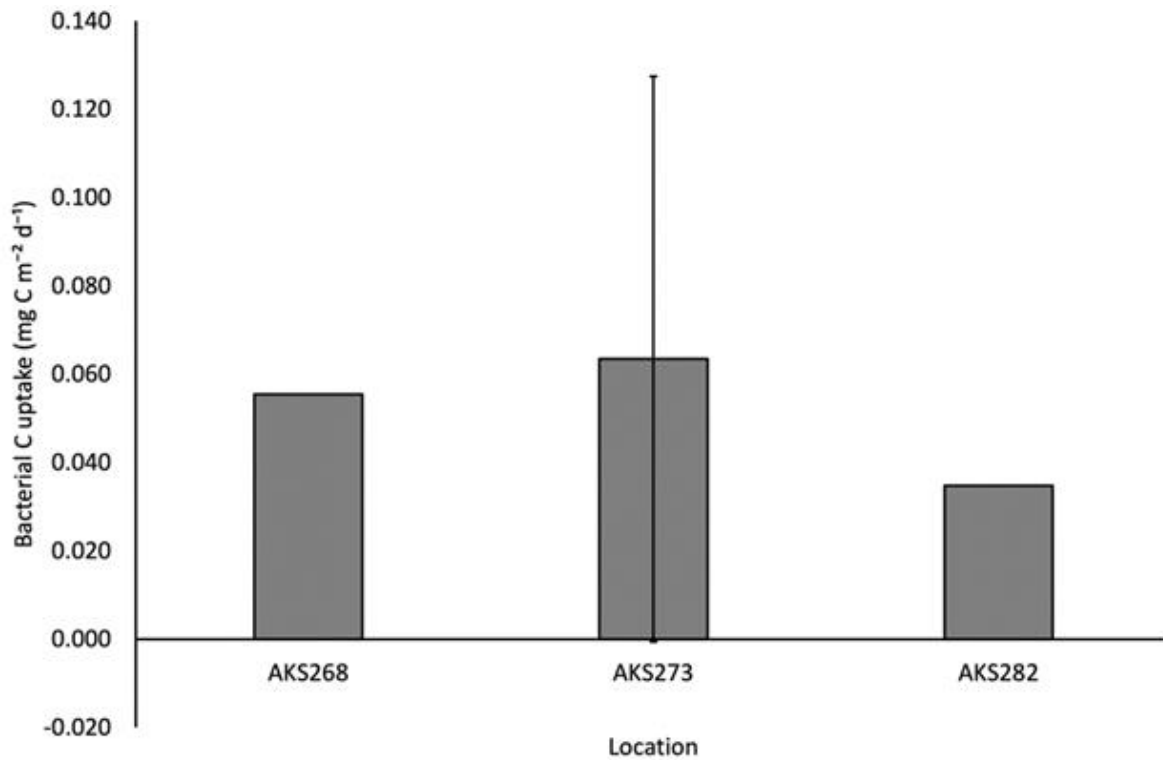
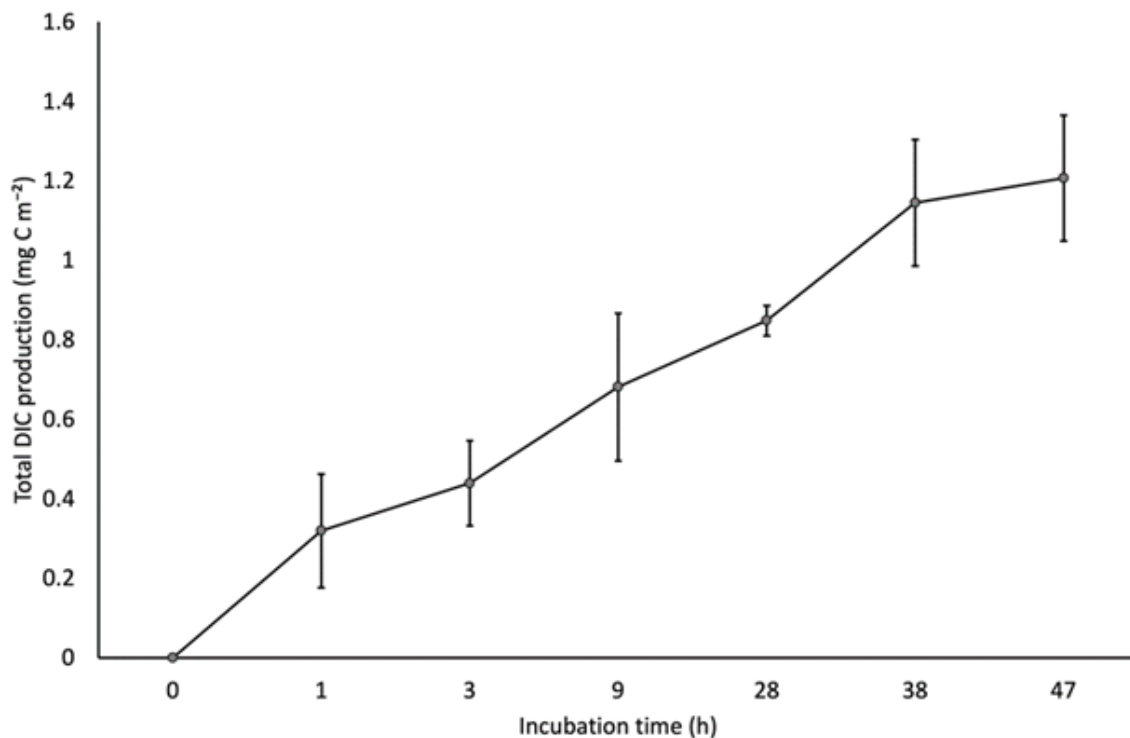


Figure 6-50 Average total DIC production (mg C m^{-2}) in algal addition experiments over the 47-hour incubation period for AKS268, AKS273 and AKS282 ($n = 3, \pm \text{SE}$; except for $t = 28 \text{ h}$, where $n = 2$).



(c) DIC production

Average total DIC production in algal addition experiments increased steadily over the 47-hour incubation period from 0 to $1.207 \pm 0.158 \text{ mg C m}^{-2}$ ($n = 3, \pm \text{SE}$; Figure 6-50). The rate of increase peaked between

0 and 1 hour at 0.319 ± 0.143 mg C m⁻² (n = 3, ± SE), then remained consistent until 38 hours, where it began to plateau towards the end of the incubation period. Average DIC production in the algal addition experiments was found to be 0.616 ± 0.081 mg C m⁻² d⁻¹ (n = 3, ± SE). Bacterial C-uptake rates were approx. 10% of the total DIC production values, which is consistent with trophic transfer efficiency in ecological food webs.

(d) Nutrient fluxes across the sediment water interface

Between background (n = 3, ± SE) and algal addition (n = 4, ± SE) experiments, ammonium flux rates ranged from -3.228 ± -1.863 to -1.448 ± 1.359 μmol/m²/h, nitrite from 0.092 ± 0.357 to 0.154 ± 0.099 μmol/m²/h, nitrate from 1.413 ± 50.08 to 36.93 ± 77.91 μmol/m²/h, NO_x from 1.505 ± 50.07 to 37.08 ± 77.96 μmol/m²/h, phosphate from 1.811 ± 2.125 to 2.584 ± 2.067 μmol/m²/h and silicate from -263.1 ± 238.9 to 56.67 ± 163.5 μmol/m²/h, respectively (Figure 6-38). After checking for normality and heteroscedasticity within the dataset, two-tailed t-tests were performed to determine if the addition of algae during in situ experiments had a significant effect on nutrient fluxes in and out of the sediment. All nutrient fluxes were found to not significantly differ between background and algal addition experiments: ammonium (t (2.7939) = 0.53137; p = 0.6345), nitrite (t (2.2132) = 0.16664; p = 0.8811, nitrate (t (4.7697) = 0.38348; p = 0.7179), NO_x (t (4.7684) = 0.384; p = 0.7175), phosphate (t (4.7444) = 0.26069; p = 0.8053) and silicate (t (3.761) = 1.1045; p = 0.335).

Figure 6-52 and Figure 6-53 depict the ranges in nutrient fluxes between deployment locations, across which all nutrients display a change between influx and efflux rates with no obvious pattern. Statistically significant differences between the CTA and PRZ and between all locations cannot yet be determined as there are insufficient sample sizes.

Figure 6-51 Average a) ammonium, b) nitrite, c) NO_x, d) nitrate, e) phosphate and f) silicate flux rates (μmol/m²/h) between background (n = 3, ± SE) and algal addition (n = 4, ± SE) experiments.

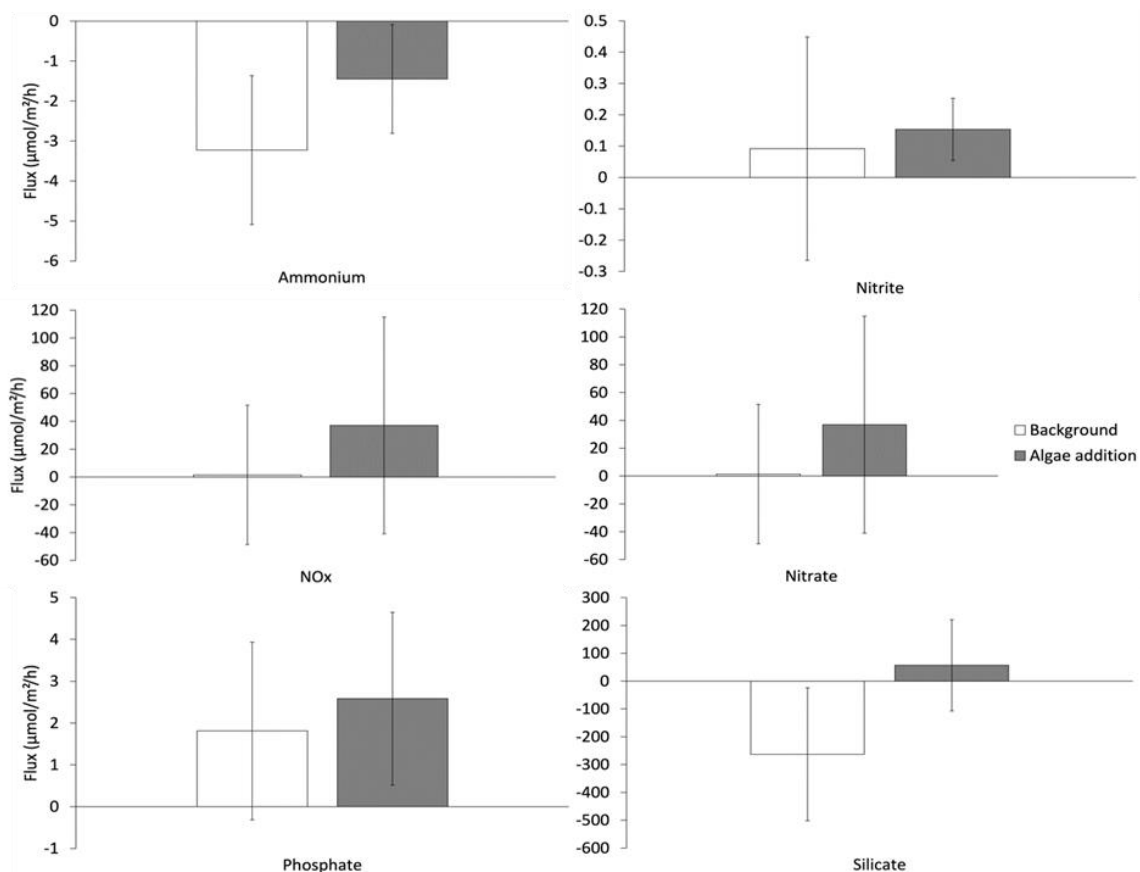


Figure 6-52 Average nitrate, NOx and silicate fluxes at four different deployment locations: AKS268 (CTA; n = 1), AKS271 (CTA; n = 2), AKS273 (CTA; n = 2), AKS282 (PRZ; n = 2).

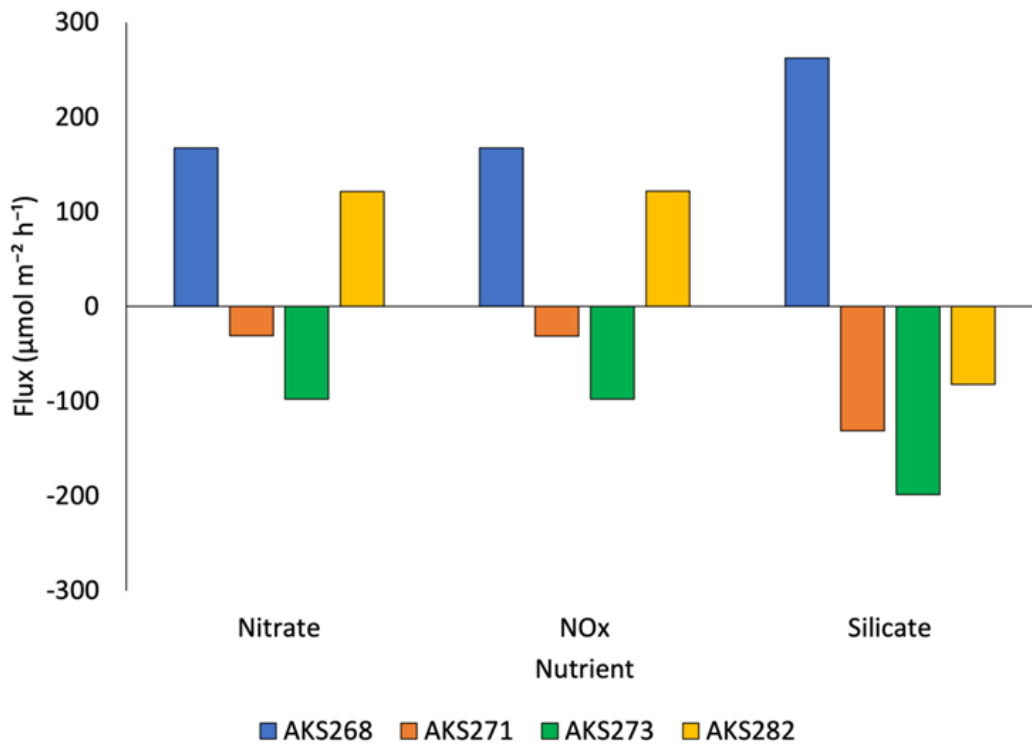
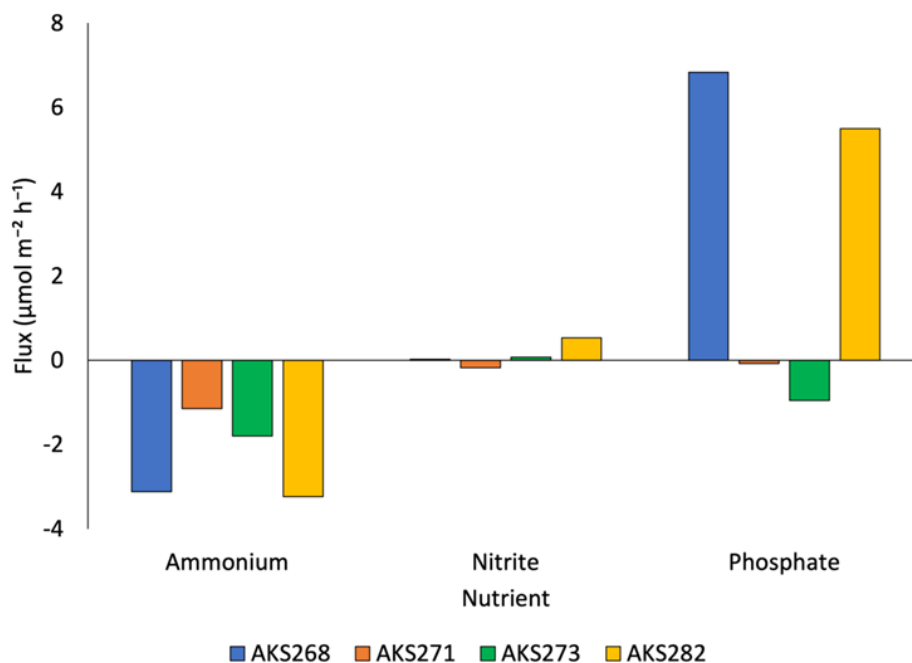


Figure 6-53 Average ammonium, nitrite and phosphate fluxes at four different deployment locations: AKS268 (CTA; n = 1), AKS271 (CTA; n = 2), AKS273 (CTA; n = 2), AKS282 (PRZ; n = 2).



Sediment community oxygen consumption (SCOC) data showed respiration rates in agreement with typical abyssal SCOC rates, and these were also consistent with rates measured in nearby license areas.

Average rates of bacterial carbon uptake, which indicate one aspect of benthic metabolic activity, a decrease from shallower to deeper sediment. Bacterial carbon uptake appeared to not significantly differ between sample sites (e.g., CTA vs. PRZ), but were lower than microbial metabolic rates measured in

the nearby OMS and UK-1 sites (Sweetman *et al.* 2019). Nutrient fluxes were not found to significantly differ between background and algal addition experiments, suggesting no change in organic matter remineralisation processes in response to phytodetrital inputs, which together with the findings of much lower bacterial C-uptake rates in NORI-D relative to the UK1 and OMS sites indicate a rather inactive microbial community at NORI-D.

Fluxes of all nutrients between deployment locations showed no clear spatial patterns and a high degree of heterogeneity across the PRZ and CTA within NORI-D. In contrast to nutrient flux data, the total DIC production rates did not appear to vary that greatly between deployment locations, suggesting a consistent pattern across the license area.

Overall, further sampling is needed from both the CTA and PRZ to properly elucidate statistically significant spatial patterns as often sample sizes were only just sufficient in size to permit statistical analyses. It may also be necessary to sample over smaller spatial scales to observe subtle changes in benthic ecosystem functions.

6.3.1 Trace Metals and Potential Toxic Elements

Identifying appropriate ecotoxicological endpoints for deep-sea taxa exposed to sediment plumes or their potentially toxic constituents, provides useful tools for evaluating the effects of such activities on the bioavailability of metals in deep-sea environments to guide regulatory decision-making and the implementation of effective mitigation measures and monitoring programmes.

Previous attempts to monitor the consequences of polymetallic nodule mining have failed to tackle the release of toxic metals, focussing rather on biological community response and recovery to sediment redeposition (Borowski and Thiel, 1998; Jones *et al.*, 2017; de Jonge *et al.*, 2020; Simon-Lledó *et al.*, 2019). The DISCOL experimental site was most recently re-surveyed in 2015, 26 years after the initial disturbance experiment, and had yet to recover to its baseline condition. The site showed significantly lower species diversity than reference sites with marked changes in community structure and impaired food-web functioning (de Jonge *et al.*, 2020; Simon-Lledó *et al.*, 2019). These results were similar to those found in simulation sites in the CCZ more than 20 years after disturbance (Jones *et al.*, 2017; Vanreusel *et al.*, 2016). To better assess the biological impact of toxic metals in the deep-sea, it is necessary to develop protocols that accurately measure the effects of contamination in the environment. Ideally, such protocols would be carried out at depth, or simulated depth (Lemaire, 2017), though this can be challenging.

As of later 2021, there are yet to be any studies assessing the metal tissue concentration in fauna inhabiting the CCZ. The only comparable study carried out in an area rich in polymetallic nodules, the Peru Basin, sampled epibenthic organisms (from the sediment or adhered to nodules) from undisturbed areas, and scavenging amphipods from the DISCOL experimental area prior to the disturbance and three years after. This study found higher concentrations in Peru Basin fauna than comparable studies in coastal and hydrothermal vent environments. It is unknown if similar situation can be expected in the CCZ, though, as the two sites have significantly different biogeochemical characteristics (Paul, 2019).

Evaluating toxicity of metals in sediment plumes requires investigating both the response of representative organisms to toxic exposures and the effects of biological and physico-chemical properties of deep-sea sediments under deep-sea conditions have on the bioavailability of metals (Koschinsky, Borowski and Halbach, 2003). The vast majority of existing ecotoxicological data is representative of shallow-water taxa in shallow-water conditions, and whether such taxa are appropriate ecotoxicological proxies for deep-sea organisms remains tentative (Brown, Thatje and Hauton, 2017; Brown *et al.*, 2017; Brown and Hauton, 2018; Brown *et al.*, 2019; Mestre *et al.*, 2019a; Mevenkamp *et al.*, 2017; Pinheiro *et al.*, 2019, 2021). The resilience of organisms to metal exposure is highly dependent on their physiology, and evidence suggests that adaptations to environmental conditions of the deep-sea,

such as high hydrostatic pressure, low temperature, and little-to-no light, may affect sensitivity to stress (Brown, Thatje and Hauton, 2017; Mestre, Calado and Soares, 2014; Mestre et al., 2019a; Somero, 1990, 1992). Likely because the energy-dependent processes of detoxification will compromise the energy available for basal maintenance in a habitat where energy constraints are already high.

Though ecotoxicological data exist for key metals likely to be released into solution by these processes for shallow-water species and a small number of deep-sea species, there are few available on the toxicity of mineral sulfides (Brown and Hauton, 2018; Simpson and Spadaro, 2016), mineral oxides, their complex dissolved components, and interacting effects that would occur within a sediment plume. No data exist for deep-sea taxa in terms of the latter, rather studies have focused on shallow-water taxa as ecotoxicological proxies for deep-sea organisms. No studies have been conducted to investigate the complex effects of combined dissolved, mineral, and particulate constituents of a sediment plume. And few studies have examined the toxicity of deep-sea sediments collected from regions, such as polymetallic nodule fields, with natural high heavy metal contents, under laboratory conditions, simulated deep-sea conditions, or *in situ*. One such study examined the toxicity of sediment elutriates from the Northwestern Mediterranean on the larvae of two shallow-water crustaceans. While exposure to concentrations of elutriate exhibited lethal and sublethal responses in both species, the chemical characterisation of elutriate was limited to a measure of total metals (Gambardella et al., 2021), not accounting for complex metal interactions that might affect bioavailability under test conditions. Research is being undertaken to better understand deep-ocean biogeochemistry; however, the antagonistic and synergistic effects of elements present in deep-sea sediments and their effects on heavy metal bioavailability and other biological effects on deep-sea biota remains unknown.

6.3.1.1 Purpose & scope

The following section describes the work conducted between 2020-2021 by the NHM, University of Gothenburg and NOC to characterise natural baseline conditions in trace metals in the tissues of key taxa in the NORI-D contract area. The scope, the survey planning and the sampling methodologies carried out to ecologically characterise seabed megafaunal communities align with International Seabed Authority ISBA/25/LTC/6 Rev 1. Annex 1 section 45 Trace Metals and potential toxic elements to provide baseline data requirements under Recommendation VI.D.40.(f).

6.3.1.2 Baseline investigations

The methods and proposed survey array for both the collector test and long-term environmental studies on NORI-D will provide data to meet the following objectives:

1. What are the baseline levels of metals in tissues of deep-sea taxa, what are the impacts of mining activities on exposure of deep-sea organisms to toxic substances, and what are the toxicological outcomes of these exposures?
2. Describe the movement of metals through the food web.

6.3.1.3 Campaign activities

(a) Survey design & site selection

During Campaign 5D and 5E, lander deployments were conducted opportunistically amid other operations throughout benthic and ROV campaigns. Deployments were spread geographically to measure depth and spatial variability (Figure 6-45).

(b) Campaign 5D

A baited trap deployed 5 times during campaign 5D (Table 6-20). The baited trap mooring consisted of a KUM Heavy Duty acoustic release, the trap, 15m of mooring line connected to 5 floatation spheres,

then an additional 5m of line connected to a flagpole with 2 flotation spheres. The trap was baited with Pacific mackerel by placing mackerel inside amphipod traps as well as in mesh netting that was tied inside the trap. Numerous fishhooks tied to 100lb monofilament line were connected to the outside of the trap and baited with Pacific mackerel. The trap was deployed 3 times in the CTA and 2 times in the PRZ of NORI-D during campaign 5D. Each deployment lasted approx. 48hrs on the seafloor.

Table 6-20 Baited trap lander deployment metadata. *Samples contain multiple organisms.

| DEPLOYMENT | STATION ID | AREA | LATITUDE (deg. dec. min) | LONGITUDE (deg. dec. min) | DEPTH (m) | # RAT TAILS | # CUSK EELS | # AMPHI-POD SAMPLES* |
|------------|------------|------|--------------------------|---------------------------|-----------|-------------|-------------|----------------------|
| AKS267 | STM_001 | CTA | 10°20.0250'N, | 117°10.5577'W | 4,287 | 2 | - | 26 |
| AKS269 | STM_014 | CTA | 10°22.7108'N, | 117°08.7293'W | 4,314 | 4 | - | 26 |
| AKS281 | SPR_033 | PRZ | 10°55.7933'N, | 116°15.7075'W | 4,257 | 3 | - | 24 |
| AKS284 | SPR_041 | PRZ | 10°50.0700'N, | 116°10.7425'W | 4,138 | 8 | 1 | 24 |
| AKS288 | STM_201 | CTA | 10°22.17'N, | 117°06.31'W | 4,147 | 7 | 1 | 31 |

(c) Campaign 5E

Campaign 5E was completed on 21/12/2021, and as a result, preliminary data are not yet available. See (Figure 6-45) for deployment locations.

6.3.1.4 Preliminary results & discussion

(a) Survey design and site selection

No data is presently available from the ecotoxicology assessments from the fishes and amphipods. This data should become available in the next 12 months as well as data on the baseline heavy metal concentrations in ophiuroids and holothurians that will be collected by the ROV during campaign 5E, and data on temporal changes in heavy metal concentrations in fish and amphipods.

Samples collected from NORI-D during Campaign 5D included deep-sea fish and large numbers of amphipods. Twenty-two rattails were caught in the baited trap, all of which were identified as *Coryphaenoides armatus*. Likewise, two cusk eel samples were captured, both of which were identified as *Barathrites iris* and are likely to be the same species as those seen on the baited-camera photographs.

The samples collected during campaign 5D/E and after test mining will undergo histological and histochemical assessments, and a small number of samples identified to genus level will be sent for transcriptomic sequencing. These analyses will help identify sublethal effects of potential toxic exposures that can be developed into effective biomarkers for monitoring purposes.

Once all samples have been collected from the remaining cruises and appropriately digested for analysis they will be sent to an ICP-MS Laboratory for quantitative trace elements analysis (including Fe, Mn, Ni, Zn, Cd, Pb, and Cu). This will be done to establish baseline metal concentrations in organism tissues from NORI-D.

6.4 Pelagic Baseline

Mid-water ecosystems have been studied very little in the CCZ, in part due to a focus on the specific effects of nodule collection on the seafloor habitats and communities. However, nodule collection and processing activities may have a variety of potential effects on biological communities in the ocean's mid-waters or pelagic realm (Christiansen *et al.* 2020; Drazen *et al.* 2019a; Drazen *et al.* 2020).

Deep mid-waters have established ecological and societal importance. These ecosystems represent more than 90% of the liveable volume on our planet (Robison 2009) contain a fish biomass 100 times greater than the global annual fish catch (Irigoien *et al.* 2014), connect shallow-living ecosystems to deeper ones including the benthos, and play key roles in carbon export (Boyd *et al.* 2019), nutrient regeneration, and in the provisioning of harvestable fish stocks (Drazen & Sutton 2017).

There have been limited studies of pelagic fauna in the benthic boundary layer (BBL) of the CCZ (Kersten *et al.* 2017; Kersten *et al.* 2019) with recent eDNA diversity studies for metazoans identifying the BBL as the most diverse region of the water column, highlighting the importance of targeted sampling within this depth horizon for baseline surveys (Laroche *et al.* 2020).

Water sampling from surface to seafloor has provided some information on surface phytoplankton (Zinssmeister *et al.* 2017) and water column microbial communities (Lindh *et al.* 2017; 2018; Shulse *et al.* 2017). These limited studies highlighted several key features of the CCZ upper and mid water column: 1) water column planktonic microorganisms are genetically distinct from those inhabiting the abyssal sediments or those associated with nodules (Lindh *et al.* 2017; Shulse *et al.* 2017); 2) the mid-water oxygen minimum zone (OMZ) plays a key role in structuring water column microbial distributions (Lindh *et al.* 2018). This OMZ varies vertically along an east-west gradient through the CCZ, with its vertical position shoaling upwards toward the eastern CCZ; and 3) water column microbial communities (eukaryotic and prokaryotic) segregate vertically, including a distinct and diverse assemblage of microbes in the mesopelagic waters (between approximately 200-1000 m; Shulse *et al.* 2017).

Studies of meso- and bathypelagic zooplankton and micronekton have been conducted around the CCZ but not within. Zooplankton and micronekton assemblages have been characterized in some areas of the central Pacific, including around Hawaii (De Forest & Drazen 2009; Drazen *et al.*, 2011; Landry *et al.* 2001; Reid *et al.* 1991; Sommer *et al.* 2017; Valencia *et al.* 2016; Young, 1978), in the equatorial region south of Hawaii (Barnett 1984; Clarke 1987) and in the Costa Rica Dome region to the east of the CCZ (Evseenko & Shtaut 2005; Maas *et al.* 2014; Wishner *et al.* 2013). Although these studies provide useful information for the wider Pacific region, they are location, taxon and/or size class specific and reveal only a partial assessment of communities.

To date, Campaign 5B and Campaign 5C have contributed to the pelagic baseline for NORI-D, collecting samples and specimens from at sites in the CTA and PRZ (Figure 6-54). ROV acquired data was collected during Campaign 5C and 5D. For each of the work scopes under the pelagic baseline, preliminary analysis is presented for Campaign 5C only.

Figure 6-54. A - Campaign 5B CTA operations; B - Campaign 5B PRZ operations; C - Campaign 5C CTA operations; D - Campaign 5C PRZ operations

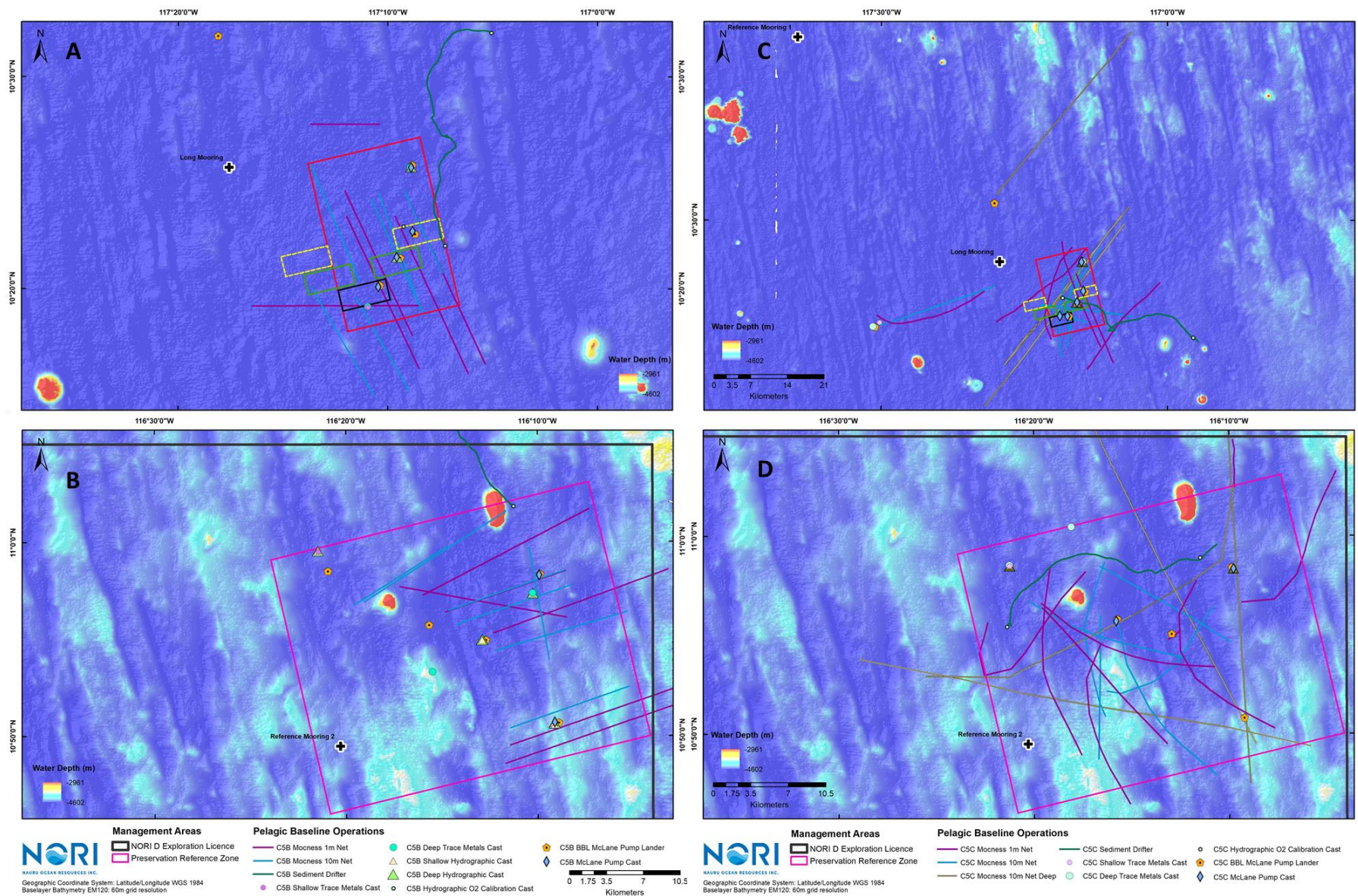
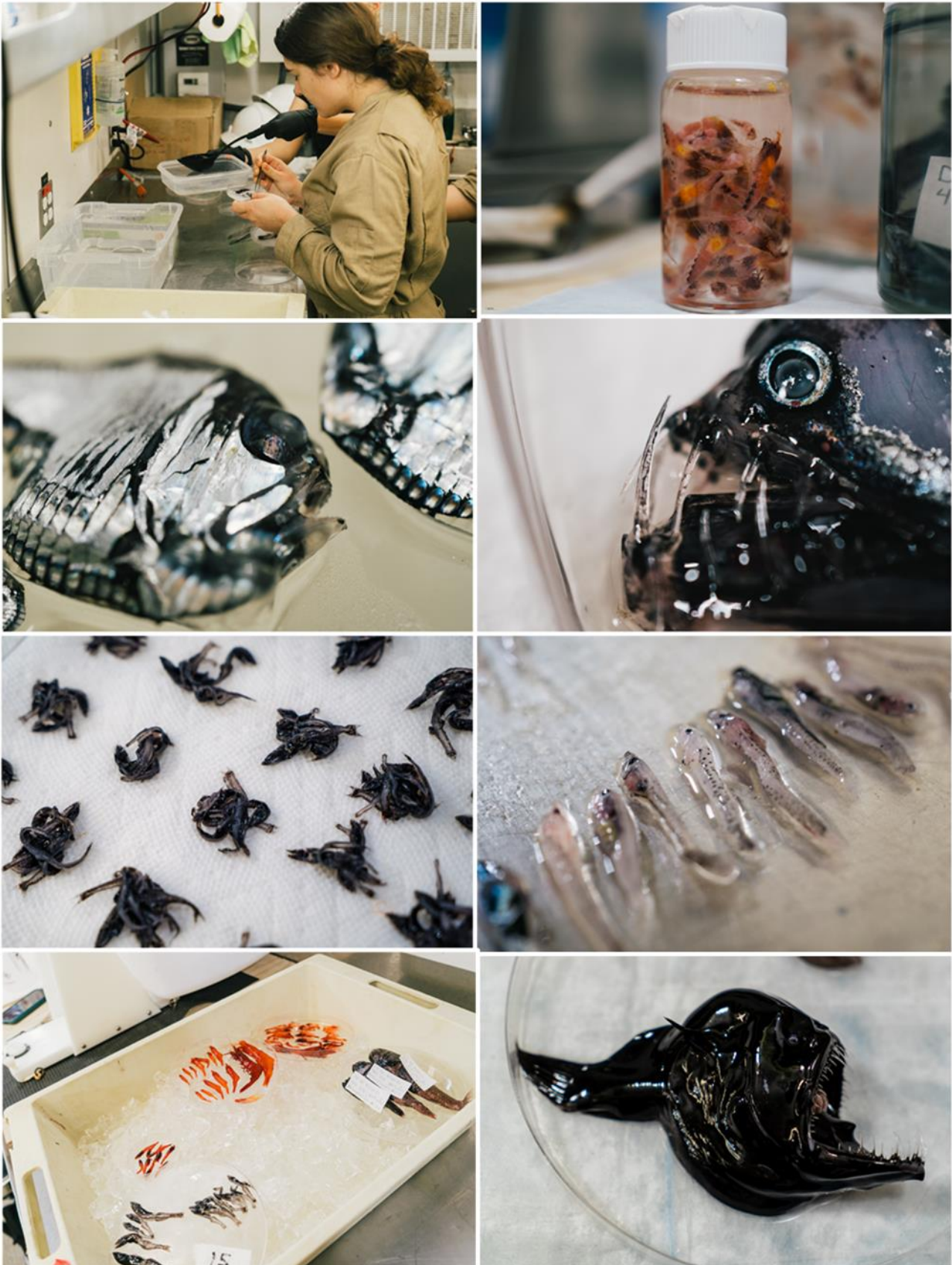


Figure 6-55. Examples of samples collected from pelagic campaigns 5B and 5C.



6.4.1 Microbial communities from surface to the benthic boundary layer

6.4.1.1 Purpose & scope

The following section describes the work conducted in 2021 by the University of Hawaii to characterise natural baseline conditions in microbial communities from the surface to the BBL in the NORI-D contract area. The scope, the survey planning and the sampling methodologies carried out to ecologically characterise microbial communities align with International Seabed Authority ISBA/25/LTC/6 Rev 1. Annex 1 section 32(d); 48. to provide baseline data requirements under Recommendations III.B.15.(d).

6.4.1.2 Baseline investigations

The methods and proposed survey array for both the collector test and long-term environmental studies on NORI-D will provide data to meet the following objectives:

- Characterise the microbial abundance and biomass (FCM), microbial diversity and community structure (16S rRNA) throughout the water column, from the surface to near the bottom

6.4.1.3 Campaign activities

(a) Campaign 5B and 5C

To characterize microbial abundance and biomass in the water column samples for flow cytometry (FCM) analysis, a total of 92 and 48 samples were collected on Campaign 5B and Campaign 5C, respectively. To characterize the diversity of prokaryotes (bacteria and archaea), a total of 93 and 72 16S rRNA samples were collected in Campaign 5B and Campaign 5C, respectively (Table 6-21 and Table 6-22).

Table 6-21 Summary of samples collected during Campaign 5B. FCM: flow cytometry, 16S: 16S rRNA genes, Nutrients: macronutrients (N+N, SRP, silicate), HPLC: photosynthetic pigments by HPLC, IFCB: imaging flow cytometry, O₂/Ar: dissolved oxygen to argon.

| AREA | CAST | DEPTH (m) | FCM | 16S | NUTRIENTS | HPLC | IFCB | O ₂ /Ar | POC |
|------|----------------|---------------------|-----|-----|-----------|------|------|--------------------|-----|
| PRZ | 1 ^a | 200 | × | × | × | - | × | - | - |
| PRZ | 1 ^a | 100 | × | × | × | × | - | - | - |
| PRZ | 1 ^a | 75 | × | × | × | × | - | - | - |
| PRZ | 1 ^a | 50/DCM ^b | × | × | × | × | × | - | - |
| PRZ | 1 ^a | 25 | × | - | × | × | - | × | - |
| PRZ | 1 ^a | 5 | × | × | × | × | × | × | - |
| PRZ | 2 ^a | 2600 | × | × | × | - | - | - | - |
| PRZ | 2 ^a | 1200 | × | × | × | - | - | - | - |
| PRZ | 2 ^a | 750 | × | × | × | - | - | - | - |
| PRZ | 2 ^a | 500 | × | × | × | - | - | - | - |
| PRZ | 2 ^a | 100 | - | - | - | - | - | - | × |
| PRZ | 2 ^a | 45/DCM ^b | × | × | × | - | - | - | × |
| PRZ | 2 ^a | 25 | × | × | × | - | - | - | - |
| PRZ | 2 ^a | 5 | - | - | - | - | - | - | × |
| PRZ | 4 | 200 | × | × | × | - | × | - | - |
| PRZ | 4 | 100 | × | - | × | × | - | - | - |
| PRZ | 4 | 75 | × | - | × | × | - | - | - |
| PRZ | 4 | 45/DCM ^b | × | × | × | × | × | - | - |
| PRZ | 4 | 25 | × | - | × | × | - | × | - |
| PRZ | 4 | 5 | × | × | × | × | × | × | × |
| PRZ | 5 | 3463 | × | × | × | - | - | - | - |
| PRZ | 5 | 3000 | × | × | × | - | - | - | - |
| PRZ | 5 | 1200 | × | × | × | - | - | - | - |
| PRZ | 5 | 500 | × | × | × | - | - | - | - |
| PRZ | 5 | 100 | - | - | - | - | - | - | × |

| AREA | CAST | DEPTH (m) | FCM | 16S | NUTRIENTS | HPLC | IFCB | O ₂ /Ar | POC |
|------|------------------|------------------------|-----|-----|-----------|------|------|--------------------|-----|
| PRZ | 5 | 75/DCM ^b | x | x | x | - | - | - | x |
| PRZ | 5 | 40/DCM ^b | x | x | x | - | - | - | x |
| PRZ | 8 | 2600 | x | x | x | - | - | - | - |
| PRZ | 8 | 1200 | x | x | x | - | - | - | - |
| PRZ | 8 | 870/LoOxy ^c | x | x | x | - | - | - | - |
| PRZ | 8 | 500 | x | x | x | - | - | - | - |
| PRZ | 8 | 200 | x | x | x | - | - | - | - |
| PRZ | 8 | 100 | x | x | x | - | - | - | - |
| PRZ | 8 | 75 | x | x | x | - | - | - | - |
| PRZ | 8 | 58/DCM ^b | x | x | x | - | - | - | - |
| PRZ | 8 | 25 | x | x | x | - | - | - | - |
| PRZ | 8 | 5 | x | x | x | - | - | - | - |
| PRZ | 10 | 200 | x | x | x | - | x | - | - |
| PRZ | 10 | 100 | - | - | - | x | - | - | x |
| PRZ | 10 | 75 | x | - | x | - | x | - | - |
| PRZ | 10 | 60/DCM ^b | x | x | x | x | x | - | x |
| PRZ | 10 | 45 | - | - | - | - | - | - | x |
| PRZ | 10 | 25 | x | - | x | x | - | x | - |
| PRZ | 10 | 5 | x | x | x | x | x | x | x |
| PRZ | 11 | 3000 | x | x | x | - | - | - | - |
| PRZ | 11 | 1200 | x | x | x | - | - | - | - |
| PRZ | 11 | 780/LoOxy ^c | x | x | x | - | - | - | - |
| PRZ | 11 | 500 | x | x | x | - | - | - | - |
| CTA | 14 | 1200 | x | x | x | - | - | - | - |
| CTA | 14 | 780/LoOxy ^c | x | x | x | - | - | - | - |
| CTA | 14 | 500 | x | x | x | - | - | - | - |
| CTA | 14 | 200 | x | x | x | - | x | - | - |
| CTA | 14 | 100 | x | - | x | - | - | - | x |
| CTA | 14 | 90/UpOxy ^d | x | - | x | x | - | - | - |
| CTA | 14 | 62/DCM ^b | x | x | x | x | x | - | - |
| CTA | 14 | 25 | x | - | x | - | - | x | - |
| CTA | 14 | 5 | x | x | x | x | x | x | - |
| CTA | TM1 ^e | 5 mab ^f | x | x | x | - | - | - | - |
| CTA | TM1 ^e | 50 mab ^f | x | x | x | - | - | - | - |
| CTA | TM1 ^e | 3000 | x | x | x | - | - | - | - |
| CTA | 17 | 1200 | x | x | x | - | - | - | - |
| CTA | 17 | 800/LoOxy ^c | x | x | x | - | - | - | - |
| CTA | 17 | 500 | x | x | x | - | - | - | - |
| CTA | 17 | 200 | x | x | x | - | x | - | - |
| CTA | 17 | 100 | x | - | x | x | - | - | x |
| CTA | 17 | 85/UpOxy ^d | x | - | x | x | - | - | - |
| CTA | 17 | 67/DCM ^b | x | x | x | x | x | - | x |
| CTA | 17 | 25 | x | - | x | x | - | x | - |
| CTA | 17 | 5 | x | x | x | x | x | x | x |
| CTA | TM2 ^e | 5 mab ^f | x | x | x | - | - | - | - |
| CTA | TM2 ^e | 50 mab ^f | x | x | x | - | - | - | - |
| CTA | TM2 ^e | 3000 | x | x | x | - | - | - | - |
| PRZ | 20 | 1200 | x | x | x | - | - | - | - |
| PRZ | 20 | 800/LoOxy ^c | x | x | x | - | - | - | - |
| PRZ | 20 | 500 | x | x | x | - | - | - | - |
| PRZ | 20 | 200 | x | x | x | - | x | - | - |
| PRZ | 20 | 100 | x | - | x | x | - | - | x |
| PRZ | 20 | 80/UpOxy ^d | x | - | x | x | - | - | - |
| PRZ | 20 | 72/DCM ^b | x | x | x | x | x | - | x |
| PRZ | 20 | 25 | x | - | x | x | - | x | - |

| AREA | CAST | DEPTH (m) | FCM | 16S | NUTRIENTS | HPLC | IFCB | O ₂ /Ar | POC |
|--------------------------------|------------------|------------------------|-----------|-----------------------|-----------|-----------|-----------|--------------------|-----------|
| PRZ | 20 | 5 | × | × | × | × | × | × | × |
| PRZ | TM3 ^e | 5 mab ^f | × | × | × | - | - | - | - |
| PRZ | TM3 ^e | 50 mab ^f | × | × | × | - | - | - | - |
| PRZ | TM3 ^e | 3000 | × | × | × | - | - | - | - |
| PRZ | 21 | 1200 | × | × | × | - | - | - | - |
| PRZ | 21 | 860/LoOxy ^c | × | × | × | - | - | - | - |
| PRZ | 21 | 500 | × | × | × | - | - | - | - |
| PRZ | 21 | 200 | × | × | × | × | × | - | - |
| PRZ | 21 | 100 | × | - | × | × | - | - | × |
| PRZ | 21 | 80/UpOxy ^d | × | - | × | × | × | - | - |
| PRZ | 21 | 71/DCM ^b | × | × | × | × | - | - | × |
| PRZ | 21 | 45 | - | - | - | - | - | - | × |
| PRZ | 21 | 25 | × | - | × | × | - | × | - |
| PRZ | 21 | 5 | × | × | × | × | × | × | × |
| PRZ | TM4 ^e | 5 mab ^f | × | × | × | - | - | - | - |
| PRZ | TM4 ^e | 50 mab ^f | × | × | × | - | - | - | - |
| PRZ | TM4 ^e | 3000 | × | × | × | - | - | - | - |
| Total samples collected | | | 91 | 73^g | 91 | 33 | 22 | 14 | 22 |

^a In these casts the carousel was malfunctioning and bottles may have been fired at wrong depths

^b DCM = deep chlorophyll maximum

^c LoOxy = lower oxycline

^d UpOxy= upper oxycline

^e this cast was conducted with the trace metal clean CTD

^f mab = meters above bottom

^g number of total samples for each pore size filter (0.2µm and 1.2µm)

Table 6-22 Summary of samples collected during Campaign 5C. FCM: flow cytometry, 16S: 16S rRNA genes, Nutrients: macronutrients (N+N, SRP, silicate), HPLC: photosynthetic pigments by HPLC, IFCB: imaging flow cytometry, O₂/Ar: dissolved oxygen to argon molar ratios, POC: particulate organic carbon.

| AREA | CAST | DEPTH (m) | FCM | 16S | NUTRIENTS | HPLC | IFCB | O ₂ /Ar | POC |
|------|------|-------------------------|-----|-----|-----------|------|------|--------------------|-----|
| PRZ | 1 | 198 | × | × | × | - | × | - | - |
| PRZ | 1 | 101 | × | - | × | × | - | - | - |
| PRZ | 1 | UpOxy ^a /78 | × | - | × | × | - | - | - |
| PRZ | 1 | DCM ^b /34 | × | × | × | × | × | - | - |
| PRZ | 1 | 25 | × | - | × | × | - | × | - |
| PRZ | 1 | 5 | × | × | × | × | × | × | - |
| PRZ | 2 | 4237 | × | × | × | - | - | - | - |
| PRZ | 2 | 4192 | × | × | × | - | - | - | - |
| PRZ | 2 | 2998 | × | × | × | - | - | - | - |
| PRZ | 2 | 1200 | × | × | × | - | - | - | - |
| PRZ | 2 | LoOxy ^c /720 | × | × | × | - | - | - | - |
| PRZ | 2 | 500 | × | × | × | - | - | - | - |
| PRZ | 2 | 100 | - | - | - | - | - | - | × |
| PRZ | 2 | 45 | - | - | - | - | - | - | × |
| PRZ | 2 | DCM ^b /33 | - | - | - | - | - | - | × |
| PRZ | 2 | 5 | - | - | - | - | - | - | × |
| PRZ | 3 | 501 | × | × | × | - | - | - | - |
| PRZ | 3 | 201 | × | × | × | - | × | - | - |
| PRZ | 3 | 101 | × | - | × | × | - | - | × |
| PRZ | 3 | UpOxy ^a /85 | × | - | × | × | - | - | - |
| PRZ | 3 | DCM ^b /45 | × | × | × | × | × | - | × |
| PRZ | 3 | 25 | × | - | × | × | - | × | - |
| PRZ | 3 | 4 | × | × | × | × | × | × | × |
| PRZ | 4 | 4221 | × | × | × | - | - | - | - |
| PRZ | 4 | 4175 | × | × | × | - | - | - | - |
| PRZ | 4 | 3000 | × | × | × | - | - | - | - |

| AREA | CAST | DEPTH (m) | FCM | 16S | NUTRIENTS | HPLC | IFCB | O ₂ /Ar | POC |
|--------------------------------|------|-------------------------|-----------|-----------------------|-----------|-----------|-----------|--------------------|-----------|
| PRZ | 4 | LoOxy ^c /782 | × | × | × | - | - | - | - |
| PRZ | 4 | 1200 | × | × | × | - | - | - | - |
| CTA | 5 | 500 | × | × | × | - | - | - | - |
| CTA | 5 | 200 | × | × | × | - | × | - | - |
| CTA | 5 | 100 | × | - | × | × | - | - | × |
| CTA | 5 | UpOxy ^a /85 | × | - | × | × | - | - | - |
| CTA | 5 | DCM ^b /63 | × | × | × | × | × | - | × |
| CTA | 5 | 45 | - | - | - | - | - | - | × |
| CTA | 5 | 25 | × | - | × | × | - | × | - |
| CTA | 5 | 5 | × | × | × | × | × | × | × |
| CTA | 6 | 4309 | × | × | × | - | - | - | - |
| CTA | 6 | 4264 | × | × | × | - | - | - | - |
| CTA | 6 | 3000 | × | × | × | - | - | - | - |
| CTA | 6 | 1200 | × | × | × | - | - | - | - |
| CTA | 6 | LoOxy ^c /636 | × | × | × | - | - | - | - |
| CTA | 7 | 500 | × | × | × | - | × | - | - |
| CTA | 7 | 200 | × | × | × | - | × | - | - |
| CTA | 7 | 100 | × | - | × | × | - | - | × |
| CTA | 7 | UpOxy ^a /75 | × | - | × | × | - | - | - |
| CTA | 7 | DCM ^b /55 | × | × | × | × | × | - | × |
| CTA | 7 | 45 | - | - | - | - | - | - | × |
| CTA | 7 | 25 | × | - | × | × | - | × | - |
| CTA | 7 | 6 | × | × | × | × | × | × | × |
| CTA | 8 | 4272 | × | × | × | - | - | - | - |
| CTA | 8 | 4221 | × | × | × | - | - | - | - |
| CTA | 8 | 3000 | × | × | × | - | - | - | - |
| CTA | 8 | 1200 | × | × | × | - | - | - | - |
| CTA | 8 | LoOxy ^c /660 | × | × | × | - | - | - | - |
| Total samples collected | | | 48 | 36^d | 48 | 20 | 13 | 8 | 15 |

^a UpOxy= upper oxycline

^b DCM = deep chlorophyll maximum

^c LoOxy = lower oxycline

^d number of total samples for each pore size filter (0.2µm and 1.2µm)

6.4.1.4 Preliminary results & discussion

(a) Flow cytometry

FCM samples from Campaign 5B and Campaign 5C are expected to be analyzed by June 2022. Samples for picoplankton enumeration will be measured using a B/D Influx flow cytometer. Three separate chlorophyll containing picoplankton populations will be enumerated by autofluorescence: *Prochlorococcus*, *Synechococcus* and picoeukaryotes (< 4 µm in size). Non-pigmented picoplankton (heterotrophic bacteria and archaea) will be enumerated using the DNA stain SYBR Green I and subtracting the previously obtained cyanobacteria concentration from the DNA positive cells. QA/QC processes include: (a) use of calibration beads of known fluorescence and scattering to normalize particle properties, (b) analytical replicates, and (c) comparison of resultant data to the historical ranges for picoplankton distributions in subtropical waters.

(b) 16S rRNA

DNA was extracted from 93 filters and a multiplexed Illumina 16S amplicon library including a mock community positive control and a sterile water negative control for a total of 95 unique samples sequenced, was constructed. The sequencing run yielded a total of 19,104,610 paired-end DNA sequences which were demultiplexed to yield a mean sampling depth of 208,078 reads per sample; there was no significant difference in sampling depth between sites ($F = 0.18$, $p = 0.67$), between size fractions ($F=0.91$, $p=0.34$), or among depth strata ($F=1.11$, $p=0.36$). Reads were trimmed, quality filtered,

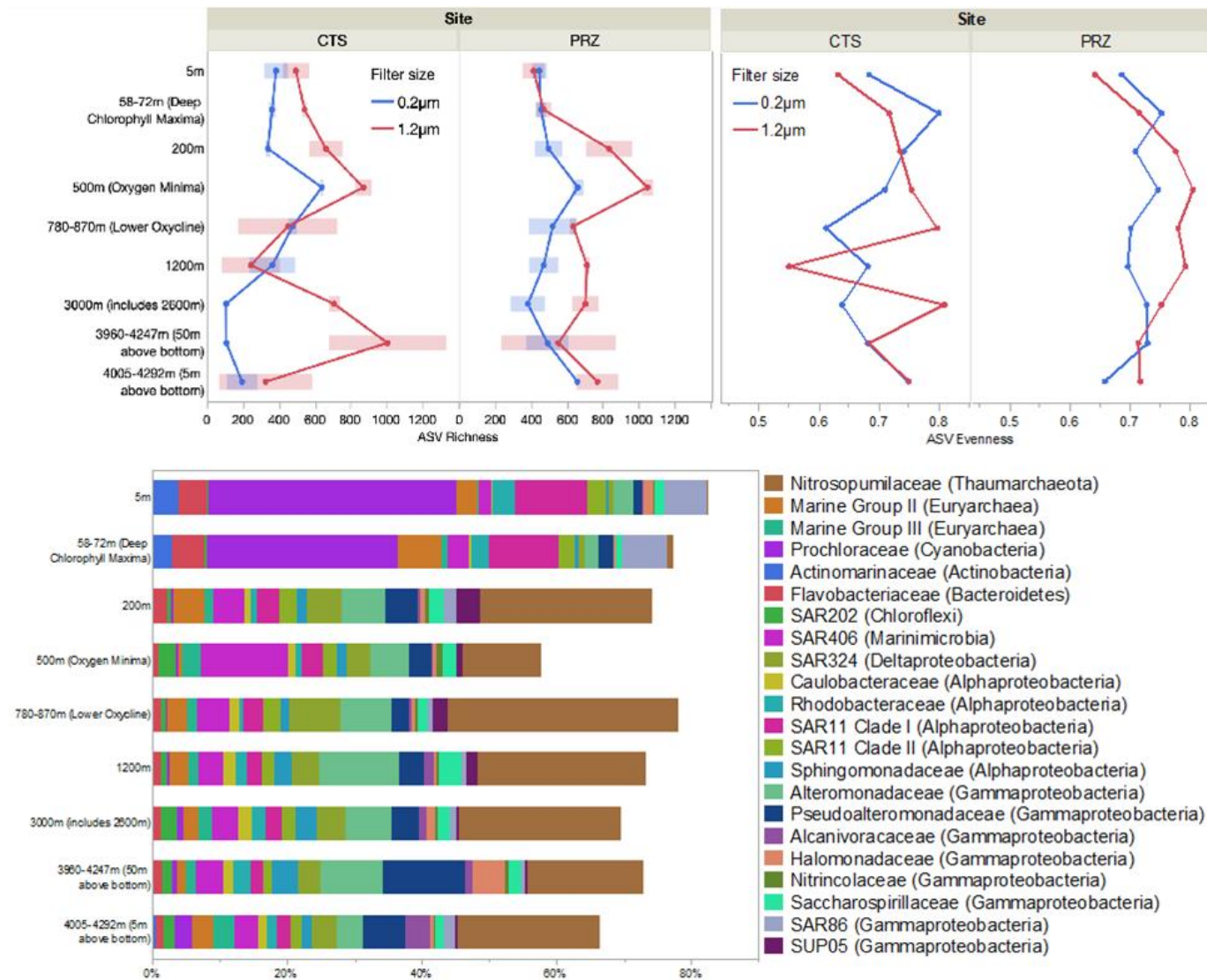
denoised, dereplicated, aligned, chimera-checked and classified through our customized bioinformatic pipeline, yielding 12,147,970 total Bacteria and Archaea sequence reads. Median final read depth per sample was 114,987 and ranged from 28,722 to 321,560; three samples failed to pass amplification verification checks along with the negative control as validated and were removed from further analysis.

To compare microbial diversity among the 90 remaining samples a random subsampling (aka rarefaction) to standardize read depth to a common minimum of 28,000 reads per sample was applied. All diversity analyses were done with unique microbial gene sequences as the operational taxonomic unit used in this work; these are typically referred to as Amplicon Sequence Variants (ASVs). Across the 90 samples, 9133 ASVs were recovered in total. Median sample ASV richness was 542 and ranged from 68 to 1331. Median sample ASV evenness was 0.74 and ranged from 0.47 to 0.84. ANOVA models were used to test whether richness or evenness differed between sites, filter size fractions or among depth strata, including interactions between factors (Figure 6-56, top).

Mean richness was significantly higher overall at the PRZ site (587) than at the CTA site (464) ($F=9.39$, $p = 0.0032$) but evenness did not differ between sites ($F=1.95$, $p=0.17$). Mean richness was also significantly higher on particles (634) than in the free-living community (417) ($F=29.83$, $p<0.0001$) while evenness did not differ by size fraction ($F=2.37$, $p=0.13$). Both metrics of diversity varied significantly among depth strata (richness $F=3.50$, $p=0.0021$; evenness $F=2.70$, $p=0.013$) and these depth distributions differed slightly between the two size fractions ($p < 0.04$) but did not differ between sites ($p > 0.13$). Richness was consistently highest at 500m depth in the particle-associated fraction.

The composition of microbial communities varied with depth and was consistent with long term observations from the North Pacific Subtropical Gyre (Figure 6-56, bottom). The most abundant taxa in the surface waters were in the family Prochloraceae, particularly the widespread photoautotrophic genus *Prochlorococcus* comprising an average of 32% of the community in the euphotic zone. Additional abundant taxa in the surface waters included the SAR11 Clade I, Flavobacteriaceae, Actinomarinaceae, and the SAR86 clade. Below the euphotic zone the most abundant taxa were in the family Nitrosopumilaceae, autotrophic Archaea that oxidize ammonia. Additional abundant taxa in the deeper waters included the SAR324, SAR406, SAR11 Clade II and the Gammaproteobacteria Alteromonadaceae and Pseudoalteromonadaceae. Abundant taxa throughout the water column included the Marine Group II and III Archaea, the Alphaproteobacteria Rhodobacteraceae, and various families within the order Oceanospirillales. The SAR202 and SUP05 clades were most abundant in specific depth horizons in the mesopelagic and oxygen minimum zones, respectively.

Figure 6-56. Microbial diversity varies among depth strata. Top panel displays variation in richness (left) and evenness (right) in the particle-associated (red) and free-living (blue) fractions at each site. Bottom panel shows the mean relative abundance of abundant families (those comprising more than 5% of sequences in any one sample).



6.4.2 Phytoplankton communities in the epipelagic zone

6.4.2.1 Purpose & scope

The following section describes the work conducted in 2021 by the University of Hawaii to characterise natural baseline conditions in Phytoplankton communities in the epipelagic zone in the NORI-D contract area. The scope, the survey planning and the sampling methodologies carried out to ecologically characterise phytoplankton communities align with International Seabed Authority ISBA/25/LTC/6 Rev 1. Annex 1 section 42(a) Phytoplankton and primary production to provide baseline data requirements under Recommendations III.A.13; III.B.15. (d)(iii); IV.B.22.

6.4.2.2 Baseline investigations

The methods and proposed survey array for both the collector test and long-term environmental studies on NORI-D will provide data to meet the following objectives:

- Characterize the composition, biomass, and productivity of phytoplankton communities in the epipelagic zone

6.4.2.3 Campaign activities

(a) Campaign 5B & 5C

To determine the biomass contributions of key phytoplankton taxa samples in the upper 200 m of the water column for the analysis of photosynthetic pigments by high performance liquid chromatography (HPLC), a total of 50 and 28 HPLC samples were collected in Campaign 5B and Campaign 5C, respectively. To further characterize the phytoplankton community, samples were collected for Imaging Flow Cytometry (IFCB). A total of 24 and 13 IFCB samples were collected in Campaign 5B and Campaign 5C, respectively (Table 6-21 and Table 6-22).

To estimate net community production in the mixed layer samples for O₂/Ar analysis in surface waters (5 and 25 m). A total of 16 and 8 O₂/Ar samples were collected in quadruplicate during Campaign 5B and Campaign 5C, respectively (Table 6-21 and Table 6-22).

Finally, to quantify gross primary production and community respiration a set of two Aandera O₂ sensors were deployed in situ for a period of three days at each sampling site (PRZ and CTA). Table 6-23 summarizes the deployments conducted on each campaign. The sensors were deployed at 15m using the sediment drifting array (Section 6.4.7), providing high-frequency O₂ measurements that allow the determination of metabolic rates from the diel changes in O₂ concentrations (Barone *et al.*, 2019).

Table 6-23 Summary of in situ optode deployments on Campaign 5B and Campaign 5C. In all occasions, two Aandera optode sensors were deployed for three days at 15 m

| 5A/5D | AREA | DATE IN | DATE OUT | LATITUDE DEPLOYMENT | LONGITUDE DEPLOYMENT | LATITUDE RECOVERY | LONGITUDE RECOVERY |
|-------|------|----------|----------|---------------------|----------------------|-------------------|--------------------|
| 5A | PRZ | 17/3/21 | 20/3/21 | 11° 01' 50.3" | 116° 11' 15.4" | 11° 15' 18.3" | 116° 25' 36.5" |
| 5A | CTA | 6/4/21 | 9/4/21 | 10° 22' 01.8" | 117° 07' 15.4" | 10° 31' 45.1" | 117° 04' 53.2" |
| 5D | PRZ | 4/10/21 | 7/10/21 | 10° 55' 31.8" | 116° 21' 20.1" | 10° 59' 33.7" | 116° 10' 38.4" |
| 5D | CTA | 13/10/21 | 16/10/21 | 10° 22' 01.2" | 117° 10' 56.5" | 10° 17' 24.6" | 116° 56' 46.5" |

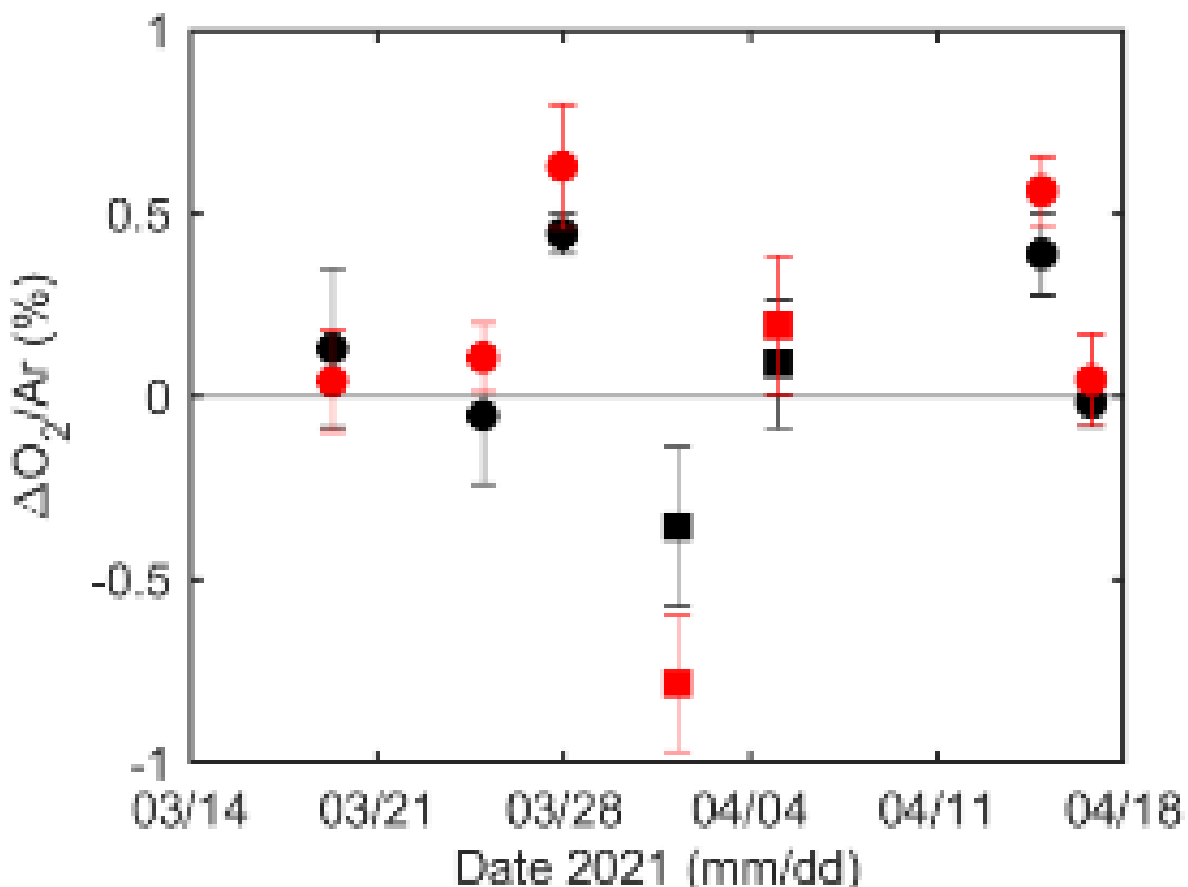
6.4.2.4 Preliminary results & discussion

(a) O₂/Ar

Net community production is an important biochemical and ecological term as it represents the balance between gross primary production (by photoautotrophs) and community respiration (by both

photoautotrophs and heterotrophs). When positive, it represents the amount of carbon available to get exported to deeper waters. Net community production in the mixed layer can be estimated from the rate of air-sea oxygen exchange derived from measurements of molar oxygen to argon ratios. This method relies on the similar physical properties of both gases but different biological behaviour (argon is biologically inert). Net community production derived from O₂/Ar measurements represents an average over the residence time of O₂ in the mixed layer prior to the measurement (typically 1-2 weeks).

Figure 6-57. Deviation of O₂/Ar from equilibrium measured in the mixed layer at 5 m (black) and 25 m (red) during Campaign 5B. Circles and squares represent samples collected at PRZ and CTA, respectively. The error bars represent the standard deviation of quadruplicate samples.



During Campaign 5B O₂/Ar was measured in surface waters (at 5 and 25m) in both sampling sites. The samples were stored and analyzed right after the cruise in the laboratory. The precision of O₂/Ar measurements, quantified as the coefficient of variation from quadruplicate samples ($\pm 0.14\%$) was found not to be as good as what we have typically obtained in the past ($\pm 0.05\%$, Ferrón *et al.* (2015)), and we suspect that this could be due to the longer storage time of the samples (up to 40 days). The deviation of O₂/Ar from equilibrium, $\Delta O_2/Ar$, represents the O₂ saturation anomaly due to biological processes, and its sign indicates whether the system is net autotrophic (positive values) or net heterotrophic (negative values). The samples collected during Campaign 5B showed high variability in $\Delta O_2/Ar$. At the PRZ site, mean $\Delta O_2/Ar$ for each cast ranged from near equilibrium (0.01%) to up to up to 0.5% (Figure 6-57), whereas the two casts conducted at the CTA site showed highly different mean values, -0.6% and 0.1%.

For comparison, mean daily $\Delta O_2/Ar$ at the Hawaii Ocean time-series station (Station ALOHA), varied between -0.09% and 1.67% over a 5-year study (Ferrón *et al.*, 2021). Whereas some degree of short-term variability in $\Delta O_2/Ar$ values is to be expected (Ferrón *et al.*, 2015, 2021), the large variations within a single site over such short time scales is surprising and could be indicative of large spatial and/or diel variability, assuming the samples are not compromised. A careful analysis to investigate these

possibilities is forthcoming. Preliminary estimates of net community production derived from mean O₂/Ar measurements at each cast are provided in Table 6-24.

Table 6-24 Preliminary estimates of net community production derived from O₂/Ar measurements collected at both sampling sites during DG5B. Values need to be revised.

| AREA | CAST | NET COMMUNITY PRODUCTION |
|------|------|--|
| PRZ | 4 | 0.81 mmol O ₂ m ⁻² d ⁻¹ |
| PRZ | 8 | 0.25 mmol O ₂ m |
| PRZ | 10 | 5.0 mmol O ₂ m |
| PRZ | 20 | 4.4 mmol O ₂ m |
| PRZ | 21 | 0.14 mmol O ₂ m |
| CTA | 14 | -4.27 mmol O ₂ m |
| CTA | 17 | 1.06 mmol O ₂ m |

(b) Gross primary productivity & respiration

Diel changes in the concentration of dissolved O₂ within the mixed layer are largely driven by biological processes. During daytime, net community production (the balance between gross primary production and community respiration) causes O₂ to increase, and during the night community respiration causes O₂ to decrease. If it can be assumed that the rate of respiration is constant throughout the day, dissolved O₂ time-series can be used to quantify metabolic rates in situ (Barone *et al.*, 2019). During baseline cruise Campaign 5B diel O₂ changes were measured by mounting two Aandera oxygen optodes at 15 m (within the mixed layer) on a free-drifting array, which was deployed for three days at each sampling site (Table 6-23).

Dissolved O₂ concentrations at the two sites displayed clear diel cycles with maxima near sunset and minima near sunrise, consistent with the variability expected from biological processes (Figure 6-58).

Preliminary estimates of gross oxygen production and community respiration in the mixed layer were obtained daily for each sensor and then averaged (Table 6-25). Metabolic rates determined with each sensor agreed within ~1% for gross oxygen production and ~5% for community respiration. The uncertainty of single rate estimates (computed as the rate standard deviation obtained by bootstrapping the residuals, as per Barone *et al.*, 2019) averaged 0.02 mmol O₂ m⁻³ d⁻¹. At the time of sampling metabolic rates at PRZ were shown to be ~40-50% larger than at CTA (t-test, p<0.02).

Net community production, determined as the difference of mean gross oxygen production and community respiration values, is 0.38 ± 0.39 mmol O₂ m⁻³ d⁻¹ for PRZ and 0.13 ± 0.16 mmol O₂ m⁻³ d⁻¹ for CTA (± propagated standard deviation), indicating net autotrophic conditions during the time of sampling.

However, rates of gross production and respiration are not significantly different (t-test, p=0.509). There is a significant positive correlation between gross oxygen production and community respiration (r² = 0.85, p = 0.0087), indicating a tight coupling between photosynthesis and respiration in this ecosystem.

Figure 6-58 Time-series of dissolved O₂ measured by two different sensors at the PRZ (left panel) and CTA (right panel) sites during DG5B. Black squares show the values of Winkler samples collected at 15 m near the time of recovery and deployment of the sediment trap array. Daytime and night-time are depicted as white and grey areas, respectively.

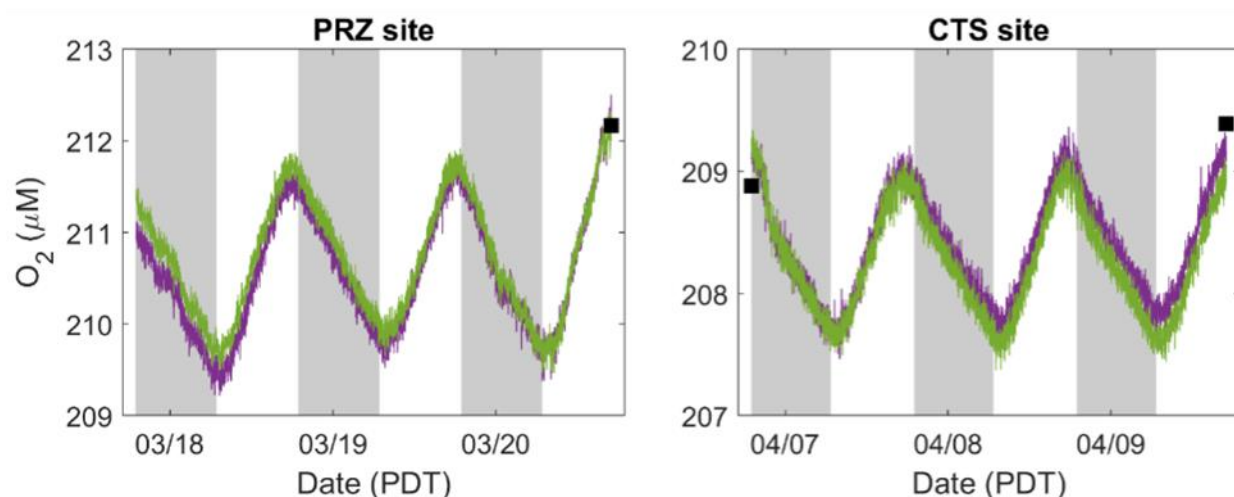


Table 6-25 Preliminary daily rates of gross oxygen production and community respiration measured with two different sensors at the PRZ and CTA sites during DG5B (\pm fit uncertainty). The values in parenthesis represent the mean \pm standard deviation (SD) from the two sensors. The means \pm SD for each site over the 3 days are also provided in bold. Units are mmol O₂ m⁻³ d⁻¹.

| AREA | STATION | GROSS OXYGEN PRODUCTION | | COMMUNITY RESPIRATION | |
|-----------|-------------------|-----------------------------------|-------------------|-----------------------------------|-----------------|
| | | SENSOR 1 | SENSOR 2 | SENSOR 1 | SENSOR 2 |
| PRZ | 3/18/2021 | 3.35 \pm 0.02 | 3.34 \pm 0.02 | 2.84 \pm 0.02 | 2.99 \pm 0.02 |
| | | (3.34 \pm 0.01) | | (2.92 \pm 0.10) | |
| | 3/19/2021 | 3.21 \pm 0.01 | 3.23 \pm 0.01 | 3.21 \pm 0.02 | 3.31 \pm 0.02 |
| | | (3.22 \pm 0.02) | | (3.26 \pm 0.07) | |
| 3/20/2021 | 4.10 \pm 0.02 | 4.19 \pm 0.02 | 3.28 \pm 0.03 | 3.51 \pm 0.03 | |
| | (4.15 \pm 0.06) | | (3.40 \pm 0.16) | | |
| - | - | 3.57 \pm 0.50 | - | 3.19 \pm 0.25 | - |
| CTA | 4/7/2021 | 2.51 \pm 0.02 | 2.50 \pm 0.02 | 2.49 \pm 0.02 | 2.60 \pm 0.02 |
| | | (2.51 \pm 0.01) | | (2.54 \pm 0.07) | |
| | 4/8/2021 | 2.32 \pm 0.01 | 2.35 \pm 0.01 | 2.12 \pm 0.02 | 2.22 \pm 0.02 |
| | | (2.34 \pm 0.02) | | (2.17 \pm 0.07) | |
| 4/9/2021 | 2.32 \pm 0.01 | 2.33 \pm 0.02 | 2.03 \pm 0.02 | 2.11 \pm 0.02 | |
| | (2.33 \pm 0.01) | | (2.07 \pm 0.06) | | |
| - | - | 2.39 \pm 0.10 | - | 2.26 \pm 0.25 | - |

(c) Satellite estimates of euphotic zone integrated primary production

Global-scale primary production models have also been used to estimate net primary production (NPP) in the NORI-D study region; these models rely on various combinations of satellite-based ocean colour, phytoplankton absorption and sea-surface temperature (Behrenfeld & Falkowski, 1997; Silsbe *et al.* 2016). The two models used include the VGPM, a chlorophyll- based model, as well as the CAFÉ model, an absorption-based model (Figure 6-59 and Figure 6-60). Each model makes different assumptions about the relationship between proxies of phytoplankton biomass and the rate and primary production

and hence both models are assessed in terms of estimated seasonality and the rate of production during Campaigns 5B and 5C. Model descriptions and source code are provided here: <http://sites.science.oregonstate.edu>.

While model coverage is not yet available for the time spanning the Campaign 5C, three preliminary conclusions can be derived from analyses to date: (1) Model predictions of the rate of NPP vary widely between models, by a factor of 2x for the euphotic zone integrated rate. It is not readily apparent which input terms lead to these model discrepancies, but the divergence is most certainly rooted in model formulations and the assumptions made. Future analyses and comparisons to in situ O₂ based rates will help inform which model may be more accurate for the region. (2) Neither model predicts any significant variability between the PRZ, CTA, or NORI-D stations; and (3) both models predict significant (2x) seasonality at all study sites with maximal production in early spring (February-March) with minimal NPP rates in winter. In combination with in-situ measurements of biomass and productivity, these data form a solid baseline for understanding the magnitude and variability of NPP in the study region.

Figure 6-59 Time-series net primary production as estimated for the PRZ, CTA, and NORI-D regions by the VPGM model (top left) and CAFÉ model (bottom left). Data encompass the DG5B campaign but not yet the DG5C campaign. (Right) The seasonal progression of net primary productivity estimated by the VPGM (top) and CAFÉ (bottom) models.

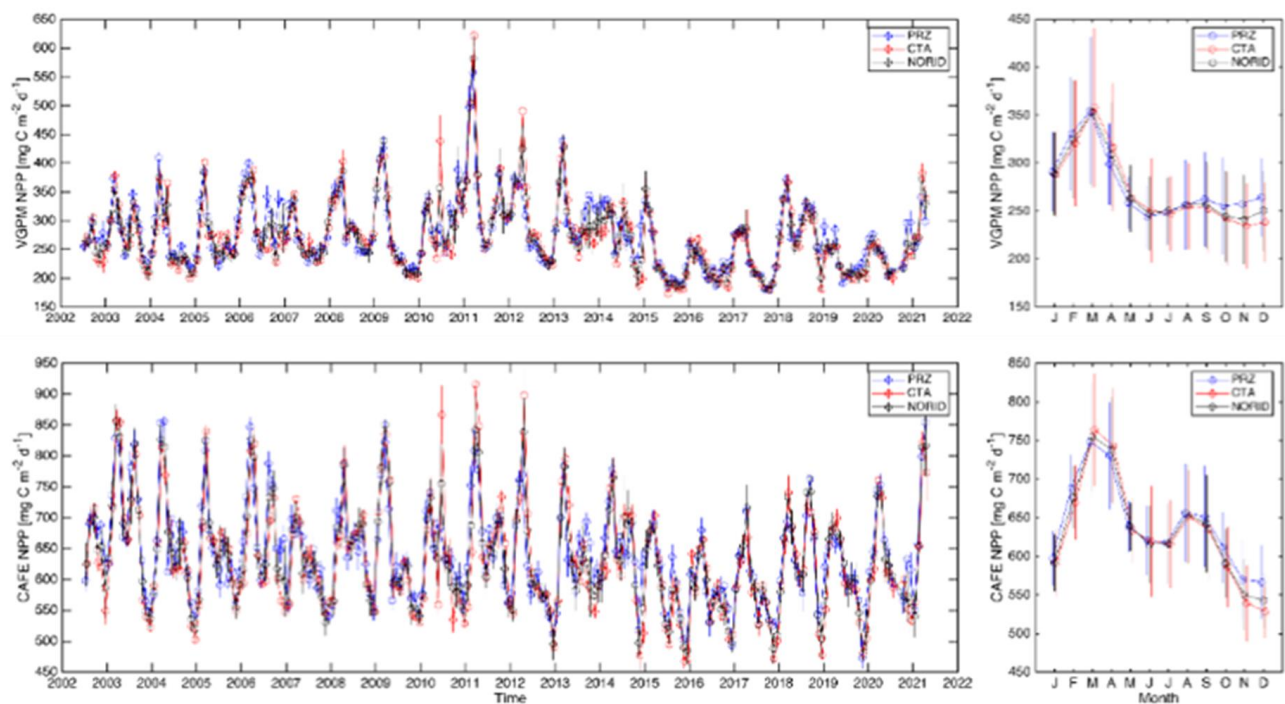
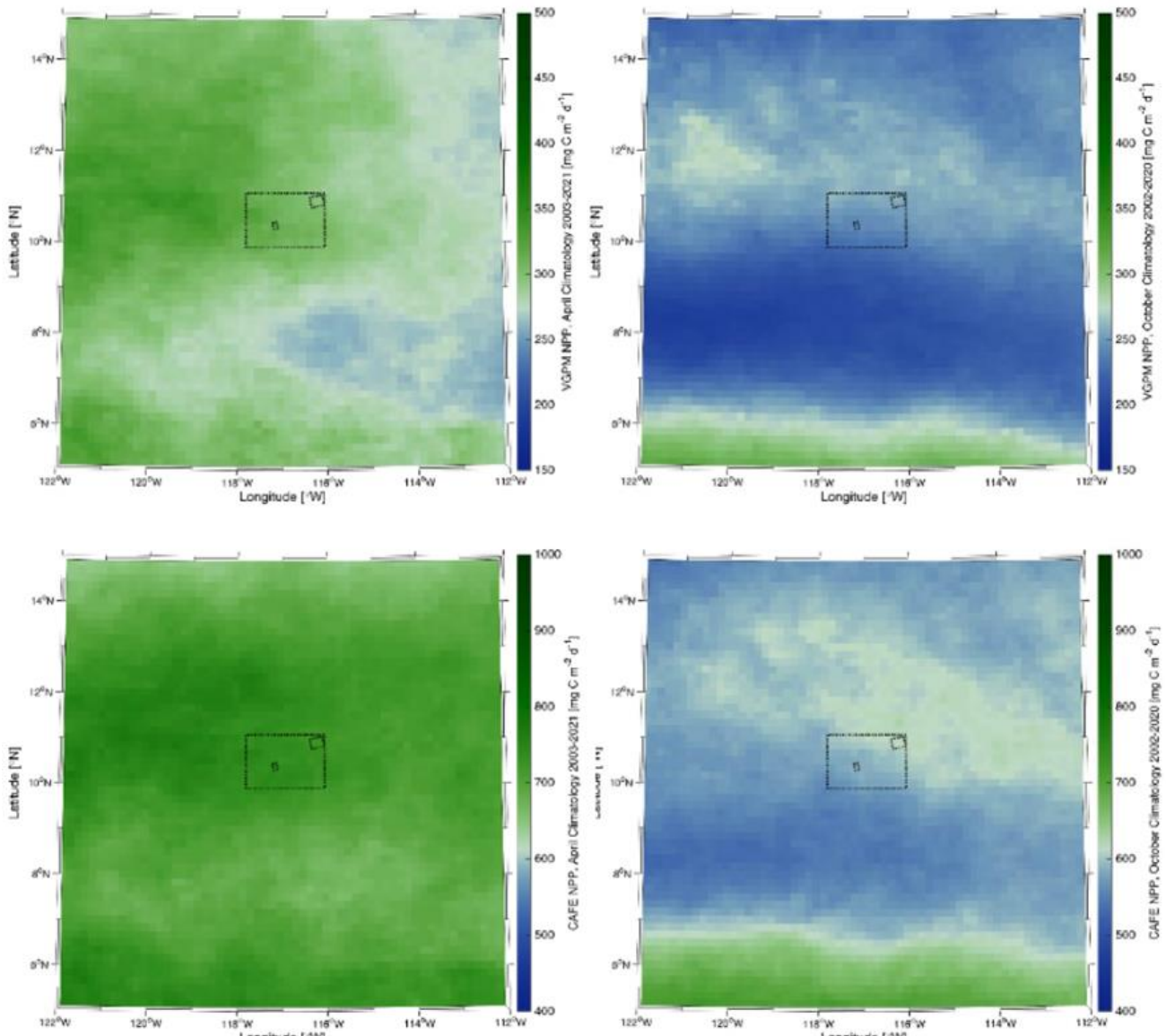


Figure 6-60. Regional maps of the monthly climatology for April (left) and October (right) as estimated from the VGPM (top) and CAFÉ (bottom) models of net primary production. While the magnitude varies between models, both approaches predict strong seasonality ($\sim 2\times$) in the study region.



6.4.3 Zooplankton community

6.4.3.1 Purpose & scope

The following section describes the work conducted in 2021 by the University of Hawaii to characterise natural baseline conditions in zooplankton communities in the NORI-D contract area. The scope, the survey planning and the sampling methodologies carried out to ecologically characterise zooplankton communities align with International Seabed Authority ISBA/25/LTC/6 Rev 1, Annex 1 section 42(b) Zooplankton (both holo- and meroplankton) and 44. Vertical migration to provide baseline data requirements under Recommendations III.B.15. (d)(iii); IV.B.22.

Collectively, these results provide baseline ecosystem information on the zooplankton as prescribed by the ISA in section III 15(e)iii and Annex 1, item 37 and for eDNA as specified in Annex 1, item 27.

6.4.3.2 Baseline investigations

The methods and proposed survey array for both the collector test and long-term environmental studies on NORI-D will provide data to meet the following objectives:

- Characterize the abundance, biomass, diversity and composition of the zooplankton community from the surface to the benthic boundary layer

6.4.3.3 Campaign 5A activities

(a) 1m² MOCNESS Sampling

Zooplankton samples were collected in spring, during Campaign 5B, across the upper 1500m of the water column within NORI-D (Table 6-26). Tows were conducted within two areas of NORI-D, the NE Preservation Reference Zone (PRZ) and the Collector Test Area (CTA). Zooplankton were collected using a 1m² Multiple Opening/Closing Nets and Environmental Sensing System (MOCNESS) equipped with 200 µm nets and cod ends, and a SeaBird SBE9 with sensors to measure pressure, temperature, conductivity, fluorescence (Seapoint), beam attenuation/transmission (WET labs transmissometer), and oxygen concentration (SBE43).

Three paired sets of tows were conducted in each of the PRZ and CTA (12 tows total) to enable resolution of zooplankton diel vertical migratory behaviour. MOCNESS tows were oblique, and approximately 7-hrs in duration. The 9 depth-stratified nets sampled from 1500 m to the sea surface, with target depths 1500-1250m, 1250-1000m, 1000-800m, 800-700m, 700-500m, 500-300m, 300-100m, 100-50m, 50-0m (Table 6-27).

Sampling in the bathypelagic was designed to sample above and below the expected discharge depth (1200m), to capture potential perturbations to communities within and immediately above midwater sediment plumes. The 1000-800m layer sampled below the oxygen minimum zone (OMZ) in the deep mesopelagic, and the 100m layer between 800-700m sampled the lower oxycline. Sampling within the OMZ was divided into the upper (100-300m), mid (300-500m), and lower (500-700m) OMZ regions, with some differences observed between the PRZ and CTA in the oxygen profiles, within the 100-300m upper OMZ (more oxygenated in the CTA). The upper oxycline was sampled at 100 – 50m in both regions, and a well-oxygenated layer from 50m to the sea surface.

Bulk plankton collected in each net was quantitatively split using a Folsom splitter onboard and allocated for different shore-based analyses as described in Table 6-28.

Table 6-26 Overview of 1m² MOCNESS tows conducted, with 6 tows in each of the reference zone (PRZ) and collector test area (CTA)

| AREA | TOW | LATITUDE | LONGITUDE | START TIME (LOCAL) | DAY/NIGHT |
|------|--------|----------------|-----------------|--------------------|-----------|
| PRZ | 1MOC1 | 10 ° 55.308 N | 116 ° 18.020 W | 19:35 | Night |
| PRZ | 1MOC2 | 10 ° 55.5479 N | 116 ° 19.268 W | 20:34 | Night |
| PRZ | 1MOC3 | 10 ° 54.082 N | 116 ° 15.925 W | 7:55 | Day |
| PRZ | 1MOC4 | 10 ° 47.601 N | 116 ° 14.890 W | 9:03 | Day |
| PRZ | 1MOC5 | 10 ° 48.479 N | 116 ° 14.372 W | 6:40 | Day |
| CTA | 1MOC6 | 10 ° 58.492 N | 116 ° 21.040 W | 22:06 | Night |
| CTA | 1MOC7 | 10 ° 26.323 N | 117 ° 11.027 W | 8:50 | Day |
| CTA | 1MOC8 | 10 ° 26.8541 N | 117 ° 10.3205 W | 8:11 | Day |
| CTA | 1MOC9 | 10 ° 26.929 N | 117 ° 13.153 W | 19:34 | Night |
| CTA | 1MOC10 | 10 ° 25.937 N | 117 ° 13.157 W | 20:55 | Night |

| AREA | TOW | LATITUDE | LONGITUDE | START TIME (LOCAL) | DAY/NIGHT |
|------|--------|---------------|----------------|--------------------|-----------|
| CTA | 1MOC11 | 10 ° 30.444 N | 117 ° 14.940 W | 10:01 | Day |
| CTA | 1MOC12 | 10 ° 19.215 N | 117 ° 05.726 W | 20:45 | Night |

Table 6-27 Depths and duration targeted for each net on each MOCNESS tow.

| NET# | START DEPTH (m) | END DEPTH (m) | FEATURE TARGETTED | DURATION OPEN (min) |
|-------|-----------------|---------------|-------------------------------------|---------------------|
| Net 0 | 0 | 1500 | Integrated net, non-quantitative | 90 |
| Net 1 | 1500 | 1250 | Bathypelagic, below discharge depth | 60 |
| Net 2 | 1250 | 1000 | Bathypelagic, above discharge depth | 60 |
| Net 3 | 1000 | 800 | below OMZ, Deep mesopelagic | 40 |
| Net 4 | 800 | 700 | Lower oxycline | 30 |
| Net 5 | 700 | 500 | Lower OMZ | 30 |
| Net 6 | 500 | 300 | Core OMZ | 30 |
| Net 7 | 300 | 100 | Upper OMZ | 30 |
| Net 8 | 100 | 50 | Upper oxycline | 12 |
| Net 9 | 50 | 0 | Oxygenated, Mixed layer (ML) | 12 |

OMZ = oxygen minimum zone. The 0 net is open when the MOCNESS enters the water and samples on the transit to the deepest sampling horizon (1500m); this net is closed simultaneously with opening the first depth stratified net, Net 1. Discharge depth (1200m) as a guide to target the net strata sampled in the bathypelagic.

Table 6-28 Examples of representative sample splitting and preservation for each tow.

| NET# | FRACT ION | SIZE FRACT ION | PRESERV ATIVE | ANALYSIS |
|--------------------|-----------|----------------|---------------|---|
| NET 0 | 1 | N/A | ETOH | DNA meta-taxonomy, DNA barcoding, targeted ID and sequencing |
| | 1/2 | N/A | Formalin | ZooScan image-based community analysis |
| | 1/4 | SM | RNALater | Metabarcoding, diversity analysis |
| | 1/4 | LG | RNALater | Metabarcoding, diversity analysis |
| | 1/4 | 0.2 | -80°C | Biomass, carbon/nitrogen content, isotope & food web analyses |
| | 1/4 | 0.5 | -80°C | Biomass, carbon/nitrogen content, isotope & food web analyses |
| | 1/4 | 1.0 | -80°C | Biomass, carbon/nitrogen content, isotope & food web analyses |
| | 1/4 | 2.0 | -80°C | Biomass, carbon/nitrogen content, isotope & food web analyses |
| | 1/4 | 5.0 | -80°C | Biomass, carbon/nitrogen content, isotope & food web analyses |
| DEEP NET | 1/2 | N/A | Formalin | ZooScan image-based community analysis |
| | 1/4 | N/A | ETOH | DNA taxonomy, DNA barcoding |
| | 1/8 | SM | RNALater | Metabarcoding, diversity analysis |
| | 1/8 | LG | RNALater | Metabarcoding, diversity analysis |
| | 1/8 | 0.2 | -80°C | Biomass, carbon/nitrogen content, isotope & food web analyses |
| | 1/8 | 0.5 | -80°C | Biomass, carbon/nitrogen content, isotope & food web analyses |
| | 1/8 | 1.0 | -80°C | Biomass, carbon/nitrogen content, isotope & food web analyses |
| | 1/8 | 2.0 | -80°C | Biomass, carbon/nitrogen content, isotope & food web analyses |
| | 1/8 | 5.0 | -80°C | Biomass, carbon/nitrogen content, isotope & food web analyses |
| SHALLOW NET | 1/2 | N/A | Formalin | ZooScan image-based community analysis |
| | 1/4 | N/A | ETOH | DNA taxonomy, DNA barcoding |
| | 1/8 | SM | RNALater | Metabarcoding, diversity analysis |
| | 1/8 | LG | RNALater | Metabarcoding, diversity analysis |
| | 1/8 | 0.2 | -80°C | Biomass, carbon/nitrogen content, isotope & food web analyses |
| | 1/8 | 0.5 | -80°C | Biomass, carbon/nitrogen content, isotope & food web analyses |
| | 1/8 | 1.0 | -80°C | Biomass, carbon/nitrogen content, isotope & food web analyses |
| | 1/8 | 2.0 | -80°C | Biomass, carbon/nitrogen content, isotope & food web analyses |
| | 1/8 | 5.0 | -80°C | Biomass, carbon/nitrogen content, isotope & food web analyses |

Net 0 was handled differently from other nets, as it is an integrated tow from the surface to the bottom of the tow. Typically, Nets 1, 2, 3, 4, 5, 6 were handled as described below for the ‘Deep Net’, while Nets 7, 8, and 9 were high biomass regions of the water column and handled as for ‘Shallow Net’ below. ETOH = 95-100% non-denatured ethanol, for both fixation and storage. Formalin and ETOH samples were stored at 4°C onboard. Size fractions of zooplankton are listed small/large (SM/LG) or by mm sizes (e.g., 0.2mm, 1.0mm).

(b) BBL Zooplankton Lander

Demersal plankton was sampled on cruise Campaign 5B using two McLane Large Volume Water Transfer Systems (WTS-LV30; McLane Research Laboratories; Plankton pumps) mounted on a free vehicle for deployment and recovery from abyssal depths (BBL Lander; Figure 6-61)(as initially described in (Kersten et al. 2019). A total of 11 successful deployments of the BBL Lander were completed (Table 6-29) with 5 sites placed within the PRZ and 6 sites in the broader CTA region (4 sites within the CTA box, 2 sites more distant but in the central- western NORI-D; Figure 6-45). Consideration of site selection took into account (a) bathymetry and benthic habitat type (e.g., nodule cover type), (b) spatial structure and distance among sites, and (c) overlap to sampling completed on Campaign 5A and ROV transect surveys, which may provide data on adult populations and possible larval sources within the BBL (as well as other ancillary data on habitat characteristics). All sites were also sampled on Campaign 5A for benthic community and biogeochemical measurements. The lander was equipped with a Kongsberg cNode MiniS 37-40V Ti USBL transponder to obtain lander position and ascent/descent rates during deployment.

Figure 6-61 Images of the BBL lander used for sampling demersal zooplankton. The McLane large-volume pumps are mounted 70 inches apart along the long axis of the lander, at an even height with the top of the frame and syntactic foam. Dual acoustic releases (Teledyne Benthos) were used to recover the lander from depth, and a separate mast & float heightened visibility of the lander at the sea surface (Xeos RDF & LED flasher beacons on the mast). When deployed at depth, the lander floats above the bottom with the pump intake at 3 mab.



Plankton pumps did not begin filtering immediately upon arrival of the lander at the seafloor, with 6.7 to 22.5 hours given for settlement of resuspended sediment. The duration of pumping ranged from 4-11 hrs at rates of 20 –30 L min⁻¹, yielding a total of 5,792 – 14,820 L filtered per pump per deployment (Table 6-29). The plankton pumps sampled at 3 meters above the seafloor, through a ~ 3 cm inlet at the top of the pump. Plankton was retained on 63 µm Nitex filters. Contamination from the midwater and surface

community is minimized by a positively buoyant ball that prevents flow across the filter when not actively pumping (on descent and ascent from the seafloor). Upon recovery of the lander on deck, the filters were immediately removed, and plankton flushed from the filter using chilled 0.2 µm filtered seawater collected from abyssal depths. Bulk plankton from each pump was quantitatively split using a Folsom plankton splitter. Quantitative 1/2 splits from one pump were preserved in 95% ETOH and 5% borate-buffered formalin. One quantitative split from the second pump was preserved in 95% ETOH, while the second 1/2 split was preserved in RNALater. Formalin samples were stored at 4°C, ETOH samples at -20 °C and RNALater samples at -80 °C following preservation. McLane filter holders were flushed with ddH₂O between deployments.

Table 6-29 Overview of lander deployments completed, listed in order of deployment.

| AREA | STATION | LANDER | EASTING | NORTHING | DEPTH (m) | PUMP | VOLUME FILTERED (l) |
|------|---------|--------|------------|--------------|-----------|------|---------------------|
| PRZ | SPR_034 | BBL1 | 591,296.74 | 1,213,062.69 | 4231.92 | A | 14,366.70 |
| PRZ | SPR_034 | BBL1 | 591,296.74 | 1,213,062.69 | 4231.92 | B | 14,820.10 |
| PRZ | SPR_033 | BBL2 | 580,733.61 | 1,208,224.28 | 4257.61 | A | 13,033.85 |
| PRZ | SPR_033 | BBL2 | 580,733.61 | 1,208,224.28 | 4257.61 | B | 5,792.00 |
| PRZ | SPR_037 | BBL3 | 586,178.69 | 1,206,806.76 | 4296.00 | A | 14,317.02 |
| PRZ | SPR_037 | BBL3 | 586,178.69 | 1,206,806.76 | 4296.00 | B | 14,539.34 |
| PRZ | SPR_041 | BBL4 | 593,090.97 | 1,198,955.66 | 4124.75 | A | 14,257.90 |
| PRZ | SPR_041 | BBL4 | 593,090.97 | 1,198,955.66 | 4124.75 | B | 8,435.66 |
| PRZ | SPR_044 | BBL5 | 570,778.14 | 1,213,230.76 | 4231.34 | A | 14,678.94 |
| PRZ | SPR_044 | BBL5 | 570,778.14 | 1,213,230.76 | 4231.34 | B | 14,067.68 |
| CTA | STM_016 | BBL6 | 483,874.05 | 1,153,059.89 | 4312.393 | A | 13,198.48 |
| CTA | STM_016 | BBL6 | 483,874.05 | 1,153,059.89 | 4312.393 | B | 14,656.86 |
| CTA | STM_014 | BBL8 | 484,132.47 | 1,147,057.46 | 4304.071 | A | 13,886.74 |
| CTA | STM_014 | BBL8 | 484,132.47 | 1,147,057.46 | 4304.071 | B | 13,808.63 |
| CTA | STM_001 | BBL9 | 481,087.98 | 1,142,600.29 | 4285.167 | A | 13,737.43 |
| CTA | STM_001 | BBL9 | 481,087.98 | 1,142,600.29 | 4285.167 | B | 7,202.04 |
| CTA | SWM_022 | BBL10 | 466,997.10 | 1,164,293.39 | 4,292.70 | A | 14,048.22 |
| CTA | SWM_022 | BBL10 | 466,997.10 | 1,164,293.39 | 4,292.70 | B | 13,705.86 |
| CTA | STM_007 | BBL11 | 482,847.49 | 1,144,973.21 | 4,283.07 | A | 14,357.34 |
| CTA | STM_007 | BBL11 | 482,847.49 | 1,144,973.21 | 4,283.07 | B | 14,179.35 |
| CTA | SWM_024 | BBL12 | 443864.26 | 1,140,404.16 | 4380.38 | A | 12,968.35 |
| CTA | SWM_024 | BBL12 | 443864.26 | 1,140,404.16 | 4380.38 | B | 13,287.20 |

Date is the deployment date, Lander Easting and Northing are the locations of the BBL Lander on the seafloor, depth is the depth of the Lander during deployment, and the volume of seawater filtered (L) by each pump (A/B) is reported at right. Two pumps (A/B) are mounted in the pump during deployment.

Table 6-30 Overview of CTD casts conducted that were sampled for eDNA.

| AREA | STATION | CTD | LATITUDE | LONGITUDE | DEPTHS SAMPLED |
|------|---------|------|-------------|--------------|---------------------------------------|
| PRZ | | CTD1 | 10° 59.554 | 116° 21.462 | 200m, 50m, 45m, 5m, Field Blank |
| PRZ | | CTD2 | 10° 59.554 | 116° 21.462 | 2600m, 1200m, 750m, 500m, Field Blank |
| PRZ | | CTD4 | 10° 57.3690 | 116° 10.2749 | 200m, 80m, 45m, 5m, Field Blank |

| AREA | STATION | CTD | LATITUDE | LONGITUDE | DEPTHS SAMPLED |
|------|---------|--------|-------------|--------------|--|
| PRZ | | CTD5 | 10° 57.3690 | 116° 10.2749 | 3000m, 1200m, 780m, 500m, Field Blank |
| PRZ | | CTD10 | 10° 50.6796 | 116° 09.1358 | 200m, 85m, 63m, 5m, Field Blank |
| PRZ | | CTD11 | 10° 50.6796 | 116° 09.1358 | 3000m, 1200m, 780m, 500m, Field Blank |
| CTA | | CTD14 | 10° 25.7117 | 117° 08.8698 | 1200m, 780m, 500m, 200m, 92m, 62m, 5m, Field Blank |
| CTA | | CTD15* | 10° 25.7278 | 117° 08.882 | 4315m (5 mab), 4263m (50 mab), 3000m |
| CTA | | CTD17 | 10° 21.48 | 117° 09.55 | 1200m, 800m, 500m, 200m, 85m, 67m, 5m |
| CTA | | CTD18* | 10° 21.48 | 117° 09.55 | 4276m (5 mab), 4231m (50 mab), 3000m, Field Blank |
| PRZ | | CTD20 | 10° 54.9525 | 116° 12.9163 | 1200m, 800m, 500m, 200m, 80m, 72m, 5m |
| PRZ | | CTD21* | 10° 54.9518 | 116° 12.915 | 4292m (5 mab), 4247m (50 mab), 3000m |
| PRZ | | CTD22 | 10° 50.5984 | 116° 09.1312 | 1200m, 860m, 500m, 200m, 80m, 71m, 5m, Field Blank |
| PRZ | | CTD23* | 10° 50.6379 | 116° 09.1277 | 4125m (5 mab), 4080m (50 mab), 3000m |

Event No includes the CTD cast #, with * indicating casts conducted with the Trace Metal (TM) CTD. Start time is local time (PT), Field blank are negative controls (filtered MilliQ water), mab = meters above bottom. Depths target specific features of the water column, e.g. upper and lower oxycline, deep chlorophyll maximum (DCM), base of epipelagic (200m).

(c) eDNA water sampling

Seawater samples for eDNA studies were obtained from the rosette on 14 CTD casts, using both the main hydrographic and trace metal CTD. The initial sampling plan was to conduct a shallow-deep CTD pair of casts in order to sample across full water column depth. Due to problems with the deep winch, samples were not obtained below ~ 3000m on several casts. In the first occupation of the PRZ, 2 high quality sets of paired CTD casts, with rosette sampling from 3000m to the surface were completed (Table 6-30). Two additional partially successful casts (CTD1, CTD2) are useful as initial test casts. Within the CTA, 2 pairs of successful casts were completed that enabled complete samples from the sea surface to the seafloor. The shallower casts were conducted on the main CTD (0-1500m), with a deep cast on the trace metal (TM) CTD. Upon return to the PRZ at the end of the campaign 5B, another pair of full casts with sampling from the sea surface to the seafloor, combining sampling 1200m to the surface on the main CTD with deep ocean sampling on the trace metal CTD.

Niskin/GoFlo bottles sampled at 5 m above bottom (5 mab), 50 meters above bottom (50 mab), bathypelagic depths (3000m, 1200m most casts), in the mesopelagic at the lower oxycline (variable, feature-targeted) and 500m, at the upper oxycline (variable, feature-targeted), the deep chlorophyll maximum (DCM; variable, feature-targeted), and at 5 m below the sea surface.

However, it became apparent that the pressure sensor on the TM CTD was possibly offset relative to the main CTD (and true values), as the apparent seafloor depths, based on pressure sensor readings and altimetry detection of the seafloor, were ~ 100m shallower than expected based on multibeam data as well as depths obtained on the BBL lander transponder for deployments in close proximity (only ~35m away in 1 case). Cross- calibration of the two systems for the oxygen sensors appeared to corroborate this hypothesis of an offset in the pressure sensor on the TM CTD.

6.4.3.4 Preliminary results & discussion

(a) 1m² MOCNESS samples

Laboratory processing of samples from the 1m² MOCNESS have been conducted for (1) biomass measurements (Table 6-31); (2) elemental composition of the whole zooplankton community (carbon,

nitrogen measurements) (Table 6-32) and DNA extractions are currently underway for metabarcoding of whole community zooplankton samples (Table 6-33).

Table 6-31 Overview of progress on processing 1m² MOCNESS samples for biomass measurements (wet weight/ dry weight).

| MOCTOW ID | DATE | DAY/NIGHT | # SAMPLES PROCESSED | COMPLETE |
|-----------------|---------|-----------|---------------------|----------|
| DG5B_PRZ_1MOC1 | 3/19/21 | Night | 49 | ** |
| DG5B_PRZ_1MOC2 | 3/21/21 | Night | 49 | ** |
| DG5B_PRZ_1MOC3 | 3/23/21 | Day | 0 | ---- |
| DG5B_PRZ_1MOC4 | 3/25/21 | Day | 54 | ** |
| DG5B_PRZ_1MOC5 | 3/26/21 | Day | 46 | ** |
| DG5B_PRZ_1MOC6 | 3/28/21 | Night | 46 | ** |
| DG5B_CTA_1MOC7 | 4/2/21 | Day | 45 | ** |
| DG5B_CTA_1MOC8 | 4/3/21 | Day | 48 | ** |
| DG5B_CTA_1MOC9 | 4/6/21 | Night | 15 | ---- |
| DG5B_CTA_1MOC10 | 4/7/21 | Night | 46 | ** |
| DG5B_CTA_1MOC11 | 4/10/21 | Day | 0 | ---- |
| DG5B_CTA_1MOC12 | 4/12/21 | Night | 47 | ** |

** = complete, ---- = in progress or not yet begun.

Table 6-32 Overview of progress on processing 1m² MOCNESS samples for elemental stoichiometry (carbon, nitrogen).

| MOCTOW ID | DATE | DAY/NIGHT | # SAMPLES PROCESSED | COMPLETE |
|-----------------|---------|-----------|---------------------|----------|
| DG5B_PRZ_1MOC2 | 3/21/21 | Night | 12 | ---- |
| DG5B_PRZ_1MOC5 | 3/26/21 | Day | 0 | ---- |
| DG5B_CTA_1MOC8 | 4/3/21 | Day | 60 | ** |
| DG5B_CTA_1MOC10 | 4/7/21 | Night | 50 | ** |

Table 6-33 Overview of progress on DNA extractions for metabarcoding of 1m² MOCNESS samples.

| MOCTOW ID | DATE | DAY/NIGHT | # SAMPLES PROCESSED | COMPLETE |
|-----------------|---------|-----------|---------------------|----------|
| DG5B_PRZ_1MOC1 | 3/19/21 | Night | 9 | 50% |
| DG5B_PRZ_1MOC2 | 3/21/21 | Night | 0 | 0% |
| DG5B_PRZ_1MOC3 | 3/23/21 | Day | 3 | 17% |
| DG5B_PRZ_1MOC4 | 3/25/21 | Day | 1 | 6% |
| DG5B_PRZ_1MOC5 | 3/26/21 | Day | 4 | 22% |
| DG5B_PRZ_1MOC6 | 3/28/21 | Night | 3 | 17% |
| DG5B_CTA_1MOC7 | 4/2/21 | Day | 1 | 6% |
| DG5B_CTA_1MOC8 | 4/3/21 | Day | 8 | 44% |
| DG5B_CTA_1MOC9 | 4/6/21 | Night | 4 | 22% |
| DG5B_CTA_1MOC10 | 4/7/21 | Night | 0 | 0% |
| DG5B_CTA_1MOC11 | 4/10/21 | Day | 9 | 50% |
| DG5B_CTA_1MOC12 | 4/12/21 | Night | 5 | 28% |
| TOTAL | | | 100 | |

There are 2 size fractions from each net and tow (SM, LG), for 218 total samples. Extractions to date have focused on the SM size fraction only.

(b) Zooplankton biomass

Zooplankton biomass in the upper 1500 m of the water column ranged from a mean of 0.2319 to 10.3783 mg m⁻³ dry weight (DW) within each depth horizon in daytime and 0.2902 to 16.2557 mg m⁻³ in each horizon during night-time over the collector test area (CTA; Figure 6-62). Comparable wet weight (WW) biomass measures ranged from a mean of 2.4565 to 85.1711 mg m⁻³ during daytime and 3.0907 to 173.7223 mg m⁻³ during nighttime (Figure 6-62).

Zooplankton biomass was highest in the well-oxygenated upper 100 m, with a maximum in daytime in the 0 – 50 m layer and maximum in nighttime in the 50 – 100 m layer. Biomass declined below this region, with a strong effect of the upper oxycline within the 50 – 100 m layer. Significant biomass remained in the 100 – 300 m and 300 – 500 m layers, in particular, during daytime, with very low biomass within the core of the oxygen minimum zone (OMZ) at 500 – 700 m (0.8392 mg m⁻³ DW, mean day).

A mild bimodal trend was visible, again in daytime, with a slight increase in biomass in the 700 – 800 m layer across the lower oxycline, with consistent declines in biomass below that to a minimum within the deepest 1250 – 1500 m layer (0.2319 mg m⁻³ DW, mean day). The overall trends in the distribution were broadly consistent between dry and wet weight measures of biomass (Figure 6-62). Greater variability in biomass occurs in the 0 – 50 m and 50 – 100 m layers (e.g., 2.43 mg m⁻³ DW st. dev., 50-100 m layer), due in part to the presence of gelatinous zooplankton.

Zooplankton biomass in the upper 1500 m of the water column over the Preservation Reference Zone (PRZ) ranged from a mean of 0.2218 to 21.6922 mg m⁻³ dry weight (DW) within each depth horizon in daytime and 0.1879 to 18.4711 mg m⁻³ in each horizon during night-time (Figure 6-63). Comparable wet weight (WW) biomass measures ranged from a mean of 2.2421 to 260.8188 mg m⁻³ during daytime and 2.1486 to 178.2184 mg m⁻³ during nighttime over the same region. Broad characteristic features of the biomass distribution were as observed over the CTA, with high biomass in the well oxygenated upper mixed layer (ML) and across the upper oxycline, and with very low biomass within the core of the OMZ at 500 – 700 m and below 1000 m (in the bathypelagic). One MOC tow over PRZ had very high biomass in the 50 – 100 m layer during daytime (1MOC4), in part due to gelatinous zooplankton.

Figure 6-62 Zooplankton biomass across the upper 1500 m of the water column during daytime and night-time over the collector test area (CTA). Mean and standard deviation of dry (top) and wet weight (bottom) are shown for 2 day and 2-night tows.

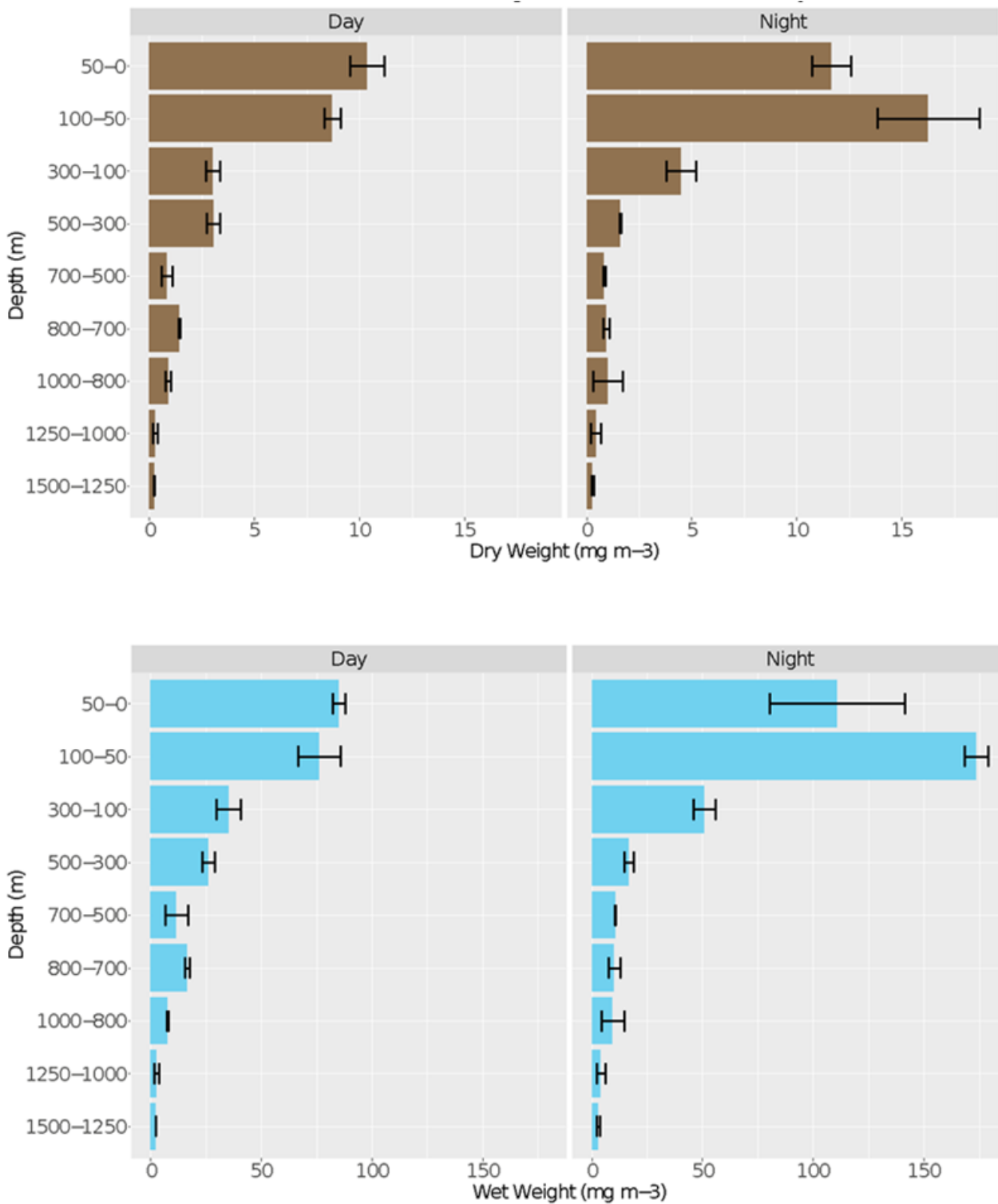


Figure 6-63 Zooplankton biomass across the upper 1500 m of the water column during daytime and nighttime over the preservation reference zone (PRZ). Mean and standard deviation of dry (top) and wet weight (bottom) are shown for 2 day and 3 night tows.

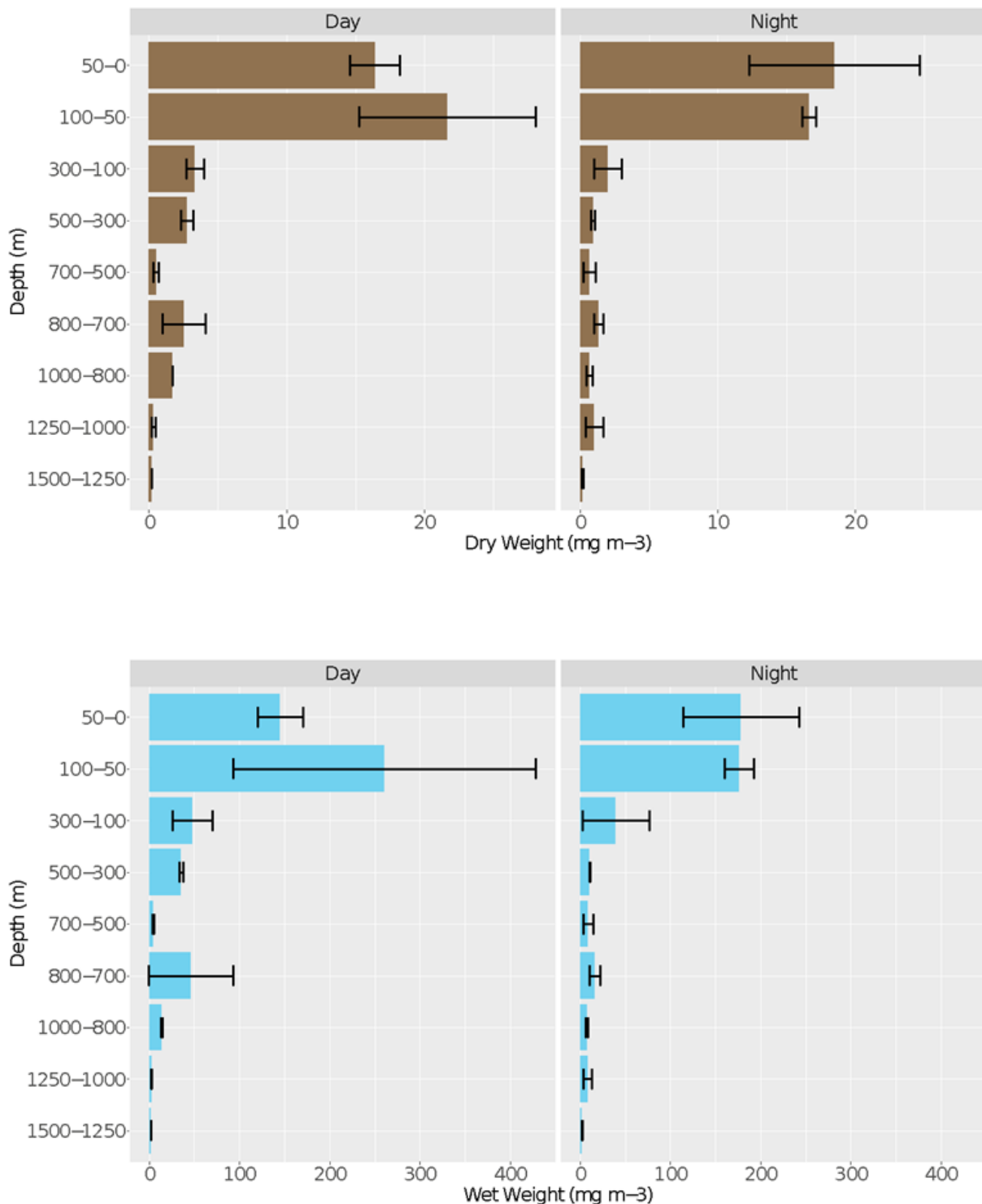
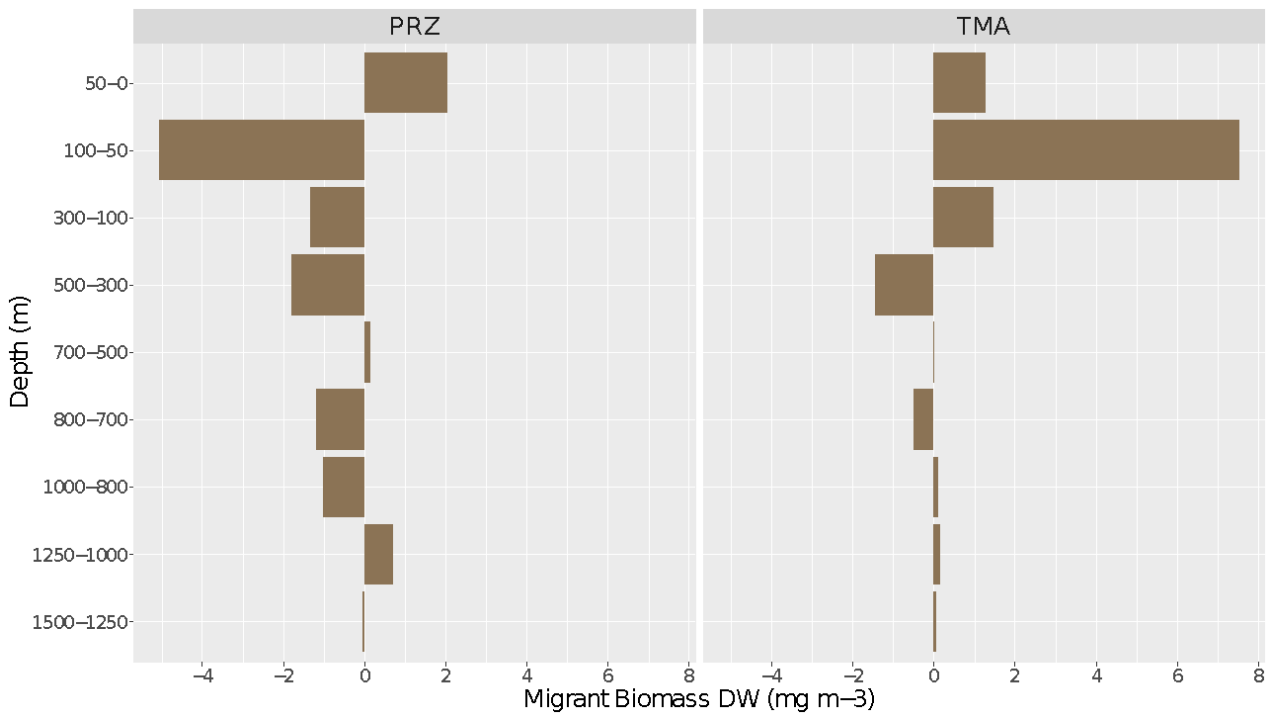


Figure 6-64 Migrant zooplankton biomass over the PRZ (left) and CTA (right) as measured by dry weight (mg m⁻³). Histogram bars to the right of 0 indicate depths that zooplankton are arriving at during night-time upward DVM migrations (in the upper ocean), while bars to the left of 0 indicate depths that zooplankton are leaving from during their return to the surface. The overall trends seen in wet biomass are comparable, but at higher total biomass (results not shown). CTA data derive from 2 day and 2 night tows; for PRZ from 3 night and 2 day tows.

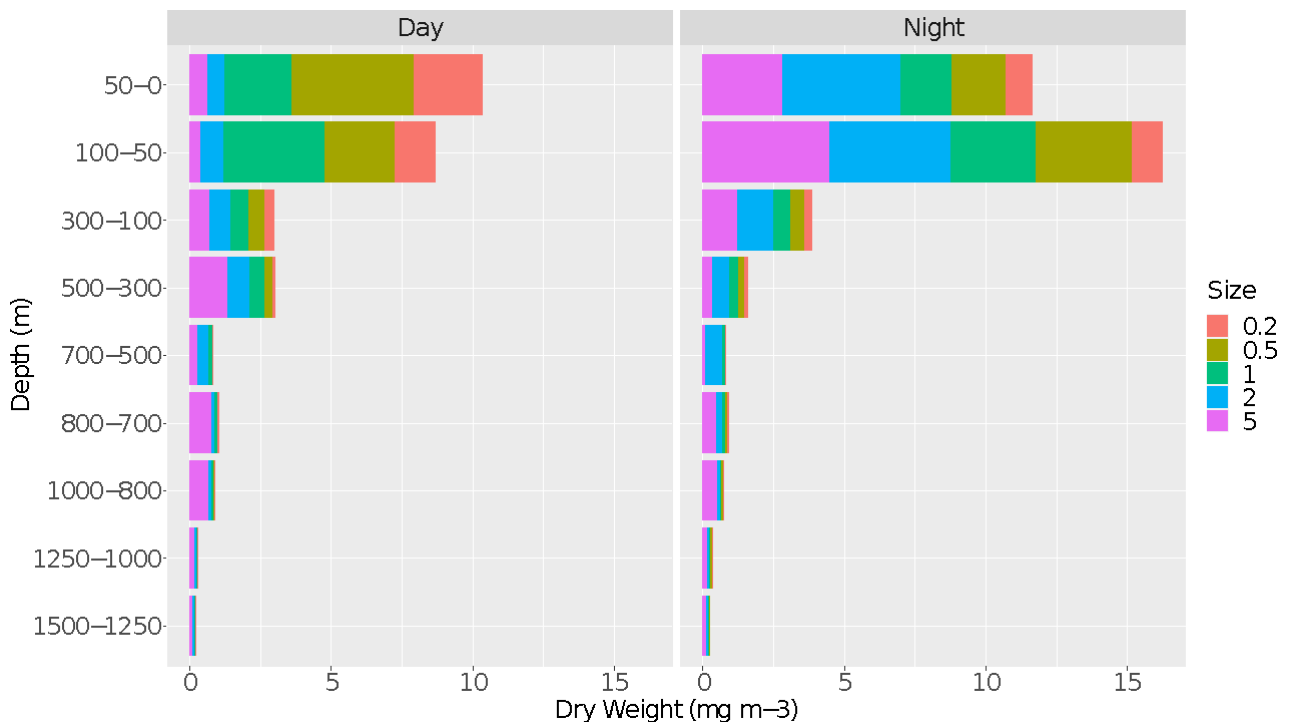


(c) Zooplankton migrant biomass

Figure 6-64 shows the overall trends in migrant biomass at the two sites given our current data (5 1m² MOCNESS tows analyzed at PRZ, 4 tows analyzed at CTA). At CTA 13.2957 mg m⁻³ dry weight (DW) migrant biomass was arriving at nighttime in the upper three layers, between 300 m and the sea surface. Migrants were departing from the 300 – 500m depth horizon, as well as from the lower oxycline, below the core of the OMZ, at 700 – 800 m. Nearly no migrant biomass was present within the core of the OMZ (500 – 700 m; all resident biomass): Based on prior work, we expect resident specialist species to occur within this layer (e.g., (Wishner et al. 2013, Wishner et al. 2020). While the total migrant biomass arriving in the upper ocean was 10.2957 mg m⁻³ dry weight (DW), the total amount leaving deeper depths was 1.9400 mg m⁻³ dry weight (DW), suggesting a deficit of 8.3557 mg m⁻³ DW due to capture avoidance in the daytime. At CTA, the total migrant biomass in the upper 300 m at night was 138.7055 mg m⁻³ wet weight (WW)(integrated 300 – 0 m).

The trends in migrant biomass for the PRZ seem to be heavily influenced by high gelatinous zooplankton biomass in 1 daytime MOC tow (1MOC4). We look forward to completing analyses on all samples, as we expect results for the 50 – 100 m layer may change. At present, 2.0536 mg m⁻³ DW migrant biomass arrives in the upper 50 m of the water column at night (Figure 6-64), while 9.3716 mg m⁻³ DW migrant biomass leaves from deeper depths. Migrants are departing from the lower oxycline and below, between 700 and 1000 m, as well as from the upper OMZ between 500 and 100m. As observed over the CTA, there appears to be no migrant biomass within the core of the OMZ at 500 – 700 m. At PRZ, there is a deficit of migrant biomass of 7.31796 mg m⁻³ DW, but in this case with higher estimates of leaving than arriving migrants. Our current data suggests that the migration extends deeper in the water column at the PRZ than the CTA, down to the base of the mesopelagic (1000 m).

Figure 6-65 Zooplankton biomass as measured by dry weight plotted for all size fractions over the CTA. Increases in DW biomass for larger size fractions in the upper ocean at night are migrants. Mean values shown.

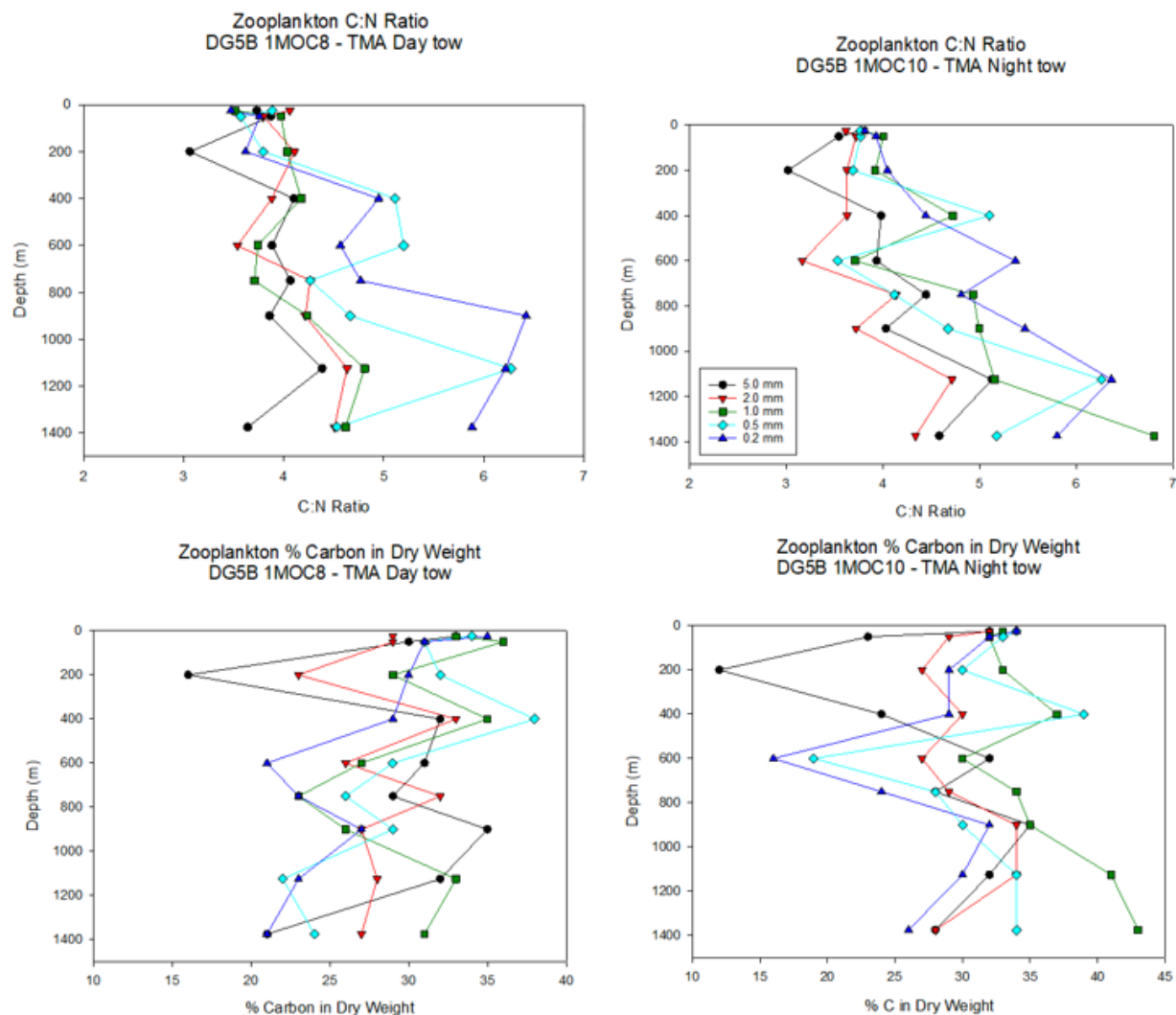


From this preliminary analysis, no significant differences were observed in zooplankton dry weight biomass between the CTA and PRZ, considered as either integrated biomass between 0 – 1500m (day/night evaluated separately) (t-test, $p=0.147$ day, $p=0.507$ night), or for distinct depth horizons 0 – 100m, 100 – 300m, 300 – 700m (OMZ), 700 – 1000m, or 1000 – 1500m ($p>0.1$ all comparisons).

(d) Zooplankton stoichiometry

Preliminary results regarding zooplankton elemental composition are shown in Figure 6-66. A consistent trend towards increasing carbon: nitrogen (C:N) ratio across depth in the water column is apparent. Initial results also suggest that the smaller zooplankton size fractions may have higher C:N ratio than larger zooplankton, which may reflect incorporation of protists (e.g. radiolarians) or detritus in addition to metazoan animals that are the targets. Plots of % carbon in zooplankton dry weight suggest low carbon content for the zooplankton community within the 100-300m layer and possibly also within the oxygen minimum zone (1MOC10). Additional replication on these measurements is needed, and samples are waiting in the queue for this analysis.

Figure 6-66 Zooplankton stoichiometry. (Top) C:N ratio across the water column for 5 size fractions in 1 day and 1 night 1m² MOCNESS tow. (Bottom) % carbon in zooplankton dry weight biomass for the same 5 size fractions. Additional replication on these measurements is currently in the sample processing queue, results are preliminary.



(e) BBL lander samples

All animals collected from Pump B on each BBL lander deployment have been sorted. Animals have been enumerated and a coarse taxonomic level classification applied. Additional work remains for finer taxonomic identification. Greater attention has been paid to date on meroplanktonic larvae (first priority), and all larvae have been imaged and body sizes measured.

Table 6-34 Overview of progress on analysing BBL Lander samples.

| EVENT# | SAMPLE HEADER | PUMP | Q1/2 PRESERVATION | Q2/2 PRESERVATION | STATUS 11/2021 |
|--------|---------------|------|-------------------|-------------------|----------------|
| PL_001 | DG5B_PRZ_BBL1 | A | EtOH | RNALater | + |
| PL_001 | DG5B_PRZ_BBL1 | B | EtOH | Formalin | * |
| PL_002 | DG5B_PRZ_BBL2 | A | EtOH | RNALater | + |
| PL_002 | DG5B_PRZ_BBL2 | B | EtOH | Formalin | * |
| PL_003 | DG5B_PRZ_BBL3 | A | EtOH | RNALater | + |
| PL_003 | DG5B_PRZ_BBL3 | B | EtOH | Formalin | * |
| PL_004 | DG5B_PRZ_BBL4 | A | EtOH | RNALater | + |
| PL_004 | DG5B_PRZ_BBL4 | B | EtOH | Formalin | * |

| EVENT# | SAMPLE HEADER | PUMP | Q1/2 PRESERVATION | Q2/2 PRESERVATION | STATUS 11/2021 |
|--------|----------------|------|-------------------|-------------------|----------------|
| PL_005 | DG5B_PRZ_BBL5 | A | EtOH | RNALater | + |
| PL_005 | DG5B_PRZ_BBL5 | B | EtOH | Formalin | * |
| PL_006 | DG5B_CTA_BBL6 | A | EtOH | RNALater | + |
| PL_006 | DG5B_CTA_BBL6 | B | EtOH | Formalin | * |
| PL_008 | DG5B_CTA_BBL8 | A | EtOH | RNALater | + |
| PL_008 | DG5B_CTA_BBL8 | B | EtOH | Formalin | * |
| PL_009 | DG5B_CTA_BBL9 | A | EtOH | RNALater | + |
| PL_009 | DG5B_CTA_BBL9 | B | EtOH | Formalin | * |
| PL_010 | DG5B_CTA_BBL10 | A | EtOH | RNALater | + |
| PL_010 | DG5B_CTA_BBL10 | B | EtOH | Formalin | * |
| PL_011 | DG5B_CTA_BBL11 | A | EtOH | RNALater | + |
| PL_011 | DG5B_CTA_BBL11 | B | EtOH | Formalin | * |
| PL_012 | DG5B_CTA_BBL12 | A | EtOH | RNALater | + |
| PL_012 | DG5B_CTA_BBL12 | B | EtOH | Formalin | * |

Key for column at right: * = Sorted and enumerated with coarse taxonomic classification; + = to be sorted and enumerated OR sequenced.

A total of 12,103 individuals were collected from one of two McLane pumps across 11 BBL lander deployments on Campaign 5B, with 6,656 individuals collected from the CTA and 5,447 collected from the PRZ. The assemblage is dominated by copepods and their nauplii comprising 97% of all individuals (Figure 6-67), broadly comparable to results found on BBL lander deployments in other CCZ exploration contract areas and APEIs. However, the ratio between copepods and nauplii is variable between the PRZ and CTA within NORI-D, and higher on average within the PRZ. Chaetognaths dominate the holoplanktonic assemblage after copepods and their nauplii. A total of 43 chaetognath individuals across 11 deployments were collected, 10 in the PRZ and 33 in the CTA. The highest density at a single site was 1 individual / m³. There appear to be at least 3 chaetognath morphotypes present within NORI-D based on head shape. Nearly nothing is currently known about these abyssal benthopelagic chaetognaths.

Benthic-associated demersal zooplankton collected include amphipods, isopods, and larval forms of polychaetes, bivalves, gastropods, barnacles, and bryozoans (Figure 6-68). Larval abundances range from 3- 26 individuals per deployment and most groups are quite patchy in occurrence. Overall, community composition is quite variable between deployments within the same site (CTA vs. PRZ).

Gastropod larvae occur in equal proportions in the CTA and the PRZ. However, polychaete larvae are notably over 6 times more abundant in the CTA than in the PRZ. Initial results suggest community differentiation between the CTA and PRZ of NORI-D based on habitat type (Section 5.17; i.e. flat, soft sediment seabed vs. topographically variable seamount or ridge type; Figure 6-69 and Figure 6-70).

Figure 6-67 Relative abundance of all major BBL zooplankton taxa from DG5B (PRZ, CTA), in comparison to other areas within the CCZ. All sites are dominated by copepods and their nauplii. Data from a total of 29 lander deployments is shown, 11 from NORI-D.

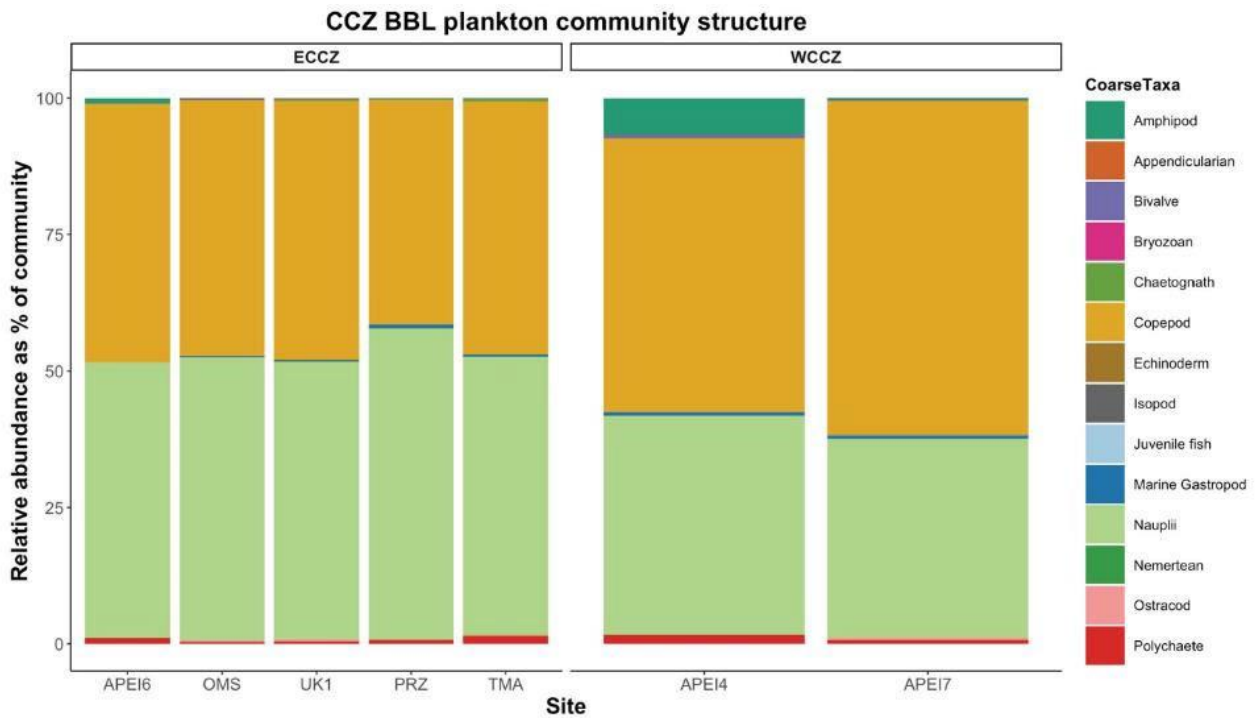


Figure 6-68 A few highlights of the diversity of animals captured in the BBL lander from Pump B on DG5B. Animals pictured here include: bryozoan larvae, chaetognath, gastropod larvae, polychaete larvae, bivalve larvae, ostracod, isopod, and amphipod. All animals captured are approximately between 3 mm and 100 µm in body size.



Figure 6-69 Community composition of meroplankton sampled from one pump across 11 BBL Lander deployments on the Campaign 5B. The outer ring of the pie chart represents the relative community composition of the CTA and the inner ring represents that of the PRZ. Polychaete larvae were over 6X more abundant in the CTA.

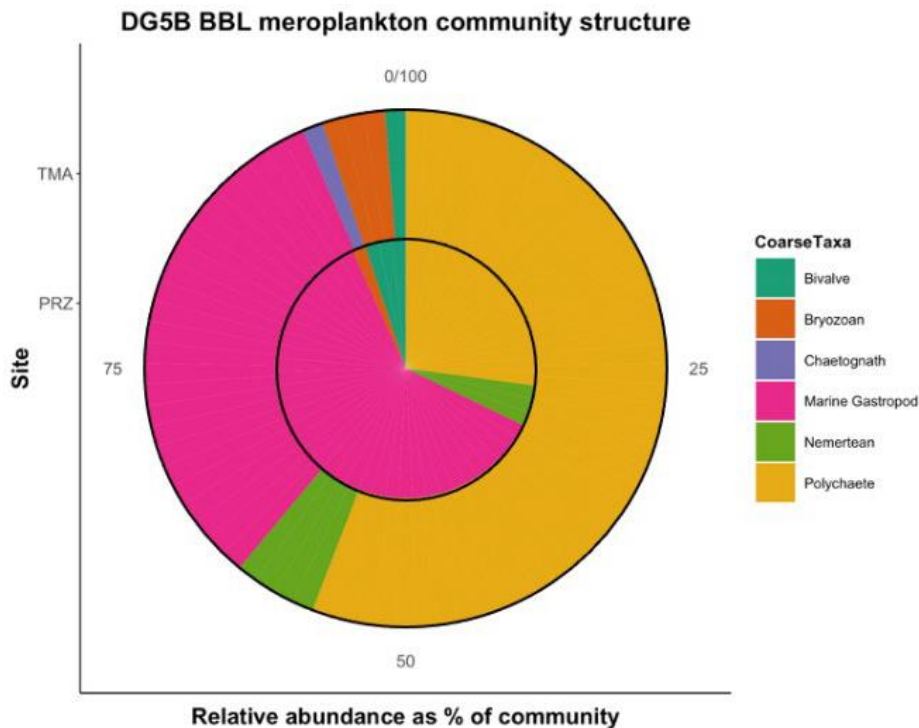
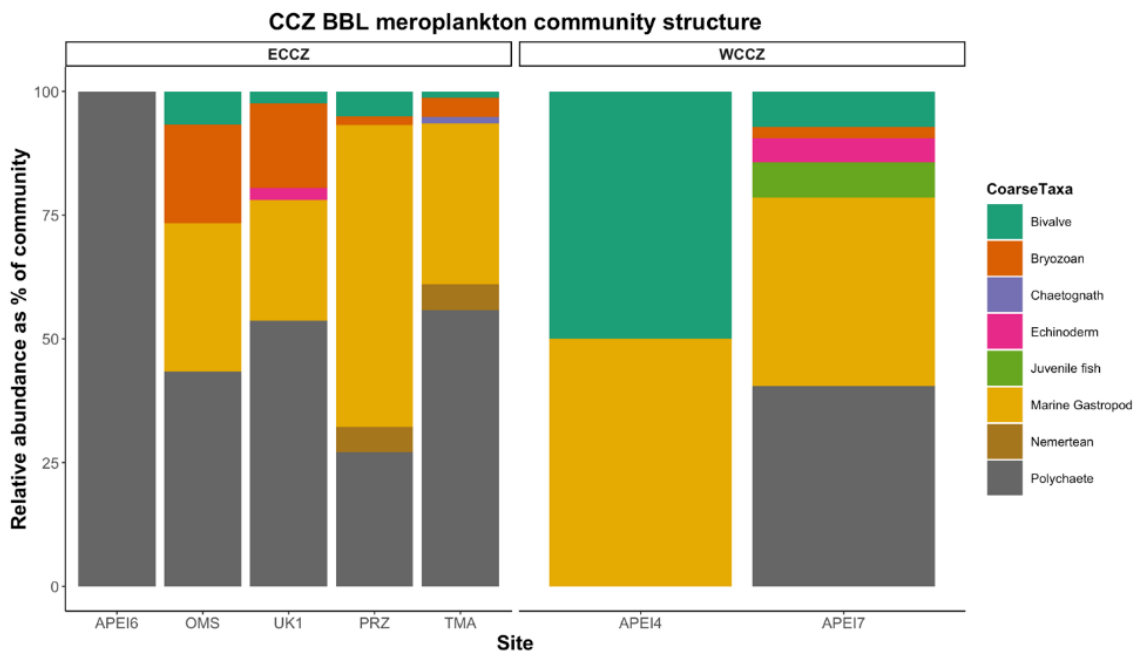


Figure 6-70 Relative abundance of BBL meroplanktonic taxa from Campaign 5B in comparison to other areas in the CCZ.



Community structure between holoplankton and meroplankton is quite consistent across the CCZ with larvae generally representing less than 1-3% of the individuals (Figure 6-70). Meroplankton were patchy in abundance (0.65 – 6.83 ind./m³, 0 – 1.4 ind./m³ in the eastern and western CCZ respectively) with taxa including polychaetes, echinoderms, bivalves, gastropods, barnacles, and bryozoans. Across all deployments and campaigns, the meroplankton community is quite under sampled, making statements

about the breakdown within this group quite difficult. Investigations are ongoing on several taxa found in NORI-D that appear unique to this region, including pelagic gelatinous polychaetes as well as several groups of chaetognaths.

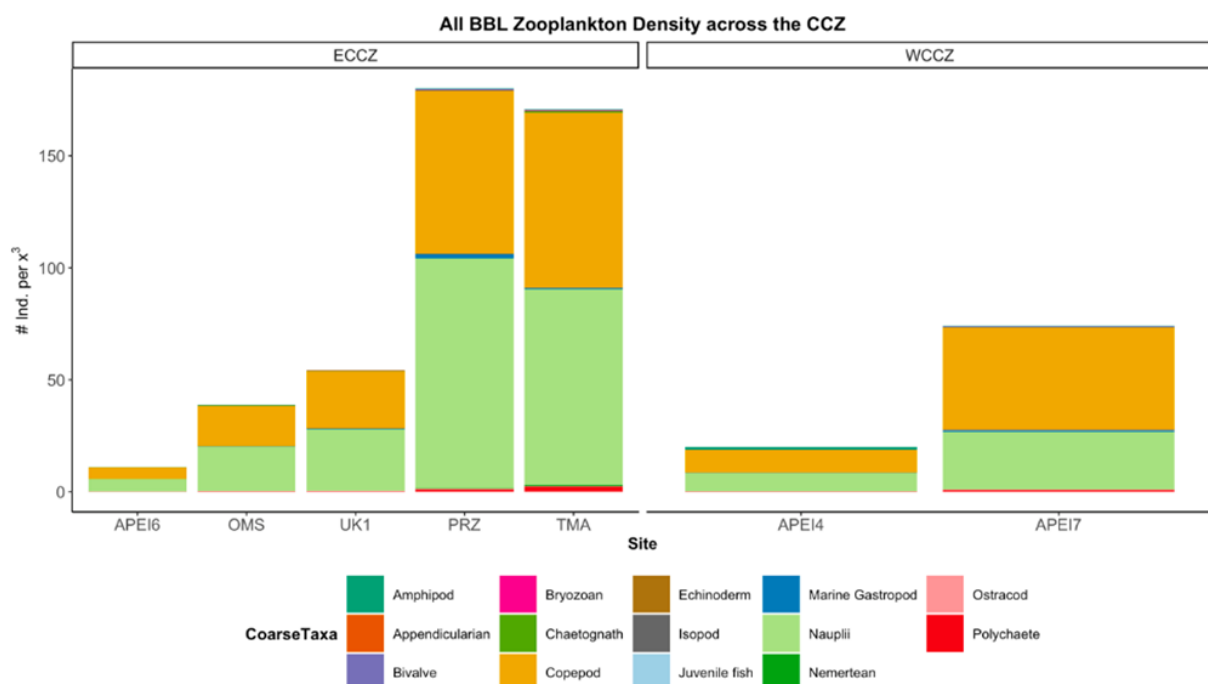
The highest densities of abyssal benthopelagic zooplankton to date have been observed in NORI-D during the campaign 5B (Table 6-35; Figure 6-70). Average BBL zooplankton densities in NORI-D, (~175 individuals/m³) were more than double those found in neighbouring east CCZ contract areas or in the west CCZ. Additional verification is underway to confirm that the normalization to seawater volumes filtered during the pump (& quantitative splitting) are accounted for correctly in for prior work in the UK1 and OMS contract areas, and on the classification of copepod molts/carapaces vs animals inferred to be captured alive (synthesis of eastern CCZ results). BBL zooplankton densities exhibited both N/S and E/W spatial gradients in the CCZ and covaried with estimated POC flux, with nearly 2X higher total density in the east (~103 ind./m³) than in the west (~59 ind./m³).

It is not yet clear what drives this spatial patterning, but factors may include sampling season, bathymetry / topography, seafloor habitat type, and near bottom ocean currents.

Table 6-35 Average BBL zooplankton densities in the PRZ and CTA of the NORI-D claim area, in comparison to other regions across the CCZ.

| AREA | AVERAGE DENSITY | S.D. |
|-------|-----------------|-----------|
| PRZ | 178.54793 | 58.294586 |
| CTA | 169.91471 | 51.59442 |
| APEI7 | 73.07203 | 65.069732 |
| UK1 | 53.86147 | 20.569165 |
| OMS | 38.45657 | 4.009814 |
| APEI4 | 20.02140 | NA |
| APEI6 | 10.97275 | NA |

Figure 6-71 Average zooplankton densities (individuals/m³) across regions of the CCZ. Data is included from DG5B represented by PRZ and CTA, as well as sampling conducted in APEIs 4 and 7 in the west and the OMS, UK1, claim areas and APEI 6 in the east. NOTE: Another scientist was involved in scope counts for other eastern CCZ areas. We need to confirm (A) that the seawater volumes that counts are normalized to are correct, and (B) how copepod carcasses were counted in this earlier work. Final numbers to be confirmed.



Upper ocean (0-1500m) zooplankton biomass results, although quite preliminary, largely follow observations reported from other areas of the eastern tropical Pacific (ETP). The overall vertical structure of biomass showed distinct features in association with the OMZ hydrographic structure. Our observations of high biomass in the upper thermocline, at the top of the upper oxycline, and also in the lower oxycline were also observed by Wishner *et al.* (2013; 2020) at sites to the east (Costa Rica Dome) and north (Tehuantepec Bowl) of the NORI-D region, although the specific depths at which these hydrographic features occurred was variable between areas.

The Tehuantepec Bowl (13 N / 105 W) also had a very broad and strong OMZ, and results from this site will be a useful comparative site for work at NORI-D. A very deep penetration of diel vertical migrators, with some animals moving to the 700-800m lower oxycline (LO), or even lower at the PRZ (down to 1000m), for their daytime resting depth, was observed. While this pattern has been reported before, the NORI-D has a particularly deep LO, and most prior studies focus on areas with a LO in the range of 500-600, closer to the daytime resting depth for deep migrating taxa in regions without OMZs. To our knowledge this is the first time sampling has been conducted into the upper bathypelagic (1000-1500m) and results from this region of the water column are particularly novel, and relevant to the discharge depth.

From these preliminary results, there is no evidence of significant differences in zooplankton biomass between the PRZ and the CTA, despite higher net community production at the PRZ. There is however high variability among tows, in particular at the PRZ, and ongoing analyses on all tows, may provide a better understanding of spatial variability.

The first DNA sequence-based surveys of the mesozooplankton for this region of the global ocean (metabarcoding) are currently ongoing. These data will help to obtain a clear resolution of the DVM behaviour and vertical profiles of the full community, as well as true estimates of zooplankton richness and diversity across the water column.

For abyssal zooplankton, preliminary results from NORI-D are presented in context relative to all other published and unpublished data on abyssal BBL larval assemblages in the CCZ (Kersten *et al.* 2017, Kersten *et al.* 2019). While overall zooplankton community composition in the NORI-D is dominated by copepods and their nauplii, as found in all other areas of the CCZ, animal abundance in the NORI-D is higher than regions in the eastern CCZ but north of our sampling sites (OMS, UK1) and in regions to the west (APEIs 4 & 7). Currently, these differences in abyssal zooplankton density look very pronounced; and it is expected that these abundances are correlated with high POC flux to the seafloor. Overall community composition of the larval assemblage specifically is broadly comparable to organisms found at other sites, including gastropods, bivalves, benthic polychaetes, bryozoans, and echinoderms. There does appear to be some spatial variability in the larval assemblage with 6X higher larval polychaete abundance in the CTA in comparison to the PRZ.

6.4.4 Gelatinous zooplankton community

6.4.4.1 Purpose & scope

The following section describes the work conducted in 2021 by JAMSTEC to characterise natural baseline conditions in gelatinous zooplankton communities in the NORI-D contract area. The scope, the survey planning and the sampling methodologies carried out to ecologically characterise these communities align with International Seabed Authority ISBA/25/LTC/6 Rev 1. Annex 1 section 42(c) gelatinous zooplankton and 44. Vertical migration. to provide baseline data requirements under Recommendations III.B.15.(d).(iii); IV.B.22.

6.4.4.2 Baseline investigations

The methods and proposed survey array for both the collector test and long-term environmental studies on NORI-D will provide data to meet the following objectives:

- Characterize the abundance, biomass, diversity and composition of the gelatinous zooplankton community from the surface to the benthic boundary layer

6.4.4.3 Campaign activities

(a) Campaign 5B & 5E survey design

Video and specimen material were collected during Campaigns 5B and 5E. The ROV *Odysseus* (Pelagic Research Services) was equipped with a 6-cannister suction sampler with a variable speed hydraulic pump, and four D-samplers (Youngbluth 1984) – two mounted on each of the two hydraulically powered swing arms.).

The pan-tilt unit-mounted main video camera was a Mini Zeus 4K (Insite Pacific Inc.). A stereo pair of IP Multi SeaCam cameras (model IPMSC-3105, DEEPSEA Power & Light) were mounted with their centres 100mm apart on a fixed bracket and facing forward. Time was synchronized using a modular NTP time server and GPS antenna. Environmental data was measured using a CTD (SBE 19plus V2 SeaCAT, Sea-Bird Scientific) with a dissolved oxygen sensor (SBE 43, Sea-Bird Scientific), transmissometer (C-Star 25cm, Sea-Bird Scientific), and a Chl a-turbidity sensor (ECO FLNTU, Sea-Bird Scientific). ROV navigation data (eg. heading, pitch, roll [iXBLUE PHINS-derived], depth [Paroscientific Digiquartz depth sensor-derived], altitude [DVL-derived]) and CTDO data was ingested, timestamped and logged using a Python script, and passed to an image annotation system (GreyBitsBox, GreyBits Engineering) that enabled real-time frame capture from the streaming 4K video, and environmental-navigation metadata extraction/association into an SQL database through the Squidle+ web interface.

A slow, oblique descent (5-10m/min) of the ROV was punctuated by horizontal transects, each of 15 minutes duration, with the main camera set on a fixed focus position in the “sweet spot” of maximum light convergence, approximately 1.5m in front of the camera’s domed viewport and the camera set at the widest imaging angle possible. ROV speed through the water was standardized by flying the ROV at the maximum speed where point-type particles looked like points rather than as lines through “streaking” associated with the slow shutter speed of the camera. Dives were done in day-night pairs to assess the diel differences in depth distributions of the organisms and the repeated horizontal transects were at the following depths: 75, 200, 350, 850, 1000, 1200, 1500m. A series of deeper dives were also carried out and these combined a medium-speed, oblique descent (15m/min) of the ROV to 1500m, followed by a slow, oblique descent (5-10m/min) with horizontal transect depths at 1750, 2500, and 3500m, and altitudes above the seafloor (approx. 4200m) as follows: 5, 10, 25, 50, 100m. Several opportunistic horizontal transects were made during Campaign 5E at depths including 50, 700 and 750m to assess the effect of oxygen concentration on the vertical distributions and activity levels of organisms.

Table 6-36 Horizontal transects and the dive numbers during which they were conducted during Campaign 5B

| CTA | | | | PRZ | | | |
|--------------|-------|------------|-------|--------------|-------|------------|------|
| Night - 75m | OY_15 | Day - 75m | | Night - 75m | | Day - 75m | |
| Night - 75m | OY_16 | Day - 75m | OY_18 | Night - 75m | OY_8 | Day - 75m | |
| Night - 75m | OY_19 | Day - 75m | OY_19 | Night - 75m | OY_20 | Day - 75m | OY_7 |
| Night - 200m | OY_15 | Day - 200m | | Night - 200m | | Day - 200m | |
| Night - 200m | OY_15 | Day - 200m | OY_18 | Night - 200m | OY_8 | Day - 200m | OY_6 |
| Night - 200m | OY_16 | Day - 200m | OY_19 | Night - 200m | OY_20 | Day - 200m | OY_7 |
| Night - 200m | OY_19 | Day - 350m | | Night - 350m | | Day - 350m | |
| Night - 350m | OY_15 | Day - 350m | OY_18 | Night - 350m | OY_8 | Day - 350m | OY_6 |
| Night - 350m | OY_16 | Day - 350m | OY_19 | Night - 350m | OY_20 | Day - 350m | OY_7 |

| CTA | | | | PRZ | | | |
|---------------|-------|-------------|-------|---------------|-------|-------------|------|
| Night - 350m | OY_19 | Day - 850m | | Night - 850m | | Day - 850m | |
| Night - 850m | OY_15 | Day - 850m | OY_18 | Night - 850m | OY_8 | Day - 850m | OY_6 |
| Night - 850m | OY_16 | Day - 850m | OY_19 | Night - 850m | OY_20 | Day - 850m | OY_7 |
| Night - 850m | OY_19 | Day - 1000m | | Night - 1000m | | Day - 1000m | |
| Night - 1000m | OY_15 | Day - 1000m | OY_18 | Night - 1000m | | Day - 1000m | OY_6 |
| Night - 1000m | OY_16 | Day - 1000m | OY_19 | Night - 1000m | OY_8 | Day - 1000m | OY_7 |
| Night - 1000m | OY_19 | Day - 1200m | | Night - 1200m | OY_8 | Day - 1200m | |
| Night - 1000m | OY_19 | Day - 1200m | OY_18 | Night - 1200m | OY_9 | Day - 1200m | OY_6 |
| Night - 1200m | OY_15 | Day - 1200m | OY_19 | Night - 1200m | OY_20 | Day - 1200m | OY_7 |
| Night - 1200m | OY_16 | Day - 1500m | | Night - 1500m | | Day - 1500m | |
| Night - 1200m | OY_19 | Day - 1500m | OY_18 | Night - 1500m | OY_8 | Day - 1500m | OY_6 |
| Night - 1200m | OY_19 | Day - 1500m | OY_19 | Night - 1500m | OY_9 | Day - 1500m | OY_7 |
| Night - 1500m | OY_15 | - | - | - | - | - | - |
| Night - 1500m | OY_16 | - | - | - | - | - | - |
| Night - 1500m | OY_19 | - | - | - | - | - | - |
| Night - 1500m | OY_19 | - | - | - | - | - | - |

During Campaign 5B, sampling was attempted on a total of 29 individual zooplankton, of which 19 were successfully captured and brought to the surface, while only the video record remains for the other 10 specimens.

After identifications were completed on fresh specimens, a small piece of tissue from each was placed in pre-chilled 99.5% ethanol in an Eppendorf tube (1.5 ml) and stored in a -80°C freezer, with the remainder of each animal being fixed and preserved as a voucher specimen in borax-buffered 5% formalin-seawater at 4°C in glass jars with no lip, making sure the jar was filled to the brim with liquid and that no air pockets remained.

One sequenced specimen was a pyrosome tunicate that was sampled during Campaign 5B using a MOCNESS net (C5b_RRZ-MOC10-Net0), rather than the ROV. During Campaign 5B all specimens for molecular analyses were snap frozen in liquid nitrogen and transported to University of Hawai'i at Manoa, where chilled ethanol was added, as above, before sending them to the JAMSTEC for processing and sequencing.

During Campaign 5E, while technical issues with the ROV prohibited in-situ surveys, a hand-held plankton net (mouth diameter 20cm, length 21.5cm, mesh size 330 µm) was modified to be towable behind the ship using a rope and a shackle weight. Primarily cnidarians, ctenophores, tunicates, polychaetes and larval stages were screened, opportunistically sampled, photographed under the dissecting microscope, and placed whole into separate Eppendorf tubes (1.5 ml) containing pre-chilled 99.5% ethanol.

(b) Video analyses

Post-cruise re-annotation was done using a video annotation plugin to Squidle+ (SquidVidPro, GreyBits Engineering) running on a GreyBitsBox (Greybits Engineering) system. Quantitative horizontal transects were analyzed by pausing the video every 2 seconds and counting all organisms. Attempts will be made to quantify the volume imaged in each of these frames but issues with the quality of the images from the IP cameras and low light levels may mean that only relative abundance estimates are possible.

For some dives, only the depth value for the ROV's Paroscientific Digiquartz depth sensor was available. During Campaign 5E, it was noticed that the discrepancy between the CTD depth values (with latitude set to 11°N) and the Digiquartz depth values (uncertain how depth is calculated) were considerable (eg. 4285.8m for CTD vs. 4297.3m for Digiquartz). Especially for the deep benthopelagic transects there may therefore be a quite marked discrepancy between depth and apparent altitude values depending on the depth data source used for that particular dive. CTDO-derived depth data was always used when available. During Campaign 5B the ROV's altitude above the seafloor was measured using an altimeter

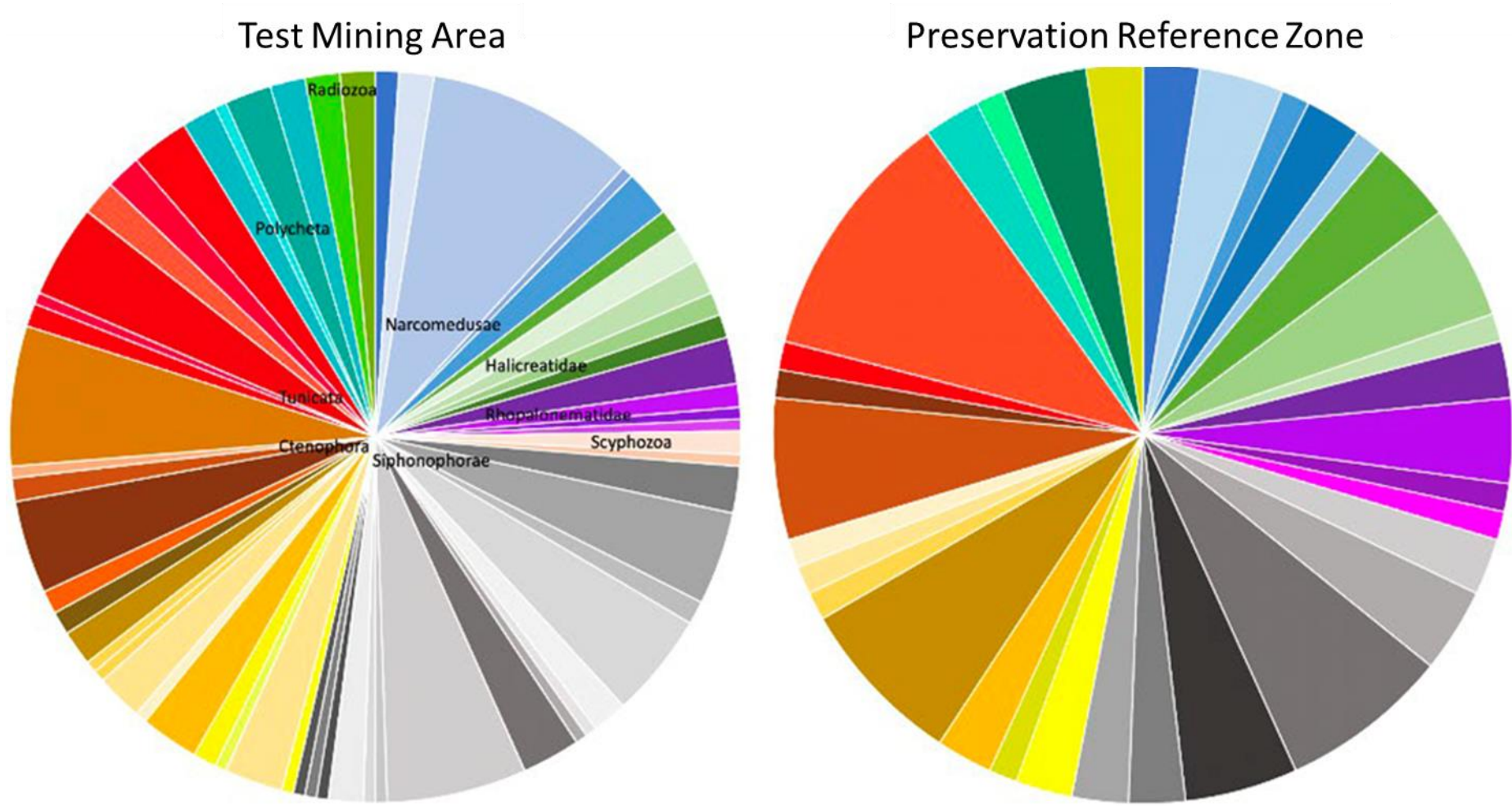
(PA200, Tritech) during benthopelagic transects by reference to a superimposed text value on the main ROV monitor in the control van.

6.4.4.4 Preliminary results & discussion

(a) Synopsis of midwater gelatinous zooplankton community composition and diversity from ROV observations

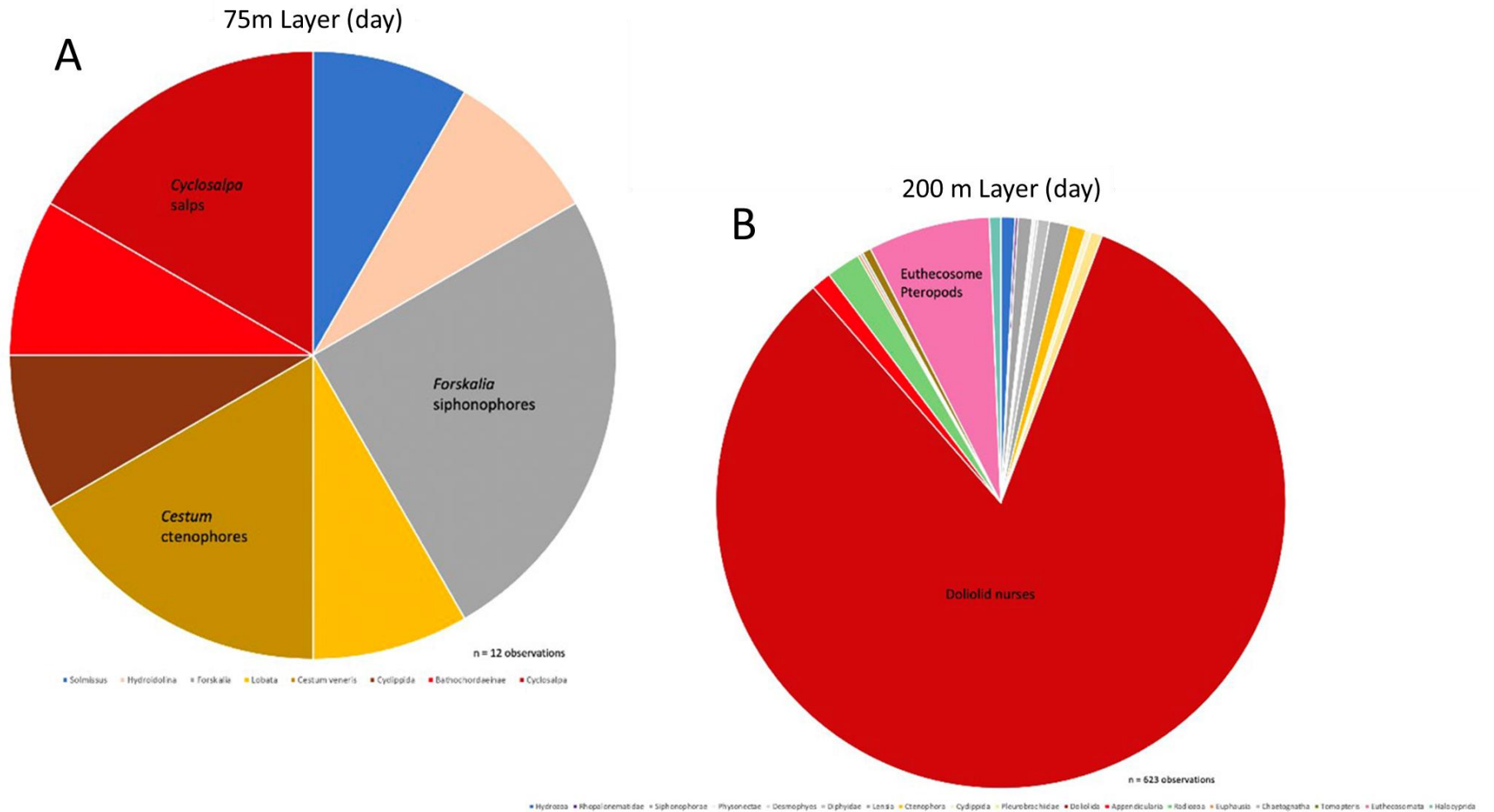
Slight differences in relative abundances of the major taxa were found between the two areas, but due to the patchy nature of planktonic ecosystems it does not appear that there is a significant difference between the two sites (Figure 6-72). Large differences in relative abundances of the major taxa were found between different depth strata (Figure 6-73).

Figure 6-72. Comparison of mid-water gelatinous zooplankton diversity between (A) Collector Test Area (CTA) and (B) Preservation Reserve Zone (PRZ)



A swarm of the scyphozoan *Pelagia noctiluca* occurred during dive OY_8, but since it was an anomalous sighting at such high densities, it was excluded from the comparison.

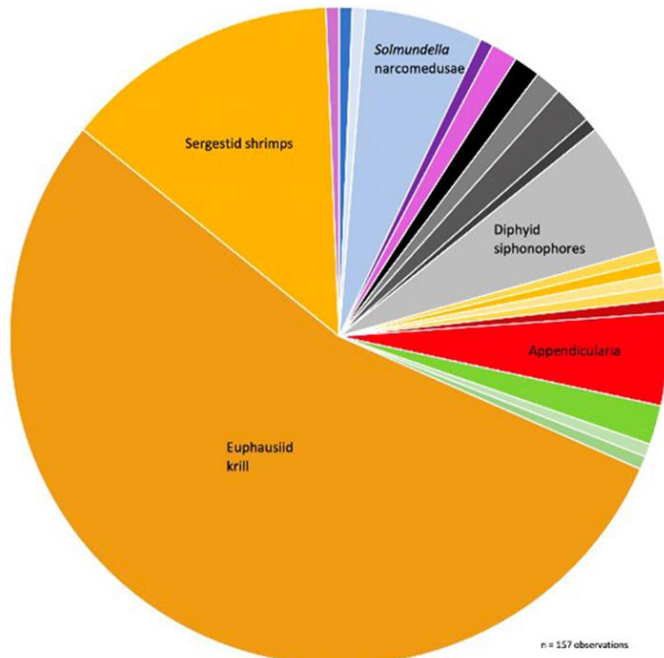
Figure 6-73. Differences in relative abundance of major taxa of mid-water gelatinous zooplankton between depth strata (A) 75m; (B) 200m; (C) 350m; (D) 850m; (E) 1000m; (F) 1200m; (G) 1500m⁷



⁷ See source document for specific species details.

C

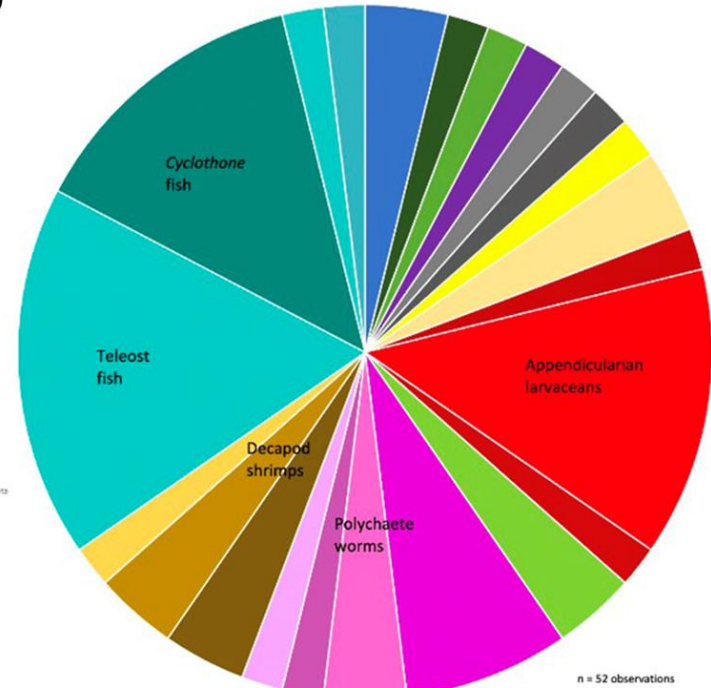
350m Layer (day)



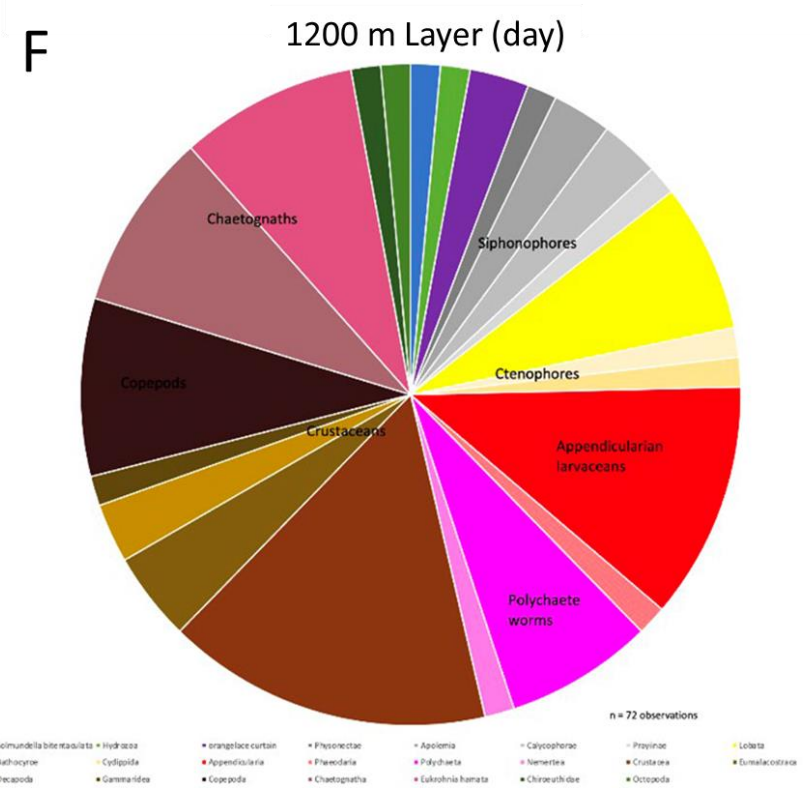
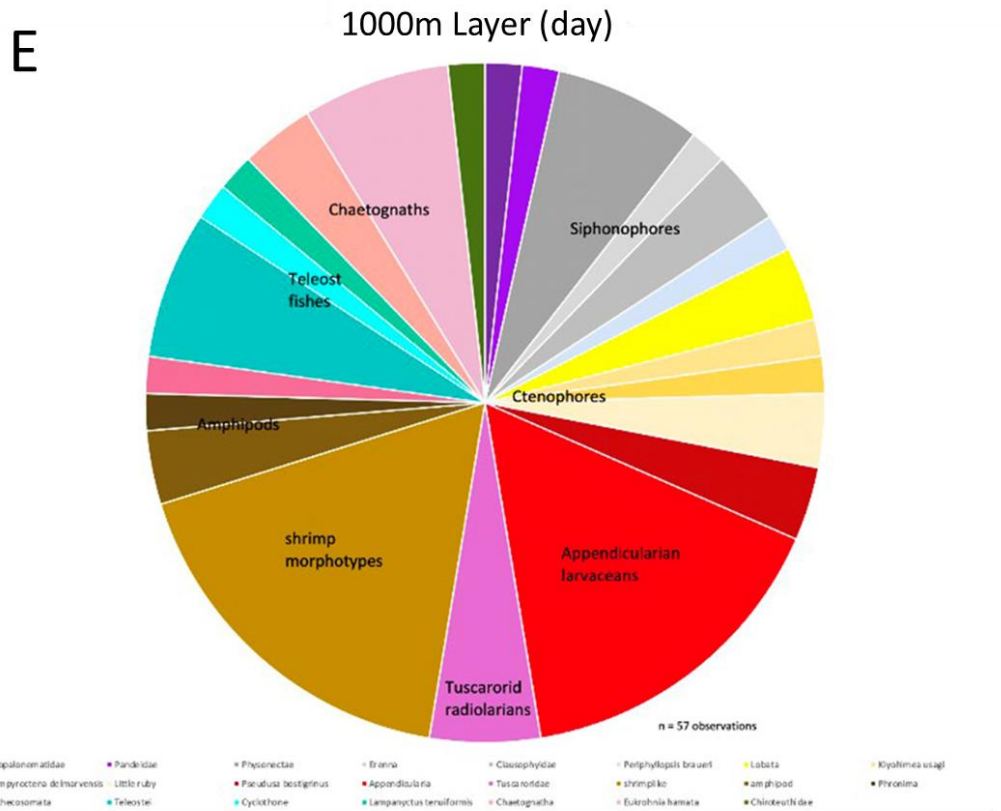
- Rotomabuxia
- Leberta
- Curidiidae
- Kryptomegastip
- Solmundella bitentaoulata
- Thalassiosira weissflogii
- Hydrus
- Trachymedusa
- Appendicularia
- Calyptrophore
- Radiosa
- Praxinos
- Cnidocystidae
- Praxinos
- Praxinos
- Euphausia
- Diphyid
- Sergestidae
- Cladocera
- Eurytemora

D

200 m Layer (day)



- Solmundella bitentaoulata
- Pseudosquilla bostigrius
- Malacostraca
- Trachymedusa
- Appendicularia
- Decapoda
- Halicreas minimum
- Fritillariidae
- Pteropoda
- Rhopalonematidae
- Tuzigoriidae
- Teleostei
- Mysis
- Polychaeta
- Cyclothone
- Praxinos
- Pteropoda meseres
- Bathylagidae
- Lamprolaima
- Tomopteris
- Nemertea
- Bathycyona



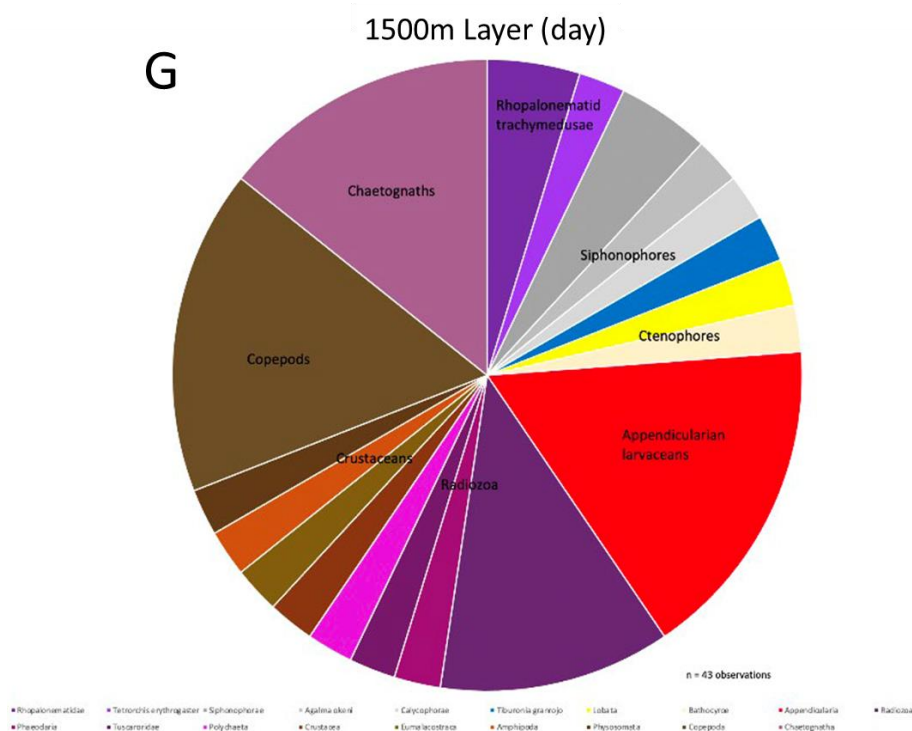


Figure 6-74 to Figure 6-78 provides some examples images captured by the ROV during Campaign 5B.

(b) Results of molecular analyses

To establish whether specimens collected in NORI-D were genetically unique (formed a separate clade from other congeners), the reference collection at JAMSTEC was leveraged for sequenceable material in the same taxonomic families as the samples from the CCZ (Table 6-38).

Table 6-37 Total of samples available for all families collected at the CCZ in Campaign 5B

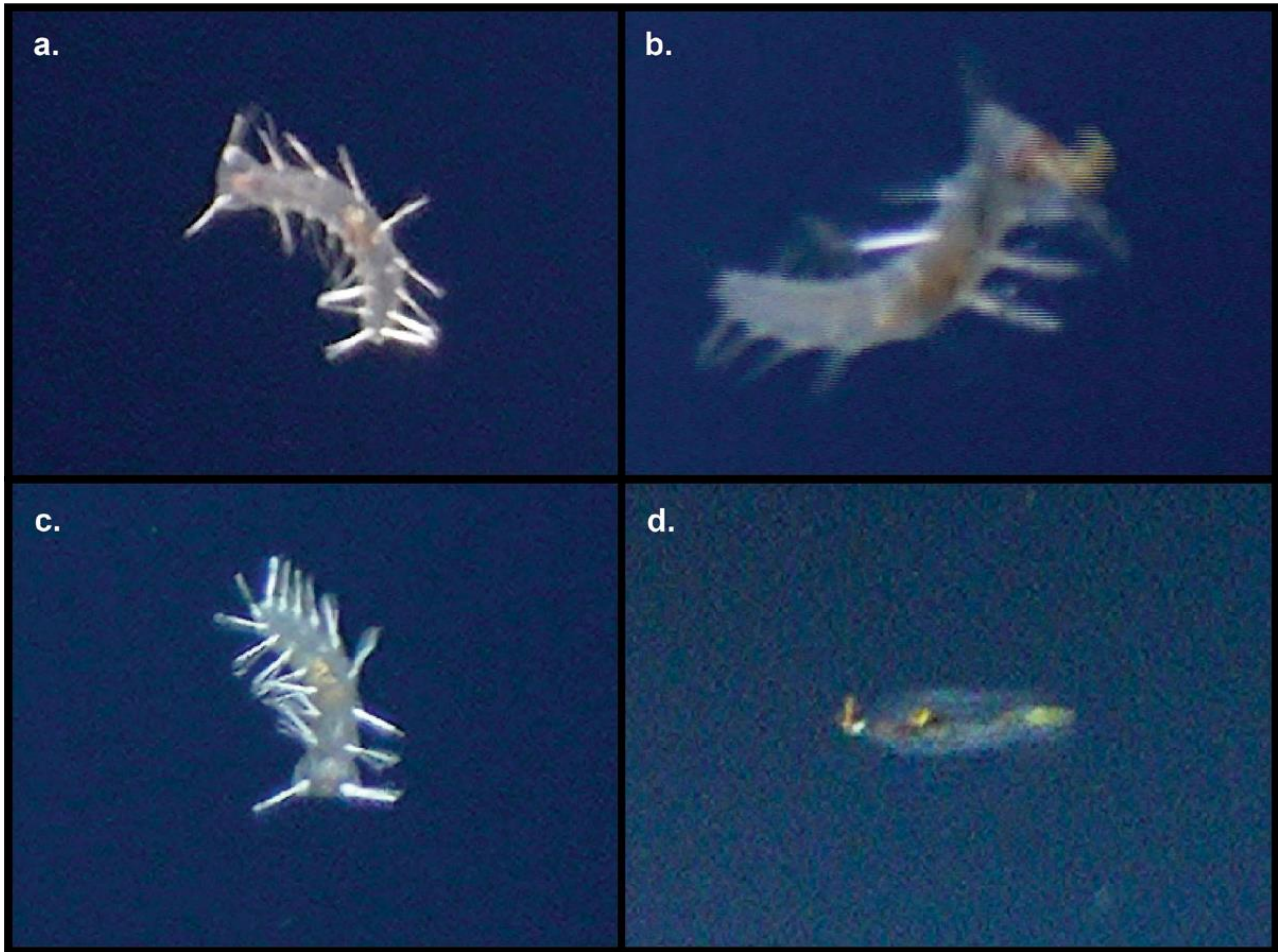
| CCZ SAMPLE FAMILIES | CCZ | JAMSTEC |
|---------------------|-----|---------|
| Atollidae | 1 | 22 |
| Aeginidae | 1 | 12 |
| Aequoreidae | 1 | 11 |
| Halicreatidae | 4 | 51 |
| Bathyctenidae | 1 | 1 |
| Beroidea | 1 | 42 |
| Eurhamphaeidae | 1 | 5 |
| Flabelligeridae | 2 | 1 |
| Pelagidae | 1 | 13 |
| Periphyllidae | 2 | 29 |
| Prayidae | 1 | 43 |
| Pyrosomatidae | 1 | 9 |
| Salpidae | 1 | 29 |

Additionally, in preparation for Campaigns 5D and 5E, a complete catalog was generated for all mesopelagic specimens with ethanol-preserved material stored in the JAMSTEC collection. The collection was grouped into cnidarians, ctenophores, and others.

Total DNA was successfully extracted from all samples collected during Campaign 5B, with double-stranded DNA concentrations ranging from 0.16 ng/ul to 120ng/ul (Table 6-38). All of the collected samples were successfully amplified and sequenced. Nonetheless, some of the samples had problems with cross contamination. Samples DL-95 and DL-102, collected on dive “C5b_ROV008 (OY_8)”, were

heavily contaminated with *Erenna laciniata* DNA. This siphonophore species was one of the specimens collected earlier on the same dive.

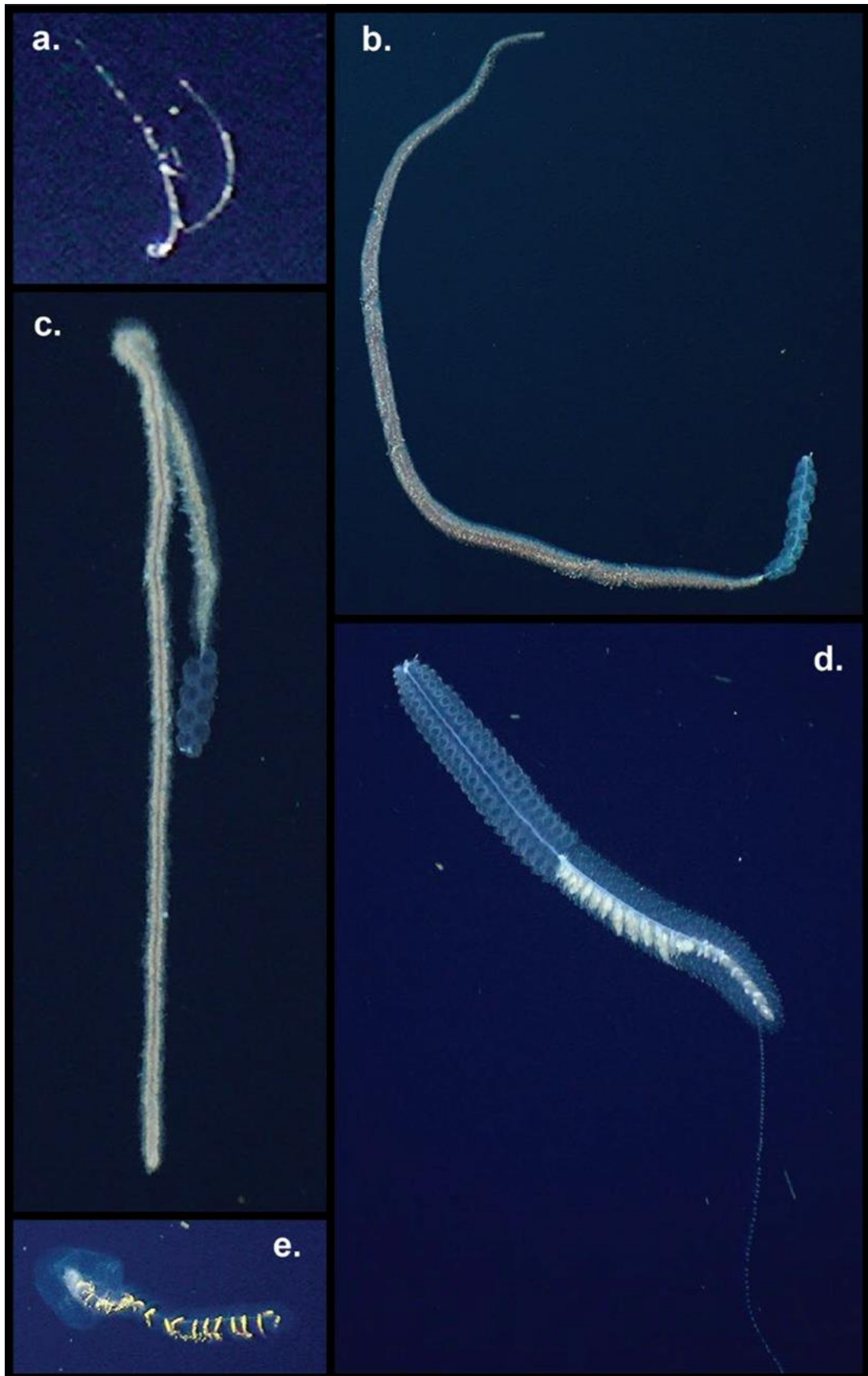
Figure 6-74 Different annelid specimens recorded from Campaign 5B.



a) DL-100, C5b_ROV013D4, *Flota vitjasi*; b) DL-106, C5b_ROV011D1, *Flota vitjasi*; c) 5b_tm010, C5b_ROV021D1, *Flota vitjasi*; d) 5b_tm011, C5b_ROV008SS3, *Poeobius* sp. See Table 2 for details.

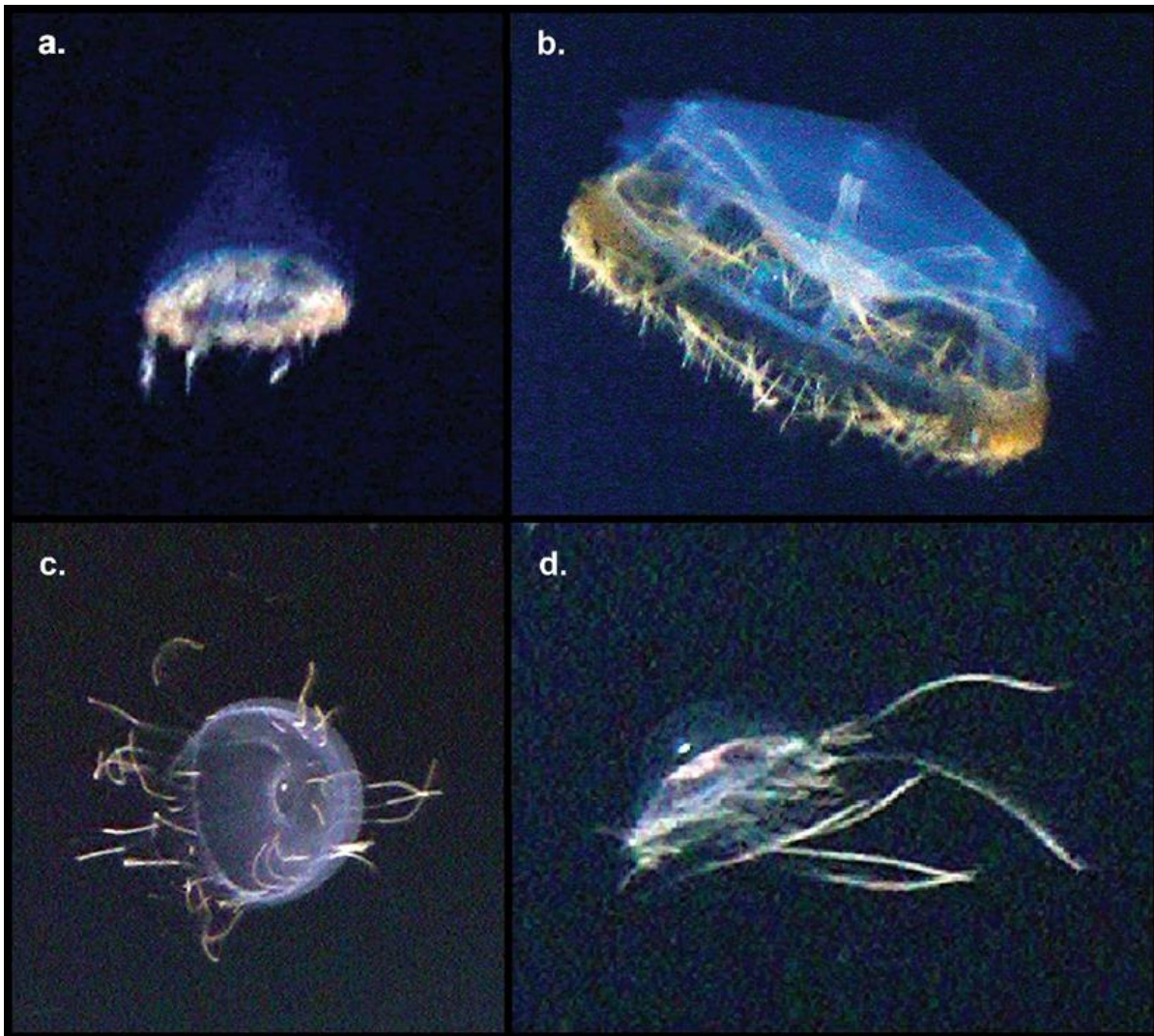
Figure 6-75

Siphonophores recorded on Campaign 5B



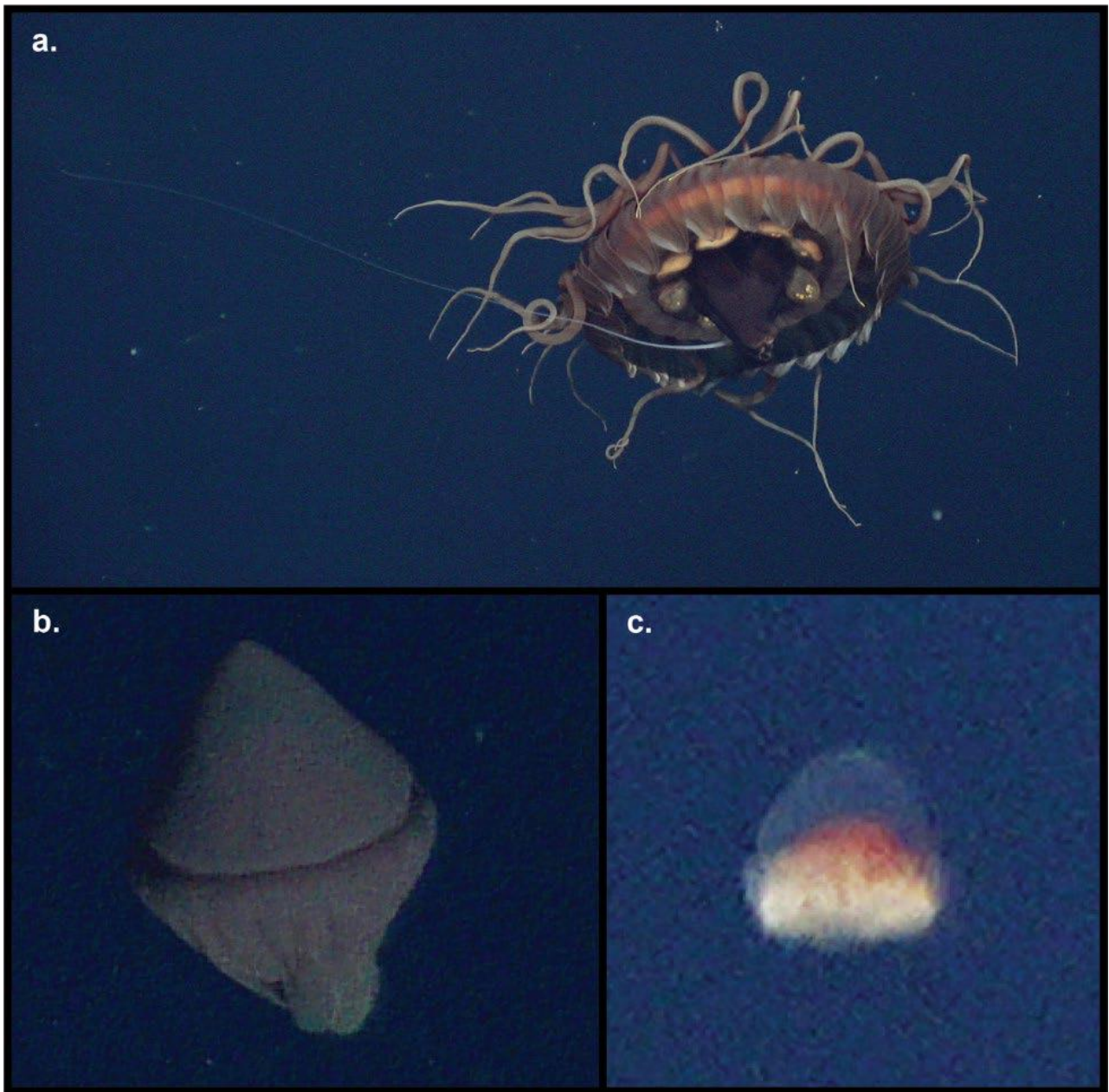
a) 5b_tm005, C5b_ROV017D1, Siphonophore sp. b) 5b_tm001, C5b_ROV006D3, *Apolesia lanosa*; c) 5b_tm002, C5b_ROV008SS1, *Apolesia lanosa*; d) DL-94, C5b_ROV008D3, *Erenna laciniata*; e) DL-110, C5b_ROV015D1, *Praya* sp. See Table 2 for details.

Figure 6-76 Medusozoans from the family Halicreatidae recorded on Campaign 5B



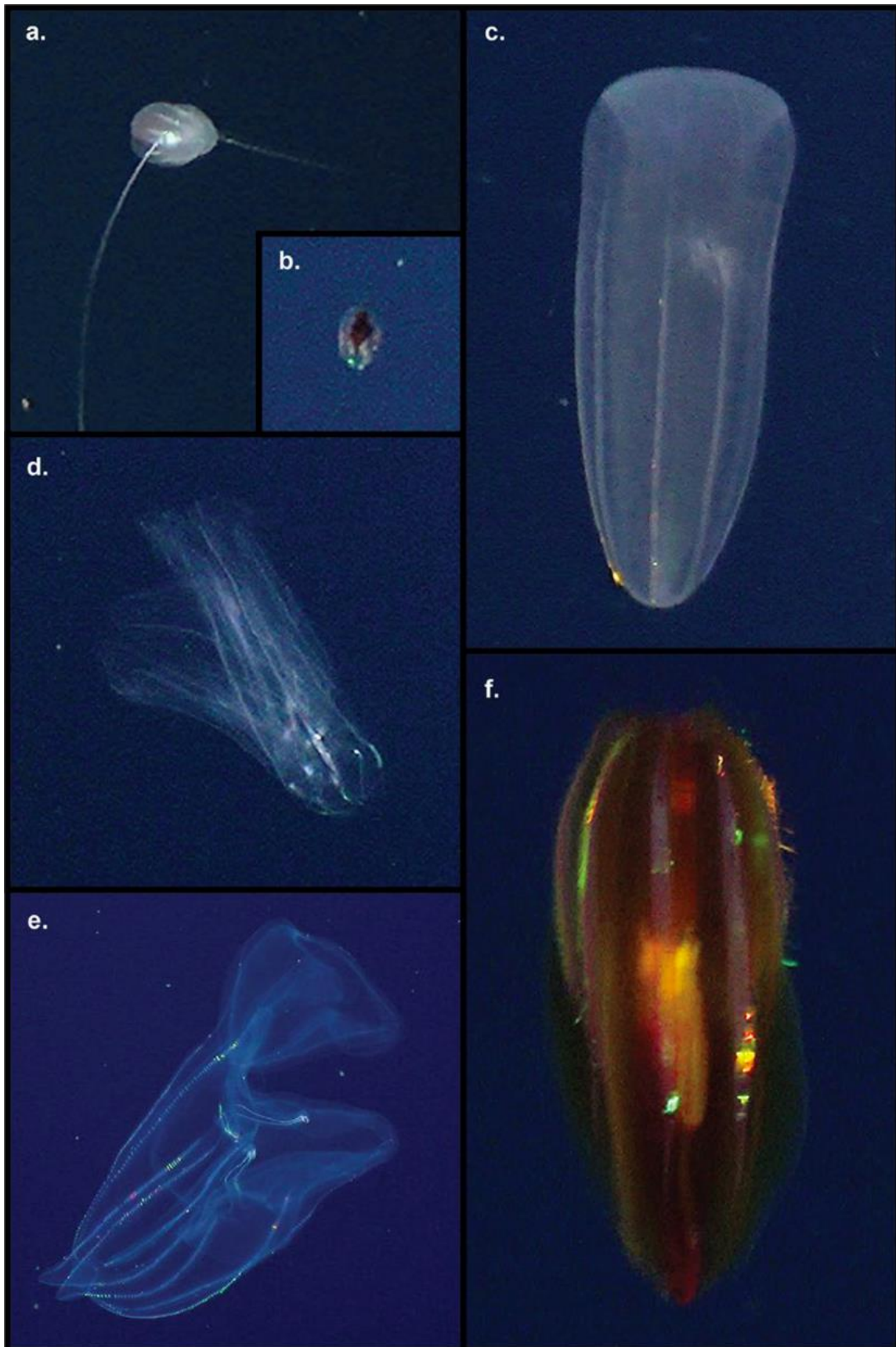
a) DL-103, C5b_ROV021D3, *Botrynema brucei*; b) DL-111, C5b_ROV018D4, *Halicreas minimum*; c) DL-104, C5b_ROV019D2, *Halitrepes valdiviae*; d) DL-108, C5b_ROV017D2, *Haliscera bigelowi*. See Table 2 for details.

Figure 6-77 Medusozoans from the order Coronatae recorded on Campaign 5B



a) DL-95, C5b_ROV008D4, *Atolla wyvillei*; b) DL-102, C5b_ROV008D2, *Periphyllopsis braueri*; c) DL-98, C5b_ROV017D3, *Periphyllopsis* sp. See Table 2 for details.

Figure 6-78 Ctenophores recorded on Campaign 5B



a) DL-99, C5b_ROV008SS2, *Bathocyroce chuni*; b) 5b_tm009, C5b_ROV020D3, *Bathocyroce chuni*; c) DL-107, C5b_ROV015D2, *Beroe cucumis*; d) 5b_tm004, C5b_ROV015D4, *Bathocyroce cf. fosteri*; e) DL-96, C5b_ROV015D3, *Kiyohimea usagi*; f) 5b_tm006, C5b_ROV018D1, Mertensiidae sp. See Table 2 for details.

Table 6-38 Samples collected on the Campaign 5B.

| SAMPLE # | DEPTH (m) | SPECIES | FOR. | PIC. | TISSUE (-40C) | Marker |
|--------------------|-----------|---------------------------------|------|------|---------------|------------|
| C5b_ROV013D4 | 3835 | <i>Flota vitjasi</i> | Y | Y | Y | COI-mtDNA |
| C5b_ROV011D1 | 4049 | <i>Flota vitjasi</i> | Y | Y | Y | COI-mtDNA |
| C5b_ROV021D1 | 4076 | <i>Flota vitjasi</i> | n | Y | n | - |
| C5b_ROV008SS3 | 1005 | <i>Poeobius sp.</i> | n | Y | n | - |
| C5b_ROV018D2 | 1001 | <i>Acanthephyra sp.</i> | n | Y | n | - |
| C5b_ROV016D3 | 1128 | <i>Pseudusa bostigrinus</i> | Y | Y | Y | COI-mtDNA* |
| C5b_RRZ-MOC10-Net0 | - | <i>Pyrosoma sp.</i> | - | n | Y | COI-mtDNA |
| C5b_ROV020D4 | 796 | <i>Vitreosalpa gemini</i> | Y | Y | n | COI-mtDNA |
| C5b_ROV019D3 | 414 | <i>Aequoridae sp.</i> | Y | Y | Y | 16S-rDNA |
| C5b_ROV008D1 | 885 | <i>Aeginura grimaldii</i> | Y | Y | Y | 16S-rDNA* |
| C5b_ROV017D1 | 2158 | Siphonophore | n | Y | n | - |
| C5b_ROV006D3 | 1268 | <i>Apolemia lanosa</i> | n | Y | n | - |
| C5b_ROV008SS1 | 1219 | <i>Apolemia lanosa</i> | n | Y | n | - |
| C5b_ROV008D3 | 1128 | <i>Erenna laciniata</i> | Y | Y | Y | 16S-rDNA |
| C5b_ROV015D1 | 346 | <i>Praya sp.</i> | Y | Y | Y | 16S-rDNA |
| C5b_ROV021D3 | 1738 | <i>Botrynema brucei</i> | Y | Y | n | 16S-rDNA |
| C5b_ROV018D4 | 1396 | <i>Halicreas minimum</i> | Y | Y | n | 16S-rDNA |
| C5b_ROV017D2 | 2404 | <i>Haliscera bigelowi</i> | Y | Y | Y | 16S-rDNA |
| C5b_ROV019D2 | 1000 | <i>Halitrephes valvidae</i> | Y | Y | n | 16S-rDNA |
| C5b_ROV019D1 | 1500 | <i>Tetrorchis erythrogaster</i> | n | Y | n | - |
| C5b_ROV008D4 | 930 | <i>Atolla wyvillei</i> | Y | Y | Y | 16S-rDNA* |
| C5b_ROV008D2 | 840 | <i>Periphyllopsis braueri</i> | Y | Y | Y | 16S-rDNA* |
| C5b_ROV017D3 | 4260 | <i>Periphyllopsis sp.</i> | Y | Y | Y | 16S-rDNA* |
| C5b_ROV018D3 | 201 | <i>Pelagia noctiluca</i> | Y | Y | Y | 16S-rDNA |
| C5b_ROV015D2 | 201 | <i>Beroe cucumis</i> | Y | Y | Y | COI-mtDNA* |
| C5b_ROV008SS2 | 1199.6 | <i>Bathycytena chuni</i> | Y | Y | Y | COI-mtDNA |
| C5b_ROV020D3 | 848 | <i>Bathycytena chuni</i> | n | Y | n | - |
| C5b_ROV018D1 | 927 | Mertensiidae | n | Y | n | - |
| C5b_ROV015D4 | 403 | <i>Bathocyroe sp.</i> | n | Y | n | - |
| C5b_ROV015D3 | 1194 | <i>Kiyohimea usagi</i> | n | Y | Y | COI-mtDNA* |

Since no remotely operated vehicle or human-occupied submersible-collected data on the gelatinous midwater fauna exists for the NORI-D area or indeed for the entire CCZ, with the single exception of five ctenophores (one at generic, one familial and three order level assignments) being reported from AUV imagery in the benthic boundary layer in the UK-1 polymetallic-nodule exploration area (Amon *et al.*, 2017), the present study has infinitely increased our knowledge of this fauna.

To maintain the link between morphology-based identifications and molecular-based identifications, the process of reverse taxonomy is advocated. This is a process in which a gene sequence (or sequences) is used as a barcode and the specimen from which the molecular material was obtained is imaged and its morphology described. The two sets of information are then published together in a scientific journal as well as added to international databanks (e.g. GenBank). These descriptions can help identify material collected by past sampling programmes. Molecular methods continue to advance rapidly, making biotic surveys at all levels, especially the level of microorganisms, much more rapid and economically feasible. Molecular sequences should be deposited in GenBank or equivalent internationally recognized sequence databases. Voucher specimens and molecular samples, including DNA extracts, should be deposited in a recognized curated collection facility such as a natural history museum and therefore be made available for wider study. [Recommendations III.B.14; III.B.15.(d).(i)–(iii) and (vii); IV.A.22] “.

Originally, the shallowest ROV transect was to be completed at 75m depth. However, oceanographic results from Campaigns 5B and 5E suggested that additional shallow transects at 50m (above the oxygen minimum layer) and a further transect at approximately 250m (within a subsurface oxygen peak at the

NORI-D area) should be completed in future campaigns. The lower limit of the oxygen minimum zone appears to be different for different faunal elements, but additional transects between 700-800m may also be warranted. Communities differed at all transect depths, but the differences were less apparent between communities below 1000m. Gelatinous fauna that are too small to be easily sampled by the ROV should be collected for DNA barcoding by gently hauled, fine-meshed, vertically towed nets, since samples captured in Campaigns 5B and 5E are heavily skewed to the larger gelatinous fauna.

There does not appear to be an appreciable difference between the overall species diversity at the CTA and PRZ sites, though the specifics of their vertical distribution show some differences.

eDNA analyses of CTD-collected seawater and plankton net samples, using the extraction techniques and primers developed in the first stage of this study, will undoubtedly increase our knowledge of the fauna of the NORI-D area. JAMSTEC will work with the team at the University of Hawaii to identify the gelatinous taxa identified by sequences from their part of the work package (Section 6.4.3).

6.4.5 Micronekton community (small fishes, squids and shrimps) using MOCNESS

6.4.5.1 Purpose & scope

The following section describes the work conducted in 2021 by University of Hawaii to characterise natural baseline conditions in mesopelagic micronekton communities in the NORI-D contract area. The scope, the survey planning and the sampling methodologies carried out to ecologically characterise these communities align with International Seabed Authority ISBA/25/LTC/6 Rev 1. Annex 1 section 42(e) mesopelagic micronekton and 44. Vertical migration to provide baseline data requirements under Recommendations III.B.15.(d).(iii); IV.B.22.

6.4.5.2 Baseline investigations

The methods and proposed survey array for both the collector test and long-term environmental studies on NORI-D will provide data to meet the following objectives:

- Characterize the abundance, biomass, diversity and community composition of the micronekton from the surface to just above the seafloor using depth discrete net tows

The goal was to sample and characterize micronekton from the surface to the seafloor as per ISBA/25/LTC/6 Rev 1 with modifications based on a workshop of midwater experts (Drazen *et al.* 2019). This was accomplished by applying two techniques. The first was towed nets, specifically the 10-meter Multiple Opening Closing Net Environmental Sampling System (MOCNESS; (Wiebe *et al.* 1985). The second was bioacoustics mounted on an autonomous platform, Saldrone (<https://www.saldrone.com/>). Additionally, ROV transects provide some anecdotal observations but the micronekton were often too fast and evasive to be quantitatively observed with this approach.

6.4.5.3 Campaign activities

(a) Survey design & site selection

The micronekton are larger and more mobile than zooplankton requiring a large net such as the 10m MOCNESS (Wiebe *et al.* 1985). This system has been used extensively off the coast of Hawaii (Choy *et al.* 2015; Gloeckler *et al.* 2018; Romero-Romero *et al.* 2019). The MOCNESS is able to monitor environmental conditions in real time and allows for 5 depth discrete samples per tow using multiple 3mm mesh nets. During Campaign 5B, the upper 1500m of the water column (epi- and mesopelagic) was sampled owing to both the high activity in this zone, and the planned test collector discharge at 1200m depth. Daily vertical migration of the community required day and night paired sampling in the upper 1500 m (Brodeur & Yamamura 2005). This active migration can contribute substantially to the biological carbon pump, comprising up to ~50% of the passive sinking flux measured with sediment traps (Davison *et al.*

2013; Ariza *et al.* 2015; Drazen & Sutton, 2017). As such this group provides essential ecosystem services and warrants characterization and study during baseline and monitoring efforts associated with deep-sea nodule collection. Additional net tows were planned to sample from 1500m to just above the seafloor (~4300m) using separate tows. This fauna has the potential to be affected by both the midwater discharge plume and the seafloor collector plume. However, during Campaign 5B, failure of the winch prevented sample collection.

The following depth strata were targeted in the upper 1500m;

- 0-70/90 (PRZ/CTA) - the upper mixed and oxygenated layer
- 70/90-450m – upper oxycline and depth of strongest acoustic scattering layers
- 450-700m – the core of the OMZ
- 700-1000m – the lower oxycline where oxygen begins increasing again
- 1000-1500m – the planned sediment discharge zone

Depth strata initially were defined as 1000-850m as the lower oxycline and 350-70m as the upper mesopelagic deep scattering layer (from Saildrone; Section 6.4.6) based on roughly 30 $\mu\text{mol l}^{-1}$ oxygen, a general value used to define OMZs (Levin 2003). However, ensuing data from the 1m MOCNESS, that had much greater vertical sampling resolution, revealed abundant populations of plankton between 700 and 800 meters, just below the core of the OMZ and at lower oxygen values that we had set our depth strata to capture. Further Saildrone data showed the strongest deep scattering layers down to 350m but in some area's layers existed to 450m (see Section 6.4.6). Thus, the sampling plan was revised after the first few tows. Three tows were conducted with the lower oxycline layer as 1000-850m before changing this to 1000-700m, to match our developing knowledge of the stratification of animal life below the OMZ.

Finally, it was found that the oxygen profile at the CTA was slightly different than at the PRZ location. At the CTA the oxygen content in the upper water column was higher. Thus, the depth strata of 0-70m from the PRZ was modified to 0-90m in the CTA. In this way these depth strata encompass the upper mixed and oxygenated layer of the water column in both locales and are comparable environmentally.

Each depth discrete net sample was sorted to family, or other broad taxonomic level at sea, counted, and weighed using a motion compensated scale (0-300g range, 0.1g precision). All sorted samples were photographed fresh to preserve natural coloration. Samples were preserved in 10% borax buffered formalin with a subset in 95% ethanol (representatives of taxa for DNA barcoding).

In the laboratory, we used diverse taxonomic keys on specific taxa to further classify specimens to genus or species, where possible. In many cases this resulted in splitting of samples created at sea (e.g., Myctophidae split into several samples representing species). These were reweighed and attribute biomass to each new finer taxonomic category. Identifications were checked by consulting taxonomic experts.

For each depth, discrete net abundance (# 10,000m⁻³) and biomass (g 10,000m⁻³) were determined by using the volume filtered for each net as generated by the MOCNESS software (LVpki).

These data were averaged between tows of the same day/night and area to generate mean depth-layer specific metrics. Evaluation of migration dynamics was accomplished by comparing day and night abundance and biomass depth profiles.

Whole epi- and mesopelagic water column (0-1500m) abundance (# 10,000m⁻³) and biomass (g 10,000m⁻³) were derived by integrating the depth layer specific values. These values were averaged for either the CTA or PRZ to represent the whole upper midwater community.

$$\text{abundance} = \Sigma(\text{net abundance} \times \text{net depth})$$

Community composition was evaluated for net specific abundance data (# 10,000m⁻³) using multidimensional scaling (MDS) and cluster analysis (group average linkage) with associated significance testing using SIMPROF (1000 permutations) in Primer v6.1 (Clarke & Gorley 2006). Family or broad group abundance data was used. Values were square root transformed and a Bray-Curtis similarity matrix was used.

6.4.5.4 Preliminary results & discussion

(a) Survey design & site selection

The MOCNESS system was deployed a total of 13 times (0-1500m depths). As per our sampling plan, 3 day and 3 night tows were conducted each in the PRZ and CTA locations (Table 6-39). An additional day tow was conducted in the PRZ. The deep MOCNESS tows (~1500-4200m) were not completed due to winch failures. However, it is important to note that these tows were completed as part of Campaign 5C and the specimens collected are currently being analysed.

Table 6-39 Metadata for 10m MOCNESS tows.

| TOW # | AREA | DAY/NIGHT | NET # | VOLUME (m ³) |
|-------|------|-----------|-------|--------------------------|
| 1 | PRZ | day | 0 | 54555 |
| 1 | PRZ | day | 1 | 118015 |
| 1 | PRZ | day | 2 | 45303 |
| 1 | PRZ | day | 3 | 84644 |
| 1 | PRZ | day | 4 | 43757 |
| 1 | PRZ | day | 5 | 22922 |
| 2 | PRZ | day | 0 | 68148 |
| 2 | PRZ | day | 1 | 99139 |
| 2 | PRZ | day | 2 | 28717 |
| 2 | PRZ | day | 3 | 45652 |
| 2 | PRZ | day | 4 | 40837 |
| 2 | PRZ | day | 5 | 22436 |
| 3 | PRZ | night | 0 | 38587 |
| 3 | PRZ | night | 1 | 76627 |
| 3 | PRZ | night | 2 | 31315 |
| 3 | PRZ | night | 3 | 50825 |
| 3 | PRZ | night | 4 | 48355 |
| 3 | PRZ | night | 5 | 23438 |
| 4 | PRZ | night | 0 | 55573 |
| 4 | PRZ | night | 1 | 78842 |
| 4 | PRZ | night | 2 | 48832 |
| 4 | PRZ | night | 3 | 41132 |
| 4 | PRZ | night | 4 | 56854 |
| 4 | PRZ | night | 5 | 27572 |
| 5 | PRZ | night | 0 | 54570 |
| 5 | PRZ | night | 1 | 86782 |
| 5 | PRZ | night | 2 | 49074 |
| 5 | PRZ | night | 3 | 42864 |
| 5 | PRZ | night | 4 | 70056 |
| 5 | PRZ | night | 5 | 22003 |
| 6 | PRZ | day | 0 | 46704 |
| 6 | PRZ | day | 1 | 87809 |
| 6 | PRZ | day | 2 | 51666 |
| 6 | PRZ | day | 3 | 44126 |
| 6 | PRZ | day | 4 | 64757 |
| 6 | PRZ | day | 5 | 13836 |
| 7 | CTA | night | 0 | 72634 |
| 7 | CTA | night | 1 | 76485 |
| 7 | CTA | night | 2 | 49756 |
| 7 | CTA | night | 3 | 39239 |
| 7 | CTA | night | 4 | 57166 |
| 7 | CTA | night | 5 | 34309 |

| TOW # | AREA | DAY/NIGHT | NET # | VOLUME (m ³) |
|-------|------|-----------|-------|--------------------------|
| 8 | CTA | night | 0 | 46358 |
| 8 | CTA | night | 1 | 73933 |
| 8 | CTA | night | 2 | 48481 |
| 8 | CTA | night | 3 | 41382 |
| 8 | CTA | night | 4 | 55651 |
| 8 | CTA | night | 5 | 28081 |
| 9 | CTA | night | 0 | 79147 |
| 9 | CTA | night | 1 | 89539 |
| 9 | CTA | night | 2 | 45751 |
| 9 | CTA | night | 3 | 42131 |
| 9 | CTA | night | 4 | 57031 |
| 9 | CTA | night | 5 | 31898 |
| 10 | CTA | day | 0 | 46368 |
| 10 | CTA | day | 1 | 60908 |
| 10 | CTA | day | 2 | 41469 |
| 10 | CTA | day | 3 | 36958 |
| 10 | CTA | day | 4 | 60346 |
| 10 | CTA | day | 5 | 20168 |
| 11 | CTA | day | 0 | 34669 |
| 11 | CTA | day | 1 | 56113 |
| 11 | CTA | day | 2 | 40452 |
| 11 | CTA | day | 3 | 36655 |
| 11 | CTA | day | 4 | 54228 |
| 11 | CTA | day | 5 | 29311 |
| 12 | CTA | day | 0 | 47415 |
| 12 | CTA | day | 1 | 59807 |
| 12 | CTA | day | 2 | 42746 |
| 12 | CTA | day | 3 | 34241 |
| 12 | CTA | day | 4 | 60610 |
| 12 | CTA | day | 5 | 20621 |
| 13 | PRZ | day | 0 | 58557 |
| 13 | PRZ | day | 1 | 73795 |
| 13 | PRZ | day | 2 | 48201 |
| 13 | PRZ | day | 3 | 47823 |
| 13 | PRZ | day | 4 | 54836 |
| 13 | PRZ | day | 5 | 26326 |

Each row provides the information when the net was closed unless otherwise specified. Ranges of conditions for a given depth strata can then be determined by comparing to the following row. For each net tow net 0 starts at the surface. Dates (yymmdd) and times (hhmmss) are UTC (local +7hrs). Local time was Pacific Daylight Savings time (the change to daylight savings occurred on the steam south to the station).

Micronekton were broadly sorted at sea (Table 6-40). The dominant fish taxa by abundance in the region were the Gonostomatid, Cyclothone spp., Myctophids, Melamphaeids, and Sternoptychidae. Dominant crustaceans include Mysids, the Penaid shrimp, Gennadas spp., the caridean shrimp family Opolophoridae, Sergestid shrimp, and euphausids (which are still being fully enumerated in the lab, so counts in Table 6-40 are far too low). The most abundant cephalopods were small juvenile squids which are challenging to identify and pelagic octopods with are mostly in the family Bolitaenidae (review of these specimens is underway). All of the fishes from Campaign 5B have been processed to the genus level.

Full identification of the shrimps and mysids from Campaign 5B and 5C are underway.

(b) Depth integrated mesopelagic micronekton abundance and biomass

Depth integrated micronekton abundance and biomass was dominated by fishes, followed by crustaceans and then cephalopods (

Table 6-41). There was generally higher fish abundance in the CTA region though crustacean and cephalopod abundances were similar. There was quite a bit of variability in abundances and biomasses between tows, more so for the biomass estimates often due to the capture of sporadic but large

individuals. Thus, differences in biomass between the regions are difficult to evaluate at this stage of analysis.

The fish community abundance is dominated by Gonostomatidae which are nearly all fish in the genus *Cyclothone* (Figure 6-79). There was a greater abundance of these fishes in the CTA region which largely drives the between region differences for fishes overall. By contrast, Melamphaidae were more abundant in the PRZ. The higher Phosichthyidae abundance in the PRZ is not significant and driven by a single very large catch in one tow. Several fish families had high biomass including the Gonostomatidae, Melamphaidae and Neoscopelidae (Figure 6-80). There was greater Gonostomatid biomass in the CTA paralleling the pattern in abundance. For the other taxa such regional differences were not apparent. With regard to biomass Gonostomatidae are not dominants because they are very small fish. The opposite is true for the Neoscopelidae, Anoplogasteridae and Lophiiformes: these taxa are less abundant but generally larger in size.

Amongst the crustaceans, there was no group that dominated in terms of abundance, however we have yet to full enumerate the euphausiids (Figure 6-79). The penaeids appear to be more abundant in the CTA and mysids may be more abundant in the PRZ but have highly variable abundance (Figure 6-79). Caridean shrimps tend to be larger than the other crustacean taxa and dominated in terms of biomass (Figure 6-80). Amphipod biomass was larger in the CTA region.

For the cephalopods, most of the Octopods are in the Bolitaenidae and they were quite abundant along with squids which are principally unidentifiable juveniles (Figure 6-79). Due to the large size of the pelagic octopods, they dominated the cephalopod biomass. Indeed, their biomass is substantial and similar to that of the caridean shrimps and several dominant fish taxa such as the Melamphaidae and Gonostomatidae. There were no significant differences apparent in cephalopod taxa biomasses between the two regions sampled.

Table 6-40 Total numbers of micronekton collected during March/April 2021 in NORI-D by broad taxa.

| MICRONEKTON | | # | TOTAL # |
|----------------|------------------|-------|---------|
| Fish | Gonostomatidae | 10097 | 13419 |
| | Myctophidae | 818 | |
| | Juvenile fish | 788 | |
| | Melamphaeidae | 658 | |
| | Sternoptychidae | 335 | |
| | Phosichthyidae | 310 | |
| | Stomiidae | 139 | |
| | Bathylagidae | 68 | |
| | Nemichthyidae | 45 | |
| | Neoscopelidae | 39 | |
| | Bregmacerotidae | 34 | |
| | Serrivomeridae | 13 | |
| | Lophiiformes | 12 | |
| | Scopelarchidae | 11 | |
| | Macrouridae | 8 | |
| | Chiasmodontidae | 5 | |
| | Leptocephalus | 5 | |
| | Anoplogasteridae | 4 | |
| | Hemiramphidae | 4 | |
| | Trachipteridae | 3 | |
| | Cetomimidae | 2 | |
| | Eurypharyngidae | 2 | |
| | Gempylidae | 2 | |
| | Alepocephalidae | 1 | |
| Astronesthidae | 1 | | |
| Caristiidae | 1 | | |

| MICRONEKTON | | # | TOTAL # |
|------------------|--------------------|----------|-------------|
| | Diplotaenia | 1 | |
| | Ipnopidae | 1 | |
| | Liparidae | 1 | |
| | Malacosteidae | 1 | |
| | Nomeidae | 1 | |
| | Ophidiidae | 1 | |
| | Paralepididae | 1 | |
| | Scorpaenidae | 1 | |
| | Unidentified | 1 | |
| | Squid | *Octopod | |
| Cranchiidae | | 6 | |
| Pyrotheuthidae | | 5 | |
| Argonauta | | 3 | |
| Enoploteuthidae | | 5 | |
| Chiroteuthidae | | 1 | |
| Histioteuthidae | | 2 | |
| Amphitretidae | | 1 | |
| Bolitaenidae | | 1 | |
| Japatella | | 1 | |
| Crustacea | Mysids | 761 | 3262 |
| | Penaid | 730 | |
| | Caridean | 530 | |
| | Sergestidae | 549 | |
| | **Euphausiids | 380 | |
| | Amphipod | 306 | |
| | Lobster phyllosome | 5 | |
| | Unknown shrimp_1 | 1 | |

* preliminary identification suggests most are Bolitaenidae, ** euphausiids are still being enumerated in the lab.

Table 6-41 Abundance and biomass (# or g /10,000m², mean ± standard deviation) of micronekton groups integrated over the top 1500m of the water column in the PRZ, CTA and averaged for both locations. Note that these values do not yet include Euphausiids as they are still being completely enumerated.

| | PRZ (n=7) | CTA (n=6) | Overall (n=13) |
|------------------------------------|----------------------|----------------------|----------------------|
| Fish abundance | 59001 ± 9450 | 74489 ± 10531 | 66149 ± 12468 |
| Fish biomass | 2473 ± 849 | 1768 ± 427 | 2147 ± 755 |
| Crustacean abundance | 15998 ± 9620 | 15247 ± 3131 | 15652 ± 7107 |
| Crustacean biomass | 940 ± 255 | 797 ± 208 | 874 ± 237 |
| Cephalopod abundance | 1501 ± 766 | 2119 ± 884 | 1786 ± 849 |
| Cephalopod biomass | 1031 ± 591 | 665 ± 511 | 862 ± 566 |
| Total micronekton abundance | 76500 ± 12378 | 91856 ± 13771 | 83587 ± 14802 |
| Total micronekton biomass | 4444 ± 1003 | 3229 ± 508 | 3883 |

Figure 6-79 Micronekton abundance by area and family or broad taxonomic group.

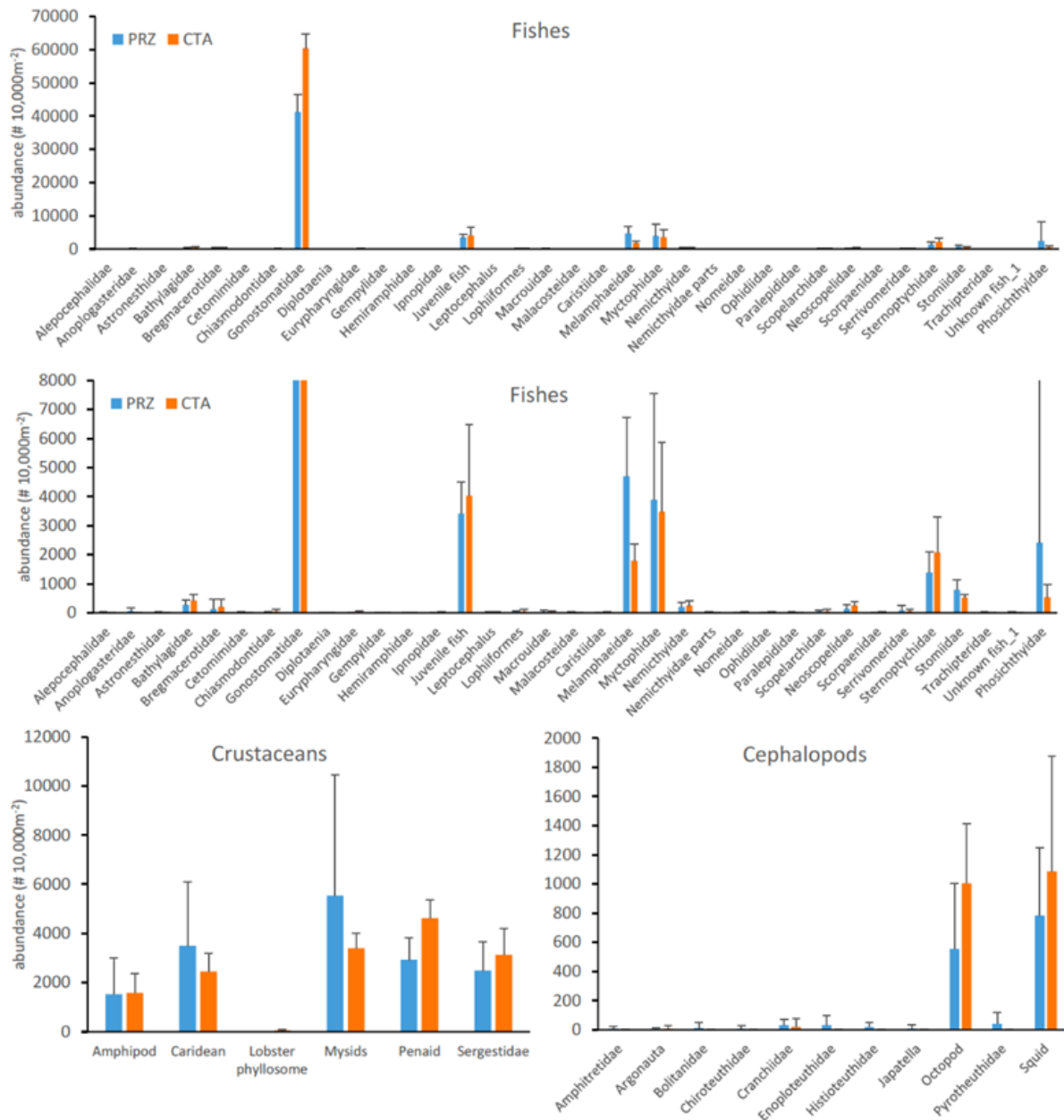
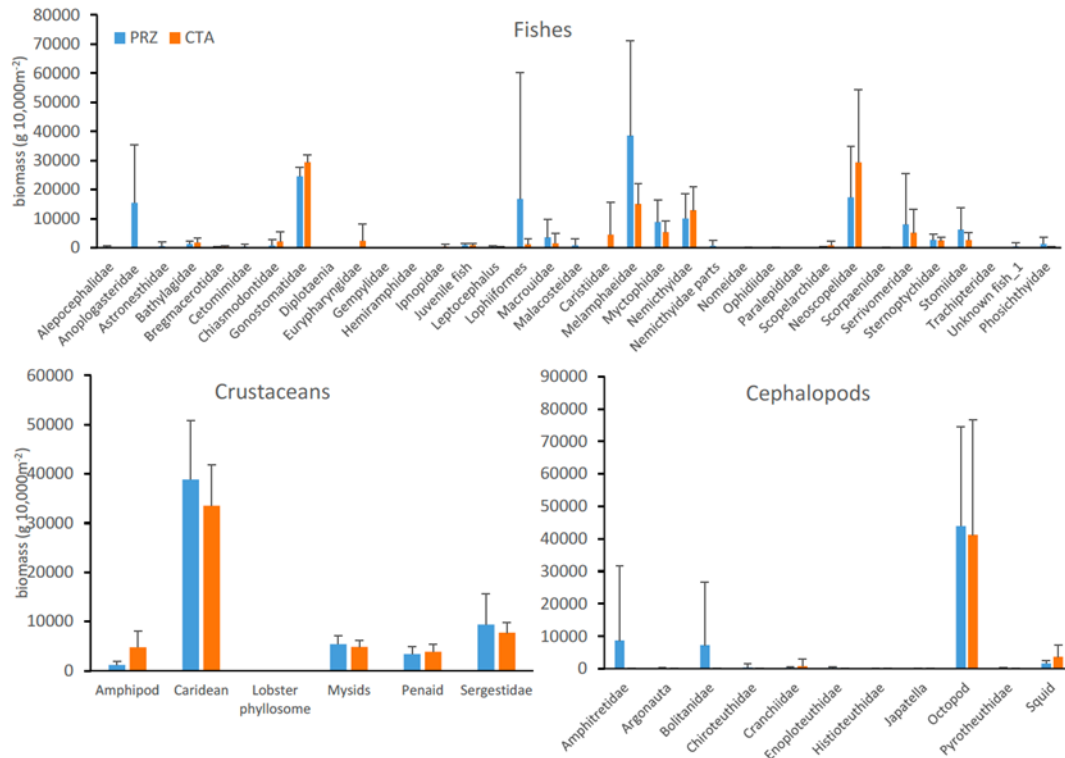


Figure 6-80 Micronekton biomass by area and family or broad taxonomic group. Note the changes in the vertical axes scaling.



(c) Depth specific mesopelagic micronekton abundance and biomass

Examination of the micronekton broad taxa by depth shows differing depths for peaks in abundance and biomass (Figure 6-81). Fish abundance is highest from 700-1000m just below the OMZ. This is largely the result of *Cyclothone* spp. which are non-migratory and dominated the fish assemblage (Figure 6-82). Other abundant fish taxa did exhibit strong vertical migration with peaks in abundance at depth during the day, typically within the OMZ core (450-700m), and closer to the surface at night (Figure 6-82). Thus, when the nonmigratory *Cyclothone* spp. are excluded, fish abundance and biomass peaks within the OMZ during the day. Crustacean abundances do show a pattern of vertical migration. However, there is a significant component of this community (both in terms of abundance and biomass) that resides at depth below the OMZ both day and night. For cephalopods, a peak in abundance is apparent in the upper oxycline (mostly juvenile squids) and a peak in biomass from 700-1000m due to the presence of the large octopods at this depth. Crustacean and cephalopod abundance and/or biomass was higher just below or just above the OMZ that directly within it. Overall, there is significant abundance and particularly biomass of micronekton from 1000-1500m, the planned discharge depth of the prototype collector vehicle.

Figure 6-81 Distributions of abundance (# 10,000m⁻³) and biomass (g 10,000 m⁻³) day and night averaged across the PRZ and CTA for fishes, crustaceans and cephalopods.

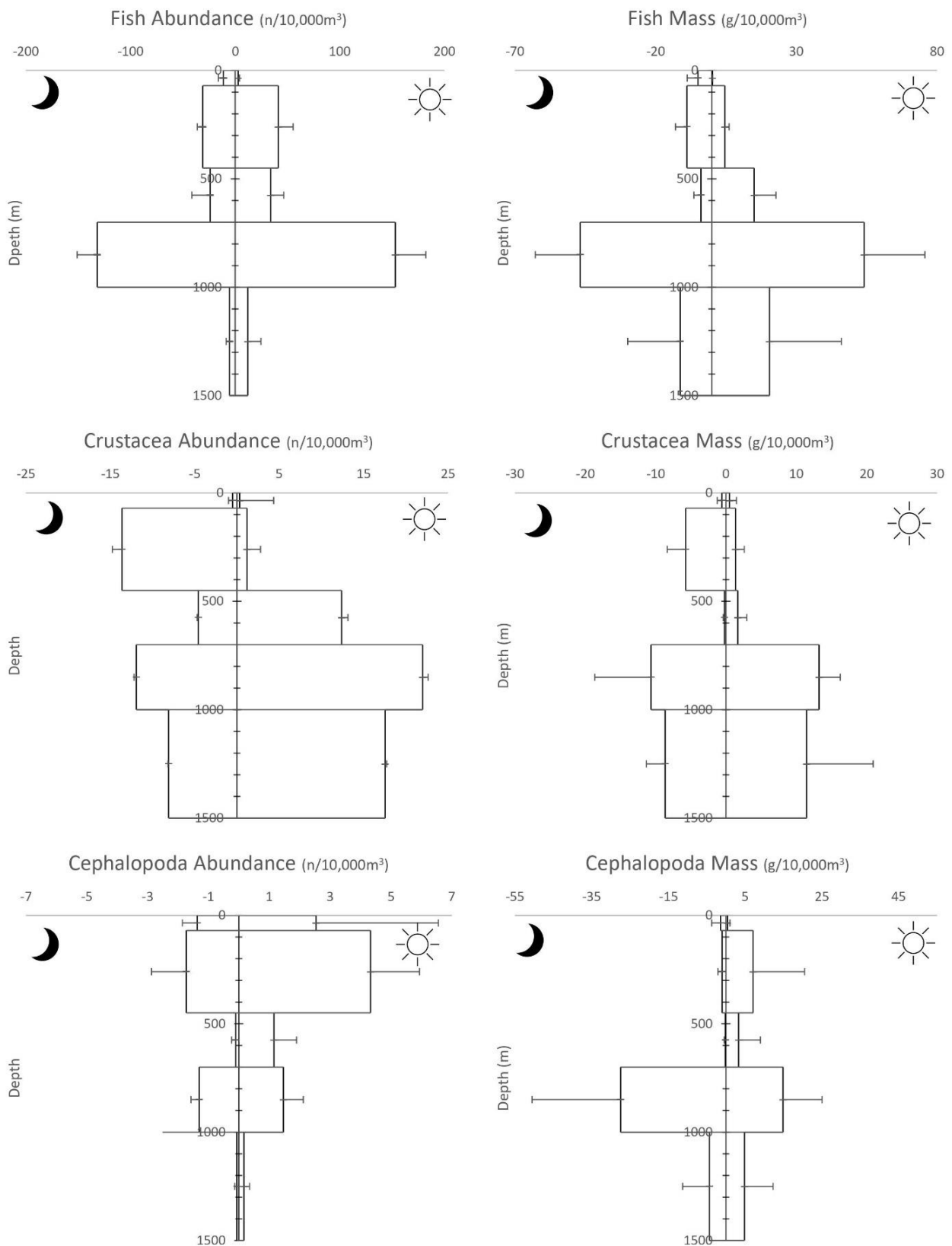
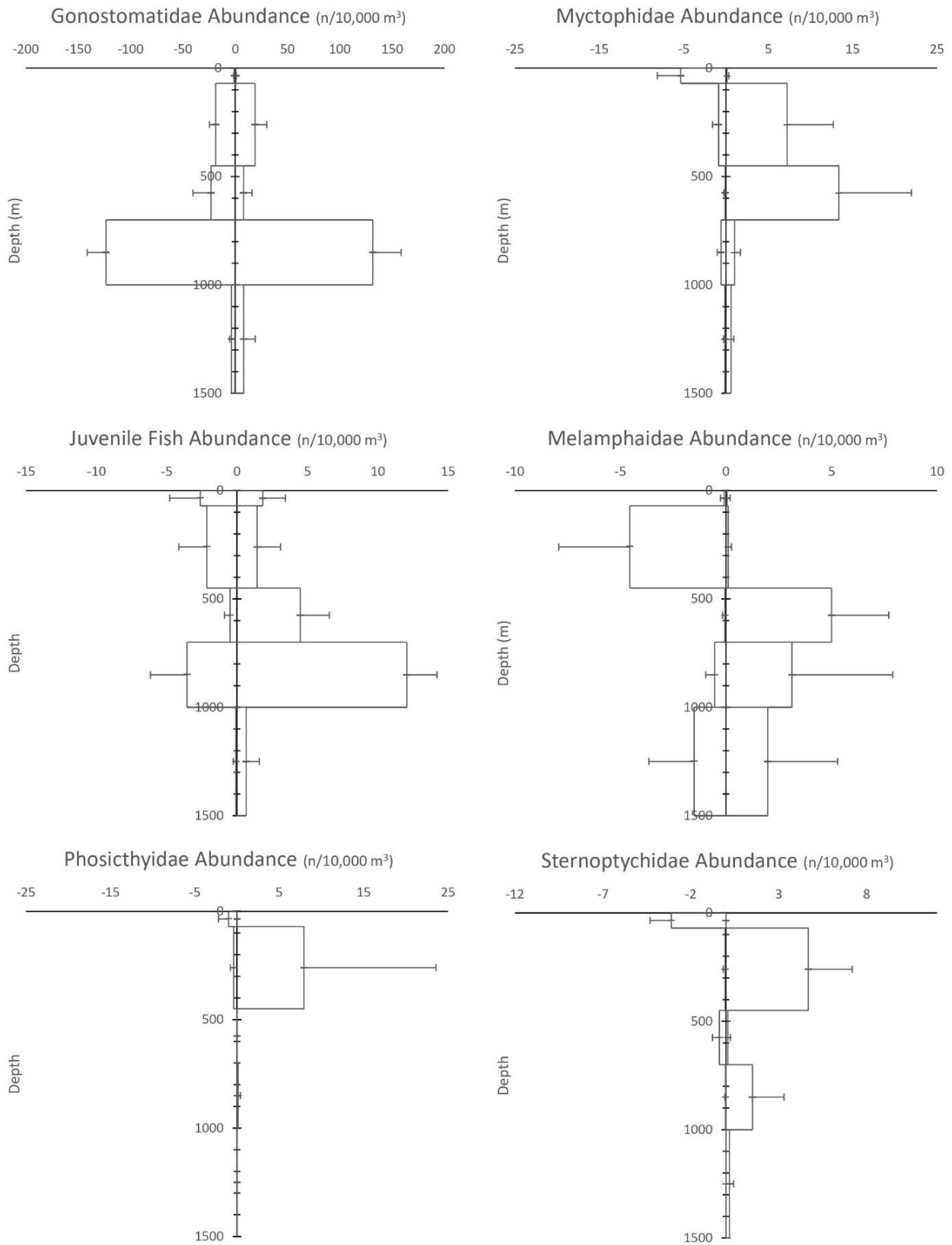


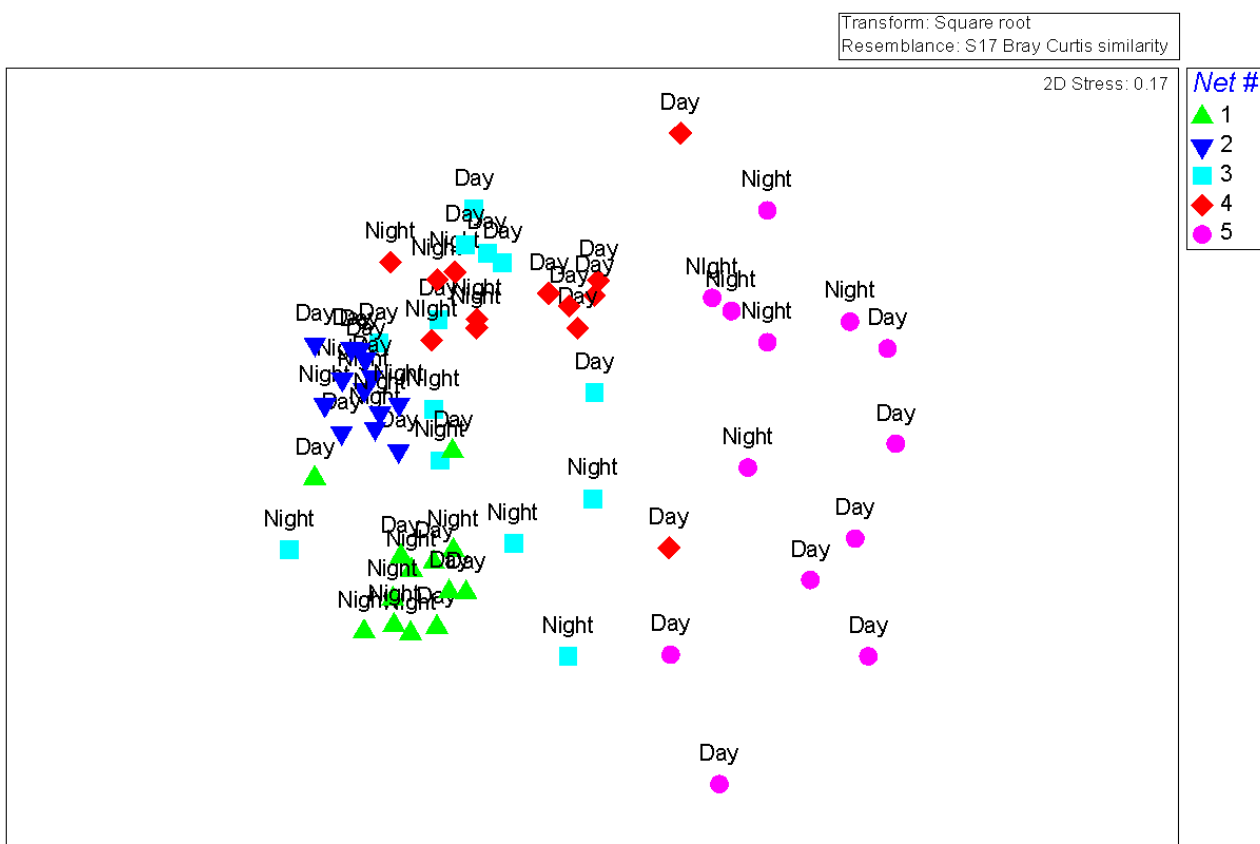
Figure 6-82 Distributions of abundance (# 10,000m⁻³) day and night averaged across the PRZ and CTA for dominant fish families.



(d) Analysis of community composition

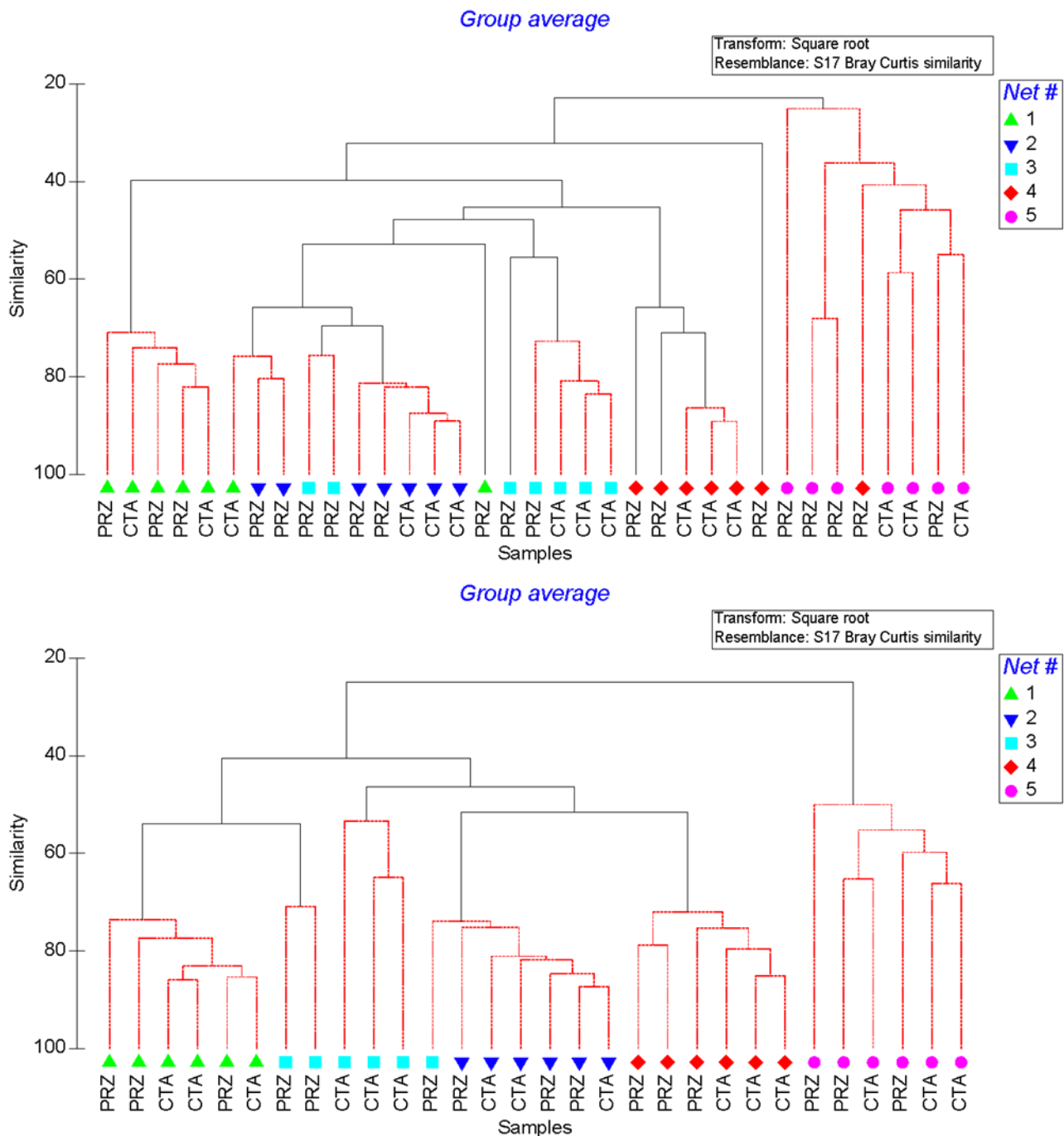
A preliminary analysis of community composition was conducted. Further analysis will need to be done when the crustaceans and cephalopods identification has been completed. This analysis clearly shows the strong structuring of the community (by family level) by depth as net samples from the same depths cluster together in multidimensional space (Figure 6-83). The changes to community composition at a given depth due to vertical migration is also apparent with samples from a given depth separating by day and night (Figure 6-83). Samples from shallower depths (nets 3-5) strongly cluster by day/night but samples from the lower oxycline and below the OMZ (nets 1, 2) do not.

Figure 6-83 MDS analysis of the micronekton community (families or broad taxa) by net. With a couple of exceptions (see above) depths are as follows: 1 = 1500-1000m, 2 = 1000-700m, 3= 700-450m, 4 = 450-70/90m, 5 = 70/90m to surface).



Given the strong influence of vertical migration the data were further separated by day and night and analyzed again to evaluate similarities between the sampling sites (Figure 6-84). From this analysis, shallow surface samples from both sites cluster together significantly (SIMPROF, $p < 0.05$). The same is true for the community from 1000 to 1500m depths (net 1). There is more structure to the daytime samples from nets 2 and 3, which is largely due to some small changes in depths samples for these nets (see methods). There does appear to be a difference in the micronekton community in the upper oxycline (70/90 to 450m; net 4). Here all the CTA samples formed a statistically significant cluster apart from the PRZ samples. Night time samples showed even stronger structuring by depth, with each depth horizon forming a statistically significant cluster (Figure 6-84, lower panel). However, differences between the sites were significant within the OMZ (450-700m, net 3).

Figure 6-84 Cluster analysis of the micronekton community (families or broad taxa) by net and by day (top panel) and night (bottom panel) to control for differences deriving from vertical migration. For net depths see Figure 5. Groups connected by red lines are significant clusters (SIMPROF, $p < 0.05$).



Our analysis represents the first depth stratified sampling of the mesopelagic micronekton community in the CCZ region. Early trawling work provided micronekton specimens from the eastern Pacific region, including in proximity to NORI-D however these samplings were frequently without the use of opening-closing nets, were opportunistic (fishes incidentally captured in plankton tows), or samples were used for taxonomic purposes and no ecological or community information was published (e.g. Wisner 1974). Therefore, earlier work and museum specimens are available for micronekton in the eastern Pacific and provide an ability to identify the fauna. However, community ecology, which is required to assess environmental baselines or evaluate environmental change in response to mining, are lacking in the eastern CCZ.

Micronekton abundance and biomass is similar to other oligotrophic regions in the North Pacific. Maynard *et al.*, (1975) reports similar abundance and biomass of total micronekton near Hawaii with similar estimates for fish abundance and biomass as well (Clarke 1973). Most other areas sampled in the Pacific are in far more productive waters such as the California current, Kuroshio current and subarctic waters where fish biomass is much higher, as expected (Brodeur & Yamamura 2005).

With regards to vertical distributions, it was somewhat surprising to find high fish biomass within the OMZ core during the day. Other studies have suggested that plankton and other taxa avoid the OMZ core (Wishner *et al.* 2013; Maas *et al.* 2014; Netburn & Koslow 2015). Given the strength and shallow depth of the OMZ in the NORI-D region it is likely that the migratory fishes must enter it during the day to avoid visual predators. Below the OMZ there are peaks in the abundance of *Cyclothone* spp., crustaceans and cephalopods, a pattern more consistent with earlier studies as cited above.

In relation to collector test preparation, it is important to note that there is a significant biomass of micronekton at the depths of the planned midwater discharge. This may be partly the result of deep distributions caused by the strong OMZ but actual drivers are unclear at this time.

There are differences in the micronekton community between the PRZ and CTA. There is inherently a lot of variability in net collection data. However, the dominant fish *Cyclothone* spp. are more abundant and have greater biomass in the CTA. These are largely nonmigratory fishes living at or just above the planned discharge depths (Brodeur & Yamamura 2005). Other taxa (e.g., Melamphaidae) are more abundant in the PRZ. Further an analysis of community composition also found differences between the two sites. The night-time communities, thus non-migrators, were different between the two sites at OMZ depths (450-700m). Daytime communities in the upper oxycline (70/90 to 450m) were also different between the sites. The reasons for differences between the PRZ and CTA are not clear at this time but may be related to slight differences in OMZ characteristics (Wishner *et al.* 2018) or due to mesoscale eddies (see Sairdron section xx).

6.4.6 Micronekton community (small fishes, squids and shrimps) using bioacoustics techniques

6.4.6.1 Purpose & scope

The following section describes the work conducted in 2021 by University of Hawaii to characterise natural baseline conditions in mesopelagic micronekton communities in the NORI-D contract area. The scope, the survey planning and the sampling methodologies carried out to ecologically characterise these communities align with International Seabed Authority ISBA/25/LTC/6 Rev 1. Annex 1 section 42(e) mesopelagic micronekton and 44. vertical migration to provide baseline data requirements under Recommendations III.B.15.(d).(iii); IV.B.22.

6.4.6.2 Baseline investigations

The methods and proposed survey array for both the collector test and long-term environmental studies on NORI-D will provide data to meet the following objectives:

- To determine proxies for mesopelagic micronekton biomass, vertical distribution and migration patterns in the top 1000m of the water column.

6.4.6.3 Campaign activities

(a) Survey design

Though bioacoustics cannot determine community composition, they have several advantages over traditional net sampling, and they are a technique strongly recommended by Drazen *et al.* (2019). Studies have been conducted worldwide showing that estimates of mesopelagic biomass from net collection

underestimate total biomass 10-fold (Irigoien *et al.*, 2014; Proud *et al.*, 2017). Further, they are an excellent way to evaluate vertical migration patterns and can detect finer scale changes in these patterns as might occur due to midwater sediment discharge (e.g. Ariza *et al.*, 2014).

Saildrone use frees up ship time and provides a stable quiet platform for bioacoustics work (De Robertis *et al.*, 2019) at two frequencies to ensonify the water column from the surface to ~1000m (38 kHz) or 250m (200 kHz). The lower frequency allows for observations of micronekton and in particular gas-bearing organisms (primarily mesopelagic fishes) that resonate most strongly at 38 kHz; the higher frequency targets large zooplankton and organisms such as crustaceans that are non-gas bearing (Davison *et al.*, 2015)

During Campaign 5B, acoustic backscatter and *in situ* oceanographic data was collected using a Saildrone uncrewed surface vehicle (USV) for 33 continuous days between 10 March and 12 April 2021. The Saildrone was mounted with a Simrad WBT mini (EK80) fisheries echo sounder (-2m) to record split-beam 38 kHz acoustic backscatter from the surface to 1000 m depth and single beam data recorded at 200 kHz from the surface to 250 m.

The echo sounder was calibrated using a 38.1 mm tungsten carbide sphere following the standard methods of Demer *et al.* (2015). Acoustic data was collected in CW mode with a ping interval of 2.25 s and pulse duration of 1024 μ s. The USV averaged a speed of 1-2 knots and survey routes were adjusted in real time to make best use of changing winds.

(b) Oceanographic variables

Surface oceanographic data including salinity and temperature (Seabird SBE 37) and photosynthetically active radiation (PAR; LI-COR LI-192SA) were collected by the Saildrone concurrently with acoustic data. It was not possible to collect chlorophyll-a via the USV during the spring survey, but 8-day and monthly satellite chlorophyll-a was extracted from NOAA OceanWatch (Aqua MODIS 0.04°) and daily data assimilative sea surface height (SSH; HYCOM GOFS 3.1 Global 1/12° Reanalysis) for comparison with acoustic backscatter and *in situ* oceanographic variables. Mesoscale features including an anticyclonic eddy and equatorial current within the survey area were initially identified from HYCOM SSH and surface currents.

(c) Acoustic data processing

Raw acoustic backscatter was analysed in the open-source fisheries acoustics data processing software, ESP3, developed by the deep-water fisheries acoustics team at National Institute of Water and Atmospheric Research (NIWA) (<https://sourceforge.net/projects/esp3/>). Acoustic files were classified as day or night after removing ± 2 hours around local sunrise and sunset to avoid DVM. Signal attenuation and sound speed were then calculated using the method of Francois & Garrison (1982) and the data was visually scrutinized to remove bad pings and signal dropouts due to internal instrument noise or surface bubbles. We set a signal-to-noise threshold of 3 dB for 38 kHz (2 dB for 200 kHz data) which removed sufficient noise at deeper depths where sound waves weakened. Area backscatter (s_a) was echo-integrated in 10 m vertical by 1 km long bins, scaled to $m^2 km^{-2}$, and the vertical profiles were averaged for each day or night. From daily/nightly s_a profiles, we calculated several acoustic metrics including total water column backscatter (total s_a ; Eq. 1) as follows:

$$Total s_a = \sum(s_{a-i}) \quad (1)$$

where s_{a-i} is the daily or nightly area backscatter for a given 10 m depth bin. We additionally calculated the weighted mean depth of backscatter (WMD; Eq. 2), a proxy for the depth of greatest micronekton density, as:

$$WMD = \frac{\sum(s_{a-i} * Depth_i)}{Total s_a} \quad (2)$$

where *Depth_i* is the mean depth for a given 10 m depth bin. Finally, we estimated the proportion of mesopelagic communities that migrated to the surface each night as DVM strength (Eq. 3), a ratio of integrated mesopelagic night-time and daytime backscatter (Klevjer *et al.*, 2016; Perelman *et al.*, 2021):

$$DVM\ Strength = 1 - \left(\frac{S_{a-meso-night}}{S_{a-meso-day}} \right), DVM\ Strength > 0 \quad (3)$$

(d) Statistics

To evaluate differences in the vertical structure of acoustic backscatter as a proxy for micronekton vertical distributions, we conducted multivariate analyses of backscatter profiles for each day or night in the two area datasets. To do this, *s_a* was aggregated into 50 m depth bins to look for broad differences in vertical structure. The data were then standardised by converting *s_a* in each 50 m depth bin to proportions of total daily or nightly backscatter. K-means clustering analysis was then performed using the ‘stats’ package in R (R Core Team, 2020). The optimal number of clusters for k-means was determined using silhouette widths, a method which measures the difference between intra-cluster similarity and similarity with the nearest cluster (Rousseeuw, 1987). Mean backscatter profiles from each cluster are presented and compared in the results.

Table 6-42 Mean daytime and nighttime 38 kHz acoustic metrics for the PRZ, CTA, and NORI-D surveys, as well as all data combined. 38 kHz data was recorded to 1000 m; epipelagic data is surface – 200 m and mesopelagic data is 200 – 1000 m.

| AREA | DAY/NIGHT | TOTAL <i>S_a</i> (m ² km ⁻²) | EPIPELAGIC <i>S_a</i> (m ² km ⁻²) | MESPELAGIC <i>S_a</i> (m ² km ⁻²) | WMD (m) | DVM STRENGTH |
|--------|-----------|---|--|--|---------|--------------|
| PRZ | day | 40.0 | 3.3 | 36.7 | 373.0 | 0.93 |
| | night | 42.0 | 39.5 | 2.5 | 103.0 | |
| CTA | day | 32.7 | 5.8 | 27.0 | 340.0 | 0.72 |
| | night | 43.4 | 38.9 | 6.8 | 107.0 | |
| NORI-D | day | 35.8 | 3.9 | 31.8 | 322.0 | 0.82 |
| | night | 34.2 | 30.6 | 3.7 | 83.4 | |
| TOTAL | day | 35.9 | 4.2 | 31.7 | 334.0 | 0.82 |
| | night | 39.4 | 35.5 | 4.3 | 92.0 | |

Table 6-43 Mean daytime and night-time 200 kHz acoustic metrics for the PRZ, CTA, and NORI-D surveys, as well as all data combined. 200 kHz data was recorded to 250 m

| AREA | DAY/NIGHT | TOTAL <i>S_a</i> (m ² km ⁻²) | WMD (m) |
|--------|-----------|---|---------|
| PRZ | day | 0.7 | 79.2 |
| | night | 3.2 | 51.0 |
| CTA | day | 0.9 | 66.0 |
| | night | 2.9 | 53.0 |
| NORI-D | day | 0.83 | 52.0 |
| | night | 2.9 | 41.0 |
| TOTAL | day | 0.8 | 60.0 |
| | night | 3.0 | 45.0 |

6.4.6.4 Preliminary results & discussion

(a) Acoustic metrics

PRZ Survey (7 Apr - 12 Apr)

38 kHz (Table 6-42): During the 6-day survey of the PRZ, mean daytime total s_a (surface – 1000 m) was roughly similar though slightly lower than night-time total s_a , with significantly higher epipelagic s_a at night and significantly higher mesopelagic s_a during the day. Mean daytime and night-time WMD at this site were 373 m and 103 m, respectively, and the mean DVM strength was 0.93. **200 kHz** (Table 6-43): Total s_a at this frequency (surface – 250 m) was higher at night-time than daytime. The mean daytime and night-time WMD in the PRZ were 79.2 m and 51 m, respectively.

CTA Survey (31 Mar - 5 Apr)

38 kHz (Table 6-42): The mean daytime total s_a during the 6-day survey of the CTA was lower than night-time total s_a , with much lower daytime epipelagic s_a and higher daytime mesopelagic s_a . At this site, the mean daytime and night-time WMD were 340 m and 107 m, respectively, and the mean DVM strength was 0.72. **200 kHz** (Table 6-43): Total night-time s_a at this frequency was higher than daytime, and the mean daytime and night-time WMD in the CTA were 66 m and 53 m, respectively.

NORI-D Survey (10 Mar - 30 Mar)

38 kHz (Table 6-42): During the full NORI-D survey, daytime and night-time total s_a were roughly similar though slightly higher during the daytime. Epipelagic s_a was significantly higher at night and mesopelagic s_a was much greater during the day, as expected from strong DVM signals in this area. Mean daytime and night-time WMD were 322 m and 83.4 m, respectively, and DVM strength had an average value of 0.82. **200 kHz** (Table 6-43): At this frequency, night-time total s_a was higher than daytime total s_a . Mean daytime and night-time WMD were 52 m and 41 m, respectively.

Total Survey (10 Mar – 12 Apr)

38 kHz (Table 6-42): For all acoustic data collected during Campaign 5B, night-time total s_a was higher than daytime s_a . This difference was largely driven by increased epipelagic s_a at night, while mesopelagic s_a decreased due to diel vertical migration. Daytime WMD throughout the survey averaged 334 m and night-time WMD averaged 92 m, and the mean DVM strength was 0.82. **200 kHz** (Table 6-43): Total s_a was higher at night-time than daytime throughout all surveys, and mean daytime and night-time WMD were 60 m and 45 m, respectively.

(b) Site comparisons

38 kHz: Daytime total s_a and mesopelagic s_a were higher in the PRZ than in the CTA, and daytime WMD was deeper in the PRZ (373 m) than in the CTA (340 m). DVM strength was also noticeably higher in the PRZ (0.93) than the CTA (0.73). Night-time mesopelagic s_a was slightly higher in the CTA than the PRZ, correlating with the decreased DVM strength in this site. **200 kHz:** Daytime and night-time total s_a were not significantly different between the two sites, but daytime WMD was noticeably deeper in the PRZ (79.2 m) than in the CTA (66 m).

38 kHz: The daytime clustering results for all acoustic data at this frequency collected during Campaign 5B resulted in two distinct data groups, roughly divided latitudinally around 10.75° – 11° N (Figure 6-85 a). Most notably, the northern data group consists of very strong daytime mesopelagic scattering layers with a peak intensity around 330 m, while the southern data group is comprised of days with much weaker and more vertically diffuse daytime mesopelagic scattering layers roughly between 250-500 m (Figure 6-85b,c). The night-time clustering results for the full dataset reveal a quite different pattern, with two distinct data groups divided roughly between the full NORI-D survey and the site-specific surveys (Figure 6-86a). These night-time groups are characterized by a strong shallower scattering layer around 35 m in the full NORI-D survey and a slightly deeper, strong scattering layer around 80 m during the site-specific

surveys (Figure 6-86b,c). The notable difference between daytime and nighttime s_a profiles is driven by strong DVM in this region; most of the acoustically detectable community appears to reside between 280-530 m during the daytime and migrate to the upper ~100 m at night.

200 kHz: Both daytime and night-time data at this frequency clustered into two groups that were similar to the night-time 38 kHz cluster groups, divided roughly between the full NORI-D survey and the following site-specific surveys (Figure 6-87a; Figure 6-88a). For the daytime data, the full NORI-D group contained slightly stronger and shallower scattering layers peaking around 45 m while the site-specific group contained slightly deeper and weaker scattering layers peaking around 75 m (Figure 6-87b,c). The night-time full NORI-D group similarly contained stronger and slightly shallower scattering layers peaking just above 50 m and the site-specific group contained weaker and deeper layers just below 50 m (Figure 6-88b,c).

Figure 6-85 K-means clustering results for daytime 38 kHz data. a) Map of daytime survey track coloured by cluster group. b) Mean vertical profiles of backscatter proportion for each cluster group. c) Mean vertical profiles of area backscatter for each cluster group.

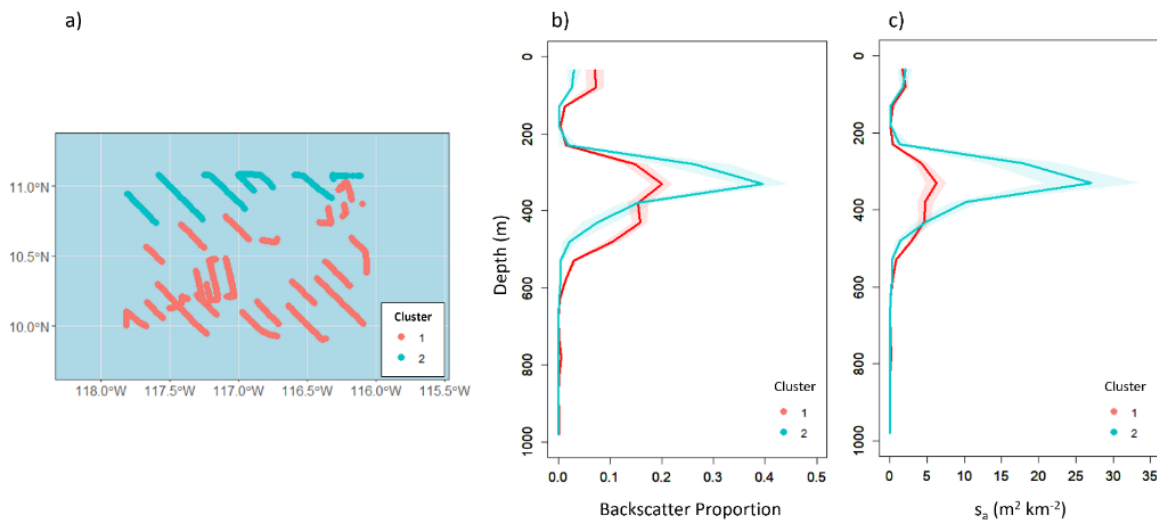


Figure 6-86 K-means clustering results for night-time 38 kHz data. a) Map of night-time survey track coloured by cluster group. b) Mean vertical profiles of backscatter proportion for each cluster group. c) Mean vertical profiles of area backscatter for each cluster group.

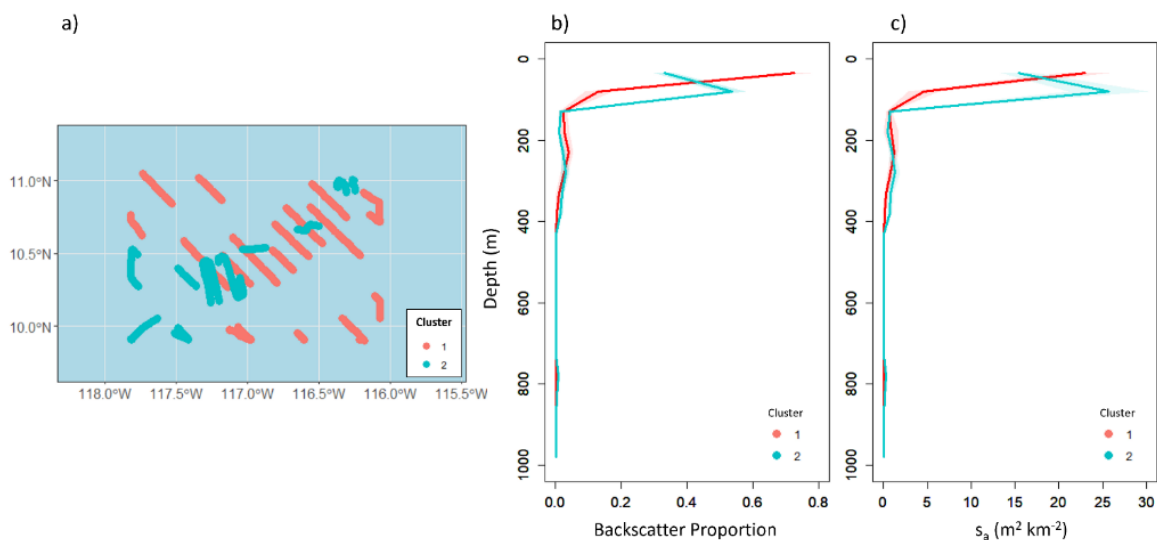


Figure 6-87 K-means clustering results for daytime 200 kHz data. a) Map of daytime survey track coloured by cluster group. b) Mean vertical profiles of backscatter proportion for each cluster group. c) Mean vertical profiles of area backscatter for each cluster group.

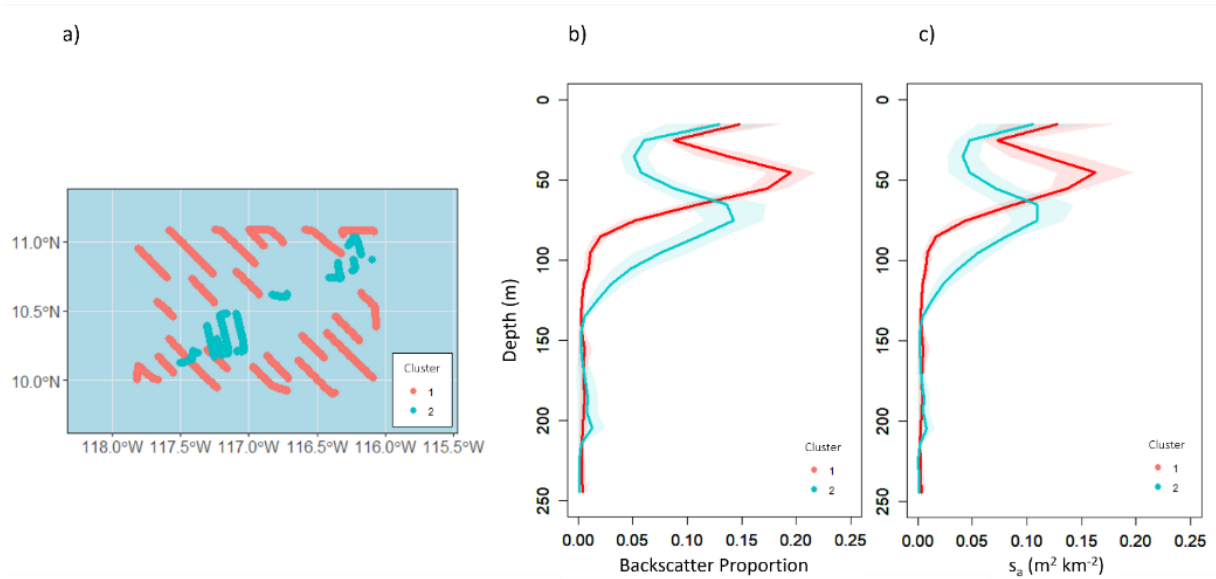


Figure 6-88 K-means clustering results for night-time 200 kHz data. a) Map of night-time survey track coloured by cluster group. b) Mean vertical profiles of backscatter proportion for each cluster group. c) Mean vertical profiles of area backscatter for each cluster group.

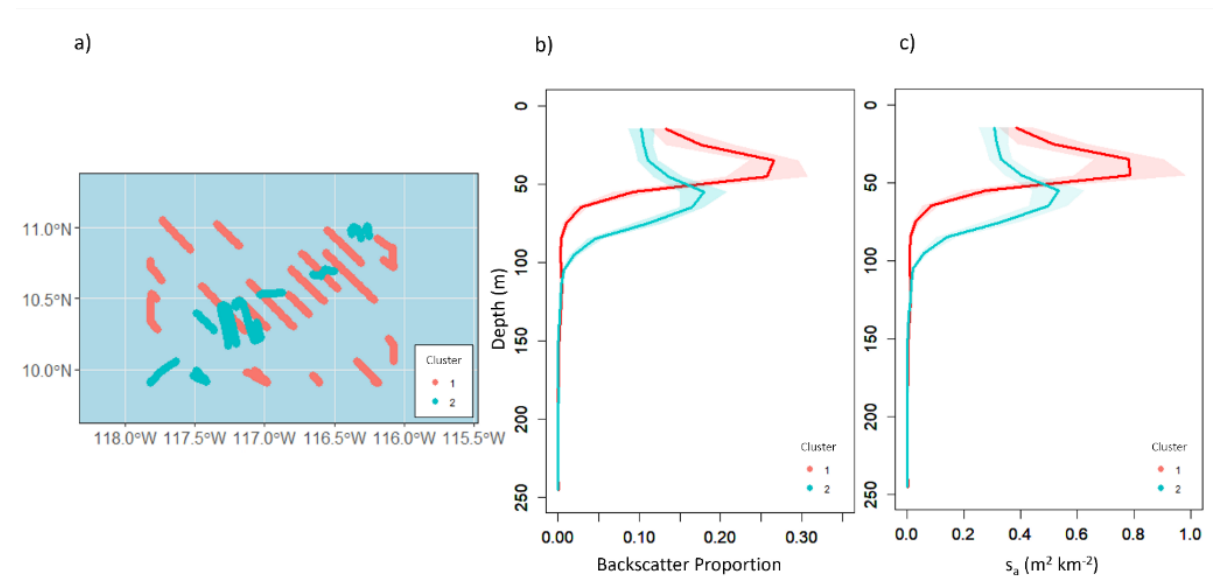
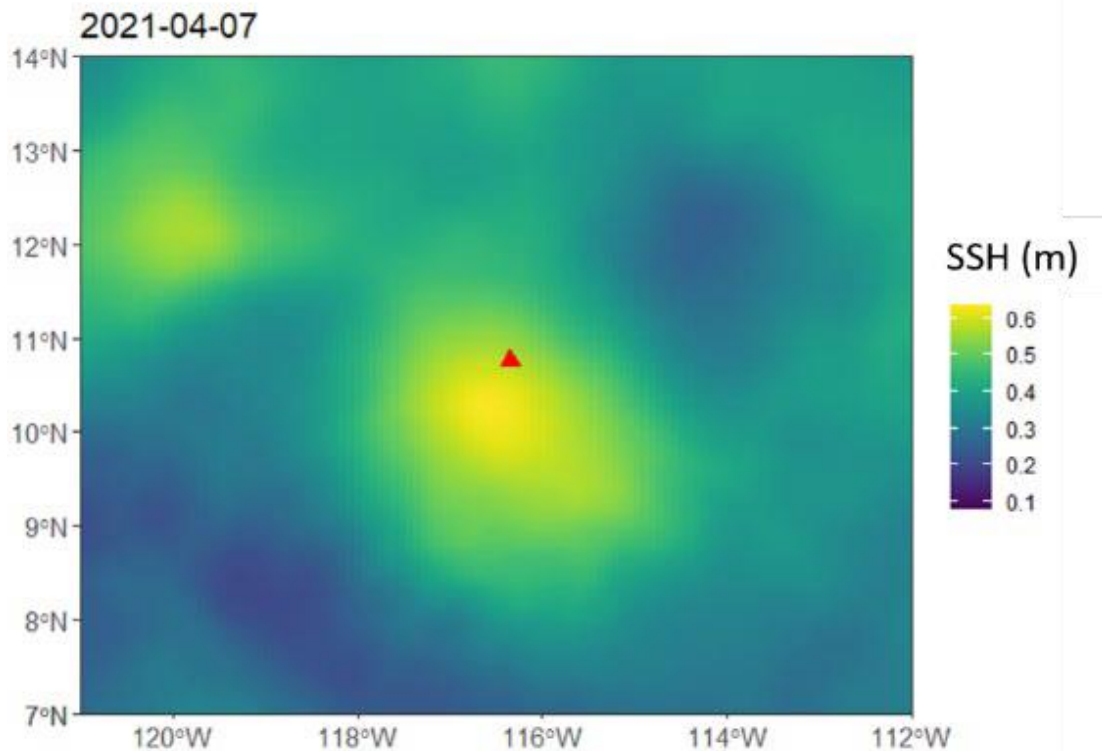


Figure 6-89 An anticyclonic eddy passed into the survey area at the end of March and persisted throughout the rest of the surveys in April. This map shows the location of the eddy (indicated by increased SSH) on 7 April and the location of the Sairldrone that day (red triangle).



Oceanographic Features

Notably, a westward-propagating anticyclonic eddy crossed into the survey area beginning at the end of March and continuing throughout the rest of the survey in April (Figure 6-89). This feature, characterized by increased sea surface height (SSH) and sea surface temperature (SST) and decreased salinity (Figure 6-90), began influencing the area towards the end of the full NORI-D survey and was present during both the CTA and PRZ surveys, corresponding roughly with the separation of night-time 38 kHz cluster groups and daytime and night-time 200 kHz cluster groups (Figure 6-86-Figure 6-88). The arrival of the eddy also corresponds with the appearance of a deep, nonmigratory scattering layer around 800 m that is mostly absent during the rest of the survey (Figure 6-92c). In addition, the North Equatorial Current (NEC) was present in the study area and identifiable from HYCOM surface currents during the month of March (Figure 6-90), prior to the arrival of the eddy. The westward-flowing current increases in strength south of ~11° N, corresponding approximately with the separation of 38 kHz daytime cluster groups (Figure 6-85).

Figure 6-90 Survey tracks of oceanographic variables including the full NORI-D survey and site-specific CTA and PRZ surveys: a) sea surface height (HYCOM), b) sea surface temperature (Saildrone Seabird SBE 37), c) salinity (Saildrone Seabird SBE 37), and d) satellite chlorophyll (8-day mean; Aqua MODIS). Grey color indicates missing data due to cloud cover.

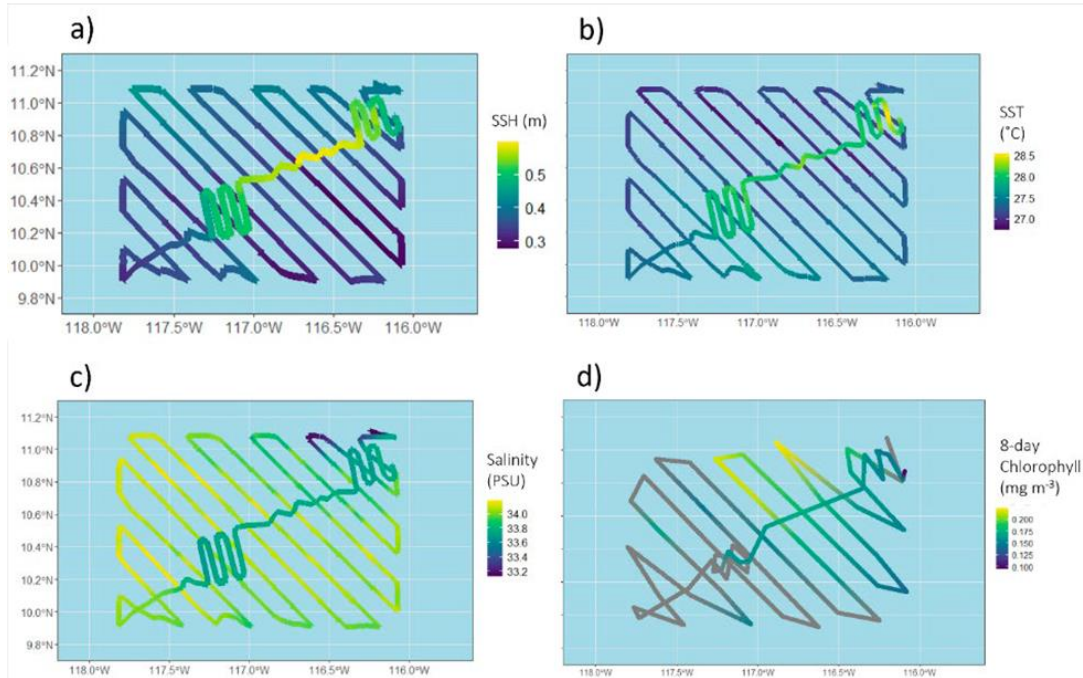


Figure 6-91 Oceanographic features with latitudinal gradients through NORI-D: a) Mean and b) standard deviation of the mean total current strength in and around the survey area for the month of March 2021, calculated from HYCOM surface currents, c) mean midwater oxygen partial pressure (pO₂) calculated from World Ocean Atlas climatology (WOA18; 1x1° resolution).

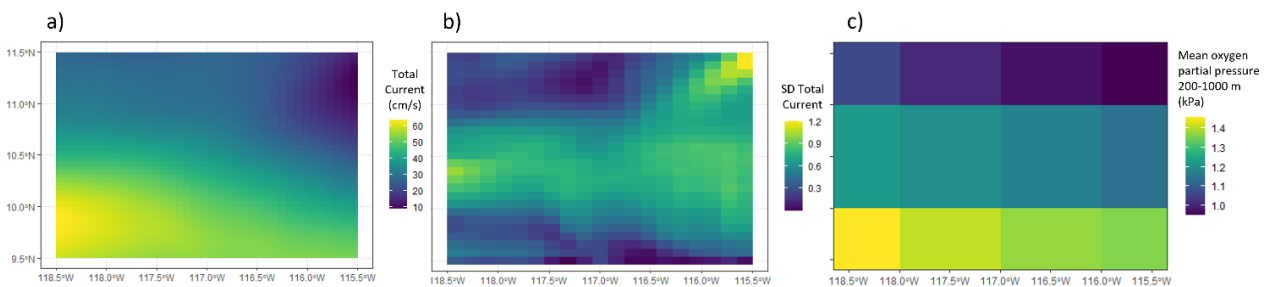
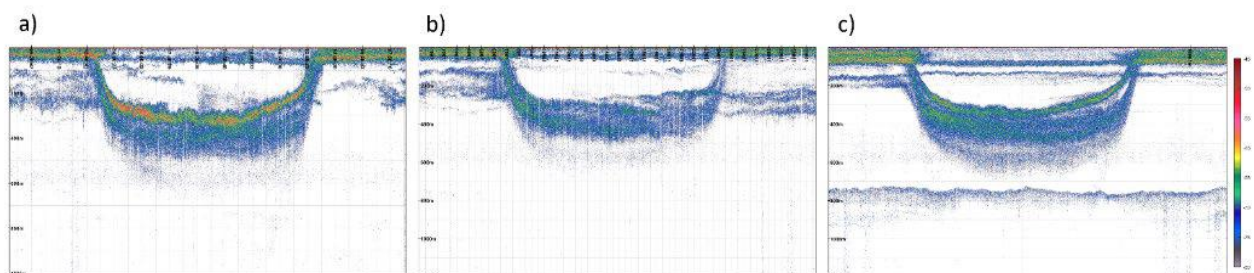


Figure 6-92 Echogram examples (0-1000 m) from 38 kHz data with one full DVM cycle showing volume backscattering strength (S_v; dB re 1 m⁻¹). a) 11 Mar 2021; north of the North Equatorial Current. b) 14 Mar 2021; within the North Equatorial Current (pre-eddy). c) 10 Apr 2021; within the North Equatorial Current (during eddy).



Area backscatter strength (s_a), is a linear proxy for biomass, abundance, or community shifts of pelagic organisms. During the spring 2021 campaign, the median daytime mesopelagic s_a within NORI-D ($25 \text{ m}^2 \text{ km}^{-2}$) was similar to and slightly higher than modelled backscatter for this area found by Proud *et al.* (2017). Based on that study, mesopelagic s_a within and around the area of NORI-D ($23 \text{ m}^2 \text{ km}^{-2}$) is higher than that of the neighboring North Pacific Subtropical Gyre ($21 \text{ m}^2 \text{ km}^{-2}$) and central/western Pacific ($20 \text{ m}^2 \text{ km}^{-2}$). Another study found that in general, the Eastern Pacific contains significantly higher daytime mesopelagic s_a than the North Atlantic, Western Pacific, and Indian Oceans (Klevjer *et al.*, 2016). Additionally, data recently collected in the central Pacific near Hawai'i found significantly lower daytime mesopelagic s_a ($\sim 13 \text{ m}^2 \text{ km}^{-2}$; Perelman *et al.*, unpublished data) than we observed within NORI-D. Our results and previous studies thus suggest that the NORI-D area contains relatively high mesopelagic biomass, or a strong sound scattering mesopelagic community, compared to published data from other oceanographic regions.

Between the two sampling sites within NORI-D, the PRZ had higher total daytime s_a (driven by higher mesopelagic s_a), deeper daytime WMD, and stronger DVM strength than the CTA at 38 kHz (Table 6-42), highlighting differences in micronekton communities between the surface and 1000 m. The PRZ also had deeper daytime WMD at 200 kHz (Table 6-43), which emphasizes differences in shallower communities with similar or higher relative acoustic responses compared to 38 kHz, such as crustaceans and large zooplankton, between the surface and 250 m. Increased daytime s_a within the PRZ could indicate higher biomass or densities of organisms compared to the CTA, but it could also indicate a community shift to species that return a stronger acoustic signal at the observed frequency and depth. In other words, the contribution of different organisms to acoustic backscatter varies greatly with frequency and depth (Bassett *et al.*, 2020), and stronger backscatter could also be indicative of a different community with stronger acoustic targets at 38 kHz at the observed depth (e.g., Davison *et al.*, 2015; Dornan *et al.*, 2019). In general, gas-bearing fishes (i.e., those with a gas-filled swim bladder) contribute most strongly to acoustic backscatter at 38 kHz. In this regard, deeper daytime WMD in the PRZ could indicate that the micronekton communities reside at deeper depths than the CTA, or it could suggest that this site harbors a different community with organisms at a slightly deeper depth returning stronger acoustic signals. Based on a previous study of scattering layers across the CCZ, the difference in DVM strength between the two sites (0.93 and 0.72 in the PRZ and CTA, respectively) may be driven by the Eastern Tropical Pacific Oxygen Minimum Zone (OMZ), in which midwater oxygen increases slightly from north to south in NORI-D (Perelman *et al.*, 2021). This is because with sufficient oxygen, more mesopelagic organisms can reside at depth at night and may not need to migrate to more oxygenated waters near the surface.

It is important to note that acoustic sampling of both the CTA and the PRZ occurred while the anticyclonic eddy was present in NORI-D. Eddies are known to influence the vertical distribution and abundance of micronekton communities (e.g., Drazen *et al.*, 2011; Penna *et al.*, 2021), and acoustically observed vertical structure and DVM behaviours in these two sites differ from those observed across NORI-D prior to the eddy. These differences are most evident in the clustering results, particularly influencing shallow scattering layers (Figure 6-86-Figure 6-88). During the night-time when most of the acoustically detectable mesopelagic communities have migrated to the surface, the shallow scattering layers at both 38 and 200 kHz are slightly deeper in cluster 2, the largely eddy-influenced group of days that occurred during the CTA and PRZ surveys, compared to cluster 1 (Figure 6-86-Figure 6-88). The eddy's influence was also evident in daytime clustering at 200 kHz, with the CTA and PRZ surveys generally comprising cluster 2 with slightly deeper scattering layers (Figure 6-87). Anticyclonic eddies are downwelling features, bringing warmer surface waters to depth. Thus, they may provide favourable opportunities for pelagic organisms to reside at deeper depths, as we observed acoustically, because warmer temperatures increase metabolic rates and ultimately growth and reproduction (Gascuel *et al.*, 2008; Proud *et al.*, 2017).

Daytime cluster groups at 38 kHz were starkly different from night-time groups at either frequency or daytime 200 kHz groups. These daytime 38 kHz groups are separated by a notable decrease in

mesopelagic scattering layer strength from north to south across the survey area, with stronger scattering layers in the north during the month of March and weaker scattering layers to the south and into April (Figure 6-85; Figure 6-92a,b). The change appears to be associated with the NEC which increases in strength from ~30 cm/s to nearly 60 cm/s around the latitude of the cluster division (~11°N) in March. While the NEC might extend (weakly) to the depth of mesopelagic scattering layers in the southern cluster (Cravatte *et al.*, 2017), it is likely that these strongly migratory communities are responding to surface changes associated with the current front. Strong gradients in physical surface properties often lead to high biological productivity, and thus oceanic fronts have been observed to influence mesopelagic fish assemblages, provide larval habitat, and act as predator foraging hot spots (e.g., Polovina *et al.*, 2001; Bakun, 2007; Netburn & Koslow, 2018). Though we were unable to collect in situ chlorophyll measurements as a proxy for productivity via the Saildrone, satellite oceanographic data suggests increased surface chlorophyll during several of the northern sampling days along the NEC front (Figure 6-90d). It is also possible that increasing midwater oxygen plays a role in these cluster separations, as oxygen partial pressure generally increases to the south in NORI-D (Figure 6-91c; Perelman *et al.*, 2021). Higher oxygen could lead to a shift in mesopelagic communities and may allow for the slightly deeper backscatter and weaker DVM strength that characterize the southern group.

The clustering results at both frequencies suggest that ephemeral oceanographic features such as mid-ocean eddies can influence the vertical structure of epipelagic communities on the scale of days to weeks. However, the NEC, a more permanent feature in this region, appears to be the dominant influence on daytime mesopelagic community structure that acoustically overshadows changes induced by the anticyclonic eddy passing through. While daytime clusters at 38 kHz were dominantly separated by latitudinal differences in mesopelagic backscatter strength, it is worth noting that focusing only on the upper 250 m of 38 kHz daytime data results in clusters very similar to those at 200 kHz, characterized by slightly shallower or deeper scattering layers prior to and during the anticyclonic eddy, respectively. This suggests that it is largely the shallow scattering layers that are responding to the eddy, and that mesopelagic communities are more strongly influenced by the NEC during the times of our observations. Time lags in productivity generation and this production reaching higher trophic levels means that the eddy may begin to influence deeper communities the longer it remains in the area (e.g., Penna & Gaube, 2020). Visual scrutiny of 38 kHz echograms does, however, reveal a clear nonmigratory scattering layer appearing around 800 m during the days and nights when the eddy is present (Figure 6-92c). This suggests that the eddy may indeed influence these mesopelagic communities, perhaps allowing certain organisms to remain at depth as productivity downwelled from the mixed layer increases food availability allowing certain organisms to reside at an acoustically-favourable depth where they may not have been detected at other depths by the 38 kHz frequency used. Because this deep, nonmigratory layer is much weaker than the strong scattering layers in the upper ~600 m of the water column, it was not a strong enough characteristic to separate the eddy-influenced days as a unique cluster in the multivariate analyses.

Overall, it appears that the latitudinal variability across NORI-D associated with the NEC confers a community or density shift of mesopelagic scattering layers that may dominate any changes induced by the eddy at deeper depths. Nevertheless, such natural variability from eddies and currents must be considered when establishing ecosystem baselines to distinguish between changes driven nodule collection or other disturbances. Since we do not have a full understanding of the frequency of mid-ocean eddies in this area nor the seasonal variability of the NEC, more sampling would be necessary to truly understand micronekton behaviour across the area. Nonetheless, our results suggest that the vertical distributions and DVM behaviours of pelagic communities across NORI-D are dynamic in space and time and highlight the important role of mesoscale oceanographic phenomena in driving this natural variability.

6.4.7 Food web linkages between trophic levels of dominant taxa

Pelagic food webs vertically connect pelagic strata and thus could translocate the impacts of dewatering plumes. Vertical migrations have a large influence on foraging ecology and sources of nutrition (Romero-Romero *et al.* 2019) and the basal sources of nutrition, surface phytoplankton, sinking marine snow, or much smaller particles changes with depth (Choy *et al.* 2015; Gloeckler *et al.* 2018b; Hannides *et al.* 2013; Romero-Romero *et al.* 2020). Knowledge of food web connections can also aid in understanding trace metal accumulation and transfer from the site of mining to surface waters or other areas removed from mining itself.

Stable isotope analyses are a very useful tool with which to characterize trophic structure in pelagic ecosystems (e.g., Choy *et al.* 2015; Popp *et al.* 2007; Romero-Romero *et al.* 2016). Furthermore, they could be used to evaluate if sediment plumes alter the isotopic composition of midwater particles and food webs. To characterize food webs during baseline studies and subsequently answer these questions after the collector tests, the stable isotopic composition of water column particles, the food of suspension feeders and size fractionated zooplankton (Hannides *et al.* 2013; Hannides *et al.* 2020), many of which are suspension feeders or omnivores, were examined. Future analyses will include several dominant micronekton which represent an intermediate trophic level to commercially important species such as tunas (Gloeckler *et al.* 2018a).

This section summarises the status of measurements of the concentration and downward flux of particulate carbon, particulate organic carbon and particulate nitrogen as prescribed by the ISA (Annex 1, 15g). In addition, the mass flux of particles and the amino acid nitrogen isotopic composition of different size classes of particles and zooplankton is reported. Carbon isotope analyses of individual amino acids are ongoing – they are complete for zooplankton from Campaign 5B but not for all of the particles and both are needed for full interpretation of the results.

6.4.7.1 Purpose & scope

The following section describes the work conducted in 2021 by University of Hawaii to develop an understanding of food web structure and function (e.g., Annex 1, 39) and the use of stable isotope analyses to understand those processes (Annex 1, 27, 30).

6.4.7.2 Baseline investigations

The methods and proposed survey array for both the collector test and long-term environmental studies on NORI-D will provide data to meet the following objectives:

Determine food web linkages between trophic levels of dominant taxa in the region using stable isotope analysis

6.4.7.3 Campaign activities

(a) Campaign 5B

Sinking Particles

Passively sinking particulate matter was collected using a surface-tethered free-floating array with 24 VERTEX-style particle interceptor (PIT) traps positioned at two depths below the euphotic zone (~65-90 m) following the protocol of (Knauer *et al.* 1979). These traps were deployed for approximately 70 to 80 hours and tracked using a surface buoy equipped with floats, a strobe, radio directional finder and Iridium satellite tracking device.

Size Fractionated Particles

Size fractionated particles were collected using in situ Large Volume Water Transfer Systems (McLane WTS-LV) equipped with either an 8 L/min or 30L/min pump head. Main sampling depths for particles covered the surface mixed layer (~25-50 m), the transition to the OMZ (70-150 m), the beginning of the mesopelagic (250 m), several depths within the mesopelagic above the proposed discharge depth (~400 and 850 m), and two depths in the upper bathypelagic (1000-1500 m). Each pump was equipped with a 142-mm diameter mini-Multiple Unit Large Volume Filtration System (mini-MULVFS) filter holder (Lam et al. 2015) with either 1 or 3 stages.

Zooplankton

Zooplankton were collected using a MOCNESS net with a 1 m² opening (see section XX). The 1-2 mm size-fractionated zooplankton was analysed throughout the sampled depths using samples from all 9 nets. Within the proposed depth range of sediment plume discharge (1000-1500 m, nets 1 and 2), zooplankton from the 0.2-0.5, 0.5-1.0, and 2.0-5.0 mm size fractions were also analysed. The carbon and nitrogen isotopic composition of size fractionated zooplankton were determined using the same methods described above for bulk isotopic composition of sinking particles. Uncertainty in measured $\delta^{13}\text{C}$ and $\delta^{15}\text{N}$ values as determined by replicate analyses was 0.2‰ for carbon and 0.3‰ for nitrogen.

AA CSIA

Size fractionated filters and zooplankton were prepared for compound-specific amino acid (AA) $\delta^{13}\text{C}$ and $\delta^{15}\text{N}$ analysis (AA-CSIA). Nitrogen isotope analysis was prioritized over carbon isotope analysis. Samples for AA-CSIA were hydrolyzed and trifluoroacetyl/isopropyl ester derivatives created using standard methods (Hannides et al. 2009). Briefly, samples were hydrolyzed (6N HCl, 150°C, 70 min) and the hydrolysate purified using low protein-binding filters and cation exchange chromatography. Purified samples were esterified using 4:1 isopropanol:acetyl chloride and derivatized using 3:1 methylene chloride:trifluoroacetyl anhydride. Trifluoroacetyl/isopropyl ester derivatives were additionally purified using solvent extraction (Ueda et al. 1989) and stored at -20°C for up to two weeks before analysis. Samples were prepared with an additional vial containing a mixture of 15 pure AAs purchased commercially (Sigma Scientific).

Calculations

Trophic position was estimated using the difference in $\delta^{15}\text{N}$ values between the trophic amino acid glutamic acid (Glx) and the source amino acid phenylalanine (Phe). This calculation assumed a $\beta\beta$ value of 3.4‰ for the difference in $\delta^{15}\text{N}$ values between Glx and Phe in primary producers and assumed that Glx was enriched in ^{15}N relative to Phe (Δ value) by 7.6‰ with each trophic transfer, e.g.:

$$\text{TP} = ((\delta^{15}\text{N}_{\text{Glx}} - \delta^{15}\text{N}_{\text{Phe}} - 3.4) / 7.6) + 1 \text{ (Chikaraishi et al. 2009a).}$$

Uncertainty in calculations of trophic position was determined using propagation of errors (Bradley et al. 2015; Jarman et al. 2017). The propagated error in this TP calculation assumed the uncertainty in $\beta\beta$ value is $\pm 0.9\text{‰}$ and the error in Δ is $\pm 1.1\text{‰}$ and used the measured analytical uncertainty in $\delta^{15}\text{N}_{\text{Glx}}$ and $\delta^{15}\text{N}_{\text{Phe}}$ based on at least triplicate analyses, when available.

Statistics

Statistical tests were conducted using SigmaPlot (v.14, Systat Software). For all statistical analyses, we considered p-values <0.05 statistically significant. Statistical differences between geographic regions were tested using one-way analysis of variance tests (ANOVAs). Data distributions were assessed using histograms, with log-transformations used to improve normality when necessary. When ANOVA results were significant, a post-hoc Tukey's Honest Significant Difference (HSD) test was conducted to determine which groups differed from others

6.4.7.4 Preliminary results & discussion

(a) Particle Standing Stock

The concentrations of particulate carbon (PC), particulate organic carbon (POC) and particulate nitrogen (PN) were measured by sub-sampling filters used on the large volume in situ pumps (McLane Pumps). The concentrations of PC, POC and PN are high at the surface and decrease exponentially with increasing depth (Figure 6-93). Concentration of PC and POC are higher than that of PN throughout the upper 1500 m at both sites. The concentration of POC is higher than that of PC in the shallowest samples at both stations and at 200 m within the OMZ at the CTA site only, otherwise the concentration of PC and POC are indistinguishable (Table 6-44). At both sites, the concentrations of PC, POC and PN are always highest in the 0.7 to 6 μm size fraction. Concentrations of PC, POC and PN in the 6 to 53 μm and >53 μm are nearly equal with the latter slightly higher at shallower depths (Table 6-44). This size distribution is particularly important at the proposed plume depths (1000-1500 m) since the discharged sediment is thought to be less than 5 μm , which overlaps with the 0.7-6 μm particle fraction. The concentrations of PC, POC and PN are only about 0.33, 0.27 and 0.03 $\mu\text{mol/L}$, respectively in the depth range of the discharge plume.

Figure 6-93 Concentrations of PC, POC and PN during Campaign 5B plotted as a function of depth at the PRZ (left) and CTA (right) sites. Values shown are the sum of concentrations measured on 0.7-6 μm , 6-53 μm and >53 μm size fractions.

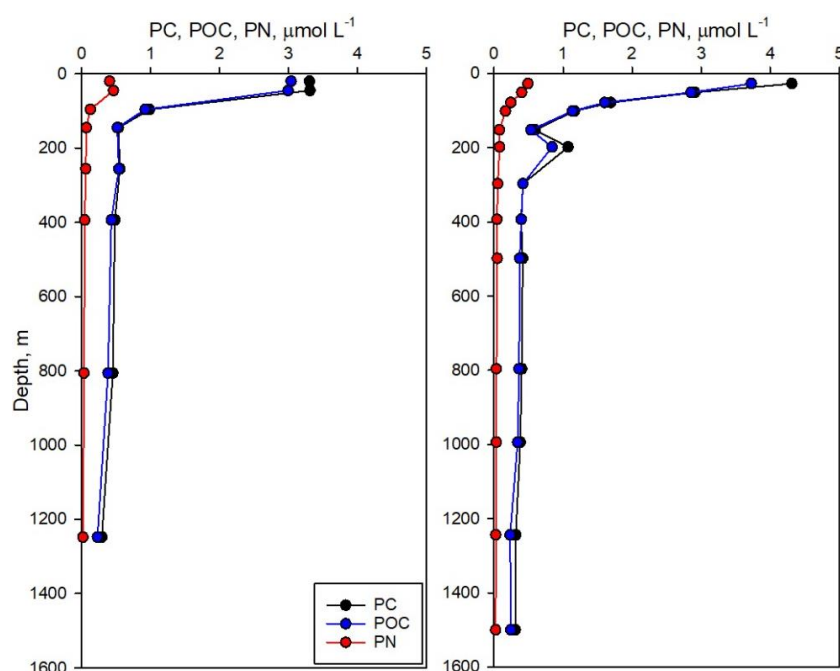


Table 6-44 Concentrations of PC, POC and PN in three size fractions of particles measured during Campaign 5B

| STATION | DEPTH (m) | 0.7-6 μm | | | 6-53 μm | | | >53 μm | | |
|---------|-----------|----------------------|-----------------------|----------------------|----------------------|-----------------------|----------------------|----------------------|-----------------------|----------------------|
| | | PC $\mu\text{mol/L}$ | POC $\mu\text{mol/L}$ | PN $\mu\text{mol/L}$ | PC $\mu\text{mol/L}$ | POC $\mu\text{mol/L}$ | PN $\mu\text{mol/L}$ | PC $\mu\text{mol/L}$ | POC $\mu\text{mol/L}$ | PN $\mu\text{mol/L}$ |
| PRZ | 20 | 2.53 | 2.37 | 0.35 | 0.26 | 0.19 | 0.01 | 0.52 | 0.48 | 0.05 |
| PRZ | 45 | 2.42 | 2.19 | 0.36 | 0.15 | 0.13 | 0.01 | 0.74 | 0.67 | 0.10 |
| PRZ | 96 | 0.77 | 0.70 | 0.11 | 0.09 | 0.10 | 0.01 | 0.13 | 0.13 | 0.02 |
| PRZ | 145 | 0.37 | 0.37 | 0.06 | 0.08 | 0.07 | 0.00 | 0.09 | 0.08 | 0.01 |
| PRZ | 256 | 0.39 | 0.39 | 0.05 | 0.10 | 0.08 | 0.01 | 0.07 | 0.07 | 0.01 |
| PRZ | 394 | 0.36 | 0.31 | 0.04 | 0.05 | 0.05 | 0.00 | 0.08 | 0.07 | 0.01 |
| PRZ | 806 | 0.34 | 0.29 | 0.03 | 0.06 | 0.06 | 0.00 | 0.06 | 0.04 | 0.00 |

| STATION | DEPTH (m) | 0.7-6 μm | | | 6-53 μm | | | >53 μm | | |
|---------|-----------|----------------------|-----------------------|----------------------|----------------------|-----------------------|----------------------|----------------------|-----------------------|----------------------|
| | | PC $\mu\text{mol/L}$ | POC $\mu\text{mol/L}$ | PN $\mu\text{mol/L}$ | PC $\mu\text{mol/L}$ | POC $\mu\text{mol/L}$ | PN $\mu\text{mol/L}$ | PC $\mu\text{mol/L}$ | POC $\mu\text{mol/L}$ | PN $\mu\text{mol/L}$ |
| PRZ | 1248 | 0.22 | 0.18 | 0.02 | 0.04 | 0.03 | 0.00 | 0.04 | 0.02 | 0.00 |
| CTA | 27 | 3.77 | 3.19 | 0.44 | 0.19 | 0.18 | 0.01 | 0.35 | 0.36 | 0.04 |
| CTA | 51 | 2.46 | 2.40 | 0.35 | 0.14 | 0.16 | 0.02 | 0.30 | 0.30 | 0.04 |
| CTA | 78 | 1.39 | 1.26 | 0.20 | 0.13 | 0.14 | 0.02 | 0.17 | 0.20 | 0.03 |
| CTA | 101 | 0.91 | 0.85 | 0.13 | 0.13 | 0.15 | 0.02 | 0.13 | 0.13 | 0.02 |
| CTA | 152 | 0.43 | 0.39 | 0.06 | 0.08 | 0.06 | 0.01 | 0.08 | 0.08 | 0.01 |
| CTA | 198 | 0.71 | 0.51 | 0.06 | 0.22 | 0.18 | 0.01 | 0.15 | 0.15 | 0.01 |
| CTA | 297 | 0.33 | 0.31 | 0.04 | 0.05 | 0.06 | 0.01 | 0.04 | 0.06 | 0.01 |
| CTA | 393 | 0.27 | 0.28 | 0.03 | 0.08 | 0.07 | 0.01 | 0.05 | 0.05 | 0.00 |
| CTA | 498 | 0.29 | 0.26 | 0.04 | 0.07 | 0.06 | 0.01 | 0.05 | 0.05 | 0.00 |
| CTA | 796 | 0.28 | 0.26 | 0.03 | 0.07 | 0.06 | 0.00 | 0.05 | 0.04 | 0.00 |
| CTA | 994 | 0.27 | 0.26 | 0.03 | 0.06 | 0.04 | 0.00 | 0.04 | 0.04 | 0.00 |
| CTA | 1244 | 0.23 | 0.18 | 0.02 | 0.04 | 0.03 | 0.00 | 0.04 | 0.03 | 0.00 |
| CTA | 1500 | 0.24 | 0.18 | 0.02 | 0.04 | 0.04 | 0.00 | 0.03 | 0.02 | 0.00 |

(b) Particle Flux

The downward flux of particles was determined using in situ particle interceptor traps (PIT) that were deployed between 70 and 90 m during Campaign 5B on sediment trap arrays. Each deployment lasted between 71 and 78 hours and had two sediment trap crosses separated vertically by 5-8 m. Each sediment trap cross held 12 PIT trap tubes. In total, each deployment resulted in 6-7 individual measurements of the mass flux of particles as well as PC, POC and PN flux. However, the distribution of organic matter across the filter was found to be heterogeneous. Consequently, we devoted 3 filters from each deployment to determine PC and PN flux and the other three to determine POC flux.

The mass flux of particles ranged from 3.95 to 5.73 g/m²/d (Table 6-45). Mass flux is variable at each site. However, the mass flux measured for sediment traps deployed at the same site but at different depths were not significantly different (one-way ANOVA $p = 0.92$ for PRZ and $p = 1.00$ for CTA). On the contrary, particle mass flux from the PRZ was significantly greater than that from the CTA (one-way ANOVA, Tukey Test, $p=0.003$) and is shown in Figure 6-94. The flux of PC ranged from 198 to 389 mg/m²/d whereas the flux of PN ranged from 26 to 58 mg/m²/d and did not differ between the PRZ and CTA sites during DG5B (Figure 6-95). The flux of POC at both sites are still being measured.

Figure 6-94 Mass flux of particles from Campaign 5B. Mass flux from the PRZ is significantly greater than that from the CTA.

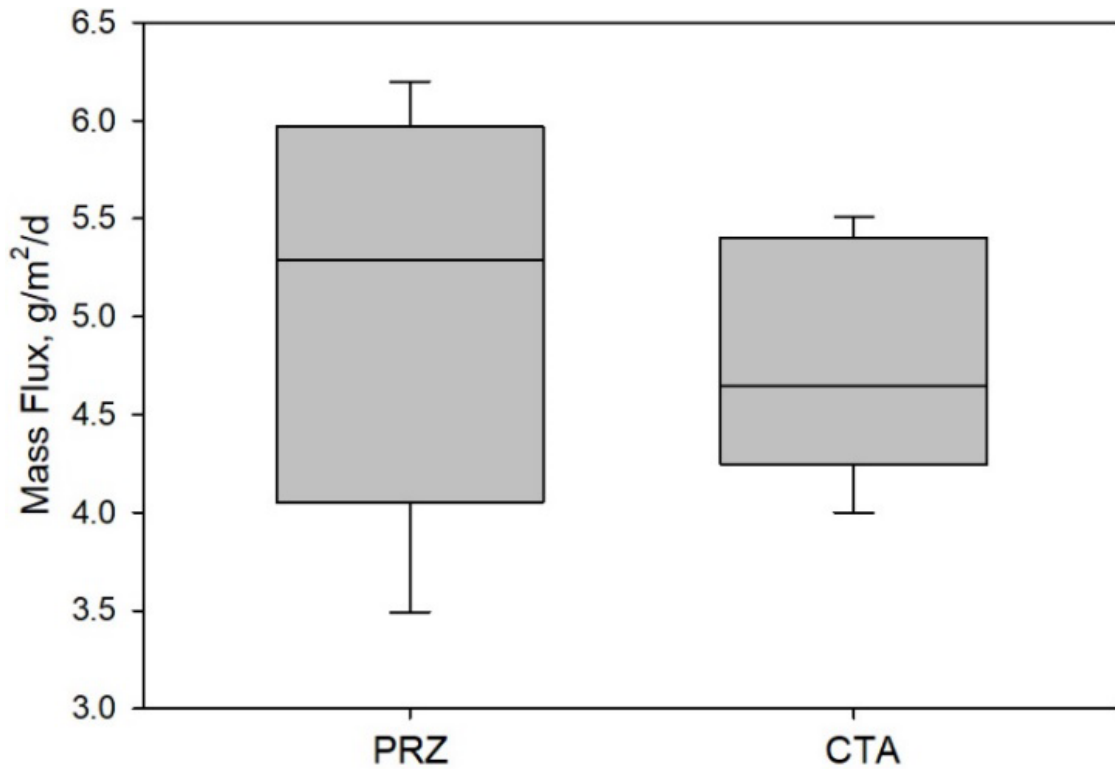


Figure 6-95 Flux of particulate carbon (PC) and particulate nitrogen (PN) from DG5B. The flux of PC and PN did not differ significantly between the PRZ and CTA sites.

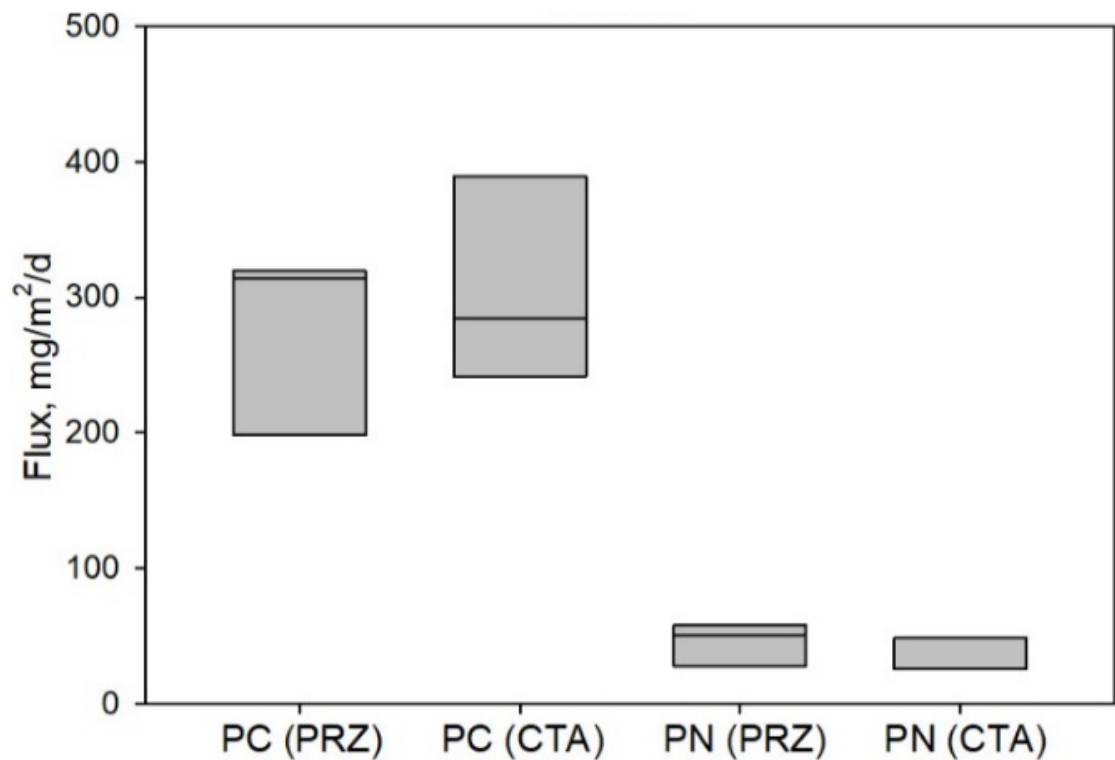


Table 6-45 Trap identification, site, hours deployed, depth of deployment and the calculated mass, PC and PN flux.

| SAMPLE # | AREA | HOURS | DEPTH (m) | MASS FLUX g/m ² /d | PC FLUX, mg/m ² /d | PN FLUX, mg/m ² /d |
|----------|------|-------|-----------|-------------------------------|-------------------------------|-------------------------------|
| Trap 1 | PRZ | 71.3 | 70 | 6.0 | 313 | 50 |
| Trap 2 | PRZ | 71.3 | 70 | 6.2 | 319 | 58 |
| Trap 3 | PRZ | 71.3 | 70 | 5.5 | NA | NA |
| Trap 4 | PRZ | 71.3 | 70 | 5.3 | NA | NA |
| Trap 7 | PRZ | 71.3 | 75 | 4.1 | NA | NA |
| Trap 8 | PRZ | 71.3 | 75 | 4.3 | NA | NA |
| Trap 9 | PRZ | 71.3 | 75 | 3.5 | 198 | 28 |
| Trap 11 | CTA | 77.7 | 82 | 4.0 | 389 | 26 |
| Trap 12 | CTA | 77.7 | 82 | 4.5 | 242 | 49 |
| Trap 13 | CTA | 77.7 | 82 | 4.3 | NA | NA |
| Trap 14 | CTA | 77.7 | 90 | 5.5 | NA | NA |
| Trap 15 | CTA | 77.7 | 90 | 5.4 | NA | NA |
| Trap 16 | CTA | 77.7 | 90 | 4.8 | 284 | 48 |

(c) Isotopic Composition of Size-Fractionated Particles

The $\delta^{13}\text{C}$ values of PC and POC were determined on bulk size fractionated particles collected using McLane Pumps at the PRZ and CTA sites during Campaign 5B. The $\delta^{13}\text{C}$ values of PC range from -26.1 to -20.5‰ whereas the $\delta^{13}\text{C}$ values of POC range from -28.5 to -22.4‰ (Table 6-46). In general, the $\delta^{13}\text{C}$ values of POC are lower than those of PC in nearly all sites and size fractions mostly likely due to contribution of carbonate organisms in PC. The only exception appears in the 0.7 to 6 μm fraction at the PRZ site, which shows some overlap in $\delta^{13}\text{C}$ values of PC and POC at a few depths (Table 6-46).

The $\delta^{15}\text{N}$ values of PN were determined on bulk size fractionated particles at the PRZ and CTA sites during SG5B (Figure 6-96). The $\delta^{15}\text{N}$ values of PN range from 1.5 to 10.0‰ (Table 6-46). However, $\delta^{15}\text{N}$ values of the different size fractions of PN differ (Figure 6-96). The $\delta^{15}\text{N}$ values of all size fractions of PN are high in the surface and decrease with depth to about 150 m. Below about 200 m, lowest $\delta^{15}\text{N}$ values are found in the 6 – 53 μm particles, intermediate $\delta^{15}\text{N}$ values are found in >53 μm particle and highest $\delta^{15}\text{N}$ values are found in the smallest size class of particles analyzed (0.7 – 6 μm).

There is overlap in the $\delta^{15}\text{N}$ values of each particle size class between sites with the exception of very low $\delta^{15}\text{N}$ values of the 0.7 – 6 μm particle in the CTA at about 50-75 m. Patterns of high $\delta^{15}\text{N}$ values of PN in the small size classes of particles, commonly referred to as suspended particles is common below about 200 m in open ocean marine environments (Sigman *et al.* 2009).

Figure 6-96 Plot of the $\delta^{15}\text{N}$ values of PN of bulk size fractionated particles. All values are given in ‰, relative AIR.

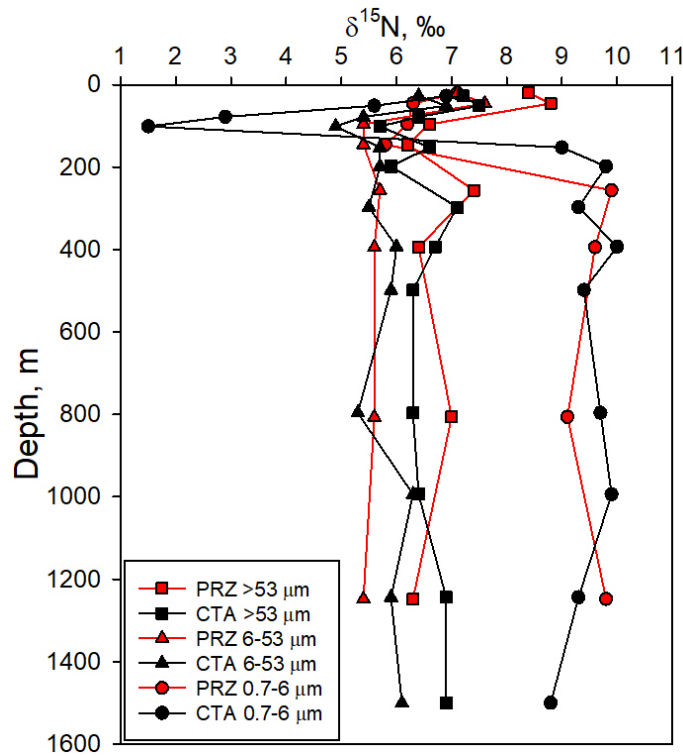


Table 6-46 $\delta^{13}\text{C}$ values of PC and POC and $\delta^{15}\text{N}$ values of PN of bulk size fractionated particles. All values are given in ‰, relative to V-PDB for $\delta^{13}\text{C}$ values and AIR for $\delta^{15}\text{N}$ values.

| STATION | DEPTH (m) | 0.7-6 μm | | | 6-53 μm | | | >53 μm | | |
|---------|-----------|---------------------------|----------------------------|-----------------------|---------------------------|----------------------------|-----------------------|---------------------------|----------------------------|-----------------------|
| | | $\delta^{13}\text{C}$ -PC | $\delta^{13}\text{C}$ -POC | $\delta^{15}\text{N}$ | $\delta^{13}\text{C}$ -PC | $\delta^{13}\text{C}$ -POC | $\delta^{15}\text{N}$ | $\delta^{13}\text{C}$ -PC | $\delta^{13}\text{C}$ -POC | $\delta^{15}\text{N}$ |
| PRZ | 20 | -22.4 | -22.9 | 7.1 | -22.8 | -25.7 | 7.1 | -25.0 | -25.5 | 8.4 |
| PRZ | 45 | -23.0 | -23.0 | 6.3 | -24.6 | -25.5 | 7.6 | -23.2 | -24.3 | 8.8 |
| PRZ | 96 | -26.1 | -26.0 | 6.2 | -25.7 | -26.4 | 5.4 | -24.4 | -25.2 | 6.6 |
| PRZ | 145 | -22.8 | -26.2 | 5.8 | -24.7 | -26.2 | 5.4 | -24.2 | -25.8 | 6.2 |
| PRZ | 256 | -23.0 | -23.8 | 9.9 | -23.9 | -25.1 | 5.7 | -23.5 | -24.6 | 7.4 |
| PRZ | 394 | -23.6 | -23.6 | 9.6 | -22.1 | -24.0 | 5.6 | -20.6 | -23.3 | 6.4 |
| PRZ | 806 | -23.6 | -24.2 | 9.1 | -23.0 | -25.5 | 5.6 | -21.1 | -24.8 | 7.0 |
| PRZ | 1248 | -21.8 | -24.0 | 9.8 | -22.3 | -25.5 | 5.4 | -22.9 | -24.7 | 6.3 |
| CTA | 27 | -24.3 | -24.7 | 6.9 | -25.3 | -25.0 | 6.4 | -22.4 | -23.4 | 7.2 |
| CTA | 51 | -24.2 | -24.2 | 5.6 | -20.5 | -23.9 | 6.9 | -21.7 | -23.5 | 7.5 |
| CTA | 78 | -25.9 | -25.8 | 2.9 | -23.6 | -24.8 | 5.4 | -23.1 | -24.4 | 6.4 |
| CTA | 101 | -25.5 | -25.9 | 1.5 | -23.9 | -25.8 | 4.9 | -23.0 | -24.9 | 5.7 |
| CTA | 152 | -23.9 | -24.9 | 9.0 | -22.6 | -25.1 | 5.7 | -22.4 | -24.7 | 6.6 |
| CTA | 198 | -21.2 | -24.6 | 9.8 | -24.3 | -27.0 | 5.7 | -22.4 | -25.6 | 5.9 |
| CTA | 297 | -21.9 | -22.9 | 9.3 | -22.9 | -24.4 | 5.5 | -22.2 | -24.0 | 7.1 |
| CTA | 393 | -21.5 | -24.4 | 10.0 | -24.8 | -25.4 | 6.0 | -23.8 | -26.3 | 6.7 |
| CTA | 498 | -21.3 | -22.4 | 9.4 | -23.2 | -24.6 | 5.9 | -21.2 | -24.2 | 6.3 |
| CTA | 796 | -22.7 | -25.5 | 9.7 | -25.0 | -25.1 | 5.3 | -25.0 | -25.9 | 6.3 |
| CTA | 994 | -23.8 | -25.1 | 9.9 | -21.1 | -25.4 | 6.3 | -21.6 | -25.7 | 6.4 |
| CTA | 1244 | -23.5 | -24.5 | 9.3 | -22.7 | -25.4 | 5.9 | -24.5 | -26.4 | 6.9 |
| CTA | 1500 | -24.7 | -24.0 | 8.8 | -23.8 | -25.5 | 6.1 | -23.5 | -28.5 | 6.9 |

(d) Bulk Isotopic Composition of Size-Fractionated Zooplankton

The $\delta^{13}\text{C}$ and $\delta^{15}\text{N}$ values of size fractionated zooplankton from the CTA site during Campaign 5B that were targeted for AA CSIA ranged from -24.5 to -20.5‰ and 10.6 to 18.7‰, respectively. (Table 6-47). Several previous AA CSIA studies of zooplankton in the Pacific Ocean targeted the 1-2 mm size fraction (Hannides et al. 2013; Hannides et al. 2020; Romero-Romero et al. 2020). Consequently, in order to directly compare the isotopic composition of zooplankton from the CCZ with these other studies, a full profile of the isotopic compositions of zooplankton in the 1-2 mm size fraction were measured (Table 6-47). In addition, we targeted samples of zooplankton from size classes 0.2-0.5, 0.5-1 and 2-5 mm collected from the proposed depth of the sediment discharge. The $\delta^{15}\text{N}$ values of the 1-2 mm zooplankton are relatively constant with depth to ~600 m, then increase to 900 m but then decrease again between 1000 and 1400 m (Figure 6-97). The $\delta^{15}\text{N}$ values of all zooplankton are higher than that of PN at the CTS (compare Figure 6-96 and Figure 6-97). Highest $\delta^{15}\text{N}$ values are observed in the smallest size class of zooplankton and the lowest values are found in the largest zooplankton. As noted above, $\delta^{15}\text{N}$ values of metazoans can vary due to: (1) changes in the $\delta^{15}\text{N}$ value of N sources driving production at the base of the food web (e.g. Rolff 2000; Syväranta et al. 2006), and (2) changes in organism trophic level, as $\delta^{15}\text{N}$ values increase with each trophic step (DeNiro and Epstein 1978; Post 2002). The expectation is that larger zooplankton which can feed on smaller zooplankton will have a higher trophic position than small zooplankton. Since $\delta^{15}\text{N}$ values are expected to increase with each trophic step, the $\delta^{15}\text{N}$ values of large zooplankton should be higher than those of smaller zooplankton. The opposite is observed. Highest $\delta^{15}\text{N}$ values are in the 0.2-0.5 mm zooplankton. Consequently, the distribution of zooplankton $\delta^{15}\text{N}$ values between 1000-1400 m are counterintuitive unless the base of their food web is formed by particles with high $\delta^{15}\text{N}$ values. Nitrogen isotopic analyses of amino acids can resolve this apparent conundrum.

Figure 6-97 Bulk tissue nitrogen isotopic composition of size fractionated zooplankton from the CTA site collected during Campaign 5B. All values are given in ‰, relative AIR.

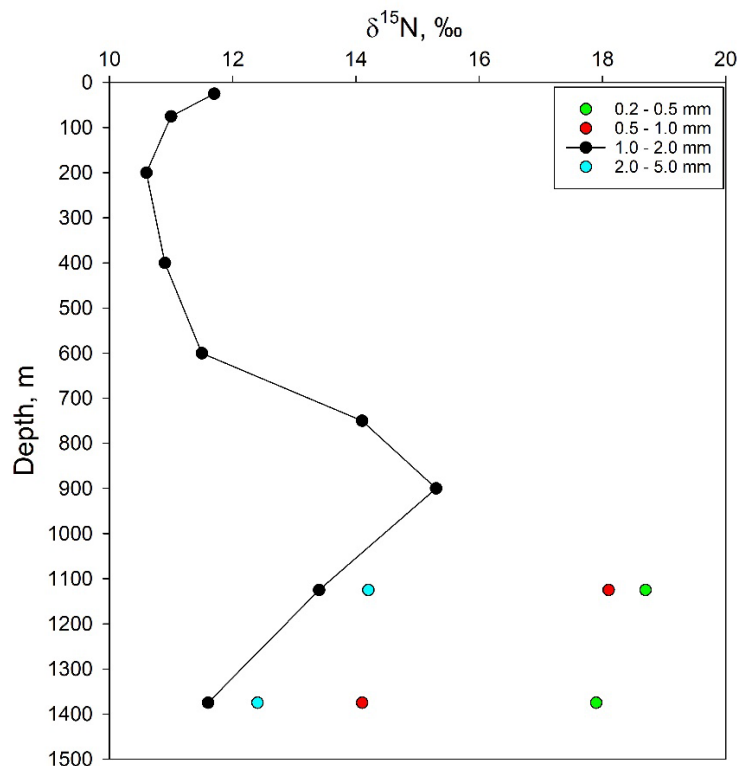


Table 6-47 Nitrogen and carbon isotopic composition of size fractionated zooplankton from the CTA site collected during Campaign 5B. All values are given in ‰, relative V-PDB for $\delta^{13}\text{C}$ and AIR for $\delta^{15}\text{N}$.

| DEPTH | SIZE FRACTION | $\delta^{15}\text{N}$ | $\delta^{13}\text{C}$ |
|-------|---------------|-----------------------|-----------------------|
| 25 | 1 - 2 mm | 11.7 | -21.6 |
| 75 | 1 - 2 mm | 11.0 | -22.1 |
| 200 | 1 - 2 mm | 10.6 | -23.7 |
| 400 | 1 - 2 mm | 10.9 | -23.6 |
| 600 | 1 - 2 mm | 11.5 | -24.1 |
| 750 | 1 - 2 mm | 14.1 | -22.4 |
| 900 | 1 - 2 mm | 15.3 | -22.4 |
| 1125 | 0.2 - 0.5 mm | 18.7 | -20.6 |
| 1125 | 0.5 - 1.0 mm | 18.1 | -22.1 |
| 1125 | 1 - 2 mm | 13.4 | -21.9 |
| 1125 | 2 - 5 mm | 14.2 | -22.0 |
| 1375 | 0.2 - 0.5 mm | 17.9 | -20.5 |
| 1375 | 0.5 - 1.0 mm | 14.1 | -22.9 |
| 1375 | 1 - 2 mm | 11.6 | -24.5 |
| 1375 | 2 - 5 mm | 12.4 | -22.4 |

(e) AA CSIA of Particles

Amino acid compound specific nitrogen isotope analysis (AA CSIA) can identify the range of particle sizes that form the base of the mesopelagic food web and have the potential to evaluate the uptake by zooplankton of sedimentary particles from the midwater discharge.

Owing to contamination, the $\delta^{15}\text{N}$ values of amino acid in 0.7-6 and $>53\ \mu\text{m}$ size classes of particles in samples from several depths at the PRZ and CTA sites during Campaign 5B, but not in 6-53 μm particles (Figure 6-98). In addition, we combined several depths at which samples were collected in order to analyze the isotopic composition of particles at depths deeper than approximately 400 m.

Key information obtained from nitrogen isotope analysis of individual amino acids includes 1) average nitrogen isotopic composition of source amino acids ($\delta^{15}\text{NSAA}$), which carries information about the organisms (phytoplankton and microbes) producing these amino acids and 2) the trophic position (TP) of particles, which can provide information about microbial reworking or inputs of fecal matter from metazoans. Combined, these measurements provide a history of the sources and microbial reworking of particles.

The difference in the $\delta^{15}\text{N}$ values of glutamic acid and lysine, which were measured in all particle samples, were used to calculate their trophic position (Figure 6-98). The trophic position of particles in the PRZ is similar to those collected from the CTA site.

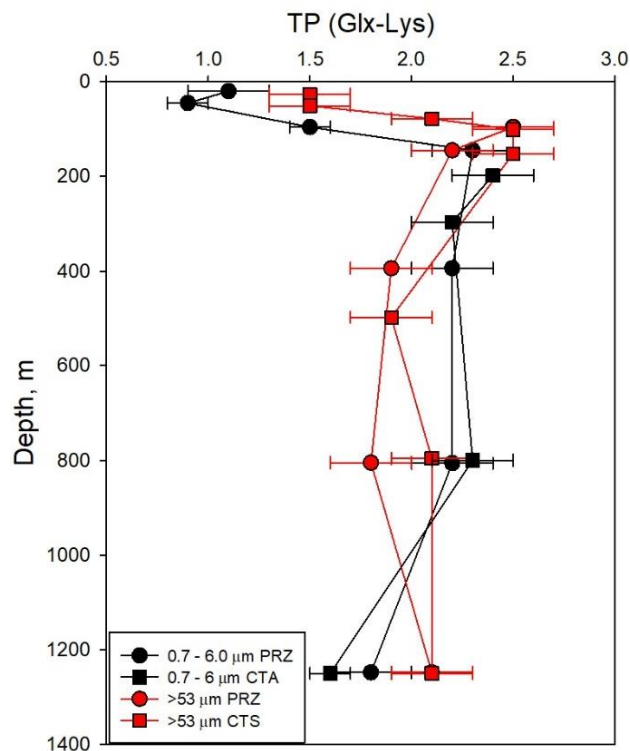
In surface waters, particle AA CSIA primarily reflects their algal origins with TP equal to ~ 1 for 0.7-6 μm particles and TP of ~ 1.5 for $>53\ \mu\text{m}$. The smaller size fraction is composed of algae and algal remains whereas the larger size fraction likely is composed of algal matter and fecal pellets. The trophic position of fecal pellets of marine zooplankton is commonly greater than 1 (Doherty et al. 2021). Below the euphotic zone particle disaggregation and microbial reworking begins and results in detrital particles that are a combination of algal remains, microbes colonizing those particles, zooplankton carcasses and fecal pellets that can contain undigested dietary material, enteric bacteria and animal biomass waste in the form of cells from animal guts (Doherty et al. 2021).

When microbes colonize particles, they release exoenzymes that break down protein. This process indiscriminately breaks the carbon-nitrogen bonds in amino acids making up protein and since C-14N bonds are weaker than C-15N bonds, the $\delta^{15}\text{N}$ values of all amino acids in the remaining particles increase with increased microbial reworking.

The extent of microbial reworking is typically greater in smaller than in larger particles, which can lead to differences in the amino acid $\delta^{15}\text{N}$ values in particles of different size (Hannides et al. 2013; Ohkouchi

et al. 2017; Romero-Romero et al. 2020). At the same time, inclusion of microbial biomass and fecal matter can increase the TP of a particle. Fortunately, the relative contributions of microbes can be recognized using essential amino acid $\delta^{15}\text{C}$ fingerprints and once complete we can distinguish if the increases in TP with increasing depth observed in Figure 6-98 are due primarily to microbial reworking or of inclusion of fecal matter in each size fraction. Carbon isotope analyses of particles are not yet complete.

Figure 6-98 Plot of the trophic position or trophic status of 0.7-6 and >53 μm particles collected during Campaign 5B. Errors shown are propagated errors from analytical measurements of the $\delta^{15}\text{N}$ values of glutamic acid and lysine and from literature values for β values ($3.9 \pm 0.5\%$) and Δ values ($5.2 \pm 0.5\%$).



The average $\delta^{15}\text{N}$ values of phenylalanine and lysine were used to calculate the $\delta^{15}\text{NSAA}$ values for samples collected during Campaign 5B (Figure 6-99). $\delta^{15}\text{NSAA}$ values of 0.7-6 and >53 μm particles are similar in the upper ~150 m of the water column and range from ~2 to 6‰ (Figure 6-100). Below about 150 m the $\delta^{15}\text{NSAA}$ values of 0.7-6 and >53 μm particles increase with depth. However, the $\delta^{15}\text{NSAA}$ values of 0.7-6 and >53 μm particles from the PRZ site diverge below 400 m. In addition, the $\delta^{15}\text{NSAA}$ values of 0.7-6 μm particles from the PRZ and CTA sites differ below about 800 m.

These observations indicate that the processes controlling the $\delta^{15}\text{NSAA}$ values of 0.7-6 and >53 μm particles are different, which has previously been observed at other sites in the Pacific Ocean (Hannides et al. 2013; Hannides et al. 2020; Romero-Romero et al. 2020). However, it is surprising that the $\delta^{15}\text{NSAA}$ values of 0.7-6 μm particles are so different between the PRZ and CTA sites given their close proximity. Phenylalanine was below the limit of detection or was severely contaminated in some samples however the $\delta^{15}\text{N}$ values of the source amino acid lysine was measured in all samples.

The $\delta^{15}\text{N}$ values of the source amino acid lysine ($\delta^{15}\text{N}_{\text{lys}}$) are shown in Figure 6-100 and confirms the variations in $\delta^{15}\text{NSAA}$ as a function of depth shown in Figure 6-99. However, $\delta^{15}\text{N}_{\text{lys}}$ values additionally indicate that >53 μm particles are much lower in the CTA site compared to the >53 μm particles in the PRZ below about 800 m. These results indicate that isotopic analyses of particles collected in the PRZ cannot be used to identify the particles forming the mesopelagic metazoan food web at the CTA site.

The $\delta^{15}\text{N}_{\text{lys}}$ values of the $>53\ \mu\text{m}$ particles is lower than the $\delta^{15}\text{N}_{\text{lys}}$ values of the $0.7\text{-}6\ \mu\text{m}$ particle at the CTA site, similar to that observed at the PRZ and other sites in the North Pacific. These results indicate that the $\delta^{15}\text{N}_{\text{lys}}$ values from the CTA site can be used to identify the size of particles that form the base of the mesopelagic zooplankton food web at the CTA site.

Figure 6-99 Plot of the average $\delta^{15}\text{N}$ values of the source amino acids phenylalanine and lysine measured in $0.7\text{-}6\ \mu\text{m}$ and $>53\ \mu\text{m}$ particles collected during DG5B. Errors shown are propagated errors from analytical measurements. All $\delta^{15}\text{N}$ values are reported in ‰ relative to AIR.

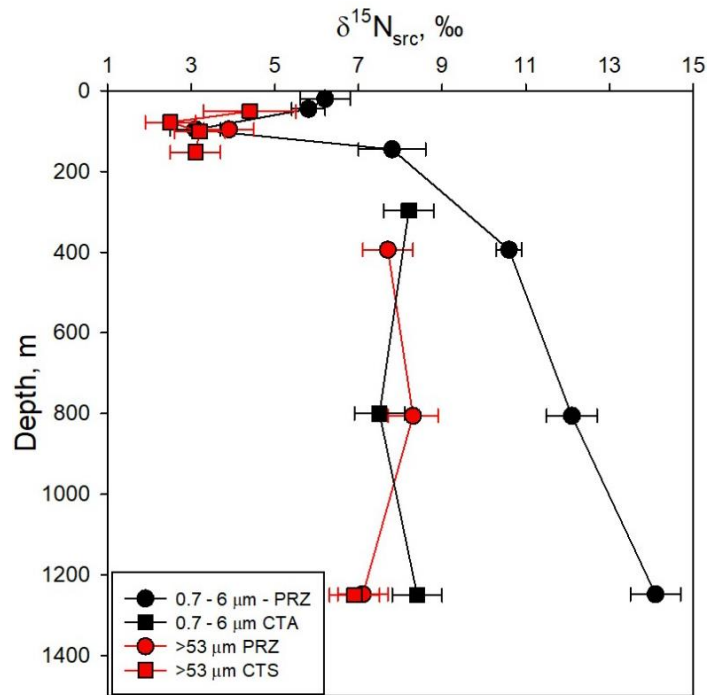


Figure 6-100 Plot of the $\delta^{15}\text{N}$ values of the source amino acid lysine measured in $0.7\text{-}6\ \mu\text{m}$ and $>53\ \mu\text{m}$ particles and zooplankton collected during Campaign 5B. Errors shown are propagated errors from analytical measurements. All $\delta^{15}\text{N}$ values are reported in ‰ relative to AIR.

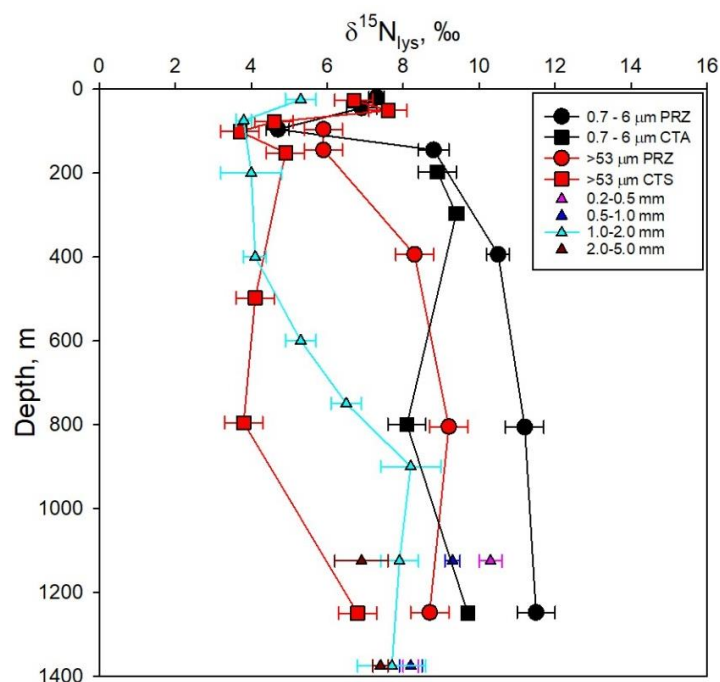


Table 6-48. Sample number, station, depth, particle size fraction and nitrogen isotopic composition of amino acids. Uncertainty represents one standard deviation from at least duplicate triplicate analysis. When no uncertainty is reported, only a single analysis was possible.

| # | AREA | (m) | SIZE | Ala | Gly | Thr | Ser | Val | Leu | Iso | Pro | Asx | Glx | Phe | Try | Lys |
|----|------|------|-------|----------|----------|---------|----------|----------|----------|----------|----------|----------|----------|----------|----------|----------|
| 15 | PRZ | 20 | 0.7-6 | 11.7±0.5 | 7.2±0.4 | 6.7±0.9 | 4.6±0.5 | 13.7±0.3 | 9.0±0.9 | 14.3±3.9 | 9.4±0.6 | 10.2±0.8 | 11.7±0.9 | 5.1±0.6 | - | 7.3±0.2 |
| 12 | PRZ | 45 | 0.7-6 | 9.6±0.3 | 5.4±0.4 | 6.5±0.2 | 4.0±0.4 | 10.2±0.3 | 7.3±0.1 | 8.4±0.6 | 8.3±0.1 | 8.9±0.2 | 10.2±0.3 | 4.8±0.2 | - | 6.9±0.4 |
| 9 | PRZ | 96 | 0.7-6 | 11.7±0.1 | 5.9±0.2 | 2.7±0.2 | 3.5±0.1 | 12.6±0.3 | 7.1±0.2 | 9.3±0.1 | 7.9±0.5 | 10.2±0.2 | 11.4±0.1 | 1.5±0.6 | 5.2±0.7 | 4.7±0.3 |
| 6 | PRZ | 145 | 0.7-6 | - | 14.7±2.1 | 4.8 | 9.1±0.8 | | 14.8±0.3 | 18.3 | 13.6±0.6 | 15.9±0.3 | 19.4±0.1 | 6.8±0.6 | 12.3±0.4 | 8.8±0.4 |
| 3 | PRZ | 394 | 0.7-6 | 21.8±0.3 | 12.7±0.8 | 9.2±0.9 | 11.3±0.8 | 18.4±0.4 | 15.8±0.1 | 17.7±0.3 | 15.5±0.1 | 16.6±0.4 | 20.7±0.6 | 10.7±0.2 | 11.8±0.3 | 10.5±0.3 |
| 25 | PRZ | 806 | 0.7-6 | - | - | - | - | - | - | - | 15.7 | 17.9 | 21.3 | 13 | - | 11.2 |
| 18 | PRZ | 1248 | 0.7-6 | - | - | - | - | - | - | - | 15.5 | 16.8 | 19.5 | 16.6 | - | 11.5 |
| 7 | PRZ | 96 | >53 | 17.1 | 7.9 | -1.5 | 6.8 | 9.8 | 12.5 | 14.1 | 10.7 | 12.5 | 17.4 | 1.9 | 10.2 | 5.9 |
| 4 | PRZ | 145 | >53 | - | - | - | 5.8 | - | - | - | 11.6 | 12.1 | 15.9 | - | - | 5.9 |
| 1 | PRZ | 394 | >53 | 17.1 | 8.1 | 0.5 | 8.2 | 4.9 | 12.9 | - | 13.7 | 13.7 | 16.9 | 7.2 | - | 8.3 |
| 24 | PRZ | 806 | >53 | 13 | 7.9 | | 7.9 | - | - | - | 11.1 | - | 13.5 | - | - | 5.3 |
| 23 | PRZ | 805 | >53 | - | 12.5 | -1.4 | 9 | - | - | - | 13 | - | 18.8 | 7.3 | 12.7 | 9.2 |
| 16 | PRZ | 1248 | >53 | 19.9 | 11.5 | 5.2 | 10.5 | 12.9 | 15.9 | 17.2 | 14.2 | 18.1 | 19.3 | 5.4 | 9.3 | 8.7 |
| 87 | CTA | 198 | 0.7-6 | - | - | - | - | - | - | - | - | - | 20 | - | - | 8.9 |
| 84 | CTA | 297 | 0.7-6 | 21.7±0.5 | 11.1±0.4 | 5.3 | 10.1±1.1 | 16.4±1.2 | 14.4±0.5 | 17.9 | 14.9±0.1 | 16.3±0.2 | 19.5±0.3 | 7.1±0.6 | 16.7 | 9.4±0.2 |
| 60 | CTA | 800 | 0.7-6 | - | - | - | - | - | 17.4 | - | 17.2 | 16.1 | 18.8 | 7 | 10.3 | 8.1 |
| 40 | CTA | 1250 | 0.7-6 | - | - | - | - | - | 15.6 | - | 12.8 | 16.3 | 16.8±0.5 | 7.1 | 17.3 | 9.7±0.5 |
| 76 | CTA | 27 | >53 | - | - | - | - | - | - | - | 10.6 | 11.9 | 13.1 | - | - | 6.7 |
| 73 | CTA | 51 | >53 | 15.9±0.1 | 8.0±0.5 | 3.0±0.8 | 6.4±0.3 | 13.4±0.1 | - | 12.0±0.1 | 11.3±0.3 | 12.5±0.5 | 14.1±0.3 | 1.3±0.9 | 7.5±0.4 | 7.6±0.5 |
| 70 | CTA | 78 | >53 | 16.5 | 7.7 | -2.8 | 3.9 | 7.6 | 10.8 | 12.3 | 9.2 | 10.8 | 14.3 | 0.5 | 5.3 | 4.6 |
| 67 | CTA | 101 | >53 | 18 | 8.6 | -2.3 | 4.7 | 7 | 9.4 | 9.5 | 9.8 | 11.9 | 15.3 | 2.8 | 10.7 | 3.7 |
| 64 | CTA | 152 | >53 | - | 11.6 | -3.3 | 6.7 | - | 12.1 | - | 11.1 | 12.8 | 16.5 | 1.3 | 5.2 | 4.9 |
| 79 | CTA | 498 | >53 | - | - | - | - | - | - | - | - | 11.4 | 12.8 | - | - | 4.1 |
| 55 | CTA | 796 | >53 | - | - | - | 5.3 | - | - | - | 9.7 | 11.3 | 13.5 | - | - | 3.8 |

Ala = alanine, Gly = glycine, Thr = threonine, Ser = serine, Val = valine, Leu = leucine, Iso = Isoleucine, Pro = proline, Asx = aspartic acid, Glx = glutamic acid, Try = tyrosine, Lys = lysine

(f) AA CSIA of Zooplankton

The carbon and nitrogen isotopic composition of individual amino acids were determined for select size-fractionated zooplankton from a night-time tow at the CTA site during Campaign 5B. A night-time tow was chosen so that it maximized the chances of collecting resident zooplankton at the depth at which they normally feed. Isotopic analysis of zooplankton from the 1-2 mm size fraction allows comparison with data on zooplankton of the same size for various sites across the North Pacific Ocean (Hannides *et al.* 2013; Hannides *et al.* 2020; Romero-Romero *et al.* 2020). Since the $\delta^{15}\text{N}$ values of source amino acids ($\delta^{15}\text{NSAA}$) do not change during trophic transfer, the average $\delta^{15}\text{NSAA}$ values in 1-2 mm zooplankton, which records the $\delta^{15}\text{N}$ value at the base of the food web, is $\sim 7\text{‰}$ and remains constant from the surface to ~ 400 m, increases to about 10‰ from ~ 400 -800 m and then decreases slightly to ~ 1400 m (Figure 6-101). This general pattern of changes in $\delta^{15}\text{NSAA}$ values with depth is common in 1-2 mm zooplankton (Romero-Romero *et al.* 2020). However, the increase in $\delta^{15}\text{NSAA}$ values with depth typically occurs at about 150-250 m, which is just below the euphotic zone at other sites in the North Pacific.

At the CTA site, the increase in $\delta^{15}\text{NSAA}$ values in 1-2 mm zooplankton coincide with the depth at which dissolved oxygen levels are the lowest within the OMZ (see section 5.11.3). The average $\delta^{15}\text{NSAA}$ values for the 0.2-0.5 mm zooplankton are higher than those of all other zooplankton within the depth range of 1000-1500 m.

We used the difference in the $\delta^{15}\text{N}$ values of glutamic acid and phenylamine to estimate the trophic position of zooplankton. The average trophic position of 1-2 mm zooplankton (TP1-2) is significantly lower between the surface and 800 m compared with average TP1-2 between 900 and 1500 m (one-way ANOVA, Tukey Test, $p = 0.03$). TP0.2-0.5 are lower than the TP of all other size fractions of zooplankton within the depth range of 1000-1500 m, although the differences are not significant (Figure 6-101). The high bulk $\delta^{15}\text{N}$ values of the 0.2-0.5 mm zooplankton (Figure 6-97) could suggest that these zooplankton have an unexpectedly high trophic position. However, the high $\delta^{15}\text{NSAA}$ values indicate that the base of the 0.2-0.5 mm zooplankton has elevated $\delta^{15}\text{N}$ values. This interpretation is confirmed by the trophic position calculated from AA CSIA and confirms that the trophic position of the 0.2-0.5 mm zooplankton is not anomalously high. TP calculated using differences in $\delta^{15}\text{N}$ values of glutamic acid and phenylalanine show the same relative patterns as TP calculated using differences in $\delta^{15}\text{N}$ values of glutamic acid and lysine although the latter are slightly higher (~ 0.5).

Comparison of the $\delta^{15}\text{N}_{\text{lys}}$ values of zooplankton and 0.7-6 and $>53 \mu\text{m}$ particles can identify the particle size forming the base of the food web (Figure 6-96). None of the zooplankton measured are obligate grazers – all have a trophic position consistent with omnivores (TP > 2 , Figure 6-95). Since these zooplankton are resident, non-migrating zooplankton, their $\delta^{15}\text{N}_{\text{lys}}$ values are set by particles forming the base of their food web as well as preying on diel vertically migrating species during the daytime that may carry a very different $\delta^{15}\text{N}_{\text{lys}}$ value than particles. From the surface to about 100 m, the $\delta^{15}\text{N}_{\text{lys}}$ values of 1-2 mm zooplankton overlaps with large and small particles. Although 0.7-6 μm particles from the CTA site have yet to be analyzed, at all sites there is overlap in the $\delta^{15}\text{N}_{\text{lys}}$ values of large and small particles near the surface. It is logical that 1-2 mm zooplankton feed within a shallow food web that base of which is dominated by large and small algae.

Below ~ 200 m and down to ~ 500 m, the $\delta^{15}\text{N}_{\text{lys}}$ values of 1-2 mm zooplankton overlap with those of $>53 \mu\text{m}$ particles (Figure 6-96). This overlap suggests that the $>53 \mu\text{m}$ particles are important in forming the base of zooplankton food web. However, given that $\delta^{15}\text{N}_{\text{lys}}$ values do not change appreciably with depth between 150 and 500 m, we cannot eliminate the possibility that carnivorous 1-2 mm zooplankton prey on vertically migrating zooplankton. Zooplankton that feed at night in surface waters inherit a $\delta^{15}\text{N}_{\text{lys}}$ value of near surface particles and those values can be passed on to resident 1-2 mm carnivorous zooplankton at depth.

Between depth of 500-1250 m, the $\delta^{15}\text{N}_{\text{lys}}$ values of 1-2 mm zooplankton become closer to the $\delta^{15}\text{N}_{\text{lys}}$ values of the 0.7-6 μm particles (Figure 6-96). This change suggests that these smaller particles may

become increasingly important at the base of the mesopelagic zooplankton food web and/or that diel vertically migrating prey that feed at the surface at night are not as abundant at these deeper depths.

Within the range of the proposed sediment discharge depths (1200 m), $\delta^{15}\text{N}_{\text{lys}}$ values of many zooplankton fall between the $\delta^{15}\text{N}_{\text{lys}}$ values of 0.7-6 and >53 μm particles (Figure 6-96). This suggests that both particle sizes are important for the zooplankton community. The $\delta^{15}\text{N}_{\text{lys}}$ values of 0.2-0.5 mm zooplankton at 1150 m overlap or are slightly greater than the 0.7-6 μm particles indicating the importance of this size class of particles to the base of at least some zooplankton. This is noteworthy because the 0.7-6 μm particles overlap with those expected in the midwater discharge.

Figure 6-101 Plot of the average $\delta^{15}\text{N}$ value of source amino acids (gly, phe, lys, ser) and trophic position as a function of depth. All samples are of size fractionated zooplankton collected during a nighttime tow (1m2, MOC10) at the CTA site during Campaign 5B. Trophic position was calculated using the difference in $\delta^{15}\text{N}$ values of glx and phe using standard methods (Chikaraishi et al. 2009a). All error bars shown were calculated using propagation of errors (Jarman et al. 2017). All $\delta^{15}\text{N}$ values are given in ‰, relative AIR.

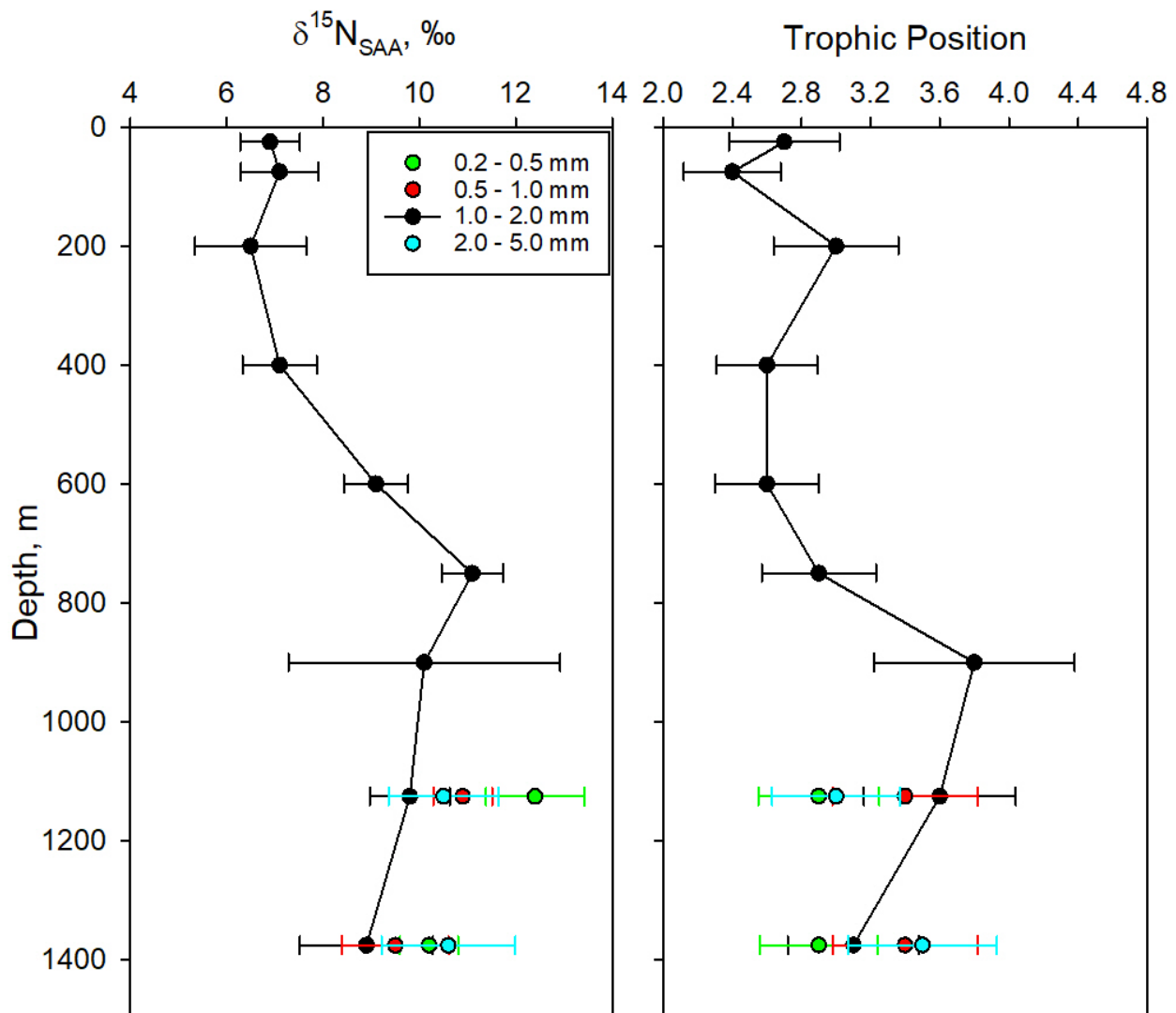


Table 6-49. Sample number, depth, zooplankton size fraction and nitrogen isotopic composition of amino acids. Uncertainty represents one standard deviation from at least triplicate analysis.

| SAMPLE | DEP | FRAC | $\delta^{15}\text{N}$, ‰ relative to AIR | | | | | | | | | | | | |
|----------|------|---------|---|----------|----------|----------|----------|----------|----------|----------|----------|----------|---------|----------|----------|
| | | | Ala | Gly | Thr | Ser | Val | Leu | Iso | Pro | Asx | Glx | Phe | Tyr | Lys |
| DG5B_413 | 25 | 1.0-2.0 | 20.9±0.2 | 9.3±0.1 | -0.7±0.1 | 8.6±0.2 | 16.3±0.3 | 15.3±0.2 | 19.9±0.9 | 13.4±0.2 | 17.9±0.5 | 20.5±0.8 | 4.4±0.5 | 5.1±0.2 | 5.3±0.4 |
| DG5B_408 | 75 | 1.0-2.0 | 22.9±0.5 | 9.1±0.5 | -0.5±0.4 | 9.6±0.3 | 15.8±0.7 | 15.1±0.3 | 16.2±0.5 | 13.5±0.2 | 16.7±0.2 | 20.4±0.5 | 6.0±0.5 | 8.2±0.5 | 3.8±0.2 |
| DG5B_403 | 200 | 1.0-2.0 | 23.0±0.4 | 9.1±0.2 | -4.6±0.9 | 8.6±0.5 | 17.4±0.6 | 17.4±0.2 | 20.3±0.7 | 14.7±0.2 | 17.3±0.2 | 22.7±0.6 | 4.4±0.6 | 8.1±0.4 | 4.0±0.8 |
| DG5B_398 | 400 | 1.0-2.0 | 23.2±0.2 | 10.6±0.4 | 1.1±0.7 | 9.0±0.5 | 16.9±0.3 | 15.6±0.5 | 17.8±0.6 | 13.7±0.3 | 15.7±0.3 | 20.4±0.1 | 4.9±0.3 | 8.2±0.7 | 4.1±0.3 |
| DG5B_393 | 600 | 1.0-2.0 | 21.7±0.3 | 14.0±0.3 | 2.4±0.1 | 12.3±0.4 | 21.2±0.6 | 15.7±0.1 | 18.0±0.9 | 12.9±0.1 | 16.2±0.2 | 20.7±0.5 | 4.9±0.2 | 9.3±0.7 | 5.3±0.4 |
| DG5B_388 | 750 | 1.0-2.0 | 27.0±0.1 | 15.5±0.2 | -4.7±0.9 | 15.5±0.5 | 23.2±0.3 | 22.0±0.4 | 22.9±0.6 | 19.9±0.1 | 20.3±0.5 | 25.2±0.2 | 7.0±0.1 | 11.8±0.8 | 6.5±0.4 |
| DG5B_383 | 900 | 1.0-2.0 | 29.5±0.6 | 14.9±0.8 | -4.8±0.3 | 14.9±0.4 | 24.4±1.0 | 24.4±0.9 | 25.8±0.7 | 21.3±0.6 | 22.7±0.2 | 26.6±0.9 | 2.2±2.6 | 18.6±0.8 | 8.2±0.8 |
| DG5B_380 | 1125 | 0.2-0.5 | 27.4±0.5 | 14.3±0.0 | -1.3±0.9 | 15.3±0.2 | 21.8±0.8 | 23.5±0.1 | 25.9±0.2 | 22.4±0.2 | 23.2±0.2 | 27.3±0.3 | 9.9±1.0 | 14.8±0.9 | 10.3±0.3 |
| DG5B_379 | 1125 | 0.5-1.0 | 28.6±0.5 | 15.2±0.0 | -6.0±0.2 | 13.9±0.2 | 23.1±0.5 | 23.2±0.3 | 24.6±0.3 | 22.5±0.1 | 22.2±0.3 | 27.0±0.5 | 5.2±0.6 | 10.4±0.3 | 9.3±0.2 |
| DG5B_378 | 1125 | 1.0-2.0 | 28.3±0.3 | 14.4±0.2 | -6.4±1.0 | 13.3±0.3 | 24.1±0.7 | 21.0±0.4 | 22.6±0.3 | 21.4±0.4 | 22.1±0.8 | 26.4±0.6 | 3.6±0.5 | 10.1±0.7 | 7.9±0.5 |
| DG5B_377 | 1125 | 2.0-5.0 | 28.2±0.5 | 13.9±0.1 | -7.0±1.1 | 13.8±0.1 | 22.4±0.1 | 22.4±0.4 | 24.1±0.3 | 21.5±0.5 | 21.1±0.6 | 25.8±0.7 | 7.2±0.9 | 11.3±0.4 | 6.9±0.7 |
| DG5B_375 | 1375 | 0.2-0.5 | 24.4±0.2 | 12.7±0.1 | -3.2±0.6 | 12.6±0.3 | 22.9±0.5 | 20.6±0.1 | 20.7±0.4 | 17.8±0.2 | 20.0±0.2 | 25.4±0.3 | 7.3±0.5 | 12.2±0.3 | 8.2±0.2 |
| DG5B_374 | 1375 | 0.5-1.0 | 26.7±0.3 | 12.5±0.6 | -1.8±0.6 | 12.7±0.5 | 20.3±0.8 | 21.2±0.8 | 23.0±0.9 | 20.1±0.5 | 20.4±0.3 | 26.0±0.7 | 4.7±0.8 | 11.3±0.5 | 8.2±0.3 |
| DG5B_373 | 1375 | 1.0-2.0 | 26.6±0.1 | 11.0±0.2 | -7.8±0.4 | 11.3±0.5 | 19.9±0.2 | 19.1±0.6 | 20.4±0.3 | 18.0±0.3 | 19.3±0.4 | 24.9±0.4 | 5.4±0.9 | 10.0±0.8 | 7.7±0.9 |
| DG5B_372 | 1375 | 2.0-5.0 | 29.7±0.7 | 14.2±1.0 | -0.1±0.8 | 13.1±0.6 | 20.8±0.1 | 23.2±0.1 | 25.0±0.4 | 24.0±0.3 | 23.6±0.2 | 29.7±0.2 | 7.6±0.8 | 9.0±0.6 | 7.4±0.2 |

Ala = alanine, Gly = glycine, Thr = threonine, Ser = serine, Val = valine, Leu = leucine, Iso = Isoleucine, Pro = proline, Asx = aspartic acid, Glx = glutamic acid, Try = tyrosine, Lys = lysine

6.4.8 Ecotoxicology studies in zooplankton and pelagic fish

For the pelagic environment, using standard ecological risk assessment procedures, baseline levels of metals, whole effluent toxicity (WET), and biomarkers of metals exposure in common taxa (i.e., metallothionein, superoxide dismutase, glutathione peroxidase, lipid peroxidation; Viarengo *et al.* 1997; Auguste *et al.* 2016) will be determined by collecting target taxa from five different depth strata spanning the surface of the ocean to the seabed in NORI-D.

These measures ensure the presence of metals, WET, and biomarker responses from common exposures are characterized prior to nodule collection activities and can serve as risk criteria for comparison to contamination levels during and following the collector test. Linking measures of exposure (i.e. metals and WET) in concentrations-response models to biomarker responses and effects measured by other researchers (e.g., micronekton abundance and biodiversity) will also identify the most sensitive responses across depth strata (e.g. bathypelagic, mesopelagic, and epipelagic) to baseline pollutant concentrations.

6.4.8.1 Purpose and scope

The following section describes the work conducted between 2020-2021 by University of Maryland to characterise natural baseline conditions in trace metals in the tissues of key taxa in the NORI-D contract area. The scope, the survey planning and the sampling methodologies align with International Seabed Authority ISBA/25/LTC/6 Rev 1. Annex 1 section 45 Trace Metals and potential toxic elements to provide baseline data requirements under Recommendation VI.D.40.(f).

6.4.8.2 Baseline investigations

The methods and proposed survey array for both the collector test and long-term environmental studies on NORI-D will provide data to meet the following objectives:

- What are the baseline levels of metals in tissues of deep-sea taxa, what are the impacts of mining activities on exposure of deep-sea organisms to toxic substances, and what are the toxicological outcomes of these exposures?
- Describe the movement of metals through the food web.

6.4.8.3 Campaign activities

To fulfil the objectives on Campaign 5B and 5C, abiotic and biotic samples were collected from other worksopes. Micronekton samples collected in coordination with the micronekton team for tissue metals and biomarker analyses. Water samples taken in coordination with the trace metals team will be analyzed for whole effluent toxicity analyses. Zooplankton samples were also collected in coordination with our team to ensure sampling techniques and processing would not compromise samples for metals analysis by our team.

A summary of the water, zooplankton, and sediment collections that were targeted thus far for contaminants and whole effluent toxicity (listed as “WET”) can be seen in Table 6-50 below (for micronekton see Table 6-52).

Table 6-50 Ecotoxicology experimental design prior to collection, study sample types and sample water column zones shifted based on logistics of biota availability during sampling.

| | Relative Sample Zones | Depths (m) | No. of Samples | | |
|----------------|-----------------------|------------|----------------|-----|-------------|
| | | | Sediment | WET | Zooplankton |
| Surface | | | | | |
| Epipelagic | 1 | 100 | | 7 | 3 |
| | 2 | 1000 | | 7 | 3 |
| Mesopelagic | 3 (OMZ) | 1500 | | 7 | 3 |
| | 4 | 3000 | | 7 | 3 |
| Bathypelagic | 5 | 4000 | 10 | 7 | 3 |

Specifically, 7-10 0.2µm filtered water samples ranging from 10-15mL per sample were collected in cleaned contaminant-free 15mL sample vials (totalling 100-105mL per depth strata) from five depth strata; targeting the epipelagic, three depth strata in the mesopelagic surrounding the assumed upper, mid, and lower bounds of where the mid-water plume will be discharged, and in the bathypelagic (Table 6-51). Water samples were collected from a total of 2 deployments in the PRZ and CTS locations. Water samples were stored and kept at 4°C after collection and will be kept at this temperature during transport back to the University of Maryland (UMD). There each water sample will be tested for whole effluent toxicity using a Microtox FX unit.

Table 6-51 Metadata for water samples collected for whole effluent toxicity (WET) in collaboration with the trace-metals team. Each row provides information on when the deployment occurred, the depth of the deployment, the number of 15ml samples that were taken from the deployment, the location of the deployment, and other relevant environmental conditions.

| SAMPLE ID | STATION | CAST | DEPTH (m) | TOTAL VOLUME (ml) |
|-----------|---------|--------|-----------|-------------------|
| 1109 | 1 PRZ | TM-008 | 1000 | 100 |
| 1129 | 1 PRZ | TM-010 | 4000 | 105 |
| 1131 | 1 PRZ | TM-010 | 3000 | 105 |
| 1134 | 1 PRZ | TM-010 | 1500 | 105 |
| 1136 | 1 PRZ | TM-010 | 1000 | 105 |
| 1165 | 2 CTA | TM-013 | 4000 | 105 |
| 1167 | 2 CTA | TM-013 | 3001 | 105 |
| 1170 | 2 CTA | TM-013 | 1499 | 105 |
| 1172 | 2 CTA | TM-013 | 1000 | 105 |
| 1173 | 2 CTA | TM-014 | 96 | 105 |

Micronekton are very mobile and many vertically migrate large distances. Food webs are vertically mixed and animals don't necessarily reside at the exact same depths every day. To accommodate this biology and the desire to sample animals with different plume exposures, non-migrators were sampled from the discharge depth (1500-1000m) that would represent the highest likelihood of exposure. Second, to sample vertical migrators that may live shallower than the discharge depth and/or move around and feed shallower than the discharge depth and likely see less exposure (Table 6-52). In collaboration with the micronekton team, 131 individual's representative of 8 micronekton taxa including 3 species of invertebrates and 5 fish species were collected using the MOC10 from several depth strata separated by migratory status (Table 6-52). Micronekton samples specifically for ecotoxicity analyses were collected from two tows in the PRZ and five tows CTA locations. These tissue samples were immediately frozen using liquid nitrogen and stored following standard procedures in a -80°C freezer (USEPA 2000, 2007). These samples will be partitioned into those for metals and those for biomarkers of metals exposure after

they are returned to UMD. Micronekton collections will be shipped frozen to UMD where they will be processed to test gills, muscle, liver, kidney, or whole body (depending on the species) for metals and biomarkers of metals exposure.

Table 6-52 Collection summary of frozen micronekton for biomarker and/or trace metal analysis. These are divided by the two sampling categories, deep non-migratory (NM) and those that migrated to shallower depths during the day (M).

| TAXON | | CATEGORY | PRZ | CTA |
|--------------------------|--------------------------|------------|-----------|-----------|
| <i>Cylothone</i> spp. | likely <i>C. alba</i> | NM | 5 | 6 |
| <i>Cylothone</i> spp. | likely <i>C. pallida</i> | NM shallow | 25 | 25 |
| Melamphaeidae | | M | 5 | 5 |
| Myctophidae | | M | 5 | 5 |
| Mysidacea | | NM | 5 | 5 |
| Sergestidae | | M | 5 | 5 |
| Bregmaceros | | M | 5 | 5 |
| Caridean shrimp | | M | 5 | 5 |
| <i>Vinciguerrria</i> sp. | | M | 5 | 5 |
| TOTAL | | | 65 | 66 |

A subset of zooplankton collected by the MOCNESS tows for biomass analysis will be used for metals analysis as well. As such, all biomass samples were collected in contaminant-free conditions. Specifically, to ensure zooplankton collections followed standard operating procedures for metals analysis, all zooplankton sampling equipment was acid washed and rinsed with distilled water before each tow (USEPA 2000; 2007). A field blank was also collected to account for any contamination that may have occurred through collection and processing.

Zooplankton samples for metals analysis were collected from the same locations in the PRZ and CTA as other ecotoxicity samples. After those zooplankton samples have been processed and analyzed for biomass, representative zooplankton samples will be shipped to UMD to be processed for metals analysis.

While all collections described in this scope of work will target five separate sampling depth strata, depth zones were adjusted based on availability and estimates of mid-water plume discharges. The five depth strata samples were collected from included approximately 100, 1000, 1500, 3000, 4000 m. In addition, all samples were collected from both the PRZ and CTS locations to ensure we could characterize the background ecotoxicity of these habitats prior to test mining. Lastly, all samples, regardless of media, were collected following United States Environmental Protection Agency (USEPA) protocols for contaminant analyses (USEPA 2000; 2007).

6.4.8.4 Preliminary results & discussion

No data is presently available from the pelagic ecotoxicology assessments. This data will become available in the next 12 months as well as data on the baseline heavy metal concentrations, and data on temporal changes in heavy metal concentrations in zooplankton and target mesopelagic taxa.

6.4.9 Marine Mammals, Birds, Turtles, Bony Fish and Sharks

Large vertebrates (particularly seabirds and marine mammals) are useful bio-indicators of the upper trophic levels of the food chain. Their distribution has the potential to reflect prey abundance lower in the food chain (e.g., phytoplankton, zooplankton, nekton and fish) and can reflect the status of the ecology of the upper water column.

6.4.9.1 Purpose and scope

The following section describes the work conducted in 2021 by Fathom Pacific Inc. to characterise natural baseline condition of marine mammals, birds, turtles and shark populations in NORI-D. The scope, the

survey planning and the sampling methodologies align with International Seabed Authority ISBA/25/LTC/6 Rev 1. Annex 1 section 51 Marine mammals, birds, turtles and sharks to provide baseline data requirements under Recommendations III.B.15.(d).(vi).

6.4.9.2 Baseline investigations

The methods and proposed survey array for both the collector test and long-term environmental studies on NORI-D will provide data to meet the following objectives:

- Determine the presence of Marine mammal, birds, turtles and sharks within NORI-D using a combination of observations

6.4.9.3 Campaign activities

(a) PelagOS observation program

The PelagOS (Pelagic Observer System) was employed to collect opportunistic data on surface observations. PelagOS is a marine monitoring application specifically designed to replace ad-hoc observations with a streamlined recording and reporting system that provides the user with a range of simple data collection and processing capabilities. Training, built-in species lists, and photo guide helps to ensure accuracy of species identification at sea which is further quality assured through validation by our offsite taxonomic experts. The PelagOS program was deployed on Campaigns 5A, B, C and D (Campaign 5C in progress at the time of writing).

(b) Hydrophone program

Moored hydrophones

The deployment of moored hydrophones has proven to be a powerful tool for investigating the presence, distribution, migration, relative abundance and behaviour of marine mammals (Erbe *et al.* 2017). Two underwater sound recorders were successfully deployed on a static mooring within NORI-D at 520 m (HTI-96-MIN hydrophone) and 4,295 m (HTI-90-U hydrophone) depth by CSA Ocean Sciences Inc (see Section 5.5.3.2)

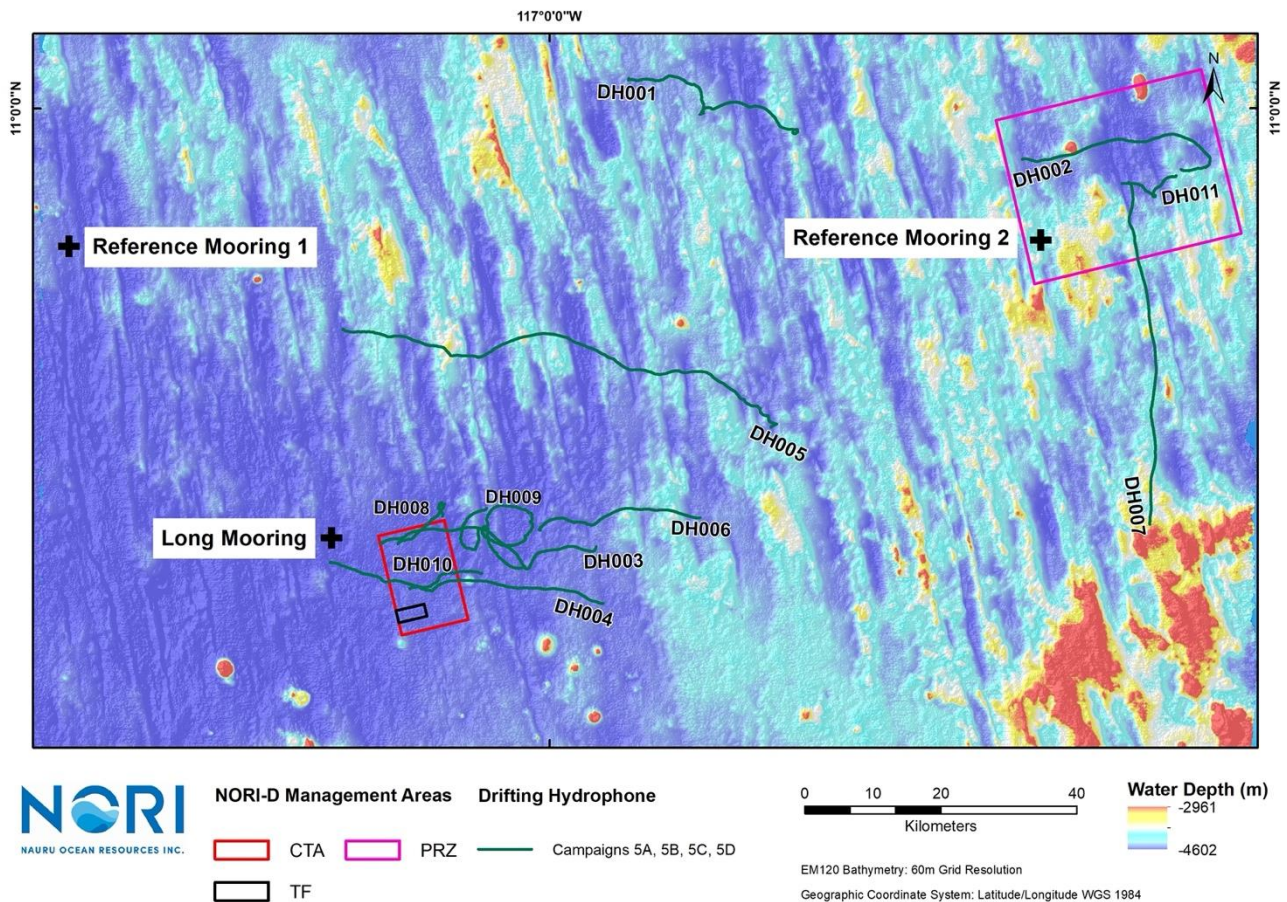
The hydrophones are tuned to detect mid to low frequency sounds that characterise the background soundscape and capable of detecting the vocalisations of baleen whales, and the clicks of large toothed whales and whistles of dolphins.

To date, there have been two deployment periods and at the time of writing the third deployment period was currently underway:

- Deployment Period 1: 14 October 2019 to 27 June 2020.
- Deployment Period 2: 28 June 2020 to 19 July 2021.
- Deployment Period 3: 21 July 2021 underway.

A bioacoustics analysis workflow has been developed, which combines automatic routines and systematic manual reviewing of recordings (Parnum 2020). Automatic detection routines include one that searches for FM signals (such as dolphin whistles and whale calls) and another for low frequency tones (e.g., blue whale calls and songs). From preliminary analysis, Delphinidae (dolphins), Physeteroidea (sperm whales), and minke whales were detected on the shallow recorder; and Delphinidae on the deep recorder.

Figure 6-102. Moored and drifting hydrophone array



The hydrophones are not capable of detecting the high frequency clicks of beaked whales that are known to occur in the region. Beaked whales are of specific relevance in the CCZ due to their occurrence in the area (Barlow *et al.* 2009) their deep-diving behaviour (Schorr *et al.* 2014) and therefore possible interaction with nodule collection activities (Marsh *et al.* 2018), and sensitivity to anthropogenic noise (Pirota *et al.* 2012).

In July 2021, an additional Ocean Instruments SoundTrap ST600HF hydrophone was procured and mounted to the mooring at a depth of 430 m depth during the mooring servicing for Deployment Period 3. The ST600HF was deployed on 21 July 2021 (Table 6-53) and the key instrument details are:

- Bandwidth: 20 Hz to 150 kHz.
- Sample rate: 192 kHz.
- Duty cycle: 1 min recording, 6 mins off (estimated 17% recording time over battery life).
- Onboard memory: 4 x 256 GB SD memory cards.

The ST600HF is a newer model that replaces the ST500HF, the latter being used on the Drifting Hydrophone array (see Section below). The ST600HF provides for more sampling rates options and various hardware, firmware and software upgrades to improve battery times and reduce self-noise. The difference between the two models is not consequential to the detectability of high frequency vocalisations.

At this time, analysis of the moored hydrophones has been completed for

- Deployment Period1: Shallow 14 October 2019 to 26 June 2020 (257 days), and Deep 14 October 2019 to 8 May 2020 (207 days).

Table 6-53 Moored ST600HF deployment details

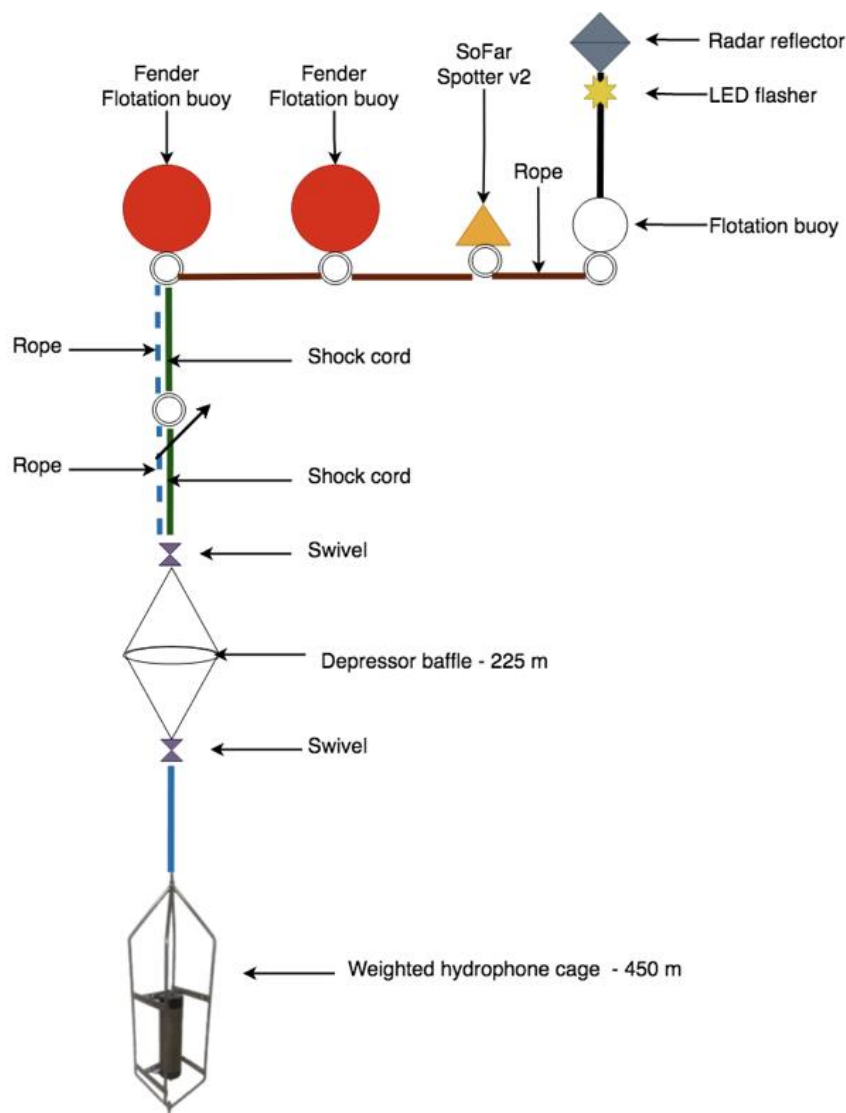
| HYDROPHONE TIME ON (UTC) | DATE AND DEPLOYMENT | SAMPLE RATE | LATITUDE | LONGITUDE | DEPTH AT SITE (m) | DEPLOYMENT DEPTH (m) |
|--------------------------|---------------------|-------------|-----------|-------------|-------------------|----------------------|
| 15:16:22 | 21/7/21 1:21 | 192 kHz | 10.428873 | -117.292850 | 4315 | 430 |

Drifting Hydrophones

A drifting hydrophone array was deployed on Campaigns 5A, 5B, 5C and 5D with the aim to increase detectability of high frequency beaked whale vocalisations. The drifting hydrophone array consists of a SoundTrap ST500HF hydrophone deployed at a depth of 450 m on a rope with surface floats and bungee lines to suppress hydrodynamic noise (Figure 6-103). A SoFar Ocean Spotter v2 float is used to track the array in real time. The ST500HF on the drifting array was set to record continuously over the duration of the deployment at a sample rate of 288 kHz. The bandwidth of the ST500HF is the same as that of the ST600HF (20 Hz to 150 kHz).

The drifting array was deployed throughout NORI-D for several days per deployment (Figure 6-102). At the time of writing, the drifting array was in operation on Campaign 5C and data were available for 10 deployments. Analysis has been completed for deployments DH_002 to DH_010.

Figure 6-103 Schematic of drifting hydrophone array



6.4.9.4 Preliminary results & discussion

(a) PelagOS Program

The PelagOS program has generated 169 biological observations as listed in Table 6-54. The observations are mapped and discoverable through the PelagOS web portal and accompanied by photographic evidence for the majority of sightings. Future work will involve quantifying sightings per unit effort, investigating temporal trends and contextualising spatially, including comparisons against inshore programs. Preliminary examination indicates that there are no differences between the observations in the PRZ (63 biological observations) and the CTA (69 biological observations), which would be expected given the wide-ranging behaviours of these species compared to the scale of NORI-D.

(b) Campaign 5A

A total of 25 biological observations were recorded by observers during Campaign 5A (examples Figure 6-104). Using PelagOS, the post-cruise quality assurance process was able to identify an additional 17 observations from photographs that were not recorded at the time. The total number of 43 biological observations in 39 days of observation is considered relatively low, this could be due to low productivity in the survey area, absence of fauna, challenging sighting conditions or a combination of all factors. Biological observations were dominated by bird species (28 records). The remaining observations were made up of 9 fish and 5 marine mammal (all cetacean) sightings. No marine reptiles were recorded during this cruise.

Birds - The most commonly recorded seabird species were the brown booby (*Sula leucogaster*) and masked booby (*Sula dactylatra*). One species of normally terrestrial bird, the cattle egret (*Bubulcus ibis*), was also recorded multiple times during the cruise. No significant bird aggregations were recorded.

Fish - Mahi mahi (*Coryphaena hippurus*) was the most commonly observed fish species (three records). Also, of note was one sighting of a manta ray (no verification image) and one sighting of tuna. No sharks were reported from this cruise.

Marine mammals - Five marine mammal sightings were recorded during the cruise, all being from the Order Cetacea and identified as bottlenose, spinner, and likely spotted dolphins. The most prevalent species of dolphin was the oceanic bottlenose dolphin (*Tursiops truncatus*) which was sighted on two occasions, most notably on one occasion, in a large group of several hundred individuals. No large whale species were visually detected during this cruise.

(c) Campaign 5B

A total of 71 biological observations were recorded by observers during Campaign 5B (examples Figure 6-105). This number is a considerable increase on the 43 biological observations observed in Campaign 5A. Biological observations were dominated by bird species (62 records). The remaining observations were made up of 1 reptile, 4 fish and 4 marine mammal (all cetaceans) sightings.

Birds - The most commonly recorded seabird species were the masked booby (*Sula dactylatra*) and brown booby (*Sula leucogaster*). Four great frigatebirds (*Fregata minor*) were also observed during this cruise, a family that was not sighted in Campaign 5A. No significant bird aggregations that may have indicated high levels of productivity were recorded.

Fish - sightings consisted of two unassigned flying fish species with one sighting estimating a school of 50 individuals. Two sightings of mahi mahi (*Coryphaena hippurus*) were also observed. No sharks were reported from this cruise.

Reptiles - One green sea turtle (*Chelonia mydas*) was recorded displaying surface active behaviour.

Marine mammals - Of the four marine mammal sightings, all were from the order cetacea and identified as three dolphins and one whale. The dolphins consisted of short-finned pilot whales (*Globicephala*

macrorhynchus; two records) and one sighting of a short-beaked common dolphin (*Delphinus delphis*). There was a single sighting of a grey whale in transit

(d) Campaign 5D

A total of 58 biological observations were recorded by observers during Campaign 5D (examples Figure 6-106). Biological observations were dominated by bird species (48 records). The remaining observations were made up of 1 fish, 1 ray, 4 reptiles and 4 marine mammals (3 cetaceans and 1 pinniped) sightings.

Birds - The most commonly recorded seabird species were the masked booby (*Sula dactylatra*; 22 records) and the red-footed booby (*Sula sula*; 10 records). The second most observed family were the tropicbirds, with eight sightings during the campaign. There was one sighting of a nominally terrestrial bird resting on the ship during the cruise. No significant bird aggregations that may have indicated high levels of productivity were recorded.

Fish - There was a single fish sighting of a billfish species during the cruise. There was also one sighting of a manta ray. No sharks were reported from this cruise.

Reptiles - Four sightings of reptiles consisted of three unassigned turtle species and one green turtle (*Chelonia mydas*) (Figure 2B)

Marine mammals – Four marine mammal sightings were recorded during the cruise, three from the order cetacea were identified as a short-beaked common dolphin (*Delphinus delphis*) an unassigned dolphin and a sperm whale. There was one sighting of an unassigned pinniped.

Table 6-54 PelagOS sightings summary, Campaigns 5A, 5B and 5D.

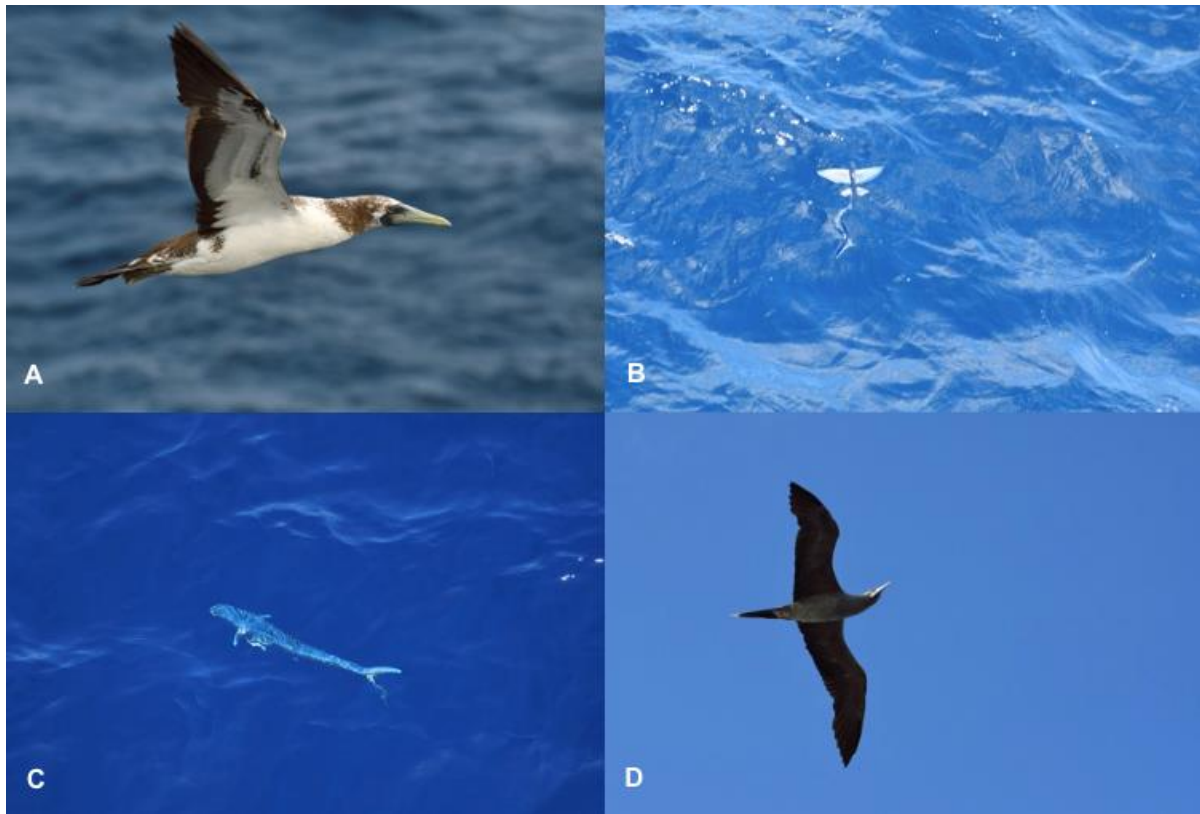
| BIOLOGICAL GROUP | NUMBER OF SIGHTINGS | NUMBER OF TAXA |
|------------------|---------------------|----------------|
| Seabirds | 1289 | 17 |
| Cetaceans | 12 | 8 |
| Fishes | 13 | 8 |
| Turtles | 5 | 2 |

Figure 6-104 Examples of surface biota observations from Campaign 5A



A) Masked booby (*Sula dactylatra*); B) Cattle egret (*Bubulcus ibis*); C) Mahi mahi (*Coryphaena hippurus*); D) oceanic bottlenose dolphin (*Tursiops truncatus*).

Figure 6-105 Examples of surface biota observations from Campaign 5B



A) Masked booby (*Sula dactylatra*); B) Flying fish; C) Mahi mahi (*Coryphaena hippurus*); D) red-footed booby (*Sula sula*)

Figure 6-106 Examples of surface biota observations from Campaign 5D



A) short-beaked common dolphins (*Delphinus delphis*); B) green sea turtle (*Chelonia mydas*); C) tropic bird (*Phaeton* sp.) D) manta ray (*Manta* sp.)

Seabirds are the most frequent observed surface species and off these, species that feed on fishes and squid species are in much higher abundance than planktivorous species (Figure 6-107; Figure 6-108). This supports the predictions from the existing literature that the NECC supports predominantly piscivorous seabirds, that in turn is indicative of an epipelagic system that supports a prey field that favours piscivores.

Figure 6-107 Abundance of seabirds recorded by PelagOS across three campaigns by trophic guild

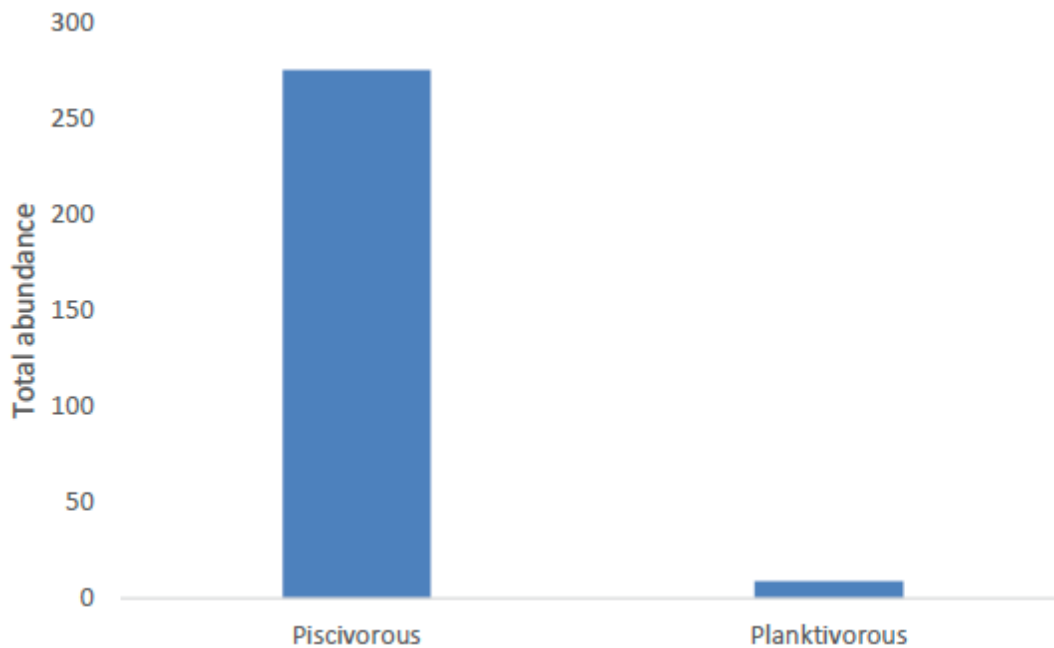
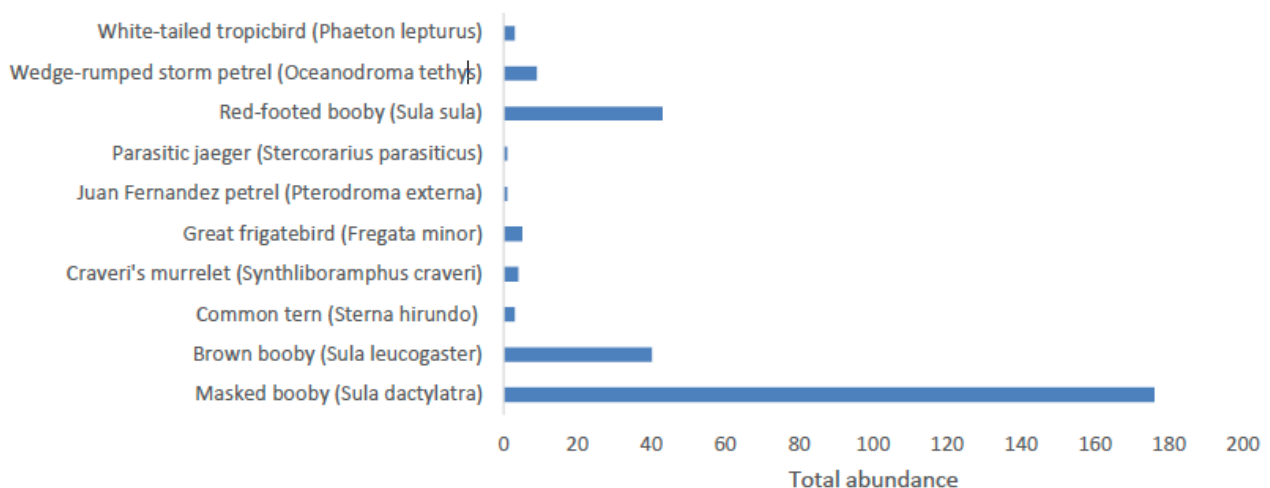


Figure 6-108 Seabird species abundance recorded by PelagOS across three campaigns



(e) Hydrophone Program

(i) *Moored hydrophones:*

- Dolphin sounds were present in most days on both recorders, and more detection occurred at night than during the day (Figure 6-109; Figure 6-110).
- Sperm whales were heard on ten separate days spread over the deployment period on both recorders, with most detections in the morning.

- Minke whales were heard on the Shallow sound recorder on 27th January 2020 and on the Deep recorder on 18th March 2020.
- Down-sweep signals recorded on the Deep static sound recorder on 19th and 30th March 2020, sound and look like north-east Pacific blue whale calls originally termed ‘S’ calls and now more regularly called ‘D’ calls. However, nothing similar to the NE Pacific blue whale ‘A’ nor ‘B’ calls were detected.

(ii) *Drifting hydrophones:*

- Dolphins were regularly detected on all of the deployments (Figure 6-111), with more detections occurring at night than during the day.
- Sperm whales were detected on four of the deployments, with more detections occurring during the day than the night.
- Clicks likely to be from beaked whales were detected on six of the deployments, with more detections occurring at night than during the day.
- Narrowband, high frequency (>100 kHz) clicks were sparsely detected on four of the deployments, with more detections occurring during the day than the night. These clicks are likely to be from dwarf sperm whales.

Figure 6-109 7-day median of percentage of hours within a 24-hour period that had dolphin whistles or clicks detected for the shallow and deep moored hydrophones.

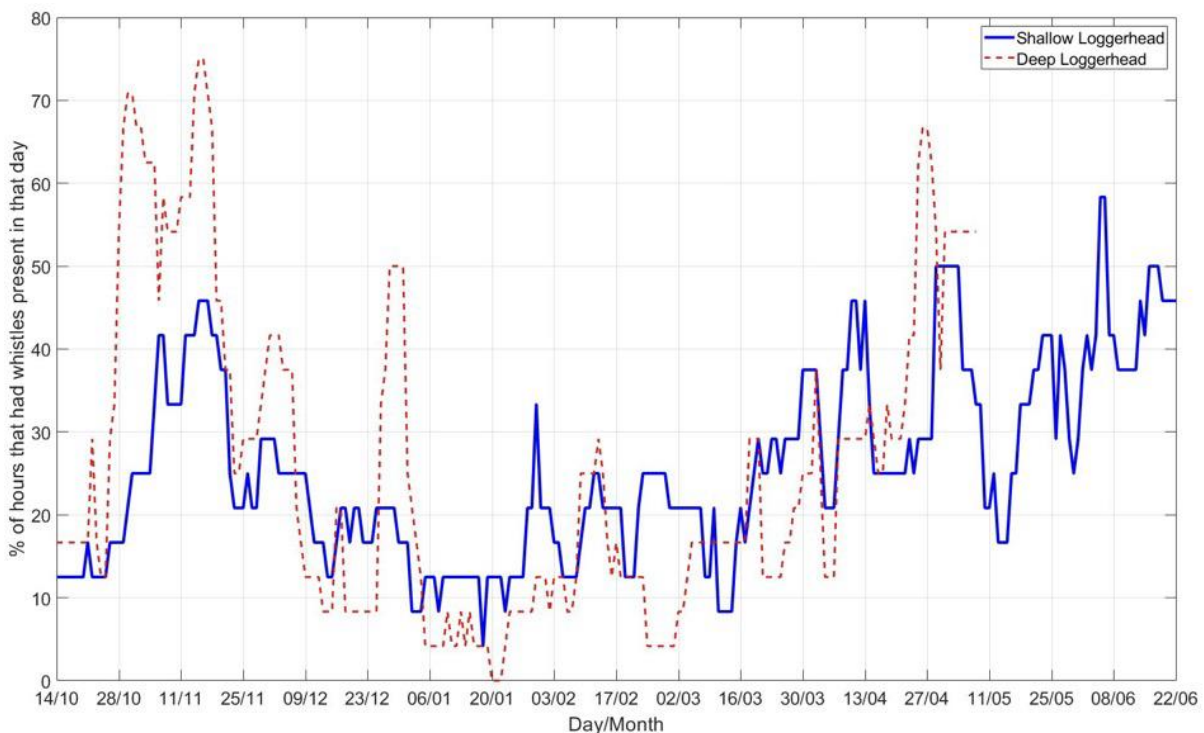


Figure 6-110 Percentage of days that had detections of dolphin whistles or clicks in an hour of day for the shallow and deep moored hydrophones

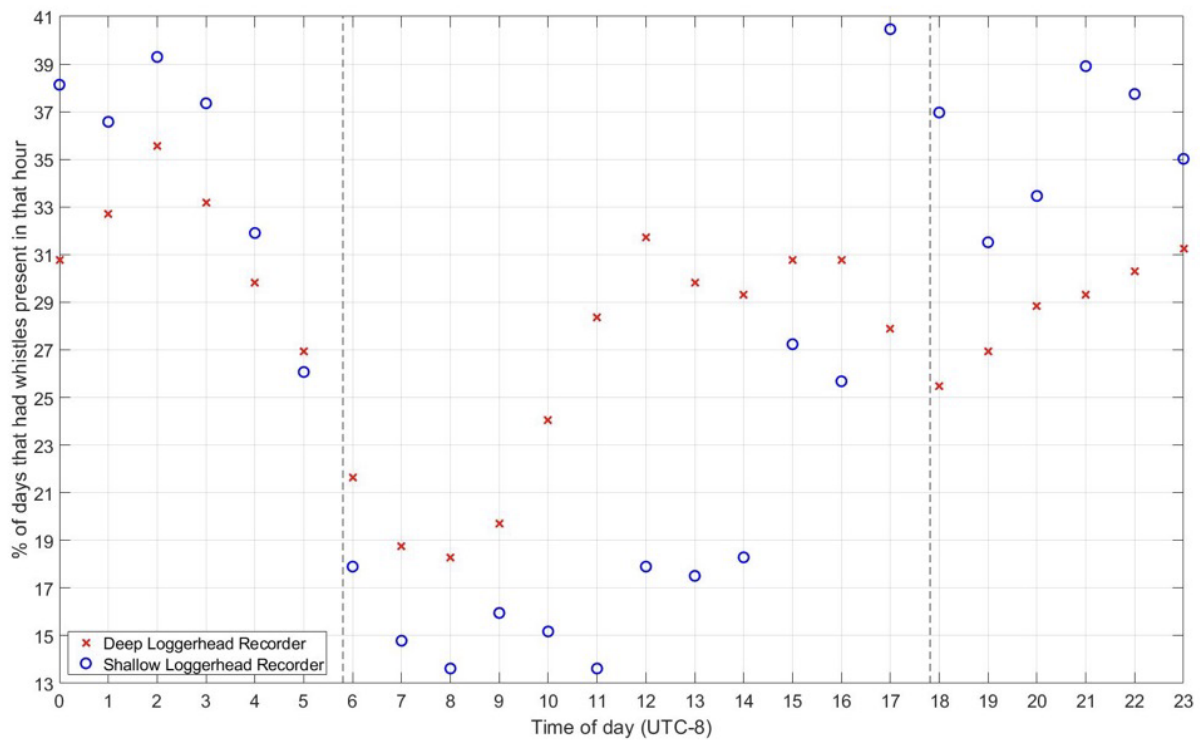
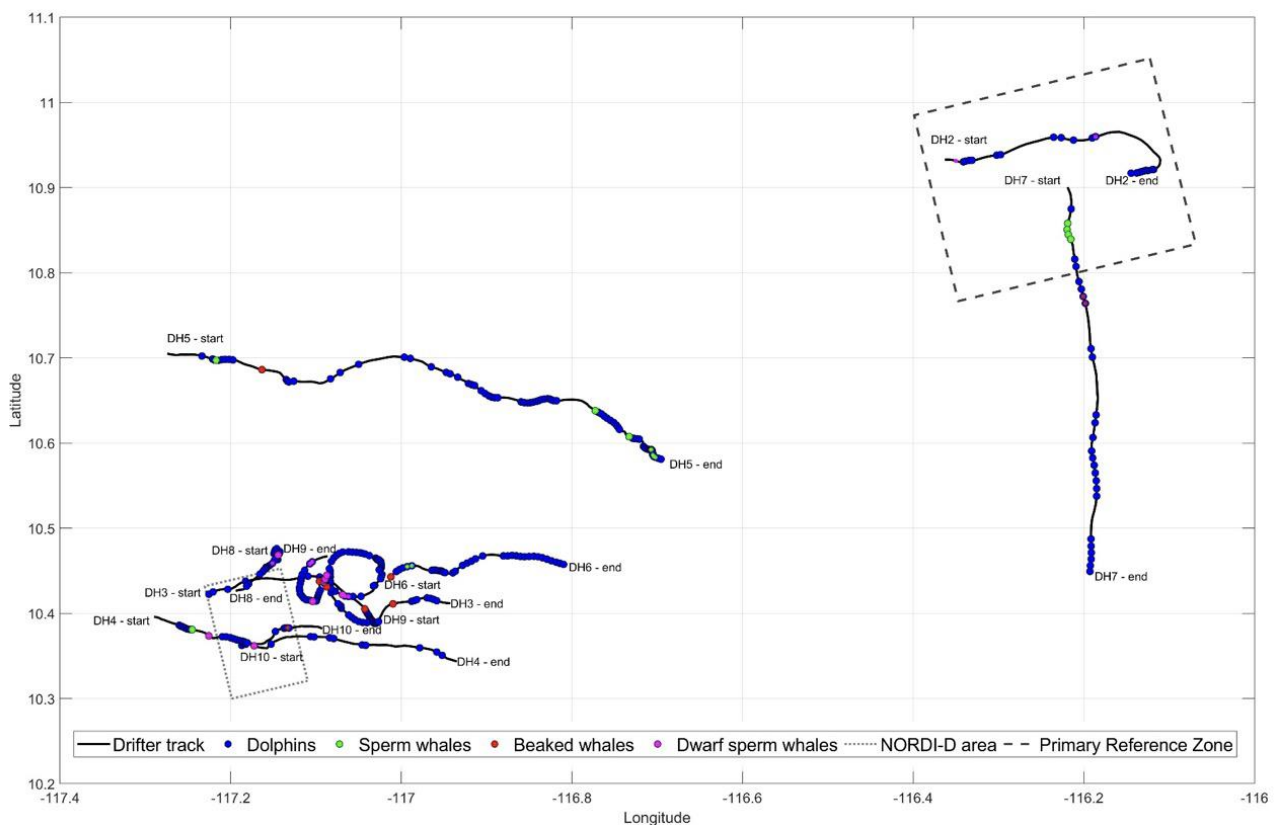


Figure 6-111 Locations of the drifting underwater sound recorder deployments and detections. Detections are shown as: Blue circles for Delphinidae species (i.e. dolphins), green circles for Physterioidea species (i.e. sperm whales), red circles for Ziphiidae species (beaked whales), and pink circles for *Kogia sima* (dwarf sperm whales). Locations are where the surface buoy was when a detection was made on the recorder.

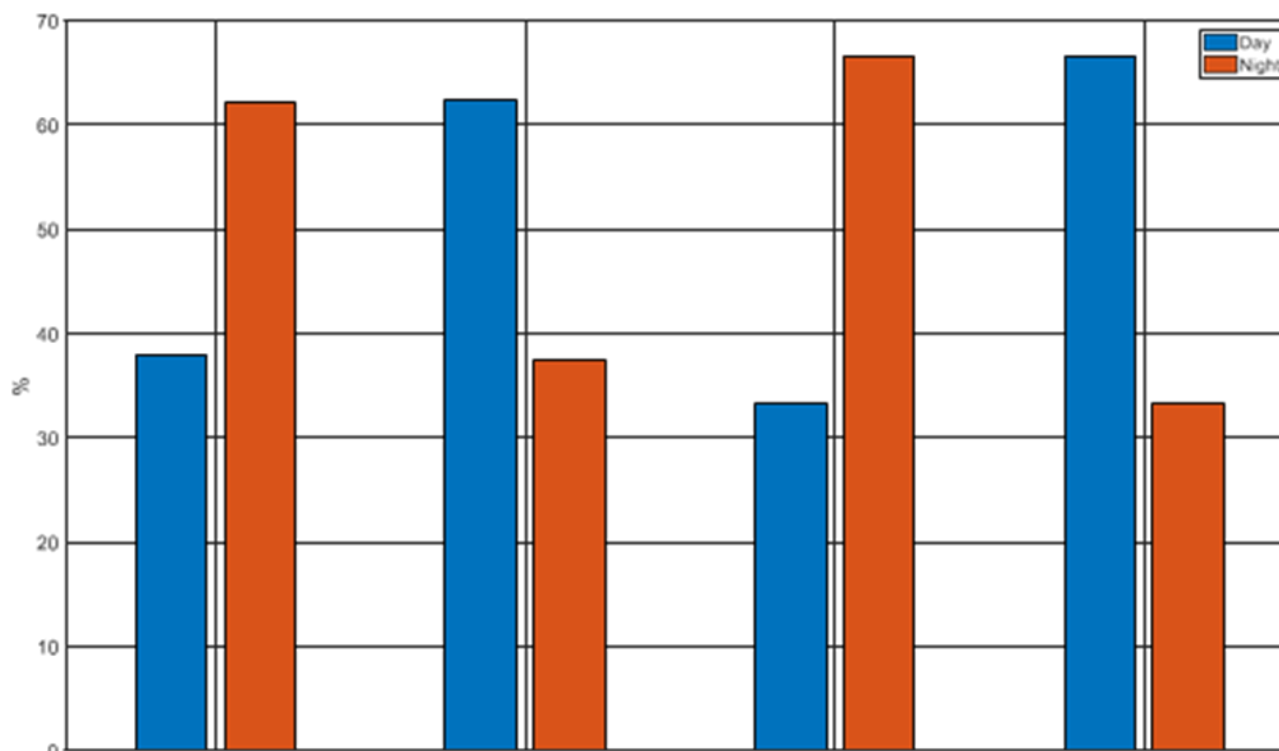


Of the nine deployments of the drifting underwater recorder analysed (DH2-DH10), Delphinidae species (dolphins) were detected on all of them, Physeteroidea species (sperm whales) on four of them, Ziphiidae species (beaked whales) on six of them, and what is likely to be *Kogia sima* (dwarf sperm whale) on four of them (Table 6-55). The occurrence of dolphin sounds in the drifting hydrophone deployments was much higher than the other marine mammals detected (Table 6-55). Detections of dolphins and beaked whales were higher at night-time than during the day, whereas the opposite trend was recorded for sperm whales and dwarf sperm whales (Figure 6-112).

Table 6-55. Percentage of survey hours within in which different marine mammals were detected in an hour, alongside the total survey hours for each deployment of the Drifting Hydrophone.

| n | % of hours surveyed where they were present in that hour | | | | Total survey hours |
|------------|--|--------------|---------------|--------------------|--------------------|
| | Dolphins | Sperm whales | Beaked whales | Dwarf Sperm Whales | |
| DH2 | 28 | 0 | 0 | 3 | 71 |
| DH3 | 32 | 0 | 2 | 0 | 88 |
| DH4 | 30 | 1 | 0 | 2 | 94 |
| DH5 | 44 | 3 | 1 | 0 | 167 |
| DH6 | 60 | 3 | 2 | 0 | 58 |
| DH7 | 46 | 7 | 4 | 0 | 56 |
| DH8 | 48 | 0 | 0 | 2 | 48 |
| DH9 | 51 | 0 | 1 | 3 | 149 |
| DH10 | 18 | 0 | 2 | 0 | 55 |
| All | 41 | 1 | 1 | 1 | 786 |

Figure 6-112. Percentage of detections made for different species/families during the day (6 am - 6pm) vs the night (6pm – 6am).



The epipelagic environment of NORI-D and the eastern CCZ region is influenced primarily by the North Equatorial Counter Current (NECC), the core of which is associated with relatively low productivity. Oceanographic processes, such as the seasonal intensification of the NECC, frontal interactions with the NEC, doming and strengthening of the thermocline ridge, phytoplankton blooms in areas of regenerated

nutrients and advection of primary production into the area, are postulated to establish periods of enhanced prey abundance that attracts pelagic predators (Fathom Pacific, 2020b).

Preliminary analysis indicates that there is a period of strengthening NECC flow in the period September to December which is known to generate increased Ekman pumping and frontal energetics which could enhance productivity and drive increased pelagic predator abundance. This is consistent with the hydrophone data which recorded increased dolphin vocalisation over these months (Figure 6-109). The tuna-dolphin-seabird (TDS) assemblage, first coined by Au and Perryman (1985) and later adopted by Ballance et al. (2006), is a characteristic pelagic phenomenon in the region that is underpinned by the counter current thermocline ridge. The TDS assemblage is reflected in commercial yellowfin and skipjack tuna fisheries catch data that shows high catch rates overlapping with the eastern CCZ. Dolphin whistles were recorded on all days in the moored hydrophones but no commercial fishing vessel have been observed at NORI-D through the PelagOS program. No tuna schools have been recorded in the PelagOS program, although surface expressions of tuna schools are relatively rare occurrences. The data indicate that NORI-D is located in area that has lower pelagic predator abundance compared to waters to the east (Eastern Pacific Warm Pool and Costa Rica Dome) and to the north (California Current and North Equatorial Current). However, the movements of wide-ranging pelagic species interact with NORI-D and these large-bodied species have high energy demands that need to be met by feeding. As such, the presence of species such as dolphins, sperm whale, manta ray and acoustic detections of substantial dolphin whistles, minke whale, sperm whale, blue whale, dwarf sperm whale and beaked whales is evidence that these species exist and feed in the NORI-D region.

Beaked whales, sperm whales and dwarf sperm whales are deep-divers that are posited as species of increased concern in terms of interaction with nodule collection activities. The occurrence of these species in the area suggests the presence of a deep prey source comprising fishes and squids that are targeted by these species.

Seabirds are the most abundant predators observed in the PelagOS program and existing data indicates that the NECC is an important foraging area for piscivorous species, particularly in the western sector (west of 120°W). The foraging behaviour of seabirds contributes to an ecological function of the open ocean by transferring nutrients to coastal environments where higher primary production occurs and, scaled-up to the population across the eastern tropical Pacific, contributes to upper ocean mixing and potentially cloud albedo effect.

Collectively, the data indicate that the pelagic ecosystem in the NORI-D region is a system that at least periodically supports piscivorous predators. This requires ecological processes that supply regenerated nutrients and primary production that underpins the development of a food chain that supports prey fish and other nekton populations.